Physical and Chemical Properties of Molten Carbonates

Kojima, Toshikatsu

(Degree)
博士（工学）

(Date of Degree)
2009-03-25

(Date of Publication)
2013-08-30

(Resource Type)
doctoral thesis

(Report Number)
甲4596

(URL)
https://hdl.handle.net/20.500.14094/D1004596

博 士 論 文

Physical and Chemical Properties of Molten Carbonates

（溶融炭酸塩の物理化学的性質に関する研究）

平成 21 年 1 月

神戸大学大学院自然科学研究科

小島 敏勝

Contents

1. General Introduction

1.1. Molten Carbonate Technologies

In 21st Century, we human beings are forced to face many crises. Depletion of oil threatens global economy to be very nervous to oil price. Climate of recent years are becoming uncomfortable in proportion to global temperature increase brought by green house effect of CO_2. Carbon dioxide and Industrial waste are getting serious problem for our environment. Today, we really need fundamental solutions for these problems in order to realize next generation's prosperity and peace.

Molten salt technologies could provide the solutions for these problems of global climate crisis, energy crisis, and pollution. There are being developed many promising technologies concerning molten salt, such as safer nuclear fission reactor with abundant resources, fuel cells, CO_2 separation and condensation, poisonous waste processing, and new material processing[1].

Among these molten salt technologies, molten carbonate technologies are very attractive and promising[2] because of its utilization for Molten Carbonate Fuel Cell (MCFC) [3]. There are many promising and interesting researches have been done for not only MCFC, but also CO_2 condensation[4-7], gasification of coal[8] or waste[9-10], nuclear fuel processing[11-14], material processing[15-17], thermal mediums[18-20], as additives to enhance the performance of Solid Oxide Fuel Cell[21-24] and so on. The needs of research for molten carbonate are becoming higher and higher.

1.2. Molten Carbonate Fuel Cell

A number of research activities concerning molten carbonate have been concentrated to MCFC R&D. The MCFC is a fuel cell which utilizes molten carbonate as electrolyte. MCFC is operated at elevated temperature, 650 °C and make electricity using hydrogen and air with a high efficiency and a low impact on the environment.

The principle of molten carbonate fuel cell is shown in Fig. 1-1. Hydrogen reacts at an electrode called as anode with carbonate ion to be water and release electrons to electric circuit. Oxygen dissolves into molten carbonate electrolyte, receives electrons at an electrode called as cathode and reacts with CO_2 to be carbonate ion. The feature of MCFC is utilizing CO_2 which will be recycled from anode exhausted gas. Electrode reactions proceed without precious metal catalyst such as Pt or Ru, and are not be poisoned with CO because of operation at elevated temperature. The materials used in MCFC are relatively lower price than that of other fuel cell, such as Polymer Electrolyte Fuel Cell. Therefore MCFC is expected to be a promising power generation technology[3]. It was demonstrated by Tanimoto[25] that a single cell of MCFC can be operated more than 40,000 hours, which is the life time needed for commercialization.

MCFC can be also utilized as separator and condenser of CO_2 [7]. Large power plants of MCFC more than 2MW had been constructed and operated. Many on-site modules of 300kW type MCFC

are produced and being operated more than 25 sites in the world and their efficiency exceed 40 %[26].

Molten carbonates are used as the electrolytes of MCFC. A MCFC is made of metal materials, ceramics and molten carbonate electrolyte. Fig.1-2 shows schematic diagram of the MCFC structure and material of components. An anode is made of porous nickel for hydrogen oxidation. A cathode is made of porous NiO for oxygen reduction. A separator is a cladding plate of nickel and stainless steel of SUS316L or SUS310. Current collectors are made of nickel for anode and stainless steel for cathode. An electrolyte matrix is made of $LiAlO_2$ powder containing liquid molten carbonate electrolyte.

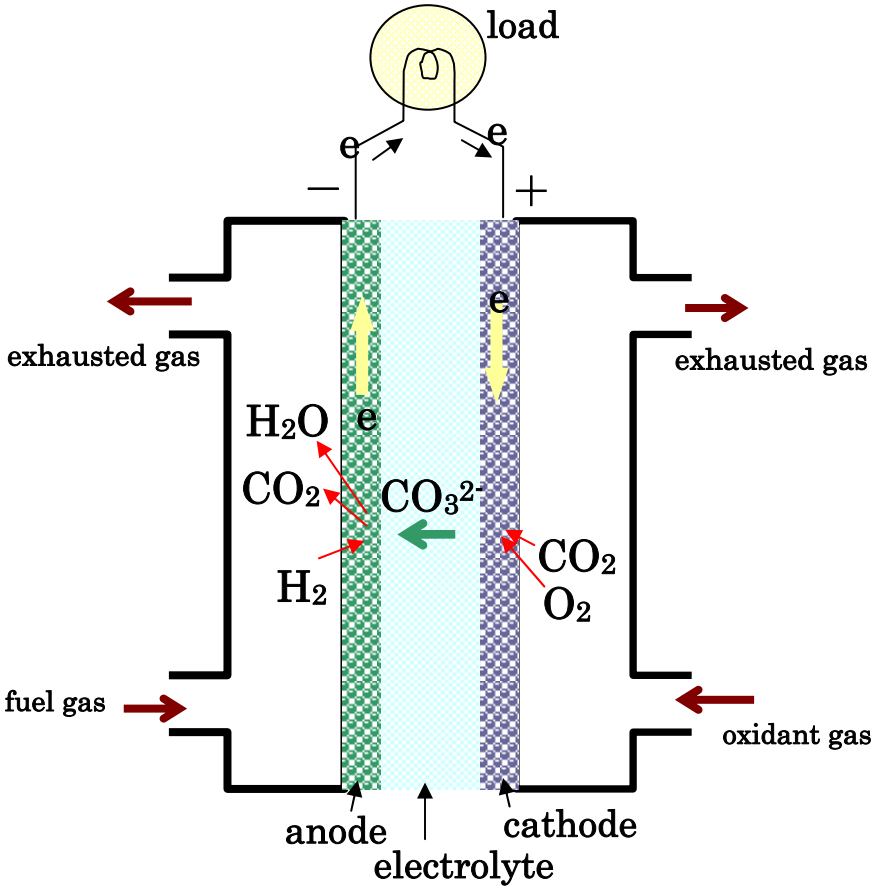

Fig. 1-1. Principle of Molten Carbonate Fuel Cell.

Molten carbonate electrolyte plays important roll in MCFC, conveying CO_3^{2-} ion from cathode to anode. Ionic conduction is related to electrical conductivity of molten carbonate. Electrical conductivity of molten carbonate is one of important physical properties, which has influence upon efficiency and output of fuel cell.

Molten carbonate should be adjusted to suitable amount in a cell among porous component properly in order to make good gas-liquid-electrode three phase reaction site. The proper volume of electrolyte can be calculated with molten carbonate density data. Molten carbonate electrolyte

distributed among porous components was retained by capillary forces which work inside small pores. The forces are originated from the surface tension of molten carbonate. The surface tension of molten carbonate distribute electrolyte among components and prevent gas cross leakage through electrolyte matrix.

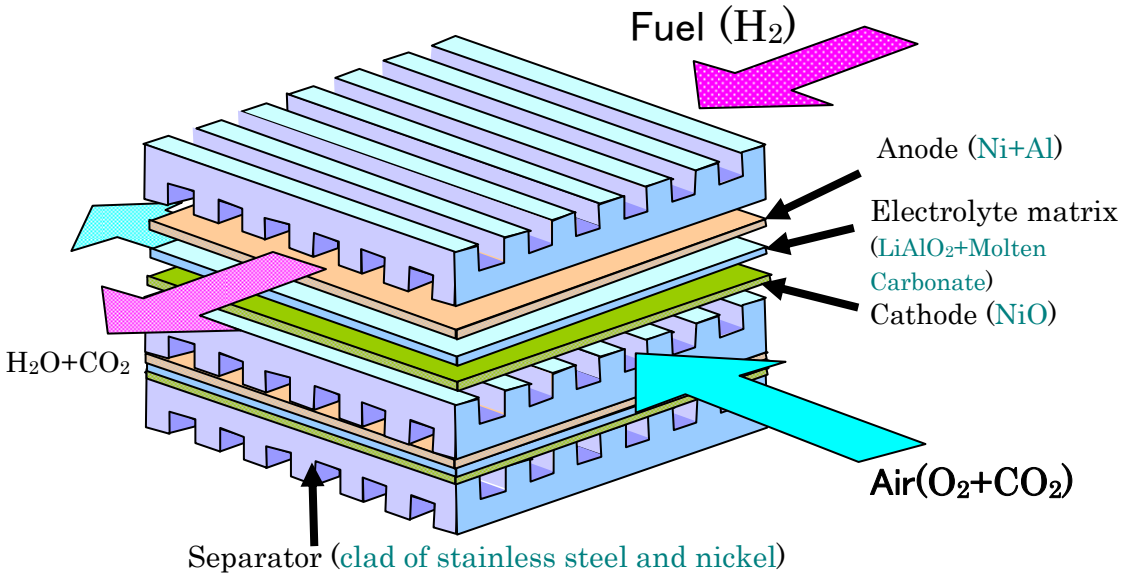

Fig. 1-2. Component and materials of Molten Carbonate Fuel Cell.

Many materials utilized in MCFC slowly corroded with molten carbonate at 650 °C. Corrosion of the materials is serious issue because corrosion reaction consume molten carbonate electrolyte, the corrosion degrade electrode function and corrosion products increase the internal resistance of cells. These corrosion reactions decrease cell performance and also life. Therefore the knowledge of reactions between materials and molten carbonate mixtures are very important not only for prevent corrosion but also for searching new materials.

Most serious problem is the dissolution of NiO cathode in molten carbonate electrolyte. Nickel dissolved as Ni^{2+} in molten carbonate, which migrates from cathode to anode then is reduced to be nickel particle. During long-term operation of MCFC, nickel particle will grow to connect each other and bring short circuit between anode and cathode. This short-circuit seriously degrade the performance of MCFC[25].

Ota et al. [27] showed that the dissolution of NiO have strong correlation with basicity of molten carbonate, which is governed by oxide ion O^{2-} and CO_2. Acidic melt such as $(Li_{0.43}K_{0.57})_2CO_3$ dissolved NiO more than basic melt such as $(Li_{0.52}Na_{0.48})_2CO_3$.

Another serious problem is metal material corrosion. Although stainless steels of type SUS316L and SUS310S have been selected, these alloys will react with molten carbonate electrode and produce corrosion scale on their surface, which consume molten carbonate electrolyte and increase

resistance of cell [28, 29]. This would result in degradation of cell performance and shortens the life of MCFC.

1.3. Molten Carbonate Mixtures

Although molten carbonate electrolyte, mainly $(Li_{0.62}K_{0.38})_2CO_3$ is used, the alternative electrolytes are recognized as promising choice for realizing long-life and high performance MCFC. There are many researches for the corrosion and reaction between molten carbonate and materials such as many kinds of metals, alloys and ceramics. However, a few kinds of carbonate mixtures have been investigated, mainly molten $(Li_{0.62}K_{0.38})_2CO_3$, $(Li_{0.52}Na_{0.48})_2CO_3$ (or $(Li_{0.53}Na_{0.47})_2CO_3$), $(Li_{0.43}K_{0.57})_2CO_3$, and $(Li_{0.435}Na_{0.315}K_{0.25})_2CO_3$.

There are many kinds of molten carbonates, and their mixtures. It is known that single carbonates containing 1+ charged cations such as Li_2CO_3, Na_2CO_3, K_2CO_3, Rb_2CO_3, and Cs_2CO_3 can exist stably as molten carbonates under CO_2[30].

It has been reported that Li_2CO_3-Rb_2CO_3, Li_2CO_3-Cs_2CO_3, Na_2CO_3-Rb_2CO_3, and Na_2CO_3-Cs_2CO_3 binary carbonate systems have some compositions of low melting point suitable for MCFC operation[31]. Smith et al. operate MCFC using $(Li_{0.75}Cs_{0.25})_2CO_3$ as electrolyte[32].

The ternary molten salt mixtures of the Li_2CO_3-Na_2CO_3-K_2CO_3 system show a large variation of physical properties, over a wide temperature range from 671 to about 1300 K, and therefore offer a wide choice of compositions and properties. Mohamedi et al. investigated oxygen solubility and Warbrug impedance in this system for MCFC[33].

The physical properties of many compositions of alkaline carbonate mixtures have not been invesitigated in Li_2CO_3-Na_2CO_3, Li_2CO_3-K_2CO_3, Li_2CO_3-Rb_2CO_3, Li_2CO_3-Cs_2CO_3, Na_2CO_3-K_2CO_3, Na_2CO_3-Rb_2CO_3, Na_2CO_3-Cs_2CO_3, Li_2CO_3-Na_2CO_3-K_2CO_3 Li_2CO_3-Na_2CO_3-Rb_2CO_3 Li_2CO_3-K_2CO_3-Cs_2CO_3 and so on. In this thesis above mentioned carbonates and mixed carbonate systems were investigated for their physical properties of density, surface tension, and electrical conductivity.

1.4. Effects of Additive and Impurities to the Nature of Molten Carbonate

So far, molten $(Li_{0.52}Na_{0.48})_2CO_3$ and $(Li_{0.62}K_{0.38})_2CO_3$ have been most frequently used as the electrolytes of MCFCs.

Some additives have been investigated in order to overcome the above-described cathode degradation. According to Doyon et al. [34], the addition of SrO effectively decreased the solubility of nickel ion in MCFC electrolyte. Tanimoto et al. reported that new electrolytes containing alkaline earth carbonates ($CaCO_3$, $SrCO_3$, and $BaCO_3$) are promising from the viewpoints of lower NiO solubility[35, 36]. Miyazaki also showed that these ternary carbonate systems have suitable melting point for MCFC operation[37]. Yanagida[38], and Tanimoto[39] et al. showed that lower corrosive

nature against stainless steel. Tanimoto also demonstrated that MCFCs utilizing electrolytes added with alkaline earth carbonates showed equivalent performance to stage-of-the-art MCFC[40]. Hatoh et al. [41] reported that the addition of alkaline earth carbonates increased the exchange current density of oxygen reduction at gold electrodes under cathode gas conditions, which means that these additives may increase the performance of the cathode.

Some mixture in the systems of Li_2CO_3-Na_2CO_3 and Li_2CO_3-K_2CO_3 can solve carbonates containing 2+ charged cations such as $MgCO_3$, $CaCO_3$, $SrCO_3$, and $BaCO_3$. Although the solubility of $MgCO_3$ is about 1mol% in molten $(Li_{0.62}K_{0.38})_2CO_3$ at 923K, $CaCO_3$, $SrCO_3$, and $BaCO_3$ are dissolved with $(Li_{0.62}K_{0.38})_2CO_3$, $(Li_{0.52}Na_{0.48})_2CO_3$ and $(Li_{0.43}K_{0.57})_2CO_3$ by no less than 30 mol%. Li_2CO_3-Na_2CO_3-$CaCO_3$, Li_2CO_3-Na_2CO_3-$SrCO_3$, Li_2CO_3-Na_2CO_3-$BaCO_3$, Li_2CO_3-K_2CO_3-$CaCO_3$, Li_2CO_3-K_2CO_3-$SrCO_3$, and Li_2CO_3-K_2CO_3-$BaCO_3$, are investigated for their physical properties in this thesis.

Several non carbonate additives also have been investigated for improving MCFC performance and durability. Terada et al reported the addition of WO_4^{2-} act as catalyst hydrogen oxidation and prevent the degradation of electrolyte supporting material, $LiAlO_2$ and metal materials[42-43].

Corrosion products and impurity would change the nature of molten carbonates. As a corrosion product from stainless steel, CrO_4^{2-} ion will dissolve into molten carbonate electrolytes [44].

Kawase reported that some impurities such as HF[45] from gasified coal accumulated as F^- in molten carbonate electrolyte.

There are many stable additives which can be dissolved or mixed with $(Li_{0.62}K_{0.38})_2CO_3$, and $(Li_{0.52}Na_{0.48})_2CO_3$ such as halogens (F^-, Cl^-, Br^-, and I^-), NO_3^-, SO_4^{2-}, CrO_4^{2-}, MoO_4^{2-}, WO_4^{2-}. These additive and impurities would change physical properties of molten carbonate electrolytes. In this thesis above the mentioned mixtures of carbonates with additives were also investigated for physical properties.

1.5. Physical Properties Molten Carbonates

The physical and chemical properties of molten carbonates are essential not only for the industrial use but also fundamental understanding their nature. Above mentioned compositions have been investigated not only in order to find new electrolyte for MCFC, but also for comprehensive understanding the nature of molten carbonate. New composition of molten carbonate would change physical and chemical properties, such as density, surface tension, electrical conductivity, acid-base property and corrosive nature. As molten carbonates would become important material for many industrial fields, the physical and chemical properties of molten carbonates should be understood and these data should be attained.

Fig 1-3 shows how physical properties of molten carbonate affect several phenomena in MCFC. In the MCFC, the data of density and molar volume of molten carbonate are needed for estimating

favorable electrolyte volume ratio in matrix of MCFC. The data of density also provides an insight into the melt structure. The surface tension of molten carbonate has relationship with the force between ionic species in it. It is also important for estimating capillary force and wettability, which work to distribute electrolyte between porous cell components of anode, cathode and electrolyte matrix and prevent gas cross-leakage through electrolyte matrix in MCFC. The surface tension also has an influence on the reactant gas solubility in molten carbonate hence MCFC performance. The electrical conductivity of molten carbonate is directly related to the output of MCFC and also provides information of ionic movement in molten carbonate.

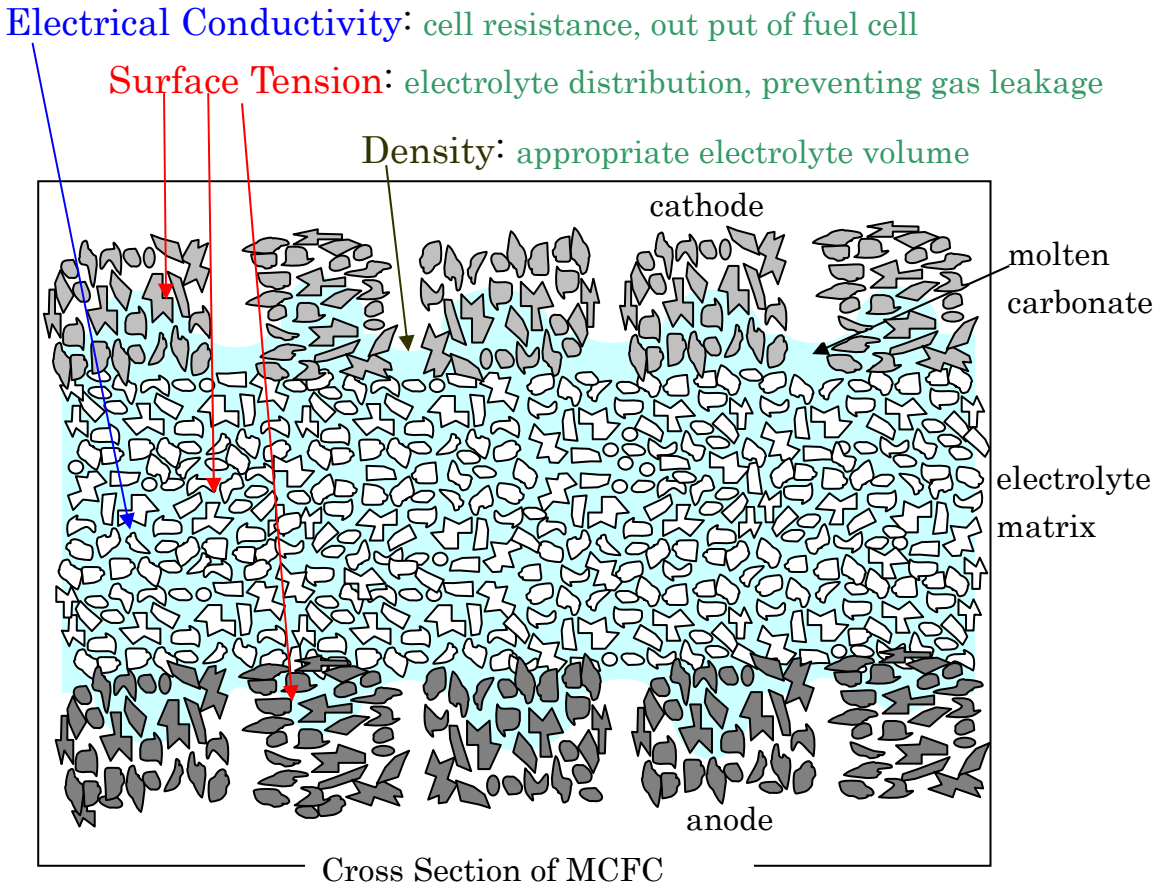

Fig. 1-3. Schematic View of Physical Properties of Molten Carbonate Affecting MCFC.

It should be pointed out that $LiAlO_2$ powder in electrolyte matrix has large surface area more than 10 m^2/g. Mizuhata and Deki reported that the physical properties such as melting point and conductivity of molten carbonate in powder of such high surface area are changed[46-48]. Understanding these phenomena is quite important for practical use of molten carbonate and solid powder mixture. This work for physical properties of molten carbonate would be foundation for understanding phenomena of liquid-solid co-existing mixture.

1.6. Material Reaction with Lanthanum in Molten Carbonates

A lanthanum species also can be dissolved by about 0.01 mole fraction from $La_2(CO_3)_2$, $(LaO)_2CO_3$, and La_2O_3, into some mixture in the molten $(Li_{0.62}K_{0.38})_2CO_3$, $(Li_{0.52}Na_{0.48})_2CO_3$ (or $(Li_{0.53}Na_{0.47})_2CO_3$), $(Li_{0.43}K_{0.57})_2CO_3$, and $(Li_{0.435}Na_{0.315}K_{0.25})_2CO_3$. Recently, many researchers reported that addition of lanthanum into molten carbonate electrolyte decrease NiO solubility, enhance oxygen solubility therefore cathode performance. Matsuzawa et al. reported that lanthanum addition make NiO solubility lower[49]. Frangini and Scaccia reported that the dissolution of oxygen in molten $(Li_{0.52}Na_{0.48})_2CO_3$ La_2O_3 added by 0.5 mol% was determined to be ten times larger than that without La_2O_3 addition[50].

I have found, however, that lanthanum react with many kinds of material to produce $LaMO_3$ (M:Al, Sc, Cr, Mn, Fe, Co, Ni, Ga, and In) perovskite compound in molten carbonates. In this thesis, these reactions summarized as novel methods for the synthesis of $LaMO_3$. The addition of lanthanum to molten carbonate electrolyte of MCFC takes place the reactions with MCFC components to produce lanthanum perovskite compounds. These new reaction would bring new materials for MCFC. This work also presents $LaMO_3$ coating method on metal or ceramic substrates and discusses the reaction mechanism of $LaAlO_3$ formation in molten carbonate on the basis of in-situ X-ray diffraction data.

1.7. Purpose of This Thesis

Recently many researchers try to use molten carbonate in many field and find out other favorable composition of molten carbonate electrolytes of MCFC. There, however, are very few investigation and data for new composition of carbonates and their mixtures.

In this thesis, I would report fundamental physical properties such as density, surface tension and electrical conductivity as well as several reactions with lanthanum to produce perovskites compounds.

Change of electrolyte composition is thought to make great influence upon the nature of electrolyte such as density, surface tension, electrical conductivity, and so on. These physical properties should have relationship with composition, ionic radius, and columbic force. These relationships between physical properties and composition, however, have not been presented for comprehensive systems of molten carbonate. In this work several interesting relationships have been found and tried to predict physical properties of molten carbonate of wide composition.

Utilization of molten carbonate in not only MCFC but also many technical fields is increasing. Corrosion protection, material synthesis and process technology utilizing molten carbonate are growing fields. Lanthanum perovskites synthesis in molten carbonate is interesting field for paving new avenue to material research, and is reported for reaction, utilization, and mechanism.

Reference

[1] Y. Ito, "Application of Molten Salts – to Energy and Environment," Industrial Publishing & Consulting, Inc., Tokyo, (2003).

[2] T. Kojima and M. Mizuhata, "R&D trend of molten carbonate," *Molten Salts*, **51**, 207-242 (2008).

[3] J. Robert Selman, "Molten-salt fuel cells—Technical and economic challenges," *J. Power Sources*, **160**, 852–857 (2006).

[4] K. Nakagawa and T. Ohashi, "A Novel Method of CO_2 Capture from High Temperature Gases," *J. Electrochem. Soc.*, **145**, 1344-1346 (1998).

[5] K. Nakagawa and T. Ohashi, "A Reversible Change between Lithium Zirconate and Zirconia in Molten Carbonate," *Denki Kagaku* (presently *Electrochemistry*), **67**, 618-621 (1999).

[6] D. Fauth, E. Frommell, J. Hoffman, R. Reasbeck, and H. Pennline, "Eutectic salt promoted lithium zirconate: Novel high temperature sorbent for CO_2 capture," *Fuel Processing Technology,* **86,** 1503-1521 (2005).

[7] K. Sugiura, K. Takei, K. Tanimoto, and Y. Miyazaki, "The carbon dioxide concentration by using MCFC," *J. Power Sources*, **118**, 218-227(2003).

[8] Y. D. Yeboah, Y. Xu , A. Sheth, A. Godavarty, and P. K. Agrawal, "Catalytic gasification of coal using eutectic salts: identification of eutectics," *Carbon*, **41**, 203-214 (2003).

[9] G. Jin, H. Iwaki, N. Arai, K. Kitagwa, "Study on the gasification of wastepaper/carbon dioxide catalyzed by molten carbonate salts," *Energy*, **30**, 1192-1203 (2005).

[10] K. Sugiura, K. Minamia, M. Yamauchi, S. Morimitsu, K. Tanimoto, *J. Power Sources*, **171** 228–236 (2007).

[11] V. A. Volkovich, T. R. Griths, D. J. Fray, M. Fields, "Oxidation of ceramic uranium dioxide in alkali metal carbonate-based melts: a study using various oxidants and comparison with UO_2 powder," *J. Nuclear Mater.*, **256**, 131-138 (1998).

[12] Y.-J. Cho, H. Yang, H. Eun, J. Yoo, and J. Kim, "Axial Gas Phase Dispersion in a Molten Salt Oxidation Reactor," *Korean J. Chem. Eng.*, **21**, 1250-1255 (2004).

[13] V. A. Volkovich, T. R. Griths, D. J. Fray, R. C. Thied, "Solubility and solubilisation enthalpies of alkali metal urinates (VI) in molten carbonate," *Phys. Chem. Chem. Phys*, **1**, 3297-3302 (1999).

[14] T. Griffiths and V. Volkovich, "A review of the high temperature oxidation of uranium oxides in molten salts and in the solid state to form alkali metal urinates, and their composition and properties," *J. Nuclear Mater.*, **274**, 229-251 (1999).

[15] P. Coursol and P. Larouche, "Using Carbonate Fluxes to Remove Oxygen and Sulfur from Blister Copper," *JOM*, 42-45 (2004).

[16] M. Tanahashi, Z. Su, K. Takeda, H. Y. Sohn, and C. Yamauchi, "The Rate of Antimony Elimination from Molten Copper by the Use of Na_2CO_3 Slag," Metallugical and Materials Transactions B, 34B, 869-879 (2006).

[17] N. M. Barbin, G. F. Kazantsev, G. K. Moiseev, and N. A. Vatolin, "Lead Recovery from PbO, $PbCl_2$, PbS, $PbSO_4$,and Their Mixtures in Carbonate Melts," *Inorganic Mat.,* **38**, 1216-1223 (2002).

[18] T. Kodama, Y.Isobe, Y.Kondoh, S.Yamaguchi, and K.-I.Shimizu, "Ni/ceramic/molten-salt composite catalyst

with high-temperature thermal storage for use in solar reforming processes," *Energy*, **29**, 895-903 (2004).

[19] T. Kodama, T. Koyanagi, T. Shimizu, and Y. Kitayama, "CO_2 reforming of methane in a molten carbonate salt bath for use in solar thermochemical processes," *Energy & Fuels*, **15**, 60-65 (2001).

[20] S. Yoshida, J. Matsunami, Y. Hosokawa, O. Yokota and Y. Tamaura, "Coal/CO_2 Gasification System Using Molten Carbonate Salt for Solar/Fossil Energy Hybridization," *Energy & Fuels*, **13**, 961-964 (1999).

[21] W. Zhu, C. Xia, D. Ding, X. Shi, and G. Meng, "Electrical properties of ceria-carbonate composite electrolytes," *Mater. Research Bulletin*, **41**, 2057-2064 (2006).

[22] J. Huang, Z. Mao, L. Yang, and R. Peng, "SDC-carbonate composite electrolytes for low-temperature SOFCs," *Electrochem. Solid-State Lett.*, **8**, A437-440 (2005).

[23] J. Huang, Z. Mao, Z. Liu, and C. Wang, "Development of novel low-temperature SOFCs with co-ionic conducting SDC-carbonate composite electrolytes," *Electrochem. Commun*., **9**, 2601-2605 (2007).

[24] J. Huang, Z. Mao, Z. Liu, and C. Wang, "Performance of fuel cells with proton-conducting ceria-based composite electrolyte and nickel-based electrodes," *J. Power Sources*, **175**, 238-243 (2008).

[25] K. Tanimoto, M. Yanagida, T. Kojima, Y. Tamiya, H. Matsumoto, Y. Miyazaki, "Long-term Operation of Small-sized Single Molten Carbonate Fuel Cells," *J. Power Sources*, **72**, 77-82 (1998).

[26] J. Daly, G. Steinfeld, D. K. Moyer, and F. H. Holcomb, "Molten carbonate fuel cell operation with dual fuel flexibility," J. Power Sources, 173, 925-934 (2007).

[27] K. Ota, S. Mitsushima, S. Kato, S. Asano, H. Yoshitake and N. Kamiya, "Solubilities of nickel oxide in molten carbonate," *J. Electrochem. Soc*., **139**, 667-671 (1992).

[28] Y. Fujita, H. Urushibata, and A. Sasaki, "The Corrosion and the Eleetrolyte Loss of the Cathode Side Current Collector Made of 16Cr-12Ni-2Mo Stainless Steel in Molten Carbonate Fuel Cells," *Denki Kagaku* (presently *Electrochemistry*), **65**, 565-573 (1997).

[29] K. Tanimoto, Y. Miyazaki, M. Yanagida, S. Tanase, T. Kojima, N. Ohtori, H. Okuyama and T. Kodama, "Corrosivity of Molten Alkali Carbonates Mixture for SUS310S," *Denki Kagaku*, **60**, 332-335 (1992).

[30] T. Kojima, M. Yanagida, K. Tanimoto, Y. Tamiya, H. Matsumoto, and Y. Miyazaki, *Electrochemistry (Tokyo, JPN)*, **67**, 593 (1999).

[31] Y. Miyazaki, M. Yanagida, S. Tanase, K. Tanimoto, T. Kojima, N. Ohtori, and T. Kodama, in the Third International Symposium on Carbonate Fuel Cell Technology, D. Shores, H. Maru, I. Uchida, and J. R. Selman, Editors, PV93-3, p. 230, The Electrochemical Society Proceedings Series, Pennington, NJ (1993).

[32] D. Smith, J. Winnick, "Cesium-Containing Electrolyte for the Molten Carbonate Fuel Cell," *Electrochem. Solid-State Lett.*, **2**, 207-209 (1999).

[33] M. Mohamedi, Y. Hisamitsu, and I. Uchida, "Ternary alkali carbonate composition-oxygen solubility relationship under atmospheric and pressurized conditions – a utility model for MCFC," *J. Appl. Electrochem*., **32**, 111–117, (2002).

[34] J. D. Doyon, T. Gilbert, G. Davies, and L Paetsch, "NiO solubility in mixed alkali/alkaline earth carbonates," J. Electrochem. Soc., 134, 3035 (1987).

[35] K. Tanimoto, Y. Miyazaki, M. Yanagida, S. Tanase, T. Kojima, N. Ohtori, H. Okuyama and T. Kodama, "Solubility of Nickel Oxide in (62+38mol%) (Li+K)CO_3 Containing Alkaline Earth Carbonate," *Denki Kagaku*, **59**, 619-622 (1991).

[36] K. Tanimoto, Y. Miyazaki, M. Yanagida, S. Tanase, T. Kojima, N. Ohtori, H. Okuyama and T. Kodama, "Effect of Addition of Alkaline Earth Carbonate on Solubility of NiO in Molten Li_2CO_3-Na_2CO_3 Eutectic," *Denki Kagaku*, **63**, 316-318 (1995).

[37] T. Kodama, *Prog. Batteries Sol. Cells,* **6**, 7 (1987).

[38] M. Yanagida, S. Baba, K. Tanimoto, T. Kojima, N. Ohtori, Y. Tamiya, T. Asai, Y. Miyazaki, and M. Azuma, "High Temperature Corrosion of Type 316L Stainless Steel with Molten Carbonate. The Effect of Alkaline Earth Carbonate Addition," *Denki Kagaku*, **64**, 542 (1996).

[39] K. Tanimoto, Y. Miyazaki, M. Yanagida, S. Tanase, T. Kojima, N. Ohtori, H. Okuyama and T. Kodama, "Corrosivity of Molten Alkali and Alkaline Earth Carbonate to SUS310S under a Simulated MCFC Cathode Environment," *Denki Kagaku*, **62**, 445-450 (1994).

[40] K. Tanimoto, T. Kojima, M. Yanagida, K. Nomura, Y. Miyazaki, "Optimization of the electrolyte composition in a $(Li_{0.52}Na_{0.48})_{2-2x}AE_xCO_3$ (AE = Ca and Ba) molten carbonate fuel cell," *J. Power Sources*, 131, 256-260 (2004)

[41] K. Hatoh, J. Niikura, E. Yasumoto, and T. Gamo, "Effect of addition of alkaline earth carbonates on the oxygen reduction reaction in molten alkali carbonates," *Denki Kagaku,* **55**, 323 (1987).

[42] S. Terada, K. Higaki, I. Nagashima, Y. Ito, "Addition of potassium tungstate to the electrolyte of a molten carbonate fuel cell," *J. Power Sources*, **83**, 178-185 (1999).

[43] S. Terada, I. Nagashima, K. Higaki, Y. Ito, "Stability of $LiAlO_2$ as electrolyte matrix for molten carbonate fuel cells," *J. Power Sources*, **75**, 223 (1998).

[44] J. P. T. Vossen, R. C. Makkus, and J. H. W. de Wit, "Corrosion behavior of chromium in molten carbonate," *J. Electrochem. Soc.,* **143**, 66, (1996).

[45] M. Kawase, Y. Mugikura, Y. Izaki, T. Watanabe, Y. Ito, "Effects of fluoride on the performance of MCFCs," *J. Power Sources*, **124**, 52-58 (2003).

[46] M. Mizuhata, Y. Harada, G. Cha, A. Béléké, and S. Deki, "Physicochemical Properties of Molten Alkali Metal Carbonates Coexisting with Inorganic Powder," *J. Electrochem. Soc.*, **151**, E179-185 (2004).

[47] M. Mizuhata, S. Suganuma, Y. Harada, and S. Deki, "Anomalous properties of $LiKCO_3$ melts coexisting with porous inorganic powder," *Electrochemistry*, **73**, 680-685 (2005).

[48] M. Mizuhata, A. Béléké, H. Watanabe, Y. Harada, and S. Deki, "Effect of γ-$LiAlO_2$ powder on ionic conductivity of coexisting single alkali carbonates, " *Electrochim. Acta*, **53,** 71-78 (2007).

[49] K. Matsuzawa, T. Mizusaki, S. Mitsushima, N. Kamiya, K. Ota, "The effect of La oxide additive on the solubility of NiO in molten carbonates," *J. Power Sources*, **140**, 258-263 (2005).

[50] S. Frangini and S. Scaccia, "The Dissolution of Oxygen in La_2O_3 -Added 52/48 mol % Li/Na Molten Carbonate Determined by Gas Solubility Measurements," *J. Electrochem. Soc.*, **152**, A2155-2158 (2005).

2. Density of Molten Carbonates

2.1. Introduction

Density and molar volume provides an insight into the melt structure. The molar volume is sensitive to the change of molten salts, such as complex species formation. For practical use, the density of molten carbonate is fundamental and essential physical properties needed for estimating favorable electrolyte volume ratio in electrolyte matrix of MCFC. The electrolyte volume should be optimized because the filling ratio of electrolyte in the open pore volume of the porous electrolyte matrix influences the endurance and the performance of MCFC.

For the study of the density of molten carbonate, Janz and Lorenz[1], Janz and Ward[2], and Spedding[3] reported single alkali, binary alkali carbonate systems, Li_2CO_3, Na_2CO_3, K_2CO_3, and their binary and ternary mixtures. Zhu et al.[4] reported data of molten Li_2CO_3, Na_2CO_3, K_2CO_3, Rb_2CO_3, and Cs_2CO_3. Liu et al.[5] reported data of molten Li_2CO_3, Na_2CO_3, K_2CO_3, and their binary and ternary mixtures containing $CaCO_3$.

No data have been reported for binary and ternary carbonate mixtures containing Rb_2CO_3, and Cs_2CO_3, $SrCO_3$, $BaCO_3$ and the mixture added with MO_4^{2-} (SO_4^{2-}, CrO_4^{2-}, MoO_4^{2-}, and WO_4^{2-}).

In this section, several molten carbonate mixtures mentioned at section 1.5 are investigated for density measurement. The influence of ionic size to physical properties of cations (Li^+, Na^+, K^+, Rb^+, Cs^+, Ca^{2+}, Sr^{2+}, and Ba^{2+}) was interesting for predict unknown data and understanding the nature of molten salts.

2.2. Experiment

2.2.1. Measurement method for the density of molten carbonates

For the measurement of density of molten salt, buoyancy method and maximum bubble pressure method are well known. The principles of methods are shown in Fig. 2-1. The buoyancy method utilizes bob dipped in molten salt. The volume of bob, V, measured using water as standard sample. The measured weight, W, changed after dipping in molten salt by buoyancy working to bob and surface tension working to string which hangs the bob. Janz et al. measured surface tension using a pin under the bob. Their method is a kind of ring method. The diameter of pin, r was measured in advance. When the pin touched the surface of molten salt, meniscus of molten salt make a force to pull down the bob by the surface tension. They measured the difference of weight, ΔF, between before and after the pin detached from the surface of molten salt.

$$\Delta F = 2\pi r\gamma \qquad [2\text{-}1]$$

where γ is the surface tension of molten salt. They measured not only surface tension but also density using surface tension. As bob is immersed inside melt, weight of bob, M, forces of buoyancy and surface tension are measured together, as noted W. The buoyancy is a product of density of melt,

ρ, and volume of bob. The density of melt can be obtain through following equation,

$$\rho = (W - M - 2\pi r\gamma)/V \qquad [2\text{-}2]$$

For a precise measurement of only density, bobs of different volume are used in order to subtract the effect of surface tension.

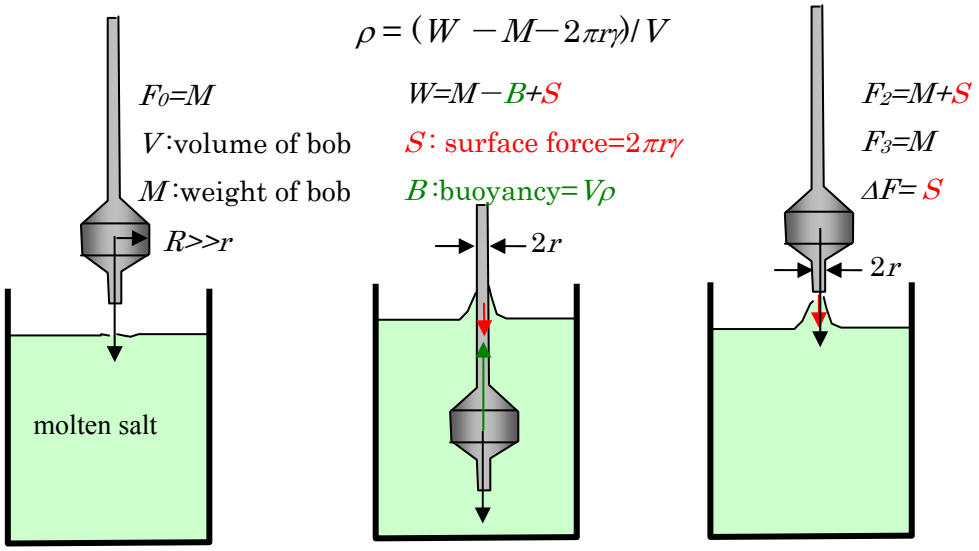

Fig. 2-1. Principle of density measurement, buoyancy method.

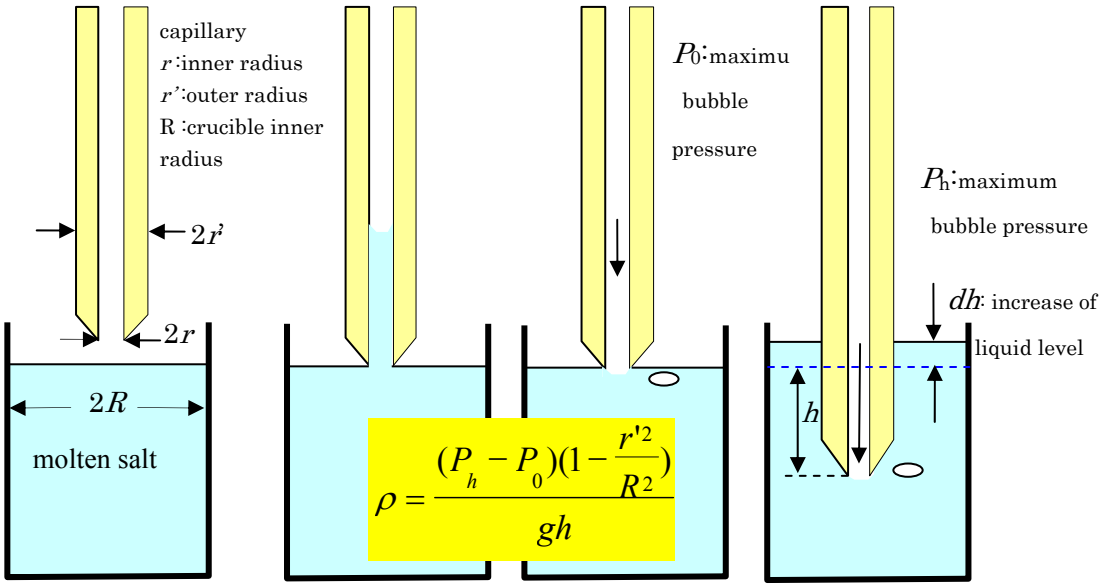

Fig. 2-2. Principle of density measurement using maximum bubble pressure method

The method of buoyancy, however, is time consuming and it is afraid that the surface of bob influences the measurement by wettability. In order to measure a number of mixtures of molten carbonate mixture, I chose maximum bubble pressure method and refine it as described in following

section.

The difficulty of density measurement with maximum bubble pressure method is scatter of measured pressure. I found the pressure deflection was suppressed by wider exit of furnace. The adoption of a laser displacement meter made measurement convenient and faster.

The principle of maximum bubble pressure method for density measurement is shown in Fig. 2-2. When a capillary is touched with melt surface, melt climbs up inside capillary by capillary force originated from surface tension of melt and this increase the pressure inside the capillary. As the pressure is increased inside capillary by sending gas, melt is pushed out and the pressure reached maximum, then finally gas bubble comes out from the tip of capillary. The maximum pressures measured when the capillary is placed on the surface and inside of melt by a depth of *h*, are denoted as P_0 and P_h, respectively. The difference between P_0 and P_h, equals to liquid column pressure, $\rho g(h+\mathrm{dh})$, where *dh* is increase of the level of surface of melt because of capillary insertion, and *g* is gravitational acceleration, 9.7975 ms^{-2} (at Ikeda City, Osaka).

$$P_h - P_0 = \rho g(h + dh) \qquad [2\text{-}3]$$

The value of *dh* is related to *h*, radius of crucible, *R* and capillary outer radius, *r'*.

$$\pi(R^2 - r'^2)dh = \pi r'^2 h \qquad [2\text{-}4]$$

$$dh = hr'^2 (R^2 - r'^2)^{-1} \qquad [2\text{-}5]$$

The density of the melt, ρ, was calculated with the following equation,

$$\rho = \frac{(P_h - P_0)(1 - \frac{r'^2}{R^2})}{gh} \qquad [2\text{-}6]$$

More precisely, actual capillary is not cylindrical but machined as truncated corn shape at the tip in order to prevent bubble staying on the tip of capillary, therefore equations from [2-4] to [2-6] changed to following, respectively,

$$\pi(R^2 - r'^2)dh = \pi(r'^2 h - \frac{2}{3}lr'^2 + \frac{1}{3}lrr' + \frac{1}{3}lr^2) \qquad [2\text{-}7]$$

$$dh = (r'^2 h - \frac{2}{3}lr'^2 + \frac{1}{3}lrr' + \frac{1}{3}lr^2)(R^2 - r'^2)^{-1} \qquad [2\text{-}8]$$

$$\rho = \frac{P_h - P_0}{g}[h + (r'^2 h - \frac{2}{3}lr'^2 + \frac{1}{3}lrr' + \frac{1}{3}lr^2)(R^2 - r'^2)^{-1}]^{-1} \qquad [2\text{-}9]$$

where *l* is height of truncated corn, *r* is inner radius of the capillary.

2.2.2. Apparatus for the measurement of density and surface tension of molten carbonates

The density and surface tension of molten carbonate mixtures were simultaneously measured using a maximum bubble pressure technique. The apparatus used for the measurements was assembled by Rigaku Denki (Tokyo). The schematic diagram of apparatus used for the

measurements is shown in Fig.2-3. The capillary (2mm inner diameter, 4mm outer diameter, 400mm in length) used for making bubbles in the melt was made of high purity alumina (Nikkato Corp., 99.5 % purity), which is wetted well with the melt. The edge of the capillary was sharpened to prevent the bubble staying on the tip of the capillary. The vertical position of the capillary tip was determined using a laser displacement meter (Keyence Corp., LB-02) which monitors the position of upper end of the capillary holder. The pressure inside the capillary was measured using a pressure transducer (MKS Instruments, Inc., Baratron 220CD), which was calibrated with the column pressure of distilled water.

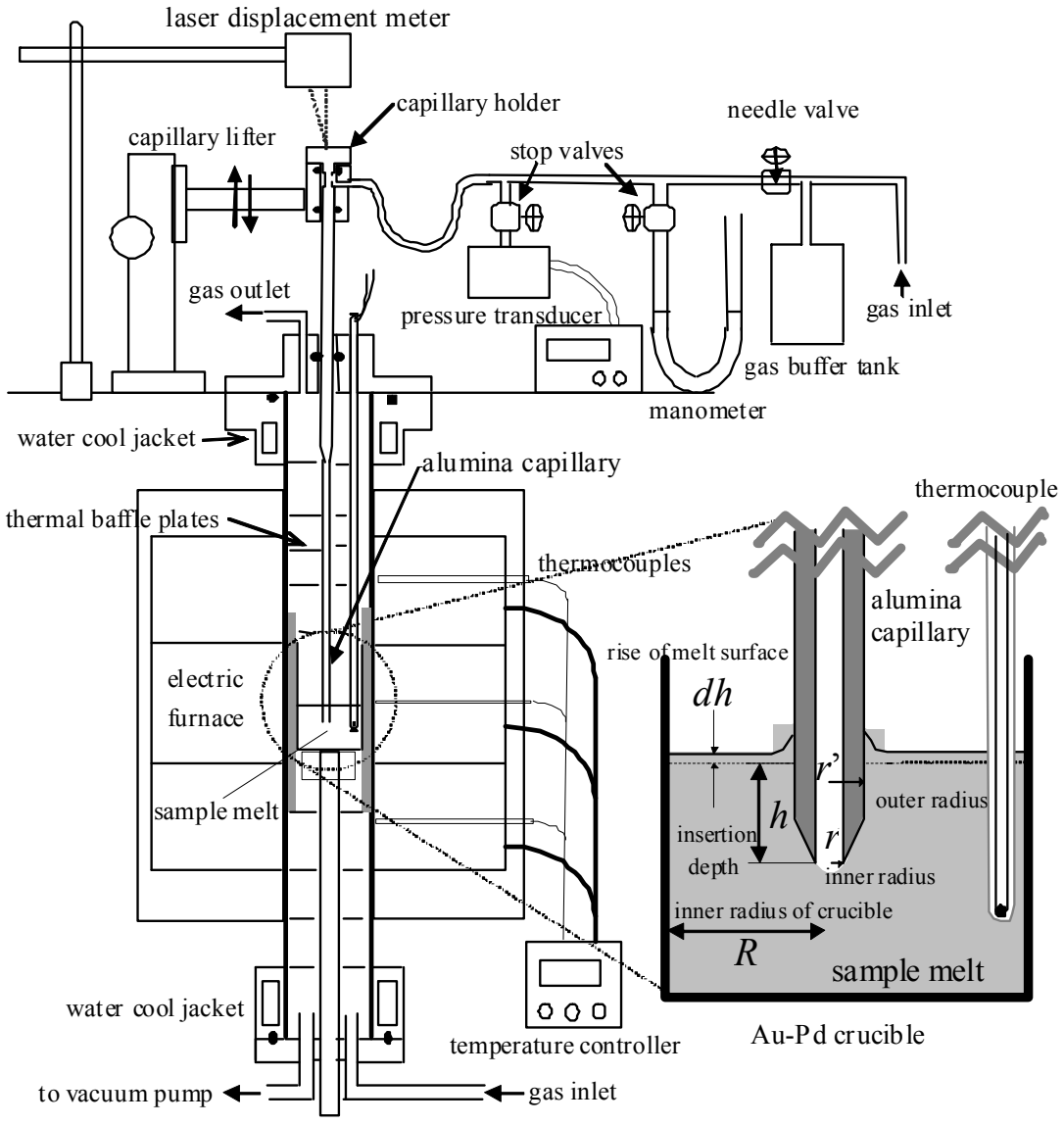

Fig. 2-3. Apparatus for simultaneous measurement of density and surface tension of molten carbonate using maximum bubble pressure technique.

2.2.3. Sample preparation

The procedure of sample preparation following is common for the measurement of density, surface tension and electrical conductivity.

The containers of molten carbonates were the crucibles made of Au-Pd (80:20 wt.%) alloy, which is stable in molten carbonate under CO_2 atmosphere[6]. The crucible for the measurement of density and surface tension was 40 mm inner diameter, 60 mm depth. A Platinel thermocouple covered with an alumina closed end tube was inserted into the sample melt for measuring the temperature.

The chemicals, Li_2CO_3 (Kanto Chemical, 99.95%), Na_2CO_3 (Nakaraitesque, 99.5%), K_2CO_3 (Nakaraitesque, 99.5%), Rb_2CO_3 (Mitsuwa's Pure Chemicals, 99%), Cs_2CO_3 (Kishida Chemical, 99.99%) $CaCO_3$ (Kanto Kagaku, 99.99%), $SrCO_3$ (Kanto Kagaku, 99.9%), and $BaCO_3$ (Kanto Kagaku, 99.9%) were used for the measurement. High purity chemicals of sodium carbonate, 99.99%, K_2CO_3 (Cerac, 99.999%), and Rb_2CO_3 (Cerac, 99.9%) were used for the measurements of single alkali carbonates.

Additives investigated were NaCl(99.5%, Kishida Chemical, Osaka, Japan), KCl (99.5%, Kishida Chemical, Osaka, Japan), Na_2SO_4(99.5%, Kishida Chemical), K_2SO_4(99.5%, Kishida Chemical), $Na_2CrO_4{\cdot}4H_2O$ (99%, Kanto Chemical, Tokyo, Japan), K_2CrO_4 (99%, Kanto Chemical), $Na_2MoO_4{\cdot}2H_2O$ (99.5%, Kishida Chemical), K_2MoO_4 (99%, Mitsuwa Chemical), Li_2WO_4 (98%, Ishizu Chemical, Osaka) and K_2WO_4 (99%, Ishizu Chemical).

These chemicals were dried at 523K in an oven more than a day, then weighed, melted in a Au-Pd alloy crucible bubbled with pure CO_2（Sumitomo Seika：99.995 %, dew point 207～209 K) more than 2 hours before measurement at about 1170K.

For x mol% addition of the anions such as SO_4^{2-}, CrO_4^{2-}, MoO_4^{2-}, WO_4^{2-}, and Cl^-, relative salts were added to carbonate in the manner of substituting carbonate ion like $(Li_{0.62}K_{0.38})_2(CO_3)_{1-x}(MO_4)_x$, (M = S, Cr, Mo, and W) and $(Li_{0.62}K_{0.38})_2(CO_3)_{1-x}Cl_{2x}$. On the other hand for the cation addition, relative additives added in the manner of substituting cation ion like $[(Li_{0.52}Na_{0.48})_{0.95}Rb_{0.05}]_2CO_3$. This formula is abbreviated to $(Li_{0.494}Na_{0.456}Rb_{0.05})_2CO_3$.

2.2.4. Measurement procedures

The density and the surface tension of molten carbonate mixtures were measured in the temperature range from about 1100 K to a temperature higher than their liquidus by 30 K.

The level of the surface of melt was detected by abrupt pressure gain when the capillary contacted the melt with moving capillary by 0.01mm at each steps. When the bubble escapes from the tip of the capillary, the pressure reaching its maximum was measured as the maximum bubble pressure. The difference of measured maximum pressure was within 0.15%. The bubbles were controlled to be made with the interval of about a few minutes. The maximum bubble pressures were measured at the both levels of surface and more than 10 mm depth in the melt.

2.3. Results

2.3.1. Evaluation of measurement accuracy

The errors estimated in the measurement of density of molten carbonates are listed in Table 2-1. The factors that cause the error of density measurement are the determination of pressure, displacement of capillary, and temperature. All the factors of the error were estimated and summed up to be less than ±0.9% for density.

In order to verify the accuracy and precision of the measurements, the density of molten NaCl - well known as a standard material - were measured from 1097 to 1179K. The results showed good agreement with literature data[7] for the density (ρ/ kg m^{-3} = 2124.6 - 0.5293T) within ±0.2%.

Table 2-1. Error factors of the density measurement of molten carbonates.

Factors	estimated error	Estimated error in density
Maximum pressure	±0.15%	±0.3%
Displacement of capillary	±40 μ m	±0.5%
Temperature	±5K	±0.1%
	Maximum Error	±0.9%

2.3.2. The results of the measurements

The density of alkali carbonates were measured as a function of temperature. The results of alkali carbonates were shown in Fig. 2-4 and Fig. 2-5 with literature data[3,4]. The results of the density of measured carbonates show good agreement with literature data.

As an example of the result measured for molten alkali binary carbonate system, the results of molten Li_2CO_3-Rb_2CO_3 binary system are plotted in Fig. 2-6.

The result measured density and temperature relationship for molten alkali ternary carbonate system are plotted in Fig. 2-5, Fig. 2-7 and Fig. 2-8.

The result measured density and temperature relationship for molten $(Li_{0.52}Na_{0.48})_2CO_3$ containing $CaCO_3$ are showed in Fig. 2-9. It is found that the density of molten carbonate mixtures containing alkaline earth carbonates increased with an increase in the amount of alkaline earth carbonates.

The result measured density and temperature relationship for molten $(Li_{0.52}Na_{0.48})_2CO_3$, $(Li_{0.62}K_{0.38})_2CO_3$ and $(K_{0.573}Li_{0.437})_2CO_3$ containing CrO_4^{2-} are showed in Fig. 2-10. Precise measurements of density had been done for CrO_4^{2-} addition. The results of small amount addition such as 1, 3 or 5 mol% showed that difference in the measurement even 2 mol% composition difference. Good resolution of data can be seen clearly in Fig. 2-10 for CrO_4^{2-} addition. Addition of CrO_4^{2-} to these carbonates made the carbonate mixtures yellow and the melt transparent deep red. Other molten mixture of carbonates and additives were transparent liquids without color.

The result measured density and temperature relationship for molten $(Li_{0.52}Na_{0.48})_2CO_3$ and $(Li_{0.62}K_{0.38})_2CO_3$ containing SO_4^{2-}, MoO_4^{2-}, WO_4^{2-}, or Cl^- are showed in Fig. 2-11.

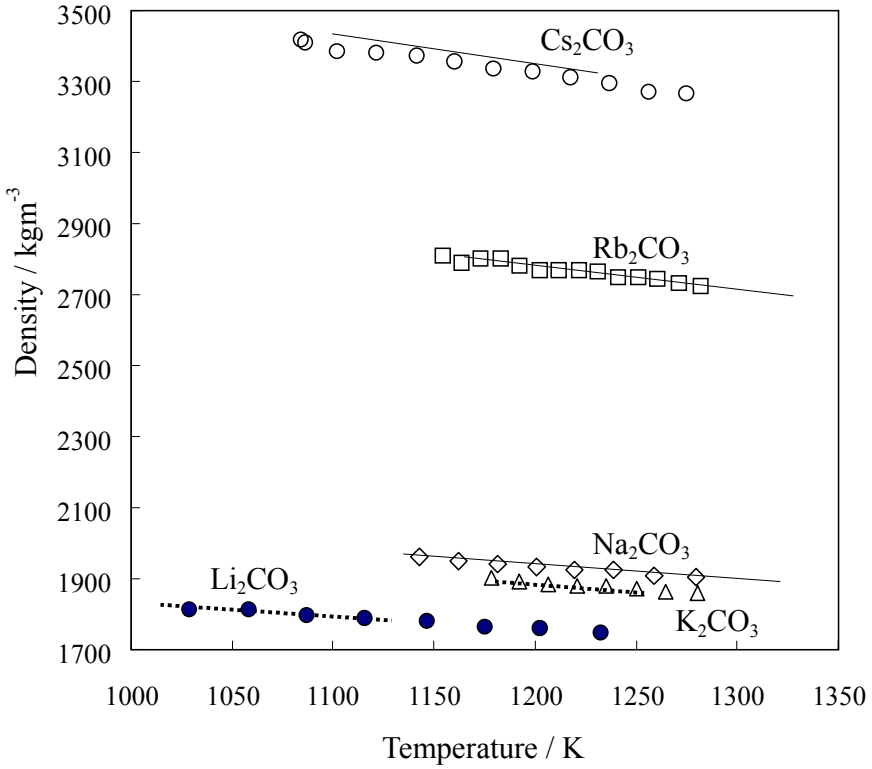

Fig. 2-4. The temperature dependence of the density of molten alkali carbonates. Li_2CO_3 ●, Na_2CO_3 ◇, K_2CO_3 △, Rb_2CO_3 □, and Cs_2CO_3 ○, solid line: ref. [4] and dash line: ref. [3].

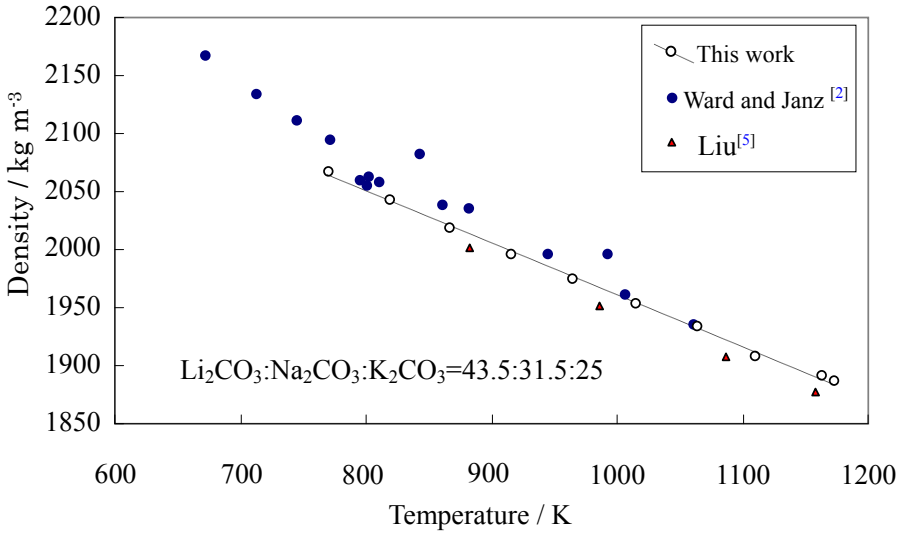

Fig. 2-5. Temperature dependence of the density of molten Li_2CO_3 - Na_2CO_3 - K_2CO_3 ternary carbonates.

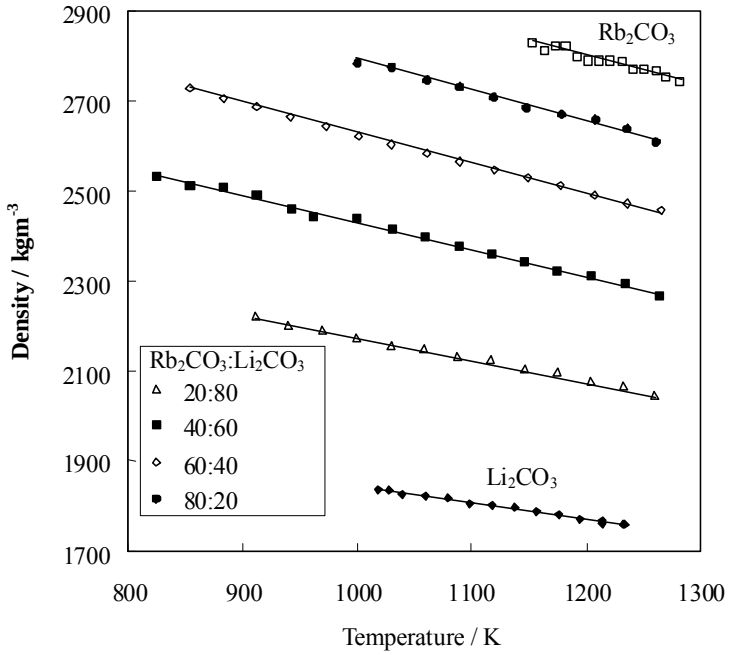

Fig. 2-6. The temperature dependence of the density of molten Li_2CO_3-Rb_2CO_3 binary carbonates.

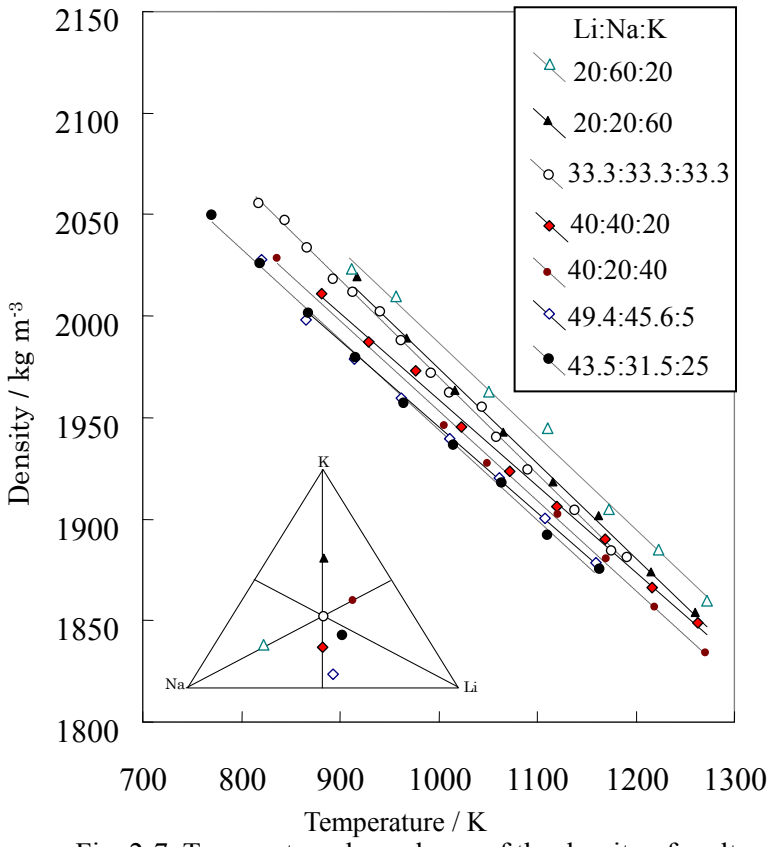

Fig. 2-7. Temperature dependence of the density of molten Li_2CO_3 - Na_2CO_3 - K_2CO_3 ternary carbonates.

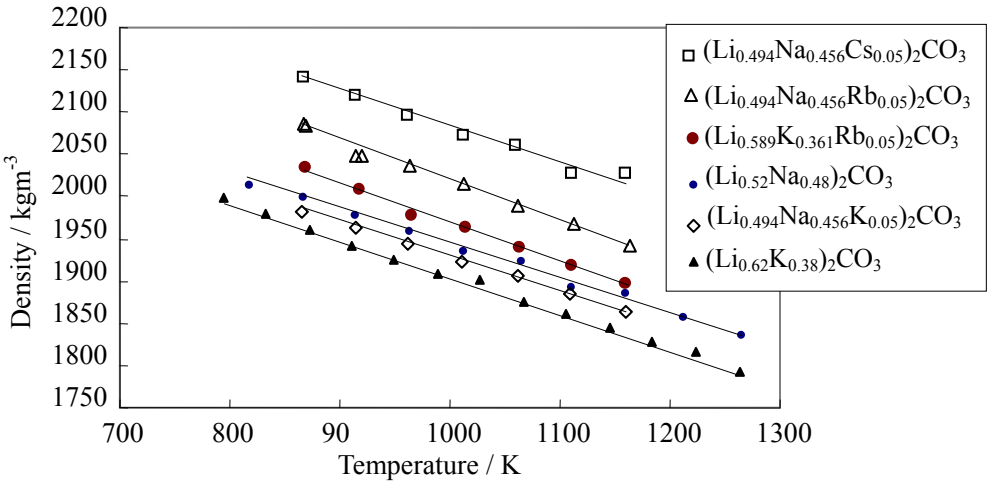

Fig. 2-8. Temperature dependence of density of molten $(Li_{0.52}Na_{0.48})_2CO_3$ and $(Li_{0.62}K_{0.38})_2CO_3$ containing alkali ion (K^+, Rb^+, or Cs^+).

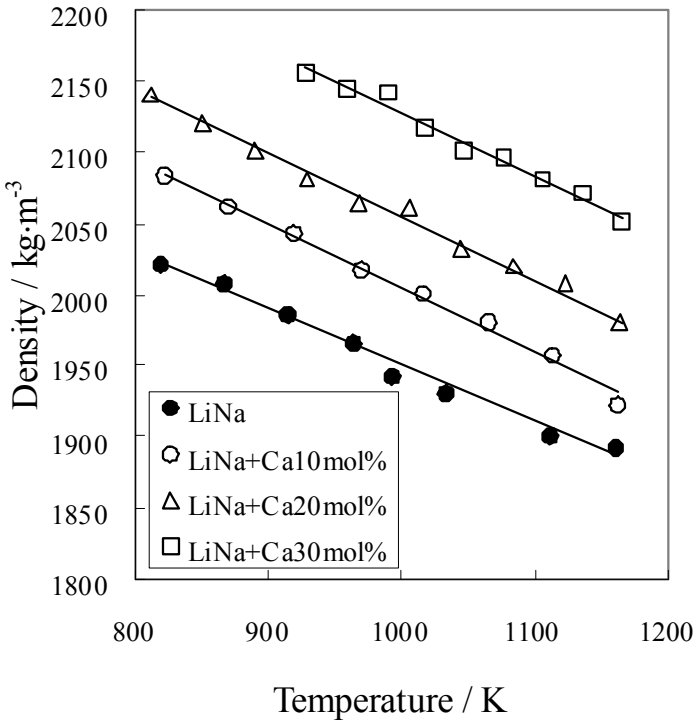

Fig. 2-9. Temperature dependence of the density of LiNa=$(Li_{0.52}Na_{0.48})_2CO_3$ with added Ca=$CaCO_3$ in the amounts of 10, 20 and 30 mol% measured under 1 atm CO_2 atmosphere.

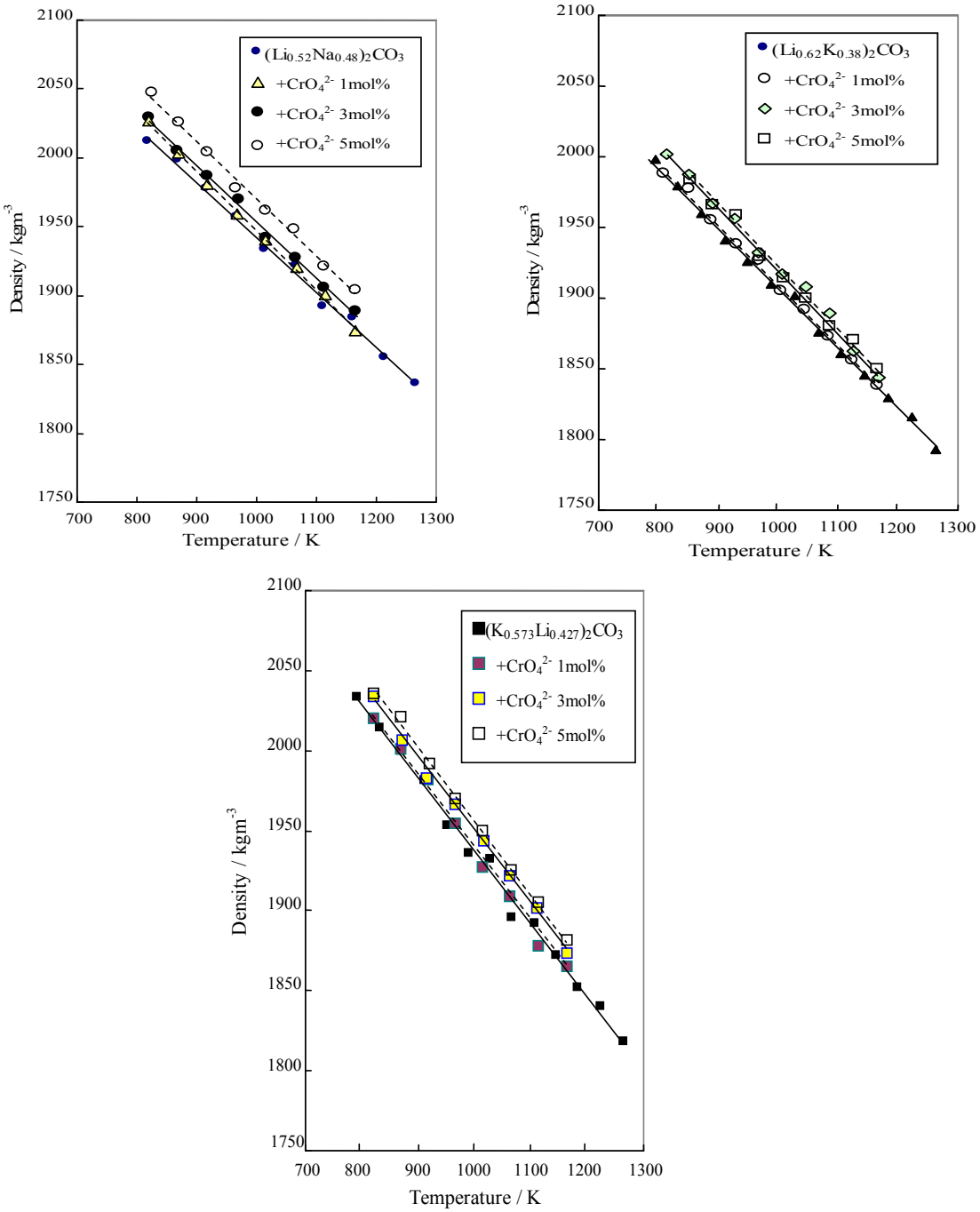

Fig. 2-10. Temperature dependence of density of molten $(Li_{0.52}Na_{0.48})_2CO_3$, $(Li_{0.62}K_{0.38})_2CO_3$ and $(K_{0.573}Li_{0.437})_2CO_3$ containing CrO_4^{2-}.

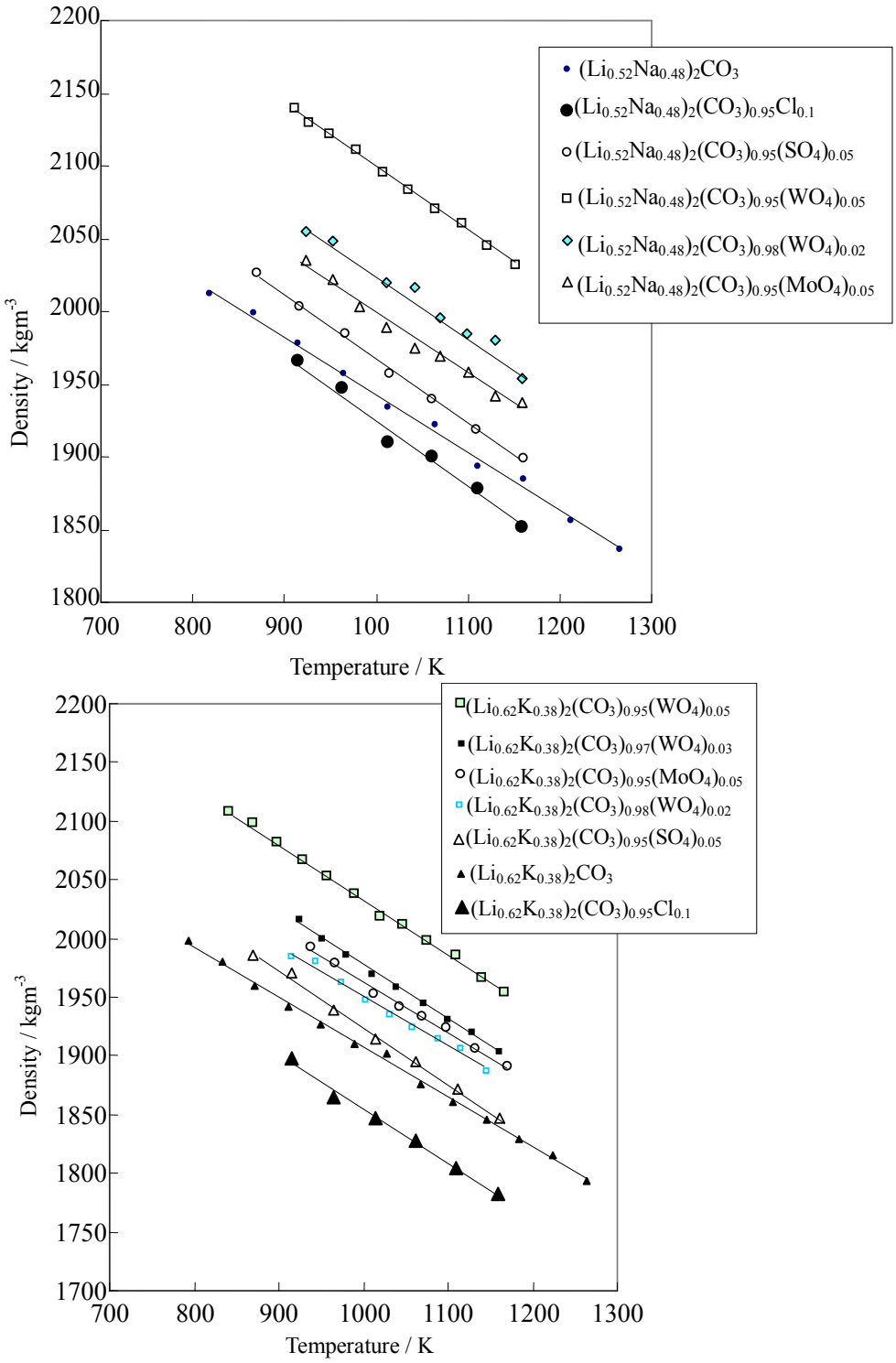

Fig. 2-11 Temperature dependence of density of molten $(Li_{0.52}Na_{0.48})_2CO_3$ and $(Li_{0.62}K_{0.38})_2CO_3$ containing SO_4^{2-}, MoO_4^{2-}, WO_4^{2-}, or Cl^-.

Table 2-2. Density of molten alkali and their binary carbonates.

Composition (mol%)	Density (kgm^{-3}) $\rho = \alpha + \beta T$		Calculated values at 1173 K (kgm^{-3})	Square of correlation coefficient	Standard deviation	Temperature range (K)
$Li_2CO_3 : Na_2CO_3$	α	β	ρ_{1173}	r^2	sd	T
100 : 0	2165	-0.3385	1768	0.982	3.5	1029 - 1231
80 : 20	2309	-0.4316	1803	0.985	0.6	940 - 1266
60 : 40	2336	-0.4177	1846	0.992	5.0	853 - 1264
52 : 48	2337	-0.3984	1869	0.996	0.4	819 - 1265
40 : 60	2473	-0.5120	1872	0.986	8.0	881 - 1264
20 : 80	2398	-0.4101	1917	0.943	8.7	1028 - 1264
0 : 100	2497	-0.4696	1946	0.992	2.0	1143 - 1258
$Li_2CO_3 : K_2CO_3$	α	β	ρ_{1173}	r^2	sd	T
90 : 10	2233	-0.3927	1773	0.954	3.5	992 - 1147
80 : 20	2264	-0.3922	1804	0.991	4.5	912 - 1264
62 : 38	2327	-0.4243	1829	0.998	3.2	794 - 1264
42.7 : 57.3	2387	-0.4547	1854	0.994	5.6	793 - 1265
20 : 80	2465	-0.4950	1884	0.998	2.0	1030 - 1263
0 : 100	2317	-0.3562	1899	0.985	1.9	1178 - 1280
$Li_2CO_3 : Rb_2CO_3$	α	β	ρ_{1173}	r^2	sd	T
80 : 20	2634	-0.4733	2078	0.997	3.4	911 - 1260
60 : 40	3006	-0.5919	2312	0.996	5.2	825 - 1265
40 : 60	3258	-0.6501	2496	0.998	3.6	854 - 1266
20 : 80	3418	-0.6505	2655	0.991	5.6	1001 - 1261
0 : 100	3565	-0.6534	2799	0.964	5.2	1154 - 1282
$Li_2CO_3 : Cs_2CO_3$	α	β	ρ_{1173}	r^2	sd	T
80 : 20	2942	-0.5235	2328	0.991	5.0	926 - 1245
60 : 40	3253	-0.4800	2690	0.987	7.5	856 - 1246
40 : 60	3858	-0.7644	2961	0.997	5.9	876 - 1266
20 : 80	3983	-0.6754	3191	0.971	13.1	952 - 1276
0 : 100	4256	-0.7750	3347	0.997	2.8	1084 - 1275
$Na_2CO_3 : K_2CO_3$	α	β	ρ_{1173}	r^2	sd	T
80 : 20	2450	-0.4328	1943	0.994	2.3	1035 - 1227
60 : 40	2492	-0.4793	1930	0.995	2.8	995 - 1227
40 : 60	2476	-0.4725	1922	0.995	2.5	1023 - 1225
20 : 80	2495	-0.4893	1921	0.995	3.7	1093 - 1229
$Na_2CO_3 : Rb_2CO_3$	α	β	ρ_{1173}	r^2	sd	T
80 : 20	2742	-0.4694	2191	0.988	3.0	1037 - 1193
60 : 40	3069	-0.5801	2389	0.998	2.8	920 - 1193
40 : 60	3348	-0.6810	2549	0.996	4.5	918 - 1189
20 : 80	3468	-0.6667	2686	0.997	2.0	1036 - 1193
$Na_2CO_3 : Cs_2CO_3$	α	β	ρ_{1173}	r^2	sd	T
80 : 20	3147	-0.6555	2378	0.986	6.1	986 - 1189
60 : 40	3538	-0.7132	2701	0.998	3.6	879 - 1186
40 : 60	3908	-0.7883	2983	0.978	11.0	930 - 1191
20 : 80	4227	-0.8654	3212	0.998	3.2	987 - 1189

Table 2-3. Density and molar volume of molten Li_2CO_3-Na_2CO_3-K_2CO_3 ternary carbonates.

Composition (mol%) Li_2CO_3 : Na_2CO_3: K_2CO_3	Density (kg m^{-3}) $\rho = \alpha + \beta T$		Calculated ρ values at 1073 K (kg m^{-3})	Square of correlation coefficient	Estimated standard deviation	Temperature range (K)	Molar Volume at 1073 K (estimated by additivity) (cm^3 mol^{-1})	
	α	β	ρ_{1073}	r^2		T_1 - T_2	V_m	
43.5:31.5:25.0	2389	-0.4447	1912	0.998	2.8	770-1163	52.35	(52.45)
33.3:33.3:33.3	2450	-0.4798	1935	0.997	2.8	817-1191	54.79	(55.21)
40:40:20	2388	-0.4288	1928	0.996	3.2	881-1262	51.66	(51.96)
40:20:40	2395	-0.4418	1921	0.998	3.3	837-1271	55.20	(55.61)
20:60:20	2449	-0.4613	1954	0.996	4.5	912-1272	54.25	(54.40)
20:20:60	2445	-0.4702	1940	0.998	3.0	917-1260	61.27	(61.70)
49.4:45.6:5.0	2344	-0.3998	1915	1.000	3.9	820-1159	47.92	(48.08)

Table 2-4. Densities of molten alkali - alkaline earth carbonate mixtures.

Composition (mol%)	Density (kg m^{-3}) $\rho = \alpha + \beta T$		Calculated values at 1123 K (kg m^{-3})	Square of correlation coefficient	Standard deviation	Temperature range (K)
	α	β	ρ_{1123}	r^2	Sd	T
Li_2CO_3 : $CaCO_3$						
90:10	2330	-0.4215	1857	0.992	2.4	988-1166
80:20	2412	-0.4339	1925	0.991	3.2	960-1163
70:40	2473	-0.4299	1990	0.990	3.3	958-1163
Li_2CO_3 : $SrCO_3$						
90:10	2431	-0.4272	1951	0.990	2.6	988-1163
80:20	2636	-0.4641	2115	0.993	2.4	989-1165
70:40	2902	-0.5472	2287	0.997	1.6	1027-1164
Li_2CO_3 : $BaCO_3$						
90:10	2527	-0.4326	2041	0.989	2.9	990-1165
80:20	2868	-0.4946	2313	0.994	5.5	969-1166
70:40	3118	-0.5043	2552	0.995	2.7	961-1166
Li_2CO_3 : Na_2CO_3 : $CaCO_3$						
46.8:43.2:10	2445	-0.4550	1934	0.995	4.8	822-1211
41.6:38.4:20	2476	-0.4348	1988	0.992	4.9	811-1164
36.4:33.6:30	2556	-0.4441	2057	0.984	4.7	928-1166
27:63:10	2491	-0.4563	1979	0.997	1.8	952-1160
24:56:20	2521	-0.4317	2036	0.986	3.2	982-1159
21:49:30	2598	-0.4543	2088	0.980	4.1	982-1157
0 : 60:40	2654	-0.4465	2153	0.979	2.8	1065-1184
Li_2CO_3 : Na_2CO_3 : $SrCO_3$						
46.8:43.2:10	2514	-0.4374	2023	0.995	4.1	812-1169
41.6:38.4:20	2681	-0.4552	2170	0.996	2.7	931-1168
36.4:33.6:30	2849	-0.4798	2310	0.990	3.1	1017-1166
27:63:10	2562	-0.4368	2071	0.995	2.4	950-1155
24:56:20	2755	-0.5003	2193	0.989	3.3	979-1157

Table 2-4. (*continued*)

Composition (mol%)	Density (kg m^{-3}) $\rho = \alpha + \beta T$		Calculated values at 1123 K (kg m^{-3})	Square of correlation coefficient	Standard deviation	Temperature range (K)
	α	β	ρ_{1123}	r^2	*Sd*	*T*
Li_2CO_3 : Na_2CO_3 : $SrCO_3$						
21:49:30	2931	-0.5335	2332	0.979	4.4	1000-1153
0 : 60:40	3039	-0.5013	2476	0.926	6.1	1079-1198
Li_2CO_3 : Na_2CO_3 : $BaCO_3$						
46.8:43.2:10	2575	-0.4156	2108	0.997	2.8	851-1165
41.6:38.4:20	2838	-0.4538	2328	0.989	5.4	853-1165
36.4:33.6:30	3147	-0.5380	2543	0.987	54	930-1164
27:63:10	2679	-0.4754	2145	0.985	4.4	952-1153
24:56:20	2917	-0.5037	2351	0.996	2.1	977-1152
21:49:30	3224	-0.5978	2553	0.990	3.7	979-1154
0 : 60:40	3424	-0.6072	2742	0.980	4.2	1046-1185
Li_2CO_3 : Na_2CO_3 : $(Ca_{0.5}+Ba_{0.5})CO_3$						
46.8:43.2:10	2503	-0.4267	2024	0.991	5.2	865-1185
41.6:38.4:20	2653	-0.4323	2168	0.994	4.6	864-1180
36.4:33.6:30	2841	-0.4782	2304	0.992	4.3	938-1182
Li_2CO_3 : K_2CO_3 : $CaCO_3$						
55.8:34.2:10	2378	-0.4217	1904	0.994	4.3	808-1161
49.6:30.4:20	2435	-0.4231	1960	0.995	3.4	846-1157
43.4:26.6:30	2488	-0.4189	2018	0.970	6.2	923-1156
38.4:51.6:10	2448	-0.4683	1922	0.996	3.5	849-1164
34.2:45.8:20	2486	-0.4677	1961	0.994	3.6	926-1163
29.9:40.1:30	2531	-0.4681	2005	0.993	3.3	1013-1162
0 : 60:40	2604	-0.4756	2070	0.986	2.2	1087-1207
Li_2CO_3 : K_2CO_3 : $SrCO_3$						
55.8:34.2:10	2488	-0.4545	1978	0.983	6.8	820-1164
49.6:30.4:20	2621	-0.4533	2112	0.984	5.0	917-1165
43.4:26.6:30	2826	-0.5137	2249	0.960	6.6	987-1134
38.4:51.6:10	2529	-0.4909	1978	0.995	4.3	820-1165
34.2:45.8:20	2630	-0.4678	2105	0.995	3.5	899-1164
29.9:40.1:30	2814	-0.5241	2225	0.987	4.2	929-1165
0 : 60:40	3034	-0.6110	2348	0.994	1.4	1141-1202
Li_2CO_3 : K_2CO_3 : $BaCO_3$						
55.8:34.2:10	2579	-0.4657	2056	0.987	5.6	883-1162
49.6:30.4:20	2787	-0.4631	2267	0.981	6.6	889-1161
43.4:26.6:30	3075	-0.5471	2461	0.994	3.7	929-1164
38.4:51.6:10	2597	-0.4839	2054	0.998	2.7	812-1166
34.2:45.8:20	2849	-0.5503	2231	0.997	2.5	890-1165
29.9:40.1:30	3042	-0.5456	2429	0.992	4.1	930-1164
0 : 60:40	3219	-0.5655	2584	0.977	3.8	1086-1205

Table 2-5. Experimental equations for density of molten $(Li_{0.52}Na_{0.48})_2CO_3$, $(Li_{0.62}K_{0.38})_2CO_3$ and $(K_{0.573}Li_{0.437})_2CO_3$ containing additives.

Composition (mol %)	Density (kg m^{-3}) $\rho = \alpha + \beta T$		Calculated value at 923K (kg m^{-3})	Square of correlation coefficient	Standard Deviation	Temperature range (K)	Molar Volume at 923 K (cm^3)
	α	β	ρ_{923}	r^2	Sd	T	V
$(Li_{0.52}Na_{0.48})_2CO_3$			1969				45.35
$(Li_{0.52}Na_{0.48})_2(CO_3)_{0.99}(CrO_4)_{0.01}$	2377	-0.4298	1980	0.999	2.0	820 - 1166	45.38
$(Li_{0.52}Na_{0.48})_2(CO_3)_{0.97}(CrO_4)_{0.03}$	2363	-0.4092	1985	0.996	3.4	820 - 1164	45.83
$(Li_{0.52}Na_{0.48})_2(CO_3)_{0.95}(CrO_4)_{0.05}$	2388	-0.4178	2002	0.994	4.1	824 - 1164	45.99
$(Li_{0.52}Na_{0.48})_2(CO_3)_{0.95}(MoO_4)_{0.05}$	2416	-0.4172	2031	0.986	4.4	923 - 1160	46.43
$(Li_{0.52}Na_{0.48})_2(CO_3)_{0.98}(WO_4)_{0.02}$	2441	-0.4142	2059	0.981	5.2	923 - 1159	45.20
$(Li_{0.52}Na_{0.48})_2(CO_3)_{0.95}(WO_4)_{0.05}$	2543	-0.4437	2133	0.999	1.4	911 - 1151	46.26
$(Li_{0.52}Na_{0.48})_2(CO_3)_{0.95}(SO_4)_{0.05}$	2409	-0.4420	2001	0.998	2.3	870 - 1160	45.53
$(Li_{0.494}Na_{0.456}Rb_{0.05})_2CO_3$	2515	-0.4828	2069	0.999	1.9	868 -1162	46.57
$(Li_{0.494}Na_{0.456}Cs_{0.05})_2CO_3$	2527	-0.4449	2116	0.998	3.9	867 - 1110	47.78
$(Li_{0.52}Na_{0.48})_2(CO_3)_{0.95}Cl_{0.1}$	2389	-0.4627	1962	0.988	6.0	915 - 1159	45.79
$(Li_{0.52}Na_{0.48})_2(CO_3)_{0.95}F_{0.1}$	2332	-0.4107	1953	0.996	2.7	873 - 1169	45.16
$(Li_{0.52}Na_{0.48})_2(CO_3)_{0.95}I_{0.1}$	2514	-0.5112	2042	0.974	2.7	903 - 994	48.47
$(Li_{0.62}K_{0.38})_2CO_3$			1935[a]				50.81
$(Li_{0.62}K_{0.38})_2(CO_3)_{0.99}(CrO_4)_{0.01}$	2336	-0.4261	1943	0.998	2.4	809 -1164	50.90
$(Li_{0.62}K_{0.38})_2(CO_3)_{0.97}(CrO_4)_{0.03}$	2360	-0.4384	1955	0.994	4.3	813 - 1167	51.15
$(Li_{0.62}K_{0.38})_2(CO_3)_{0.95}(CrO_4)_{0.05}$	2394	-0.4562	1973	0.994	4.0	852 - 1166	51.26
$(Li_{0.62}K_{0.38})_2(CO_3)_{0.95}(MoO_4)_{0.05}$	2391	-0.4285	1995	0.993	3.2	937 - 1169	51.78
$(Li_{0.62}K_{0.38})_2(CO_3)_{0.98}(WO_4)_{0.02}$	2390	-0.4385	1985	0.991	3.2	916 - 1145	51.42
$(Li_{0.62}K_{0.38})_2(CO_3)_{0.97}(WO_4)_{0.03}$	2443	-0.4649	2014	0.998	1.9	924 - 1161	51.62
$(Li_{0.62}K_{0.38})_2(CO_3)_{0.95}(WO_4)_{0.05}$	2505	-0.4718	2070	0.998	2.6	841 - 1167	52.05
$(Li_{0.62}K_{0.38})_2(CO_3)_{0.95}(SO_4)_{0.05}$	2408	-0.4831	1962	0.997	2.8	869 - 1162	51.03
$(Li_{0.589}K_{0.361}Rb_{0.05})_2CO_3$	2442	-0.4663	2012	0.997	3.1	868 - 1161	52.18
$(Li_{0.62}K_{0.38})_2(CO_3)_{0.95}Cl_{0.1}$	2281	-0.4288	1885	0.997	2.0	965 - 1159	52.45
$(Li_{0.62}K_{0.38})_2(CO_3)_{0.95}F_{0.1}$	2304	-0.4103	1925	0.997	2.5	853-1169	50.50
$(Li_{0.437}K_{0.573})_2CO_3$			1967				56.29
$(Li_{0.437}K_{0.573})_2(CO_3)_{0.99}(CrO_4)_{0.01}$	2414	-0.4761	1975	0.995	4.5	821 - 1164	56.22
$(Li_{0.437}K_{0.573})_2(CO_3)_{0.97}(CrO_4)_{0.03}$	2399	-0.4489	1985	0.997	3.0	821 - 1165	56.50
$(Li_{0.437}K_{0.573})_2(CO_3)_{0.95}(CrO_4)_{0.05}$	2416	-0.4598	1992	0.998	2.5	823 - 1164	56.83

2.4. Discussion

2.4.1. Molar volume of molten carbonate systems

From the density, ρ, data measured in this work, the molar volume of molten carbonate mixtures, V_M, can be calculated using the following equation,

$$V_M = (\sum_i X_i M_i) / \rho \qquad [2\text{-}8]$$

where X_i and M_i are the mole fraction and formula weight of the carbonate component *i*, respectively.

Assuming that the additive property of molar volume holds in molten carbonates, the

following equation would hold in the mixtures,

$$V_M = \sum_i V_i^0 X_i \qquad [2\text{-}9]$$

where V_i^0 and X_i are the molar volume and the mole fraction of component, *i*, respectively.

The molar volume of binary molten carbonate systems are detailed in Fig. 2-12 for the systems of Li_2CO_3-X_2CO_3 (X: Na, K, Rb, and Cs) and in Fig. 2-13 for the systems of Na_2CO_3-Y_2CO_3 (Y: K, Rb, and Cs) at 1173K. The dependence of molar volume on the composition in each system almost seems to be linear. Therefore, one can calculate the density of any composition in binary alkali carbonate without large error. There, however, were positive deviation from the additive rule of molar volume observed in the molten binary carbonate Li_2CO_3-Rb_2CO_3 and Li_2CO_3-Cs_2CO_3 systems. On the other hand, the molar volume in Na_2CO_3-K_2CO_3, Na_2CO_3-Rb_2CO_3 and Na_2CO_3-Cs_2CO_3 systems seems to be ideal relation or show slight negative deviation from additive rule. These deviations from additivity are shown in Fig. 2-14. In Li_2CO_3-Rb_2CO_3 and Li_2CO_3-Cs_2CO_3 systems, there are relatively large positive deviations.

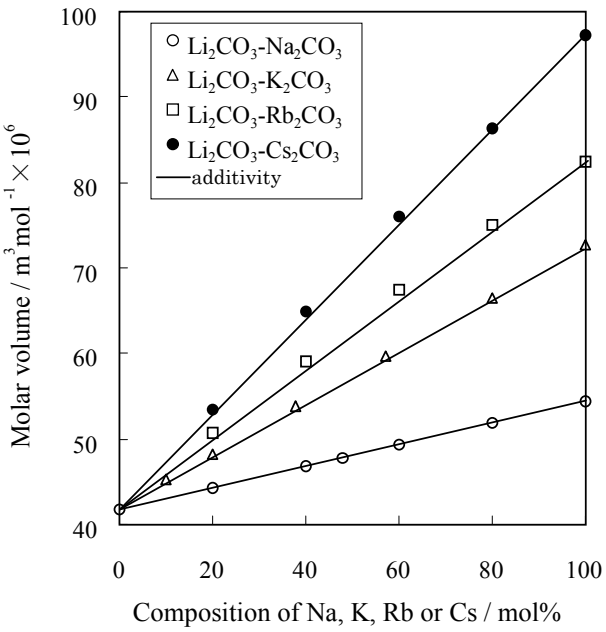

Fig. 2-12. The molar volume of Li_2CO_3-Na_2CO_3(○), Li_2CO_3-K_2CO_3(△), Li_2CO_3-Rb_2CO_3(□) and Li_2CO_3-Cs_2CO_3(●) binary carbonate system at 1173K, solid line: calculated from additivity.

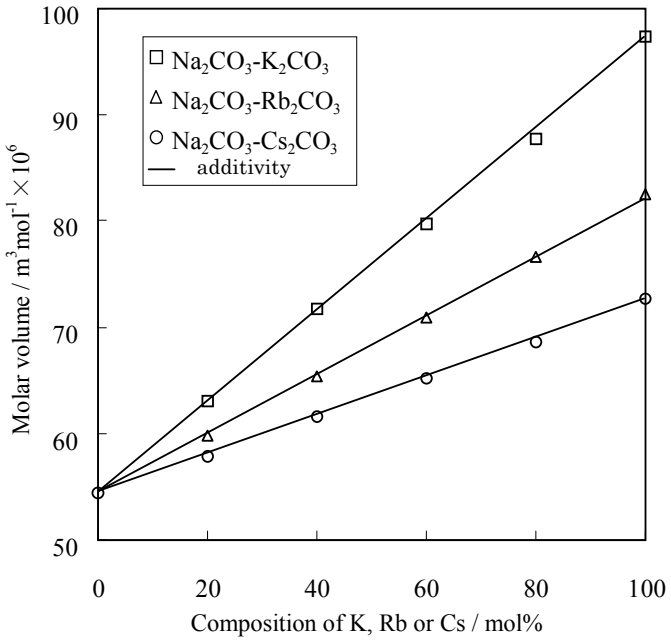

Fig. 2-13. The molar volume of Na_2CO_3-K_2CO_3(○), Na_2CO_3-Rb_2CO_3(△) and Na_2CO_3-Cs_2CO_3(□) binary carbonate system at 1173K, solid line: calculated from additivity.

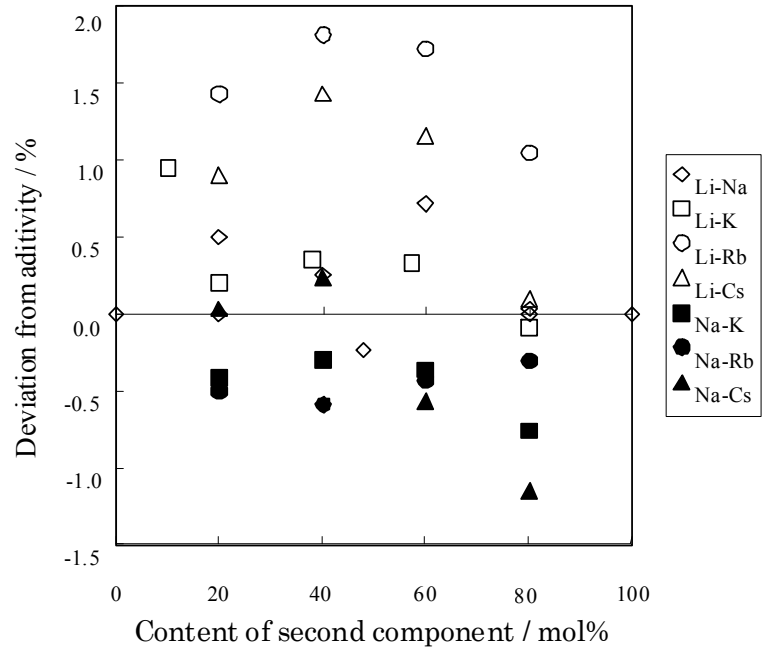

Fig. 2-14. The deviation of molar volume from additivity in the systems of Li_2CO_3-X_2CO_3 (X: Na, K, Rb and Cs) and Na_2CO_3-Y_2CO_3 (Y: K, Rb and Cs) at 1173K.

In these systems, large Rb or Cs cations increase the distance between carbonate ions, so lithium ion is forced to occupy larger space than that in pure molten Li_2CO_3. This is the cause of the positive deviation from the additive rule of molar volume in these systems. And the prolonged distance between lithium ion and carbonate ion weakens the strong ionic interaction, i.e., the surface tension.

For the system of Li_2CO_3-Na_2CO_3-K_2CO_3, Table 2-3 shows that the molar volume of the Li_2CO_3-Na_2CO_3-K_2CO_3 ternary system is also in good accordance with values estimated using the data of three single molten carbonates of Li_2CO_3, Na_2CO_3, and K_2CO_3 within experimental error (±0.7 %). The molar volume in molten ternary alkali carbonates can be calculated using additivity. The relationship between the composition and the physical property of a ternary system is depicted as a regular triangle diagram and contour lines of physical property. The points at vertex, on side, in regular triangle diagram denote pure components, binary mixture and ternary mixture, respectively. The molar volume of the Li_2CO_3-Na_2CO_3-K_2CO_3 ternary system at 1073 K is shown in Fig. 2-15, together with contour lines estimated using additivity.

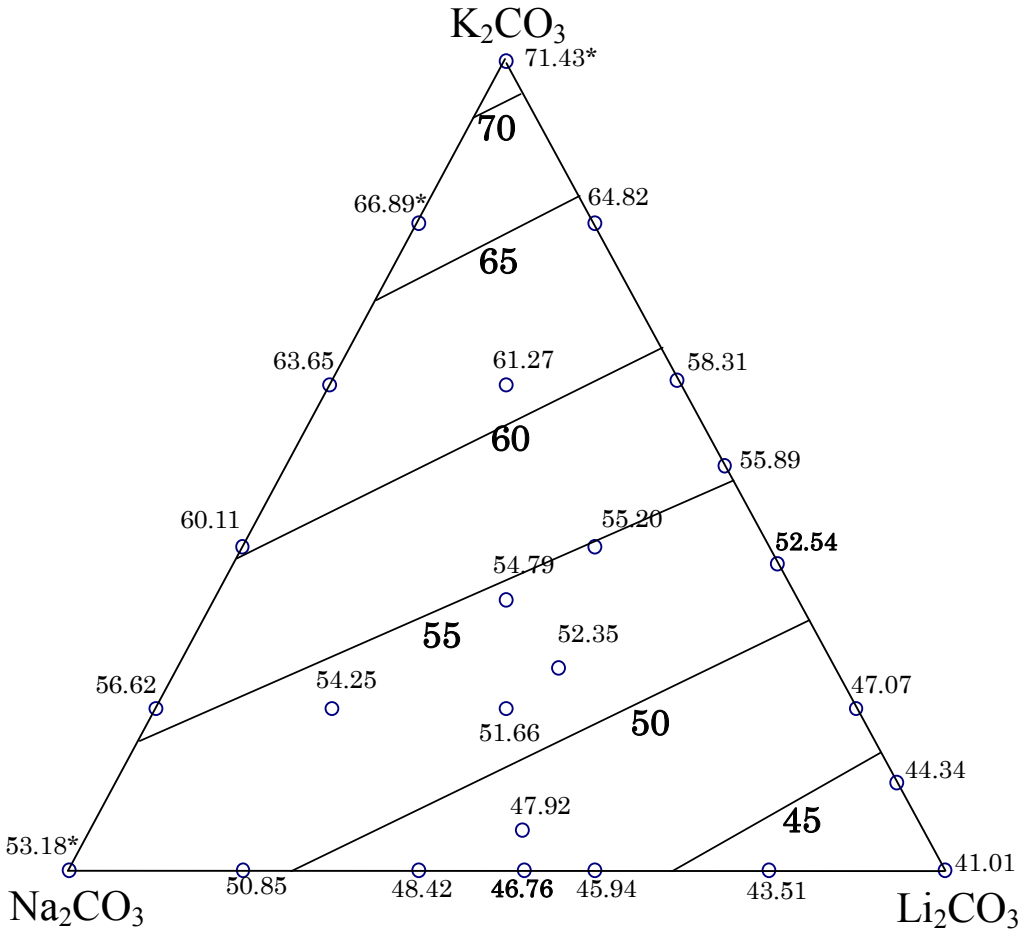

Fig. 2-15. Contour diagram of molar volume (cm^3 mol^{-1}) of molten Li_2CO_3-Na_2CO_3-K_2CO_3 system at 1073K. (* extrapolated values)

For Molar volume of alkali-alkaline earth carbonate systems, the equivalent density data for alkaline earth carbonate is not available, as they exist as solids over the temperature range used in this work. Therefore values of V_i^0 in ternary carbonate systems were derived from the experimental data by the least-squares method using equation [6] with V_M, and X_i as parameters. The value of V_i^0 obtained from equation [6] is the apparent molar volume of the pure component in the molten carbonate mixture, and is therefore denoted as $V_i'^0$.

Density data converted from $V_i'^0$ values obtained at several temperatures in ternary carbonate systems are summarized in the form of an empirical equation in Table 2-6. The density data of Li_2CO_3, Na_2CO_3, and K_2CO_3 obtained from values showed good agreement with this work and literature data within an error of ±0.6%.

Table 2-6. Calculated density of molten carbonates in ternary molten carbonate systems using the additive property of molar volume.

Components in ternary system	$\rho = \alpha' + \beta' T$		Density at 1123K (kg m^{-3})	Molar Volume at 1123K (cm^3)
	α'	β'	ρ_{1123}	V_{1123}
Li-Na-Ca system				
$CaCO_3$	3047	-0.4531	2538	39.43
Na_2CO_3	2488	-0.4606	1971	53.78
Li_2CO_3	2225	-0.3968	1779	41.52
Li-Na-Sr system				
$SrCO_3$	4171	-0.6637	3426	43.10
Na_2CO_3	2480	-0.4523	1972	53.76
Li_2CO_3	2221	-0.3928	1780	41.51
Li-Na-Ba system				
$BaCO_3$	4902	-0.7695	4038	48.87
Na_2CO_3	2492	-0.4630	1972	53.74
Li_2CO_3	2200	-0.3728	1781	41.48
Li-K-Ca system				
$CaCO_3$	3137	-0.5802	2485	40.28
K_2CO_3	2409	-0.4351	1920	71.99
Li_2CO_3	2220	-0.3883	1784	41.43
Li-K-Sr system				
$SrCO_3$	4478	-0.9739	3384	43.63
K_2CO_3	2408	-0.4375	1917	72.09
Li_2CO_3	2201	-0.3761	1779	41.53
Li-K-Ba system				
$BaCO_3$	4971	-0.7620	4115	47.96
K_2CO_3	2411	-0.4479	1908	72.43
Li_2CO_3	2211	-0.3720	1793	41.21

The $V_i'^0$ values of alkaline earth carbonates showed a small difference between molten Li_2CO_3-Na_2CO_3 and molten Li_2CO_3-K_2CO_3. The value of $V_i'^0$ of $CaCO_3$ in molten Li_2CO_3-Na_2CO_3

was smaller than that in molten Li_2CO_3-K_2CO_3 by 2.1% at 1123K. On the other hand, the V_i^0 of $BaCO_3$ in molten Li_2CO_3-Na_2CO_3 was larger than that in molten Li_2CO_3-K_2CO_3 by 1.9% at 1123K. These differences may arise from the different interactions of alkaline earth cations with Na^+ or K^+.

The data in Table 2-6 can be used to estimate the molar volume and density of carbonate mixtures. The calculated densities and molar volumes showed good agreement with measured data within an error of 1.0%. The molar volume of the Li_2CO_3-Na_2CO_3-$CaCO_3$ ternary system is shown in Fig. 2-16 together with contour lines estimated using the parameters in Table 2-6.

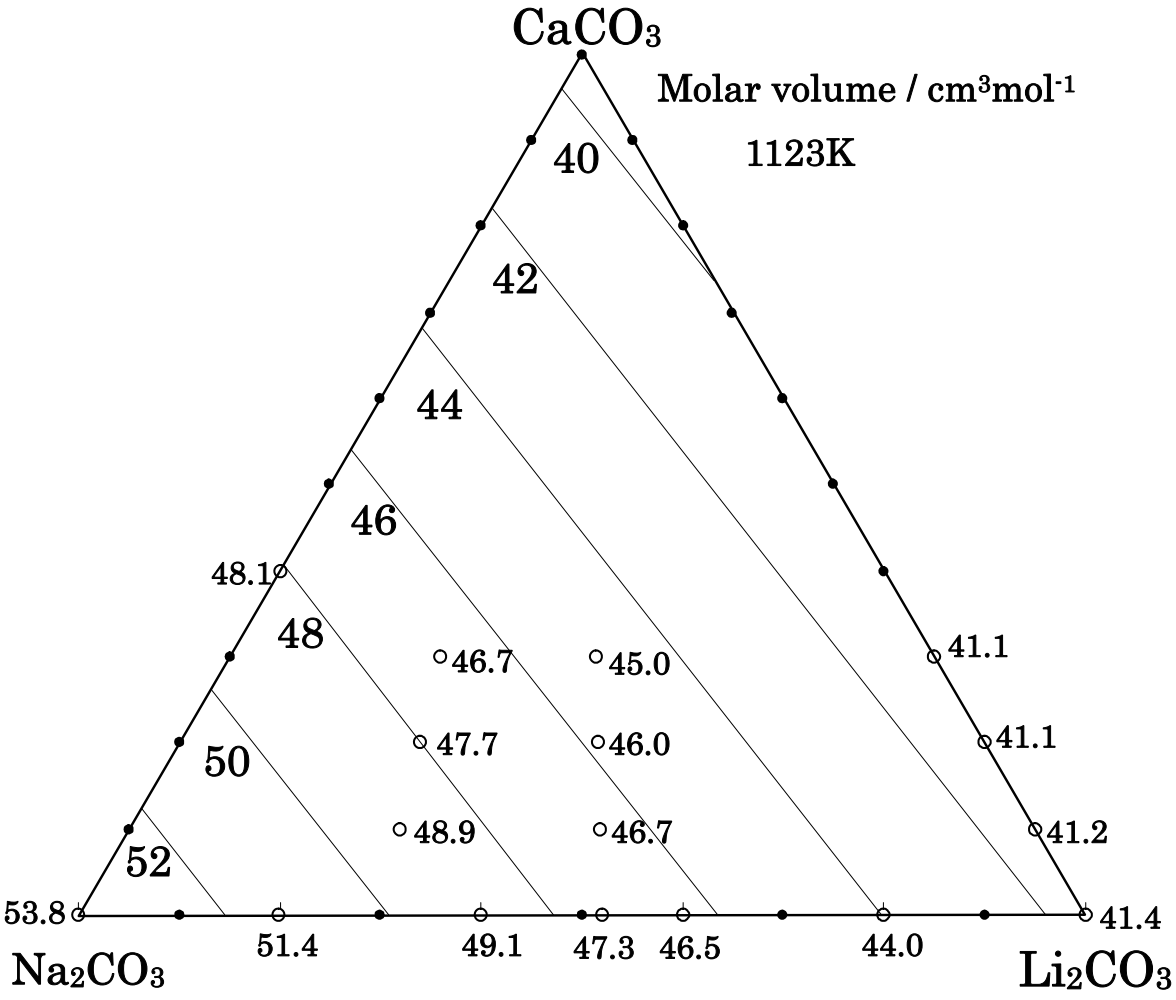

Fig. 2-16. Experimentally measured molar volumes of molten Li_2CO_3-Na_2CO_3-$CaCO_3$ at 1123K (○) and contour lines calculated from the additive property.

2.4.2. Relationship between the molar volume and ionic radii

The molar volume of alkali carbonates and alkaline earth carbonates increased with an increase in the ionic radii of cations contained in each carbonate melt. There can be seen a linear relationship between the molar volumes of the molten carbonates and their cationic volumes, calculated using radii of 6 coordination[8], as shown in Fig. 2-17. The intercept of this plot should be the molar

volume of the carbonate ion, 34.73 cm^3 mol^{-1} at 1123K.

Using this type of plot at several temperatures, the relationship between the ionic radii and the molar volumes of ions in molten carbonates can be described as the following empirical equation.

$$V_{ion} = \frac{4}{3}\pi r_{ion}^3 N(1.89 + 6.27 \times 10^{-4} T) \qquad [2\text{-}9]$$

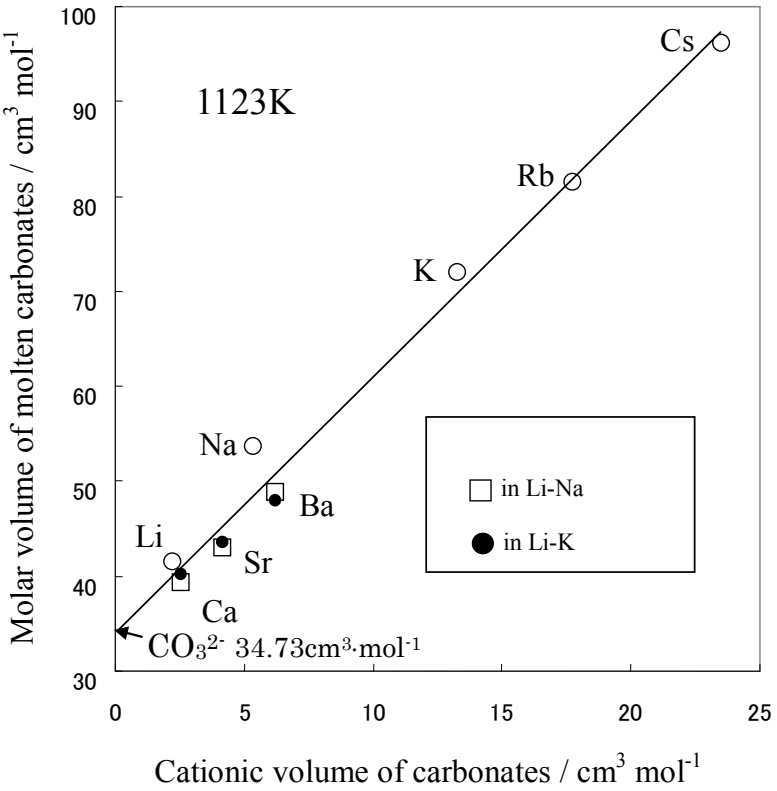

Fig. 2-17. The relationship between molar volume of molten carbonates and their cationic volume of carbonate calculated from ionic radii.

where V_{ion} is the molar volume of an ion in molten carbonates, and r_{ion} is the ionic radius of 6 coordination, T is the absolute temperature, and N is Avogadro's number. Inverting this equation, the apparent ionic radius of the carbonate ion can be obtained as 174 pm. This value is quite similar to that of 178pm reported as the thermochemical ionic radius[9]. Using equation [2-9], the molar volume of a carbonate mixture containing some ions of known ionic radius can be estimated and the ionic radius can also be estimated from the density data.

2.4.3. Estimation of molar volume of quaternary system

Recently it has been reported that quaternary carbonate mixtures such as $(Li_{0.52}Na_{0.48})CO_3$+$Ca_{0.5}Ba_{0.5}CO_3$ (in the amounts of 10, 20 and 30 mol%) are promising as MCFC

electrolytes[10].

The molar volume of $(Li_{0.52}Na_{0.48})CO_3$-$Ca_{0.5}Ba_{0.5}CO_3$ was estimated following equation

$$V_M = \sum_i X_i V'^0_i = X_{Li} V'^0_{Li} + X_{Na} V'^0_{Na} + X_{Ca} V'^0_{Ca} + X_{Ba} V'^0_{Ba} \qquad [2\text{-}10]$$

The V'^0_i s were obtained from the data of Table 2-6. In spite of the large temperature extrapolation under the melting point, the estimated values show good agreement with measured values within an error of 0.3%, as shown in Fig. 2-18.

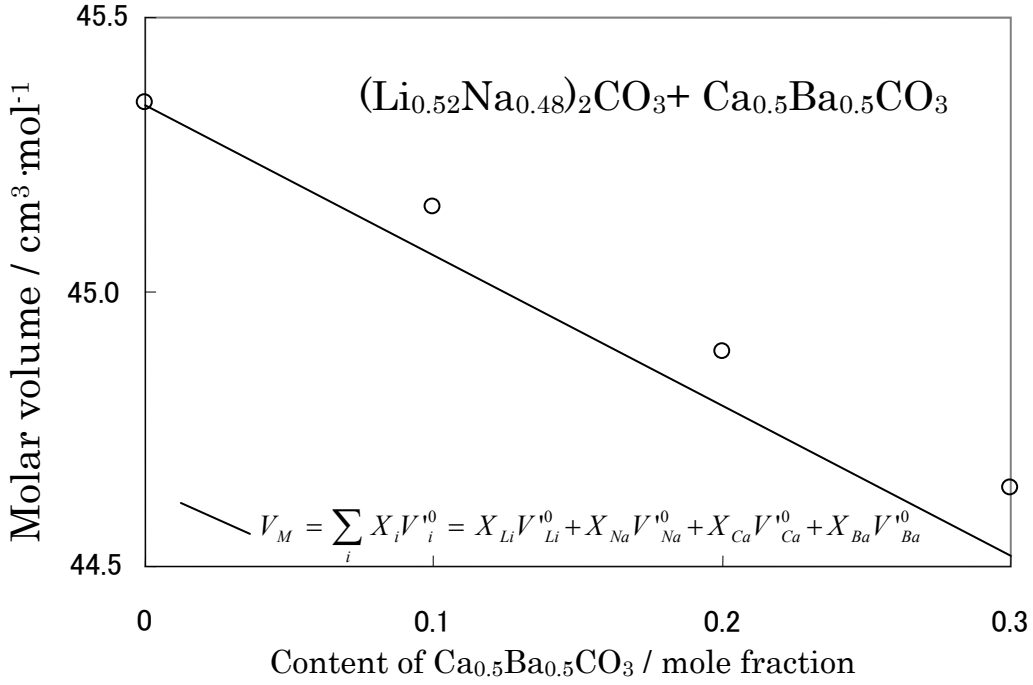

Fig. 2-18. Molar volume of $(Li_{0.52}Na_{0.48})_2CO_3$ with added $Ca_{0.5}Ba_{0.5}CO_3$ at 923K and estimated values shown as a line.

2.5. Conclusion

The density, and molar volume of binary, ternary, and quaternary molten carbonate mixtures of alkali carbonates (Li_2CO_3, Na_2CO_3 and K_2CO_3) and alkali carbonate added with several additives such as alkaline earth carbonates ($CaCO_3$, $SrCO_3$, and/or $BaCO_3$) and MO_4^{2-} (SO_4^{2-}, CrO_4^{2-}, MoO_4^{2-}, and WO_4^{2-}) were measured using a maximum bubble pressure technique with good accuracy.

Assuming that their properties are additive, the predicted molar volume of ternary mixtures agreed well with measured ones within 0.7%.

The molar volume of Li_2CO_3-Rb_2CO_3 and Li_2CO_3-Cs_2CO_3 systems shows positive deviation.

The addition of alkaline earth carbonates resulted in an increase in the density of molten carbonate mixtures. The molar volumes of single molten carbonates in molten carbonates have been derived from the density data of ternary molten carbonate mixtures. The obtained molar volume of a single molten carbonate can be inverted to estimate the molar volume and density of mixtures within an error of 1%.

Apparent molar volumes of single molten carbonates can be estimated from the ionic radii of the component ions. The molar volumes of mixtures also can be estimated from the ionic radii of the components without measuring the density, and conversely the ionic radius in a molten carbonate also can be estimated from density measurements.

These methods for estimating the density, and molar volume of molten alkali - alkaline earth carbonates can be extended to multi-component systems and lower temperature than the melting point of single molten carbonates with good agreement.

Reference

[1] G. J. Janz and M. R. Lorenz, "Molten carbonate electrolytes: physical properties, structure, and mechanism of electrical conductance," *J. Electrochem. Soc.*, 108, 1052 (1961).

[2] A. T. Ward and G. J. Janz, "Molten carbonate electrolytes: electrical conductance, density and surface tension of binary and ternary mixtures," *Electrochimica Acta*, 10, 849 (1965).

[3] P. L. Spedding, *J. Electrochem. Soc.*, **117**, 177 (1970).

[4] Zhu Hong-Min, T. Sato, T. Yamamura, K. Shimakage and T. Ejima, *J. Japan Inst. Metals*, **55**, 937 (1991).

[5] Q. Liu and R. A. Lange, *Contrib. Mineral Petrol.*, **146**, 370 (2003).

[6] G. J. Janz and A. Conte, Corr., 20, 237 (1964).

[7] G. J. Janz, *J. Phys. Chem. Ref. Data*, **17**, 1 (1988).

[8] R. D. Shannon, *Acta Crystallogr., Sect. A: Cryst. Phys., Diffr., Theor. Gen. Crystallogr.*, **A32**, 751 (1976).

[9] H. D. B. Jenkins, and K. P. Thakur, *J. Chem. Educ.*, **56**, 576 (1979).

[10] A. C. Schoeler, T. D. Kaun, I. Bloom, M. Lanagan, and M. Krumpelt, *J. Electrochem. Soc.*, **147**, 916(2000).

3. Surface Tension of Molten Carbonates

3.1. Introduction

One of physical properties of molten salts, surface tension is important for not only their industrial use but also better understanding their nature. The surface tension of molten salt has relationship with the force between ionic species in it. Surface tension is also sensitive to the formation of complex in molten salt. It is also important for estimating capillary force and wettability, which work to distribute electrolyte between porous cell components of anode, cathode and electrolyte matrix and prevent gas cross-leakage through electrolyte matrix in MCFC. The surface tension also has an influence on the reactant gas solubility in molten carbonate hence MCFC performance[1].

For the study of the surface tension of molten carbonate, Janz and Lorenz[2,3], Ward and Janz [4],and Smirnov and Stepanov[5] reported single alkali, binary alkali carbonate systems, Li_2CO_3, Na_2CO_3, K_2CO_3, and their binary and ternary mixtures. Liu et al. [6] reported data of Li_2CO_3, Na_2CO_3, K_2CO_3, and their binary and ternary mixtures containing $CaCO_3$.

No data have been reported for binary and ternary carbonate mixtures containing Rb_2CO_3, and Cs_2CO_3, $SrCO_3$, $BaCO_3$ and the mixture added with MO_4^{2-} (SO_4^{2-}, CrO_4^{2-}, MoO_4^{2-}, and WO_4^{2-}).

In this section, several molten carbonate mixtures mentioned at section 1.5 are investigated for surface tension measurement. The influence of ionic size to physical properties of cations (Li^+, Na^+, K^+, Rb^+, Cs^+, Ca^{2+}, Sr^{2+}, and Ba^{2+}) and additives MO_4^{2-} (SO_4^{2-}, CrO_4^{2-}, MoO_4^{2-}, and WO_4^{2-}) was interesting for predict unknown data and understanding the nature of molten salts. I will present interesting relationship between surface tension and composition in ternary molten carbonate system.

3.2. Experiment

3.2.1. Measurement method for the surface tension of molten carbonates

For the measurement of surface tension of molten salt, pin-detachment method and maximum bubble pressure method are well known. Janz et al.[2-4] measured surface tension using a pin under a bob. Their method is a kind of ring method. The principles of pin-detachment methods are shown in Fig.3-1. The whole weight of the bob and the pin, M. The diameter of pin, r was measured in advance. When the pin touched the surface of molten salt, meniscus of molten salt make a force to pull down the pin by the surface tension. They measured the difference of weight, ΔF, between before and after the pin detached from the surface of molten salt.

$$\Delta F = 2\pi r\gamma \qquad [3\text{-}1]$$

where γ is the surface tension of molten salt. They measured not only surface tension but also density using surface tension.

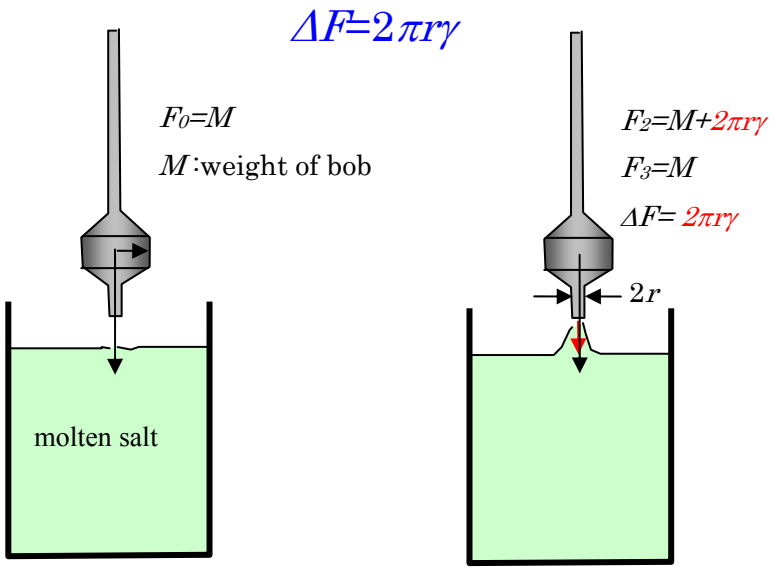

Fig. 3-1. Principle of surface tension measurement, pin-detachments method.

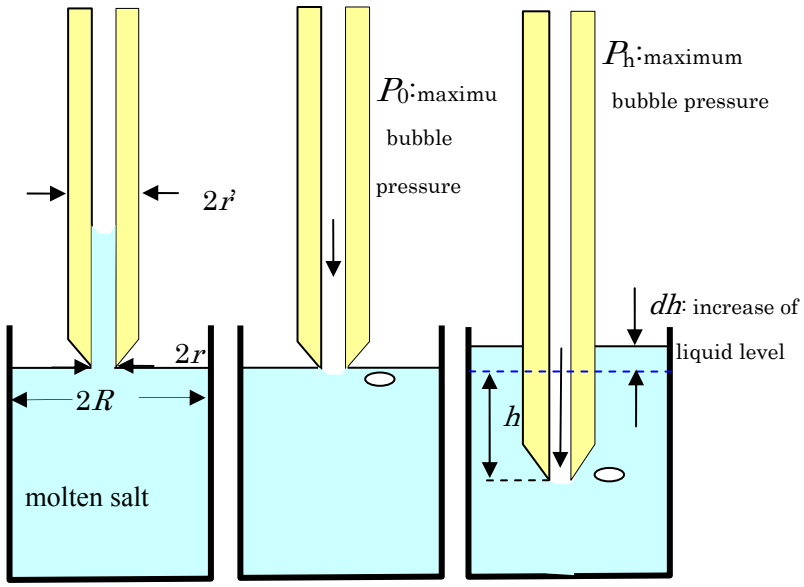

Fig. 3-2. Principle of surface tension measurement using maximum bubble pressure method

The pin-detachment method, however, is time consuming and it is afraid that the surface of bob influences the measurement by wettability. Some metals show low wettability for molten carbonate depending on atmosphere or temperature. Wettability is described as contact angle, θ. The force pulling molten salt decreases to $\gamma\cos\theta$. It was reported that the contact angles for Au was lower than 90 degree.

In order to measure a number of mixtures of molten carbonate mixture, I chose maximum bubble

pressure method and refine it as described in following section.

The difficulty of surface tension measurement with maximum bubble pressure method is scatter of measured pressure. I found the pressure deflection was suppressed by wider gas exit of furnace. The adoption of a laser displacement meter made measurement easier and faster.

The principle of maximum bubble pressure method for density measurement is shown in Fig. 3-2. When a capillary is touched with melt surface, melt climbs up inside capillary by capillary force originated from surface tension of melt and this increase the pressure inside the capillary. As the pressure is increased inside capillary by sending gas, melt is pushed out and the pressure reached maximum, then finally gas bubble come out from the tip of capillary. At that time a contact line of molten carbonate and capillary go through the place where apparent contact angle θ almost become zero because of curve near the near the exit of capillary then the bubble pressure would also become maximum. The maximum pressures measured when the capillary is placed on the surface and inside of melt by a depth of *h*, are denoted as P_0 and P_h, respectively. As described section 2.2.1, density can be obtained from the difference between P_0 and P_h. The relationship between maximum pressure inside capillary and capillary force induced by surface tension is expressed as following equation.

$$\pi r^2 P_0 = 2\pi r\gamma + \alpha \qquad [3\text{-}2]$$

where α is a contribution of buoyancy made by half bubble pushing out into the melt.

$$\gamma = \frac{r}{2}(P_0 - \alpha) \qquad [3\text{-}2]$$

Schrödinger[7] analyzed α and reported following equation for surface tension.

$$\gamma = \frac{rP_0}{2}\{1 - \frac{2}{3}\frac{\rho g r}{P_0} - \frac{1}{6}(\frac{\rho g r}{P_0})^2\} \qquad [3\text{-}3]$$

It should be noted that the density data is need to obtain surface tension for using equation [3-3].

3.2.2. Measurement procedures

As mentioned 2.2.3, sample preparation and apparatus for the measurement of density and surface tension of molten carbonates is common.

The surface tension of molten alkali carbonates were measured in the temperature range from about 1100 K to a temperature higher than their liquidus by 30 K.

The level of the surface of melt was detected by abrupt pressure gain when the capillary contacted the melt. When the bubble escape from the tip of the capillary, the pressure reaching its maximum was measured as the maximum bubble pressure. The bubbles were controlled to be made with the interval of about a few minutes. The maximum bubble pressures were measured at the both levels of

surface and more than 10 mm depth in the melt in order to obtain density of melt.

The value of capillary radius, r at room temperature was determined through the measurement with doubly distilled water at room temperature using high purity Ar gas (Iwatani gas, 99.9995%, dew point 203 K) and was estimated at high temperature considering thermal expansion of alumina.

3.3. Results

3.3.1. Evaluation of measurement accuracy

Errors estimated in the measurement of surface tension of molten carbonates are listed in Table 3-1. The factors contributing to the error of surface tension are determination of the inner diameter of capillary, detection of melt's surface, density, measurement of the maximum bubble pressure and temperature of the melt. All the factors of the error were estimated and summed up to be less than $\pm 1.0\%$ for surface tension measurements.

Table 3-1. Errors estimated in the measurement of surface tension of molten carbonates.

Factors	Estimated error in each measurements	Estimated error in surface tension
pressure measurement	±0.15%	±0.15%
detaction of surface	±20 μ m	±0.15%
capillary radius	±5 μ m	±0.5%
density of melt	±0.9%	±0.03%
temperature	±5K	±0.2%
	Maximum Error	±1.0%

In order to verify the accuracy and precision of the measurements, the density and the surface tension of molten NaCl, well known as a standard material[8] were measured from 1097 to 1179K. The results showed good agreement with literature data of the surface tension (γ / mN m^{-1} = 190.2 - 0.07167T) within ±0.8%.

3.3.2. The results of the measurements

The surface tension of alkali carbonates were measured as a function of temperature. The results of alkali carbonates were shown in Figs. 3-3 with literature data[3,5]. Although the results of the surface tension of single alkali carbonate, Li_2CO_3 and K_2CO_3 shows good agreement with literature data, there was disagreement between our results and reported ones for Na_2CO_3 by max. 2%, Rb_2CO_3 by max. 4% and Cs_2CO_3 by max. 2% as shown in Fig. 3-3. The reason for these discrepancies is not clear. The disagreement may be come from the difference of the measurement technique, usage of less wettable materials which contact with the melt (Au-Pd(80:20wt%) alloy pin or platinum capillary), inadequate preparing or handling of those salts in earlier investigations.

As an example of the result measured for molten alkali binary carbonate system, the results of molten Li_2CO_3-Rb_2CO_3 binary system are plotted in Fig. 3-4. Several data of the surface tension in

Li_2CO_3-Na_2CO_3, Li_2CO_3-K_2CO_3, and Na_2CO_3-K_2CO_3 have been reported. The results of these systems are plotted with literature data in Fig. 3-5 for Li_2CO_3-Na_2CO_3 and Li_2CO_3-K_2CO_3 systems and Fig. 3-6 for Na_2CO_3-K_2CO_3 system. Our result seems to agree well with previous data.

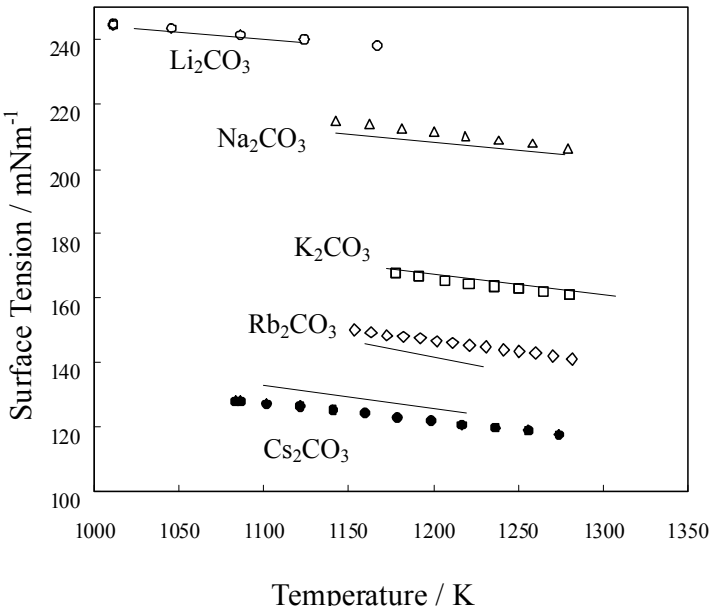

Fig. 3-3. The temperature dependence of the surface tension of molten alkali carbonates. Li_2CO_3(○), Na_2CO_3(△), K_2CO_3(□), Rb_2CO_3(◇), and Cs_2CO_3(●), solid line: [8].

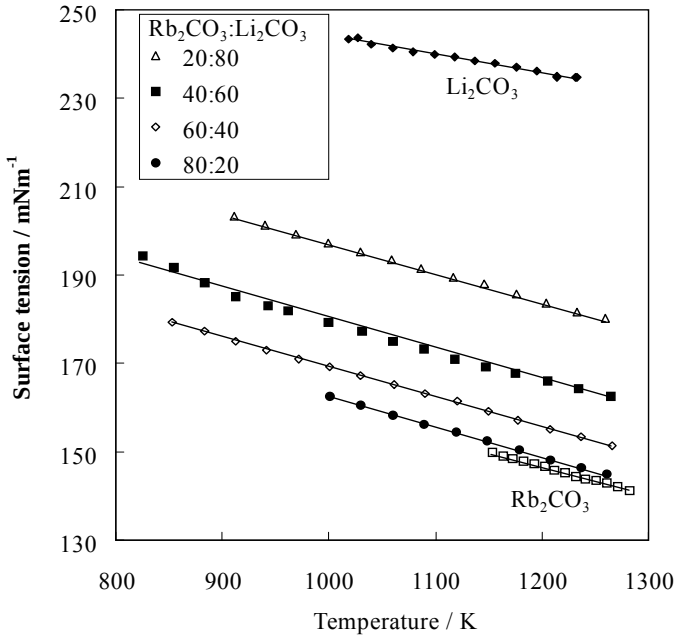

Fig. 3-4. The temperature dependence of the surface tension of molten Li_2CO_3-Rb_2CO_3 binary carbonates.

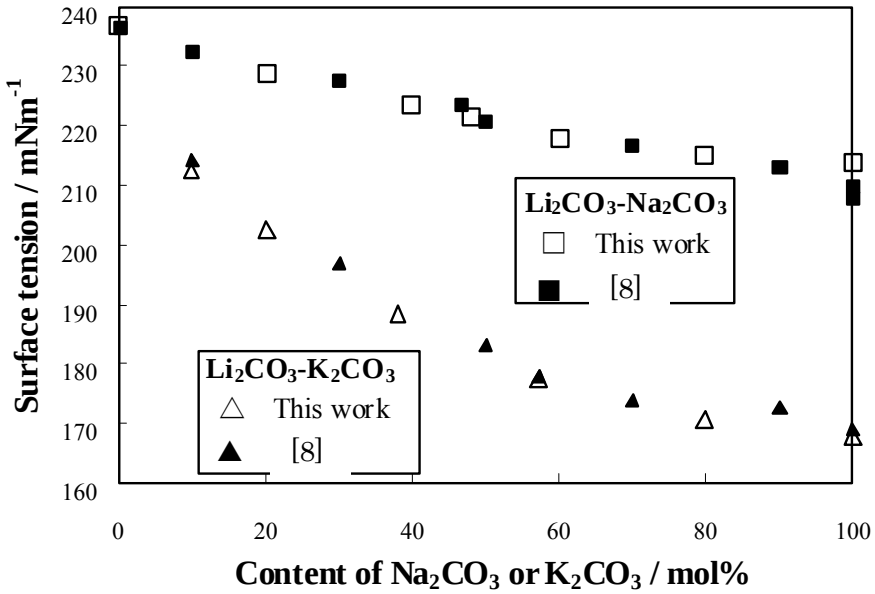

Fig. 3-5. The surface tension of molten Li_2CO_3-Na_2CO_3 (□) and Li_2CO_3-K_2CO_3 (△) systems of this work, (■) (▲): [8]) at

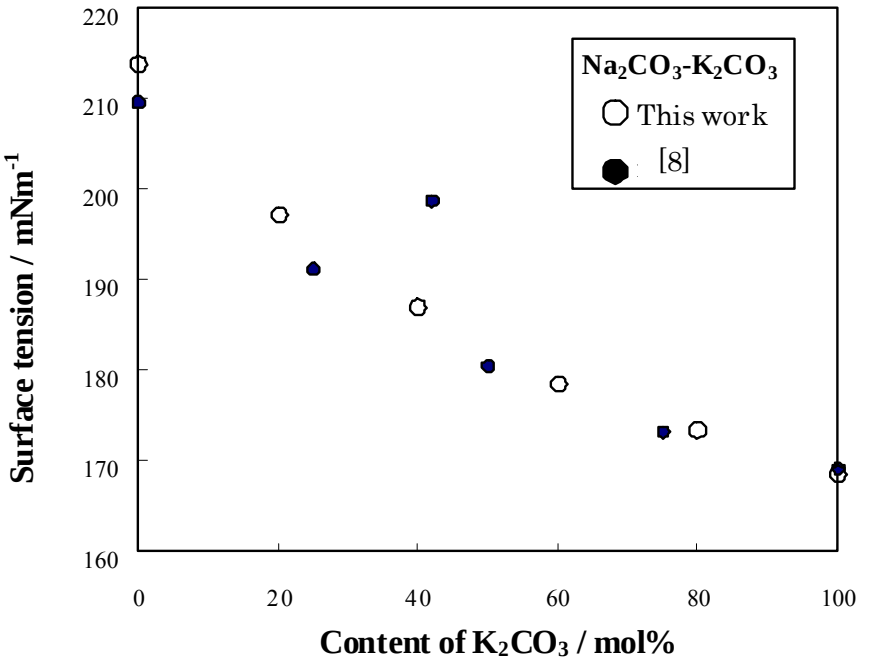

Fig. 3-6. The surface tension of molten Na_2CO_3-K_2CO_3 (○) systems of this work, (●): [8]) at 1173K.

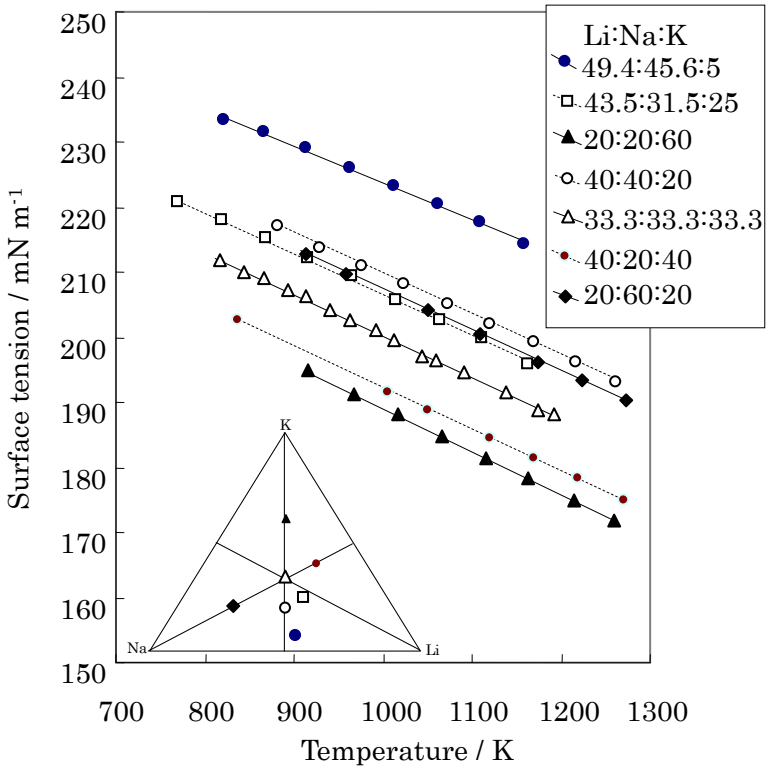

Fig. 3-7. Temperature dependence of the surface tension of molten Li_2CO_3 - Na_2CO_3 - K_2CO_3 ternary carbonates.

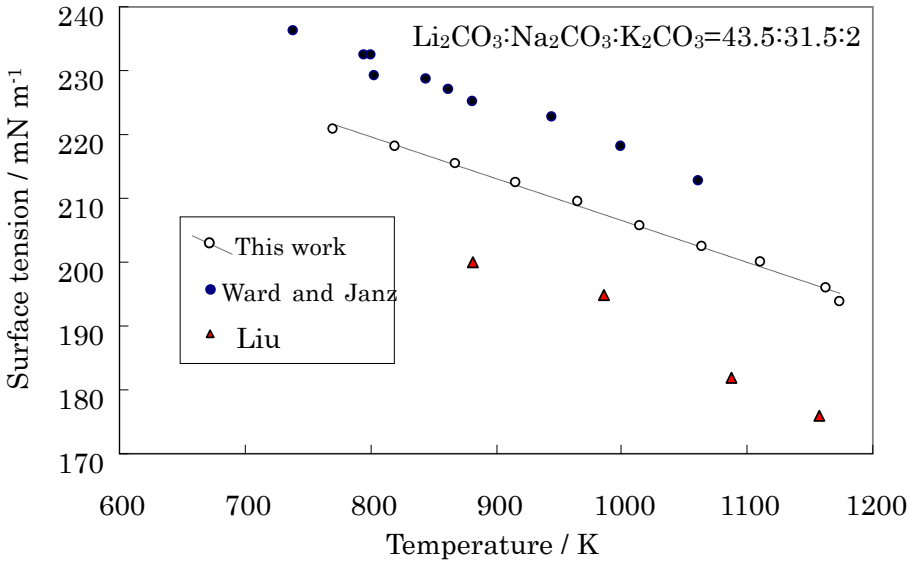

Fig. 3-8. Comparison of the results of surface tension measurements with those in the literature.

The data of the surface tension of the MCFC electrolytes, Li_2CO_3-Na_2CO_3 (52:48 mol%) and Li_2CO_3-K_2CO_3 (62:38 mol%) have not been reported. The surface tension of Li_2CO_3-Na_2CO_3 (52:48 mol%) at 923 K was 236 mNm^{-1} which is higher than that of Li_2CO_3-K_2CO_3 (62:38 mol%), 205 mNm^{-1}. Higher surface tension of MCFC electrolyte is favorable for preventing cross-leakage.

The results of surface tension of Li_2CO_3-Na_2CO_3 -K_2CO_3 systems are plotted in Fig. 3-7.

Our data, and that reported by other authors, are shown in Fig. 3-8 [4,6] . The surface tension showed significant differences from that measured by Ward and Janz[4] and by Liu et al. [6] These differences can probably be attributed to different measurement methods and to differences in the materials which contacted the molten carbonates.

The surface tensions of $CaCO_3$ added to molten Li_2CO_3-Na_2CO_3 (52:48mol%) are plotted as a function of temperature in Fig. 3-9. It was shown that the addition of alkaline earth carbonate to alkali carbonate resulted in increase of surface tension of mixture.

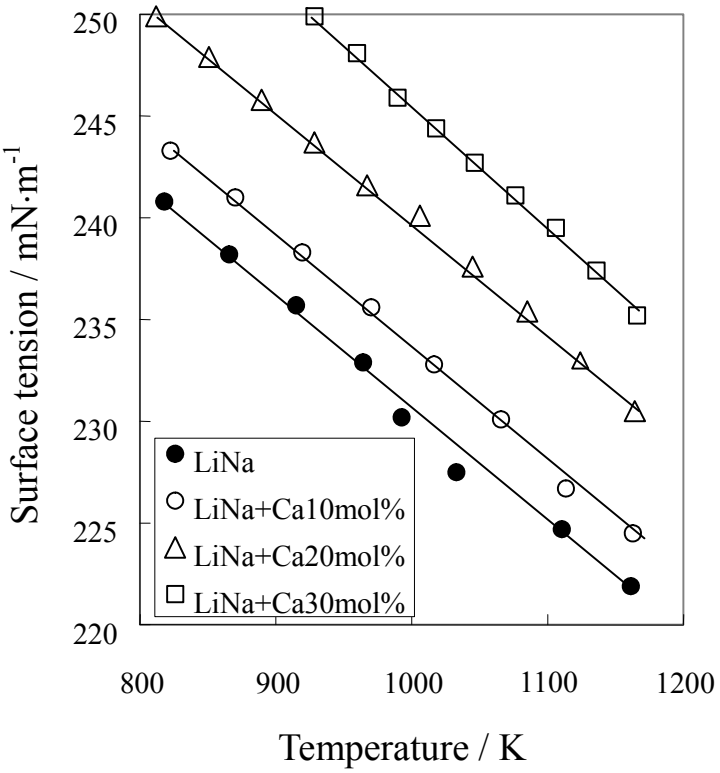

Fig. 3-9. Temperature dependence of the surface tension of $(Li_{0.52}Na_{0.48})_2CO_3$ with added $CaCO_3$ in the amounts of 10, 20 and 30 mol% measured under 1 atm CO_2 atmosphere.

Surface tension of molten carbonates are plotted as a function of temperature in Fig. 3-10 for alkali ion (Rb^+ or Cs^+) addition, Fig. 3-11 for CrO_4^{2-} addition and Fig. 3-12 for SO_4^{2-}, MoO_4^{2-}, WO_4^{2-} and

Cl^- addition, respectively. It was shown that the addition of these additives alkali carbonate mixture resulted in decrease of surface tension of mixture.

Precise measurements of density, surface tension and conductivity had been done for CrO_4^{2-} addition. The results of small amount addition such as 1, 3 or 5 mol% showed that difference in the measurements even 2 mol% composition change. Good resolution of data can be seen clearly in Fig 3-11 for CrO_4^{2-} addition.

Surface tension of carbonate mixtures show linear relationship with temperature for all composition measured in this work. The surface tension of molten salt mixtures decrease linearly with an increase in temperature. Empirical equations for the surface tension, γ (mN m^{-1}), were used as follows,

$$\gamma = a + bT \qquad [3\text{-}4]$$

where T (K) is absolute temperature. These equations fit the measured data well over a wide temperature range. The constants a and b are calculated from experimental data by the method of least mean squares and are given in Table 3-2 for surface tension of single and binary alkali carbonate mixtures, in Table 3-3 for ternary alkali carbonate mixtures, in Table 3-4 for alkali-alkaline earth carbonate mixtures, and Table 3-5 for alkali carbonate containing several additives, respectively.

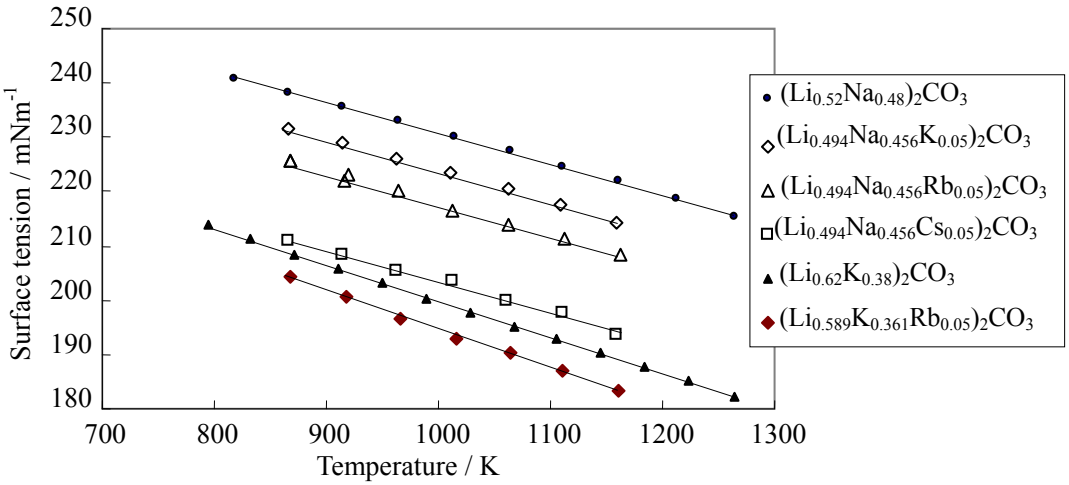

Fig. 3-10. Temperature dependence of surface tension of molten $(Li_{0.52}Na_{0.48})_2CO_3$ and $(Li_{0.62}K_{0.38})_2CO_3$ containing alkali ion (K^+, Rb^+, or Cs^+).

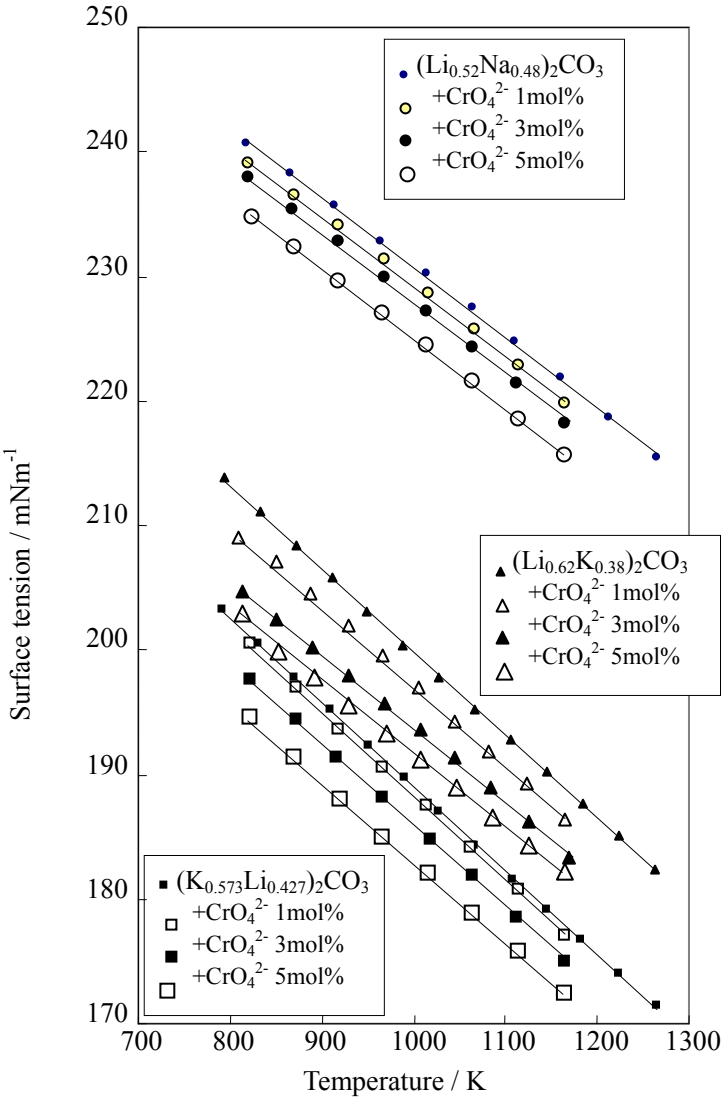

Fig. 3-11. Temperature dependence of surface tension of molten $(Li_{0.52}Na_{0.48})_2CO_3$, $(Li_{0.62}K_{0.38})_2CO_3$ and $(K_{0.573}Li_{0.437})_2CO_3$ containing CrO_4^{2-}.

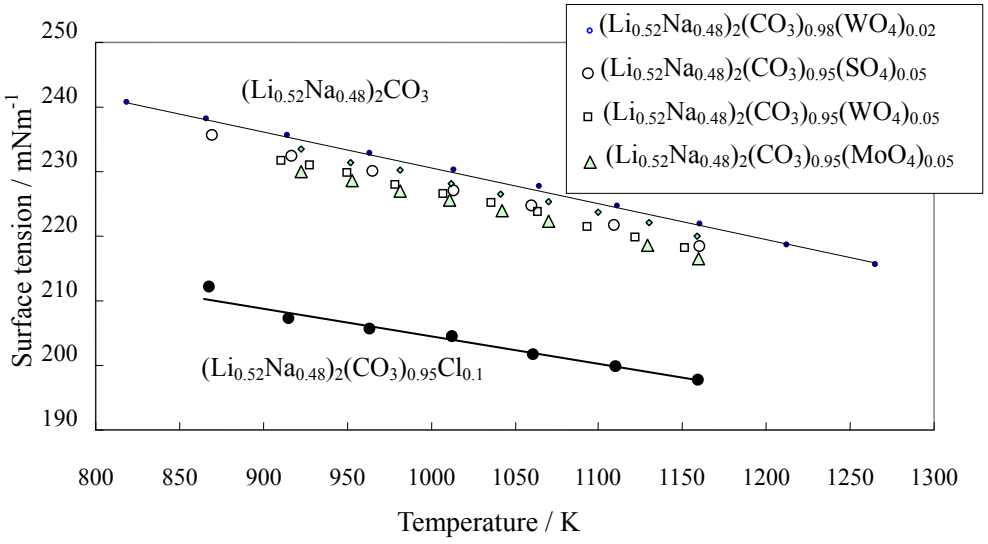

a) molten $(Li_{0.52}Na_{0.48})_2CO_3$ containing SO_4^{2-}, MoO_4^{2-}, WO_4^{2-}, or Cl^-.

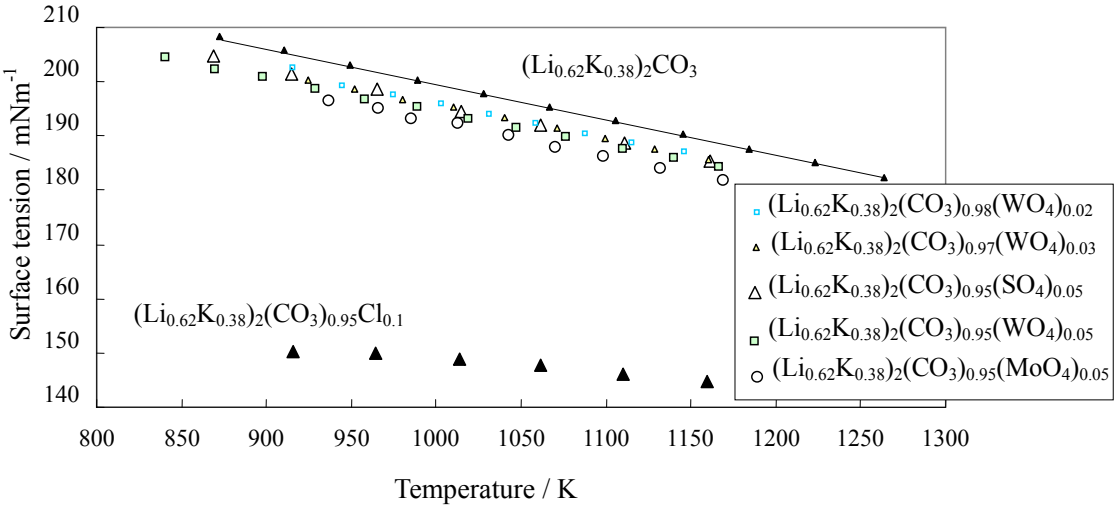

b) molten $(Li_{0.62}K_{0.38})_2CO_3$ and $(K_{0.573}Li_{0.437})_2CO_3$ containing SO_4^{2-}, MoO_4^{2-}, WO_4^{2-}, or Cl^-.

Fig. 3-12. Temperature dependence of surface tension of a) molten $(Li_{0.52}Na_{0.48})_2CO_3$, b) $(Li_{0.62}K_{0.38})_2CO_3$ and $(K_{0.573}Li_{0.437})_2CO_3$ containing SO_4^{2-},

Table 3-2. Surface tension of molten alkali carbonates

Composition (mol%)	Surface tension (mNm^{-1}) $\gamma = a + bT$		Calcurated value at 1173 K (mN/m)	Square of correlation coefficient	Standard deviation	Temperature Range (K)
$Li_2CO_3 : Na_2CO_3$	*a*	*b*	γ_{1173}	r^2	*sd*	T
100 : 0	285.2	-0.04100	237.0	0.992	0.30	1018 - 1235
80 : 20	294.3	-0.05588	228.7	0.998	0.31	940 – 1266
60 : 40	289.7	-0.05622	223.8	0.999	0.24	853 – 1264
52 : 48	287.1	-0.05578	221.6	0.999	0.26	819 – 1265
40 : 60	287.1	-0.05891	217.9	0.999	0.26	881 – 1264
20 : 80	285.7	-0.05997	215.3	0.999	0.18	1028 - 1264
0:100	287.1	-0.06254	213.7	0.999	0.10	1149 - 1286
$Li_2CO_3 : K_2CO_3$						
90 : 10	288.1	-0.06431	212.6	0.996	0.17	992 - 1147
80 : 20	276.1	-0.06215	203.2	0.999	0.22	912 - 1264
62 : 38	266.5	-0.06637	188.7	1.000	0.16	794 - 1264
42.7 : 57.3	256.8	-0.06733	177.8	0.999	0.39	793 - 1265
20 : 80	247.0	-0.06464	171.2	1.000	0.08	1030 - 1263
0:100	244.3	-0.06473	168.4	1.000	0.05	1182 - 1285
$Li_2CO_3 : Rb_2CO_3$						
80 : 20	263.8	-0.06616	186.2	1.000	0.17	911 - 1260
60 : 40	250.5	-0.07025	168.0	0.991	0.99	825 - 1265
40 : 60	236.5	-0.06687	158.0	1.000	0.12	854 - 1266
20 : 80	230.3	-0.06759	151.0	1.000	0.13	1001 - 1261
0:100	226.4	-0.06599	149.0	0.999	0.10	1157 - 1286
$Li_2CO_3 : Cs_2CO_3$	*a*	*b*	γ_{1173}	r^2	sd	T
80 : 20	235.1	-0.06403	160.0	0.999	0.20	926 - 1245
60 : 40	224.6	-0.06892	143.7	0.997	0.52	856 - 1246
40 : 60	205.0	-0.06139	132.9	0.998	0.34	876 - 1266
20 : 80	201.5	-0.06342	127.1	0.998	0.32	952 - 1276
0:100	186.8	-0.05359	124.0	0.998	0.16	1093 - 1285
$Na_2CO_3 : K_2CO_3$						
80 : 20	266.4	-0.05909	197.1	0.999	0.15	1035 - 1227
60 : 40	259.4	-0.06179	186.9	0.999	0.15	995 - 1227
40 : 60	255.5	-0.06563	178.5	1.000	0.10	1023 - 1225
20 : 80	248.7	-0.06426	173.3	1.000	0.01	1093 - 1229
$Na_2CO_3 : Rb_2CO_3$						
80 : 20	253.4	-0.05811	185.3	0.998	0.14	1037 - 1193
60 : 40	243.3	-0.06251	170.0	1.000	0.09	920 - 1193
40 : 60	234.0	-0.06258	160.6	1.000	0.10	918 - 1189
20 : 80	229.9	-0.06496	153.7	1.000	0.08	1036 - 1193
$Na_2CO_3 : Cs_2CO_3$						
80 : 20	223.7	-0.05010	165.0	0.995	0.29	986 - 1189
60 : 40	215.0	-0.05505	150.4	0.999	0.18	879 - 1186
40 : 60	203.2	-0.05643	137.0	0.999	0.20	930 - 1191
20 : 80	199.7	-0.05998	129.3	1.000	0.09	987 - 1189

Table 3-3. Surface tension of molten Li_2CO_3-Na_2CO_3-K_2CO_3 ternary carbonates.

Composition (mol%) Li_2CO_3 : Na_2CO_3: K_2CO_3	Surface tension (mN m^{-1}) $\gamma = a + bT$		Calculated γ value at 1073 K (mN m^{-1})	Square of correlation coefficient	Estimated standard deviation	Temperature range (K)	Estimated γ value with eq. [3-10] (mN m^{-1}) (diff. %)†	Estimated γ value using binary data (mN m^{-1}) (diff. %)‡
	a	b	γ_{1073}	r^2		T		
43.5:31.5:25.0	270.2	-0.06337	202.2	0.999	0.33	770-1163	213.0 (5.4)	202.6 (0.2)
33.3:33.3:33.3	264.8	-0.06443	195.7	0.999	0.19	817-1191	206.6 (5.6)	196.5 (0.5)
40:40:20	271.8	-0.06220	205.1	1.000	0.17	881-1262	215.2 (5.0)	206.5 (0.7)
40:20:40	260.6	-0.06473	191.1	1.000	0.17	837-1271	204.2 (6.9)	192.4 (0.7)
20:60:20	269.4	-0.06212	202.8	1.000	0.15	912-1272	211.7 (4.5)	205.4 (1.2)
20:20:60	256.3	-0.06703	184.4	1.000	0.09	917-1260	191.9 (4.1)	183.9 (-0.3)
49.4:45.6:5.0	280.9	-0.05707	219.7	1.000	0.31	820-1159	226.4 (3.1)	221.1 (0.6)

†: difference % between measured data and those estimated using equation [3-10]

‡: difference % between measured data and those estimated from binary data using equation [3-18]

Table 3-4. Surface tensions of molten alkali - alkaline earth carbonate mixtures.

Composition (mol %)	Surface tension (mN m^{-1}) $\gamma = a + bT$		Calculated value at 1123K (mN m^{-1})	Square of correlation coefficient	Standard Deviation	Temperature range (K)
	a	b	γ_{1123}	r^2	sd	T
Li_2CO_3 : $CaCO_3$						
90:10	291.4	-0.04288	243.2	0.990	0.27	988-1166
80:20	291.3	-0.03925	247.2	0.997	0.17	960-1163
70:30	288.7	-0.03165	253.2	0.974	0.40	953-1163
Li_2CO_3 : $SrCO_3$						
90:10	293.2	-0.04372	244.1	0.99	0.28	988-1163
80:20	294.4	-0.04084	248.5	0.988	0.28	989-1165
70:30	296.7	-0.03687	255.3	0.990	0.19	1027-1165
Li_2CO_3 : $BaCO_3$						
90:10	294.8	-0.04506	244.2	0.994	0.21	990-1165
80:20	297.5	-0.04239	249.9	0.995	0.20	969-1166
70:30	306.0	-0.04495	255.5	0.997	0.20	961-1166
Li_2CO_3 : Na_2CO_3 : $CaCO_3$						
46.8:43.2:10	290.8	-0.05681	227.0	0.998	0.39	822-1211
41.6:38.4:20	294.0	-0.05381	233.6	0.998	0.28	811-1164
36.4:33.6:30	305.8	-0.05995	238.5	0.998	0.24	928-1166
27:63:10	288.5	-0.05753	223.9	0.999	0.17	952-1160
24:56:20	289.6	-0.05506	227.8	0.999	0.09	982-1159
21:49:30	299.8	-0.05900	233.5	0.996	0.23	982-1157
0 : 60:40	299.9	-0.05730	235.6	0.997	0.14	1065-1184
Li_2CO_3 : Na_2CO_3 : $SrCO_3$						
46.8:43.2:10	291.4	-0.05489	229.8	0.999	0.23	812-1169
41.6:38.4:20	297.7	-0.05585	235.0	0.998	0.23	931-1168
36.4:33.6:30	301.3	-0.05422	240.4	0.997	0.20	1017-1166
27:63:10	289.5	-0.05770	224.7	0.999	0.14	950-1155
24:56:20	295.4	-0.05868	229.5	0.999	0.12	979-1157

Table 3-4. (*continued*)

Composition (mol %)	Surface tension (mN m^{-1}) $\gamma = a + bT$		Calculated value at 1123K (mN m^{-1})	Square of correlation coefficient	Standard Deviation	Temperature range (K)
	a	b	γ_{1123}	r^2	sd	T
Li_2CO_3 : Na_2CO_3 : $SrCO_3$						
21:49:30	295.2	-0.05388	234.7	0.997	0.17	1000-1153
0 : 60:40	306.3	-0.06119	237.6	0.992	0.24	1079-1198
Li_2CO_3 : Na_2CO_3 : $BaCO_3$						
46.8:43.2:10	293.4	-0.05663	229.8	0.998	0.27	851-1165
41.6:38.4:20	297.4	-0.05619	234.3	0.997	0.37	853-1165
36.4:33.6:30	300.6	-0.05477	239.1	0.990	0.48	930-1164
27:63:10	286.7	-0.05513	224.8	0.998	0.17	952-1153
24:56:20	295.6	-0.05915	229.2	0.998	0.18	977-1152
21:49:30	294.7	-0.05460	233.4	0.997	0.20	979-1154
0 : 60:40	296.7	-0.05454	235.5	0.996	0.18	1046-1185
Li_2CO_3 : Na_2CO_3 : $(Ca_{0.5}+Ba_{0.5})CO_3$						
46.8:43.2:10	296.5	-0.06041	228.7	0.997	0.55	865-1185
41.6:38.4:20	294.8	-0.05488	233.2	0.998	0.82	864-1180
36.4:33.6:30	302.0	-0.05752	237.4	0.987	0.99	938-1182
Li_2CO_3 : K_2CO_3 : $CaCO_3$						
55.8:34.2:10	271.7	-0.06833	195.0	1.000	0.17	808-1161
49.6:30.4:20	275.3	-0.06768	199.3	1.000	0.10	846-1157
43.4:26.6:30	277.4	-0.06320	206.4	0.997	0.31	923-1156
38.4:51.6:10	262.1	-0.06790	185.8	1.000	0.13	849-1164
34.2:45.8:20	264.5	-0.06660	189.7	1.000	0.11	926-1163
29.9:41.1:30	270.7	-0.06744	195.0	0.999	0.17	1013-1162
0 : 60:40	257.7	-0.06320	186.7	0.998	0.11	1087-1207
Li_2CO_3 : K_2CO_3 : $SrCO_3$						
55.8:34.2:10	269.9	-0.06655	195.2	1.000	0.15	820-1164
49.6:30.4:20	274.7	-0.06627	200.3	0.999	0.18	917-1165
43.4:26.6:30	287.6	-0.07225	206.5	0.997	0.27	987-1134
38.4:51.6:10	262.5	-0.06806	186.1	1.000	0.07	820-1165
34.2:45.8:20	268.6	-0.06982	190.2	0.999	0.18	899-1164
29.9:41.1:30	272.7	-0.06816	196.2	0.997	0.21	929-1165
0 : 60:40	259.9	-0.06396	188.1	0.980	0.26	1141-1202
Li_2CO_3 : K_2CO_3 : $BaCO_3$						
55.8:34.2:10	271.0	-0.06601	196.9	0.999	0.25	883-1162
49.6:30.4:20	275.9	-0.06705	200.6	0.997	0.36	889-1161
43.4:26.6:30	275.3	-0.06162	206.1	1.000	0.11	929-1164
38.4:51.6:10	261.5	-0.06803	185.1	1.000	0.10	812-1166
34.2:45.8:20	268.9	-0.07044	189.8	0.999	0.19	890-1165
29.9:41.1:30	270.7	-0.06622	196.3	0.997	0.33	930-1164
0 : 60:40	262.4	-0.06519	189.2	0.998	0.13	1086-1205

Table 3-5. Experimental equations for surface tension of molten $(Li_{0.52}Na_{0.48})_2CO_3$ and $(Li_{0.62}K_{0.38})_2CO_3$ containing additives.

Composition (mol %)	Surface tension (mN m^{-1}) $\gamma = a + bT$		Calculated value at 923K (mN m^{-1})	Square of correlation coefficient	Standard Deviation	Temperature range (K)
	a	b	γ_{923}	r^2	Sd	T
$(Li_{0.52}Na_{0.48})_2CO_3$			235.6			
$(Li_{0.52}Na_{0.48})_2(CO_3)_{0.99}(CrO_4)_{0.01}$	285.2	-0.05583	233.7	0.999	0.19	820 - 1166
$(Li_{0.52}Na_{0.48})_2(CO_3)_{0.97}(CrO_4)_{0.03}$	285.4	-0.05749	232.3	0.999	0.22	820 - 1164
$(Li_{0.52}Na_{0.48})_2(CO_3)_{0.95}(CrO_4)_{0.05}$	281.3	-0.0563	229.3	1.000	0.14	824 - 1164
$(Li_{0.52}Na_{0.48})_2(CO_3)_{0.95}(MoO_4)_{0.05}$	282.8	-0.05672	230.4	0.996	0.32	923 - 1160
$(Li_{0.52}Na_{0.48})_2(CO_3)_{0.98}(WO_4)_{0.02}$	284.8	-0.05570	233.4	0.998	0.24	923 - 1159
$(Li_{0.52}Na_{0.48})_2(CO_3)_{0.95}(WO_4)_{0.05}$	283.4	-0.05651	231.2	0.998	0.22	911 - 1151
$(Li_{0.52}Na_{0.48})_2(CO_3)_{0.95}(SO_4)_{0.05}$	285.4	-0.05751	232.3	0.999	0.24	870 - 1160
$(Li_{0.494}Na_{0.456}Rb_{0.05})_2CO_3$	277.8	-0.05992	222.5	0.998	0.30	868 - 1162
$(Li_{0.494}Na_{0.456}Cs_{0.05})_2CO_3$	258.7	-0.05506	207.9	0.997	0.51	867 - 1110
$(Li_{0.52}Na_{0.48})_2(CO_3)_{0.95}Cl_{0.1}$	243.6	-0.03944	207.2	0.984	0.44	868 - 1159
$(Li_{0.52}Na_{0.48})_2(CO_3)_{0.95}F_{0.1}$	287.8	-0.05685	235.3	0.999	0.18	873-1169
$(Li_{0.62}K_{0.38})_2CO_3$			205.2			
$(Li_{0.62}K_{0.38})_2(CO_3)_{0.99}(CrO_4)_{0.01}$	262.0	-0.06477	202.2	0.999	0.22	808 - 1164
$(Li_{0.62}K_{0.38})_2(CO_3)_{0.97}(CrO_4)_{0.03}$	253	-0.05923	198.3	0.999	0.22	813 - 1167
$(Li_{0.62}K_{0.38})_2(CO_3)_{0.95}(CrO_4)_{0.05}$	248.7	-0.05714	196.0	1.000	0.11	852 - 1166
$(Li_{0.62}K_{0.38})_2(CO_3)_{0.95}(MoO_4)_{0.05}$	256.8	-0.06409	197.6	0.999	0.34	937 - 1169
$(Li_{0.62}K_{0.38})_2(CO_3)_{0.98}(WO_4)_{0.02}$	258.0	-0.06198	200.8	0.999	0.43	945 - 1145
$(Li_{0.62}K_{0.38})_2(CO_3)_{0.97}(WO_4)_{0.03}$	258.1	-0.06220	200.7	0.999	0.15	924 - 1161
$(Li_{0.62}K_{0.38})_2(CO_3)_{0.95}(WO_4)_{0.05}$	255.6	-0.06110	199.2	0.999	0.18	841 - 1167
$(Li_{0.62}K_{0.38})_2(CO_3)_{0.95}(SO_4)_{0.05}$	261.3	-0.06542	200.9	0.999	0.25	869 - 1162
$(Li_{0.589}K_{0.361}Rb_{0.05})_2CO_3$	265.8	-0.07134	200.1	0.997	0.44	868 - 1161
$(Li_{0.62}K_{0.38})_2(CO_3)_{0.95}Cl_{0.1}$	175.7	-0.02654	151.2	0.994	0.18	965 - 1159
$(Li_{0.62}K_{0.38})_2(CO_3)_{0.95}F_{0.1}$	266.5	-0.06873	203.1	0.999	0.23	853-1169
$(Li_{0.437}K_{0.573})_2CO_3$			194.7			
$(Li_{0.437}K_{0.573})_2(CO_3)_{0.99}(CrO_4)_{0.01}$	255.9	-0.06753	193.6	1.000	0.17	821 - 1164
$(Li_{0.437}K_{0.573})_2(CO_3)_{0.97}(CrO_4)_{0.03}$	251.8	-0.06582	191.0	1.000	0.07	821 - 1165
$(Li_{0.437}K_{0.573})_2(CO_3)_{0.95}(CrO_4)_{0.05}$	247.5	-0.06453	187.9	1.000	0.09	823 - 1164

3.4. Discussion

3.4.1. Surface tension and ionic distance

Smirnov et al. [5] reported that the surface tension of alkali halide shows linear with their cubic root of molar volume. In the case of molten alkali carbonates, we observed also a linear relationship between the surface tension and the cubic root of molar volume as shown in Fig. 3-13.

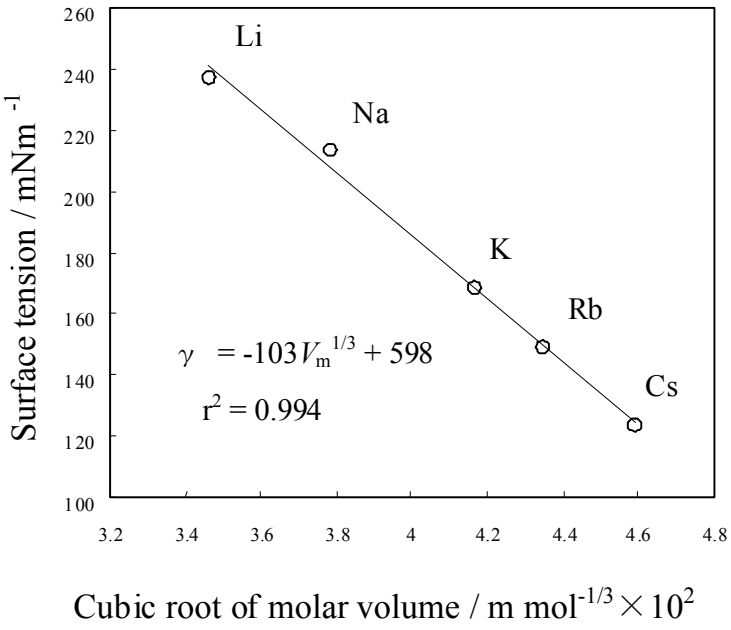

Fig. 3-13. The relationship between the surface tension of alkaline carbonate and their cubic molar volume.

It is observed an apparent linear relationship between the radius[9] of alkali cation and the surface tension of molten alkali carbonate as shown in Fig. 3-14. The surface tension of molten single alkali carbonate decrease with increase of alkali cation's radius. As the radius of cation increase, the distance between cation and anion increase, which resulted in the decrease of coulombic force and the number of ions in unit area. This is the explanation for the decrease of the surface tension lower. The addition of Rb_2CO_3 or Cs_2CO_3 increases molar volume hence the distance between carbonate ions. The change of inter ion distance may decrease anion cation coulombic interaction, hence result in decrease of the surface tension. The larger inter ion distance would change the site of Li^+ or Na^+ ion around carbonate ion suggested by Spedding[10]. This structural change of melt would be the cause of deviation of molar volume from additivity.

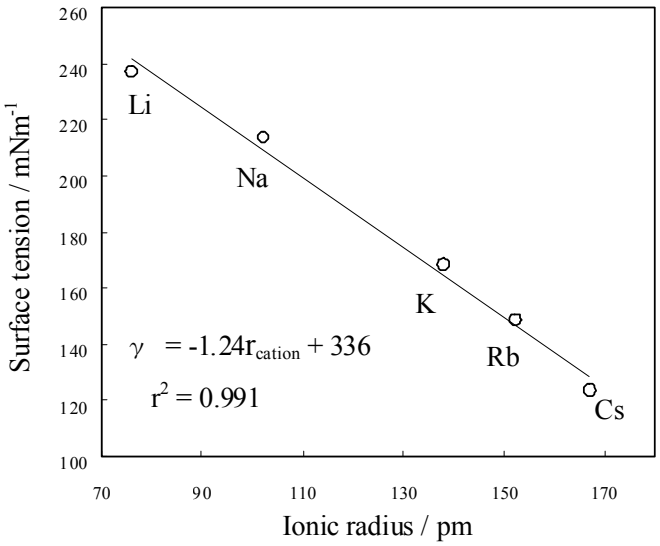

Fig. 3-14. The relationship between the surface tension of alkaline carbonate and ionic radius of alkaline ion.

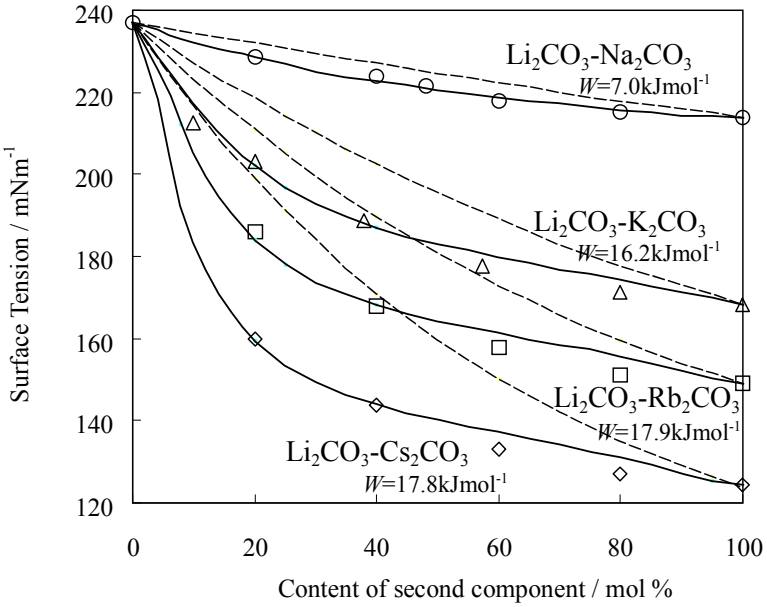

Fig. 3-15. The surface tension of molten Li_2CO_3-Na_2CO_3(○), Li_2CO_3-K_2CO_3(□), Li_2CO_3-Rb_2CO_3(□) and Li_2CO_3-Cs_2CO_3(□) binary carbonate systems at 1173K, and calculated isotherm using Guggenheim's equation for perfect (dash line), and regular solution using interaction parameter, *W*,(solid line).

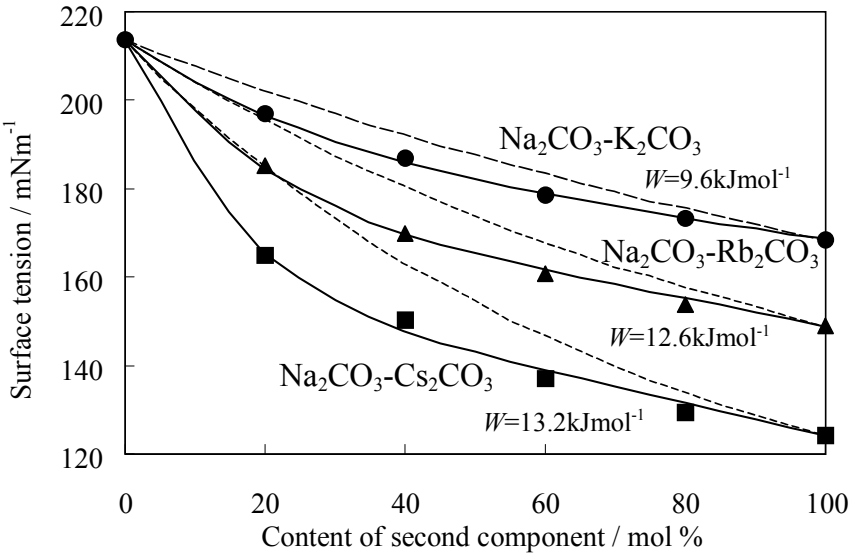

Fig. 3-16. The Surface tension of molten Na_2CO_3-K_2CO_3(●), Na_2CO_3-Rb_2CO_3(▲) and Na_2CO_3-Cs_2CO_3(■) binary carbonate systems at 1173K, and calculated isotherm using Guggenheim's equation for perfect (dash line), and regular solution using interaction parameter, *W*,(solid line).

3.4.2. Surface tension and composition of binary molten alkali carbonate mixtures

The dependence of surface tension on composition measured in molten Li_2CO_3-X_2CO_3 (X= Na, K, Rb and Cs) and Na_2CO_3-Y_2CO_3 (Y= Na, K, Rb and Cs) binary carbonate systems at 1173 K shown in Figs. 3-15 and 3-16, respectively. In any systems it can be seen that the increase of larger cation's content makes the surface tension of the mixture lower. The bigger difference of the cationic size, the more effectively the larger cation decreases the surface tension of the mixture. Therefore, Cs_2CO_3 and Rb_2CO_3 can act as surfactant, which effectively decrease the surface tension of molten carbonate mixture.

Uhlig[1] investigated the relationship between the gas solubility and the surface tension. Blander[11] et al. applied the theory to molten salt and reported that the lower the surface tension, the more gas dissolves into the melt. Therefore the addition of Cs_2CO_3 or Rb_2CO_3 to molten carbonate electrolyte is expected to increase the gas solubility thus increase electroactive species then the performance of MCFC.

The relationship between the surface tension and the composition of binary solution were investigated by Guggenheim[12], Belton and Evans[13]. Using Guggenheim's equation for perfect solution, one can calculate the surface tension of the mixture at any composition only with the value of the surface tension and the molar volume of pure component.

Guggenheim's equation for perfect solution are:

$$\gamma = \gamma_A^0 + (kT/a)\ln(X_A^{'}/X_A) \qquad [3\text{-}5]$$
$$\gamma = \gamma_B^0 + (kT/a)\ln(X_B^{'}/X_B)$$

$$a = X_A(V_A^0/N)^{2/3} + X_B(V_B^0/N)^{2/3} \qquad [3\text{-}6]$$

where γ is the surface tension of binary mixture γ_A^0 and γ_B^0 are the surface tension of pure component A and B, respectively. X_A and X_B are mole fractions of component A and B in the bulk melt. $X_A^{'}$ and $X_B^{'}$ are mole fractions of component A and B at the surface of melt and. a is the average area of molecular at the surface of melt. V_A^0 and V_B^0 are molar volume of pure component A and B, respectively. *N* is Avogadro number. *k* is Boltzmann constant.

Janz and Lorenz[3] used the Guggenheim equation for perfect solution in order to estimate the surface tension of Li_2CO_3-Na_2CO_3 and Li_2CO_3-K_2CO_3 systems. As shown in Figs. 3-15 and 3-16, depicted as dash lines, the measured value in Li_2CO_3-Na_2CO_3 and Na_2CO_3-K_2CO_3 system shows small deviation from estimation, but in other binary systems shows quite large negative deviation from estimated values. Therefore it was found that Guggenheim equation for perfect solution is not to suitable for estimating the surface tension of Li_2CO_3-K_2CO_3 system and alkali binary carbonate systems containing and Rb_2CO_3 or Cs_2CO_3.

Guggenheim also proposed another equation[12] for regular solution on the assumption of a quasi-crystalline model, in which each molecule is arranged on a lattice point and it is distribute randomly in both the bulk and surface layer. It was found that following Guggenheim's equation for regular solution can correlate surface tension and composition with good agreement using the values of the surface tension and molar volume of pure component and fitting values of interaction parameter W, which is related to mixing enthalpies, ΔH_M with an equation of $W = \Delta H_M/(X_A X_B)$. In the following equation $w = W/N$ was used. The w is defined such that if one starts with two pure liquids and interchanges an interior A molecule with an interior B molecule the total increase of potential energy is $2w$.

$$\gamma = \gamma_A^0 + kT/a \cdot \ln(X'_A/X_A) + l(X'^2_B - X_B^2)w/a - mX_B^2 w/a \qquad [3\text{-}7]$$
$$\gamma = \gamma_B^0 + kT/a \cdot \ln(X'_B/X_B) + l(X'^2_A - X_A^2)w/a - mX_A^2 w/a$$

$$\mathrm{a} = X'_A(V_A^0/N)^{2/3} + X'_B(V_B^0/N)^{2/3} \qquad [3\text{-}8]$$

$$X_A + X_B = X'_A + X'_B = 1 \qquad [3\text{-}9]$$

where l and m are the proportions of nearest neighbors which occupy the same lattice plane and the next lattice plane, respectively. Hence they should have the relation of $l+2m=1$. For closed packed structure, l and m are 0.5 and 0.25, respectively, and were used for calculation.

Using W fitted to measured value in each system, unknown values, γ, a, and $X_A^{'}$ (or $X_B^{'}$)

are solved out from equations [3-7] to [3-9] for whole composition. The calculated surface tension γ of binary systems is shown as solid line curves in Figs. 3-15 and 3-16. The calculated curves correlated the measured values with good agreement.

The obtained W are expected to be related to the mixing enthalpies ΔH_M with the equation of $W = \Delta H_M /(X_A X_B)$. Andersen et al. [14] reported the mixing enthalpies in binary molten carbonate systems measured by means of calorimetric experiments. The W calculated from ΔH_M with the equation of $W = \Delta H_M /(X_A X_B)$ are minus ones, while W from surface tension are plus ones. It is found that $W = -\Delta H_M /(X_A X_B)$ should be applied for the Guggenheim's equation instead of $W = \Delta H_M /(X_A X_B)$ in order to correlate the surface tension of the molten binary carbonate systems of this work. The values W from surface tension and calculated from $^{\Delta H_M}$ with the equation $W = -\Delta H_M /(X_A X_B)$ for each binary carbonate systems are listed in Table 3-6. The W of the surface tension show difference from the ones calculated from Andersen's mixing enthalpy. From these results, binary molten carbonate systems of this work are thought to be different from the model system from which Guggenheim's equation is derived. Therefore, the model of Guggenheim's equation can not be fully applied to these systems. It is, however, notable that the Guggenheim's equation for regular solution can correlate between the surface tension of binary alkali carbonate systems and their composition. This equation is still useful from the viewpoint of estimating the surface tension of unknown composition of the binary system.

Table 3-6. Interaction parameter *W* from Andersen[14] and estimated from surface tension result.

Systems	Temperature K	*W* from surface tension kJ·mol^{-1}	*W* from Andersen kJ·mole^{-1}
Li_2CO_3-Na_2CO_3	1178	7.0	10 - 12
Li_2CO_3-K_2CO_3	1178	16.2	27 - 37
Li_2CO_3-Rb_2CO_3	1178	17.9	24 - 39
Li_2CO_3-Cs_2CO_3	1135	17.0	29 - 50
Na_2CO_3-K_2CO_3	1178	9.6	5.1 - 6.3
Na_2CO_3-Rb_2CO_3	1178	12.6	8.1 - 8.6
Na_2CO_3-Cs_2CO_3	1135	13.2	8.4 - 8.9

3.4.3. Surface tension and composition of the mixture in Li_2CO_3-Na_2CO_3-K_2CO_3 ternary system

The surface tension of the Li_2CO_3-Na_2CO_3-K_2CO_3 ternary system at 1073 K is shown in Fig. 3-17 together with contour lines. The relationship between the surface tension and the composition of binary solution were investigated by Guggenheim[12]. This relationship was extended to a ternary molten carbonate. The surface tension (γ) of an ideal solution consisting of components *i* is given by

$$\gamma = -\frac{kT}{s}\ln\left\{\sum_i X_i \exp(-\gamma_i \frac{s}{kT})\right\} \qquad [3\text{-}10]$$

where γ_i is the surface tension of pure component *i*. X_i is the mole fraction of component *i* in the

bulk melt, k is the Boltzmann constant, s is the average area of molecules at the surface of the melt and is given approximately by

$$s \approx \sum_i X_i (V_i / N)^{2/3} \qquad [3\text{-}11]$$

where N is the Avogadro number. Table II shows that the γ values estimated using equation [3-10] were higher than those measured by no more than +7%.

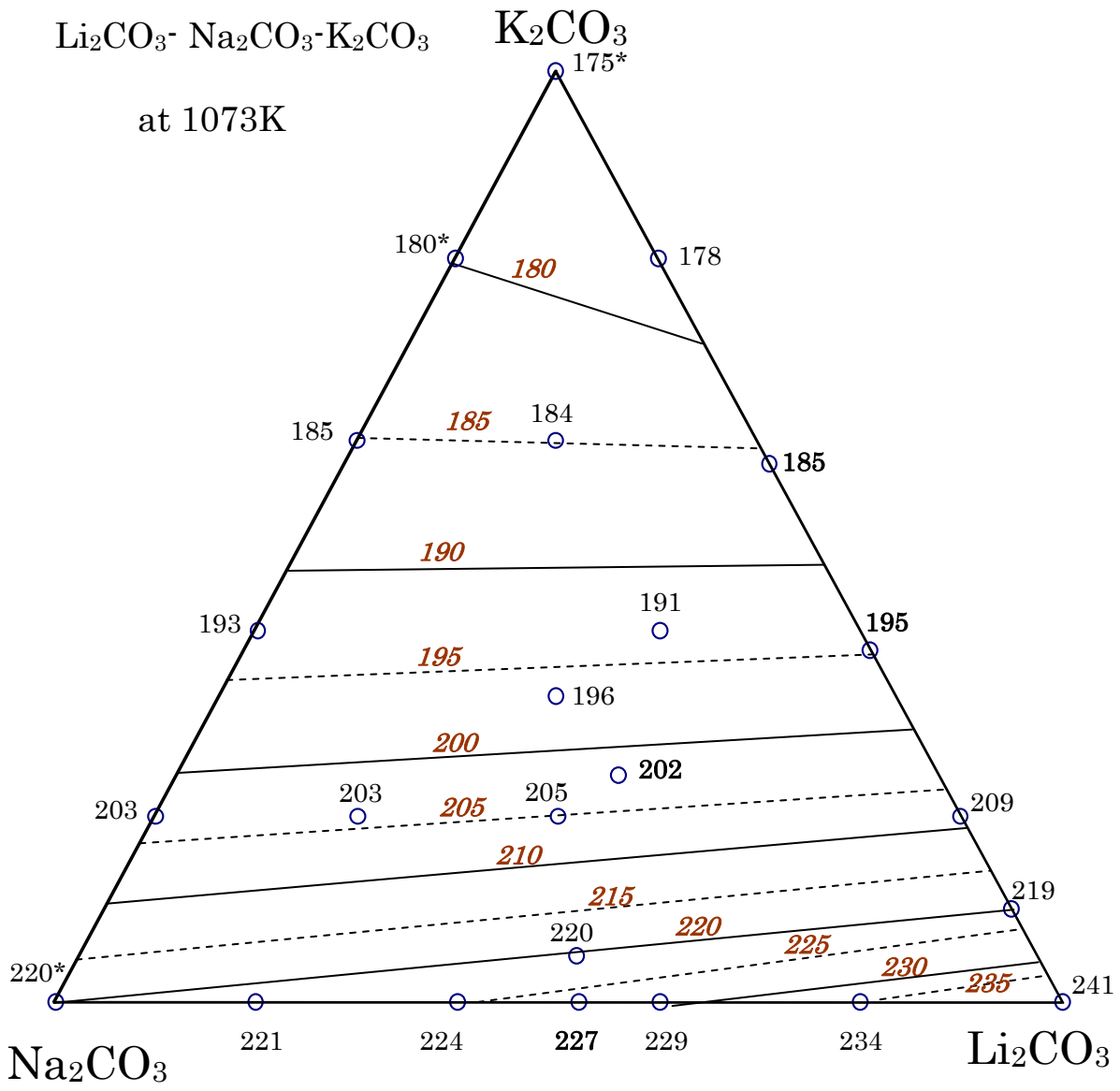

Fig. 3-17. Contour diagram of the surface tension in the molten Li_2CO_3-Na_2CO_3-K_2CO_3 system at 1073 K (mN m^{-1}). (*extrapolated value)

In Fig. 3-17 the contour lines of surface tension are drawn as straight lines between two binary carbonate compositions of the same surface tension calculated from measured binary carbonate data.

It can be seen that such straight contour lines fit well the surface tensions of binary and ternary carbonates. Supposing the contour lines are almost straight, any composition in ternary compositions should lie on a line between two binary carbonates of the same surface tension. Therefore, the surface tension of any composition of Li_2CO_3 - Na_2CO_3 - K_2CO_3 can be calculated using the following method using the data from the three binary carbonate systems, Li_2CO_3-Na_2CO_3, Li_2CO_3-K_2CO_3, and Na_2CO_3-K_2CO_3.

The mole fractions of Li_2CO_3, Na_2CO_3, and K_2CO_3 are set to be x, y, and z, respectively. As $x + y + z = 1$, any composition in the Li_2CO_3-Na_2CO_3-K_2CO_3 system can be depicted as (x, y). Further on, the compositions in the binary systems of Li_2CO_3-Na_2CO_3, Li_2CO_3-K_2CO_3, and Na_2CO_3-K_2CO_3 are depicted as (x_1, y_1), $(x_2, 0)$, and $(0, y_3)$, respectively.

Now we shall consider a line $y = px + q$ which goes through a point of a composition (a, b) of the ternary carbonate mixture using parameters p and q. If the line passes through a composition of binary system Li_2CO_3-Na_2CO_3, (x_1, y_1), then it fulfills the following relationships.

$$b = pa + q: \quad x_1 + y_1 = 1: \quad y_1 = px_1 + q \qquad [3\text{-}12]$$

Therefore

$$(x_1, y_1) = \left(\frac{1 - b + pa}{1 + p}, \frac{b - pa + p}{1 + p}\right) \qquad [3\text{-}13]$$

If the line passes through a composition of binary system Li_2CO_3-K_2CO_3, $(x_2, 0)$, then it fulfills the following relationships.

$$b = pa + q: \quad px_2 + q = 0 \qquad [3\text{-}14]$$

Therefore

$$(x_2, 0) = \left(\frac{pa - b}{p}, 0\right) \qquad [3\text{-}15]$$

Finally, if the line passes through a composition of binary system Na_2CO_3-K_2CO_3, $(0, y_3)$, then it fulfills the following relationships.

$$b = pa + q: \quad y_3 = q \qquad [3\text{-}16]$$

Therefore

$$(0, y_3) = (0, \ b - pa) \qquad [3\text{-}17]$$

If contour lines of surface tension are straight, there exists a line through (a, b) and two of points (x_1, y_1), $(x_2, 0)$, or $(0, y_3)$. The surface tensions of the three compositions are equal. Let us denote the surface tension of a composition (x, y) in a system as $\gamma_{system}(x, y)$. Then $\gamma_{LiNaK}(a, b)$ can be made equal to two of the following three expressions by adjusting p.

$$\gamma_{LiNa}\left(\frac{1 - b + pa}{1 + p}, \frac{b - pa + p}{1 + p}\right): \quad \gamma_{LiK}\left(\frac{pa - b}{p}, 0\right): \quad \gamma_{NaK}(0, \ b - pa) \qquad [3\text{-}18]$$

The values of $\gamma_{LiNa}(x_1, y_1)$, $\gamma_{LiK}(x_2, 0)$, and $\gamma_{NaK}(0, y_3)$ can be obtained from binary data using polynomial functions relating surface tensions and compositions. Therefore, changing the value of p

to produce two equal surface tension allows one to obtain the $\gamma_{LiNaK}(a, b)$ value. Then the line $y = px + q$ indicate the compositions of which surface tension equals to $\gamma_{LiNaK}(a, b)$.

Using the above approach, it was found that the estimated surface tensions of the ternary carbonates listed in Table 3-3 agreed well with the measured data within 1.2%. This result suggested the contour lines in the surface tension plots are indeed almost straight lines. It also means that mixing of two components of the same surface tension makes little change in the surface energy in the Li_2CO_3-Na_2CO_3-K_2CO_3 system. We can summarize this phenomenon in this system by the statement that the mixture of two components A and B of the same surface tension ($\gamma_A = \gamma_B$) shows almost the same surface tension before mixing. Therefore the surface tension of the mixture consists of components A and B of the same surface tension show following relationship:

$$\gamma_A = \gamma_B \approx \gamma_{XA+(1-X)B} \qquad [3\text{-}19]$$

where X is the fraction of A in the mixture.

In Fig. 3-17, the contour lines are calculated using the method above mentioned. As shown in Fig. 6, the contour lines are straight ones and the values of calculated contour lines agree well with measured data.

There have been sporadic reports of the surface tension of common anion molten salt ternary systems, such as $PbCl_2$-NaCl-KCl, $PbCl_2$-KCl-LiCl, [15,16] and LiF-ThF_4-BeF_2 [17]. In these systems, the authors did not report straight contour lines such as we have observed. This difference may be attributable to surface active complexes reported to be present in these systems. The surface active complexes would have relatively weaker interaction and make surface tension lower than that expected without the complexes.

Contour lines in alkali-alkaline earth ternary carbonate systems (Li_2CO_3-Na_2CO_3-MCO_3 and Li_2CO_3-K_2CO_3-MCO_3, M:Ca, Sr, and Ba) seem to be straight as shown in following section.

The surface tension of molten $CaCl_2$-$MgCl_2$-NaCl and $CaCl_2$-$MgCl_2$-KCl systems[8] was calculated using binary data via the above-mentioned methods. The data can be estimated at 1173 K within 6%. Therefore the surface tension of molten $CaCl_2$-$MgCl_2$-NaCl and $CaCl_2$-$MgCl_2$-KCl systems can be described using straight contour lines.

It is expected that in general the surface tensions of common anion molten salt ternary systems that do not contain complex ions can be predicted with good accuracy using above mentioned method and three sets of binary data.

3.4.4. Surface tension of alkali carbonate added alkaline earth carbonate

It has been reported that the equations [3-10] and [3-11] can be fitted well with the reported data of similar systems such as LiCl-$CaCl_2$ and LiCl-$BaCl_2$[8]. Equations [3-10] and [3-11] were fitted to the experimental data of molten binary Li_2CO_3-alkaline earth carbonates as shown in Fig. 3-18. From

these equations hypothetical surface tensions of molten single alkaline earth carbonates were estimated and are summarized in Table 3-7. The surface tensions of molten single carbonates follow the order of $BaCO_3$ > $SrCO_3$ > $CaCO_3$ > Li_2CO_3 > Na_2CO_3 > K_2CO_3 > Rb_2CO_3 > Cs_2CO_3. Such an order also can be seen for their chlorides, bromides, and iodides[8].

The estimated surface tension for binary Na_2CO_3 - $AeCO_3$ (Ae =Ca, Sr, and Ba) and K_2CO_3 - $AeCO_3$ using equations [3-10] and [3-11] and data in Table 3-4, however, showed a positive deviation from measured data at 1123K by about 3% for Na_2CO_3 - $AeCO_3$ (Na:Ae = 60:40 mol%) and about 7% for K_2CO_3 - $AeCO_3$ (K:Ae = 60:40 mol%). These deviations may arise from non-ideality in these systems.

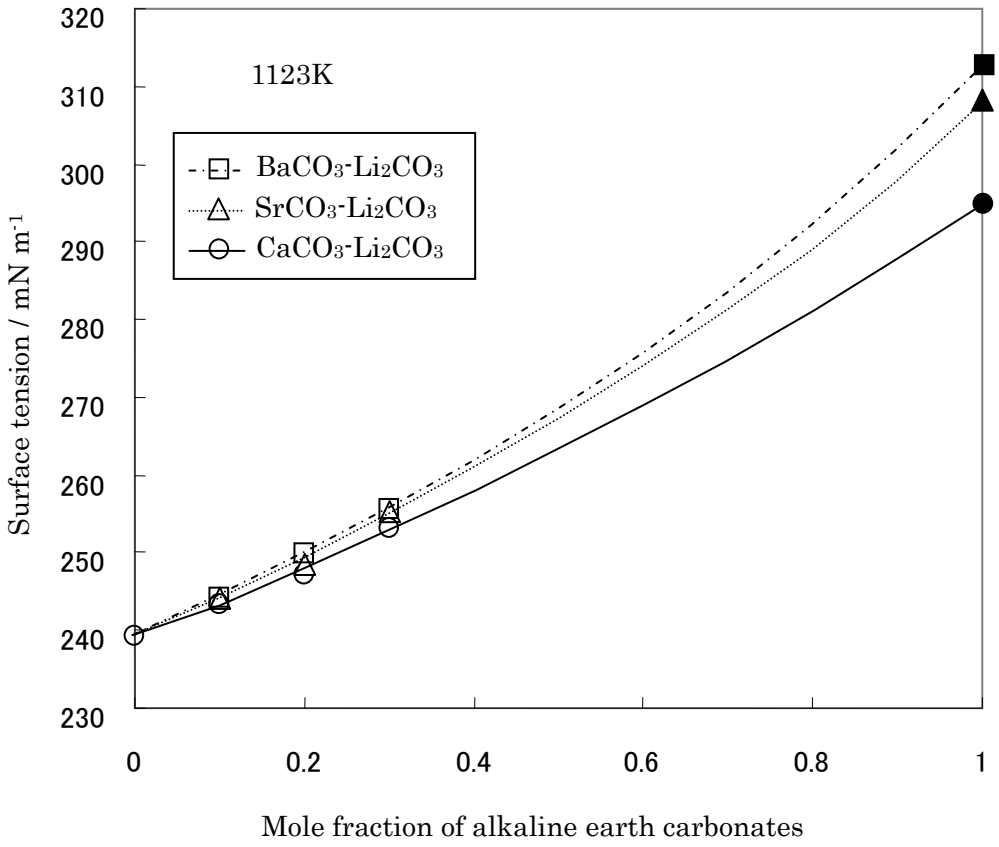

Fig. 3-18. The surface tension of Li_2CO_3-alkaline earth carbonates shown as open points and estimated value fitted to Guggenheim's equation shown as lines and solid points.

The surface tension of molten carbonate mixtures containing added alkaline earth carbonates increased linearly with an increase in the mole fraction of alkaline earth carbonate as shown in Fig 3-19. Therefore the empirical equation for estimating the surface tension of the mixture can be written as

$$\gamma_{mix} = \gamma_{alkali} + \lambda X_{A.E.} \qquad [3\text{-}20]$$

where γ_{alkali} is the surface tension of the molten alkali carbonate mixture before addition of alkaline earth carbonate and γ_{mix} is that for a mixture with added alkaline earth carbonate having a mole fraction, $X_{A.E.}$. λ is the slope of the plot $\gamma_{mix} - \gamma_{alkali}$ v.s. $X_{A.E.}$.

Table 3-7. Hypothetical surface tension of molten alkaline earth carbonates.

Alkaline earth carbonate	Surface tension (mNm^{-1}) $\gamma = a' + b'T$		Calculated value at 1123K (mNm^{-1})
	a'	b'	γ_{1123}
$CaCO_3$	315.0	-0.0180	294.8
$SrCO_3$	357.9	-0.0452	307.1
$BaCO_3$	411.3	-0.0880	312.5

It was found that equation [3-20] with a value of λ can be used to estimate the surface tension in the whole ternary system as shown in Fig. 3-20 within an error of about 1%. The values of λ were obtained for 6 ternary carbonate systems as listed in Table 3-8. The measured surface tensions and calculated contour diagrams for Li_2CO_3-Na_2CO_3-$CaCO_3$ at 1123K are shown in Fig. 3-21. It can be seen that the calculated contour diagrams agree well with the measured values.

The increase in the surface tension by the addition of an alkaline earth carbonate depends only on the mole fraction of the alkaline earth carbonate. This means that, for the increase in surface tension, the interaction between an alkaline earth ion and a carbonate ion is more important than that between an alkaline earth ion and alkali ions.

Table 3-8. The parameter λ of the relationship $\gamma_{mix} = \gamma_{alkali} + \lambda X_{AE}$, for molten Li_2CO_3-Na_2CO_3 or Li_2CO_3-K_2CO_3 containing alkaline earth (Ca, Sr or Ba) carbonates at 1123K.

Ternary carbonate systems	λ ($mN \cdot m^{-1}$mole-fraction^{-1})	Square of correlation coefficient r^2
Li_2CO_3-Na_2CO_3-$CaCO_3$	45.16	0.98
Li_2CO_3-Na_2CO_3-$SrCO_3$	51.56	0.99
Li_2CO_3-Na_2CO_3-$BaCO_3$	49.01	0.98
Li_2CO_3-K_2CO_3-$CaCO_3$	42.54	0.96
Li_2CO_3-K_2CO_3-$SrCO_3$	46.39	0.96
Li_2CO_3-K_2CO_3-$BaCO_3$	47.78	0.97

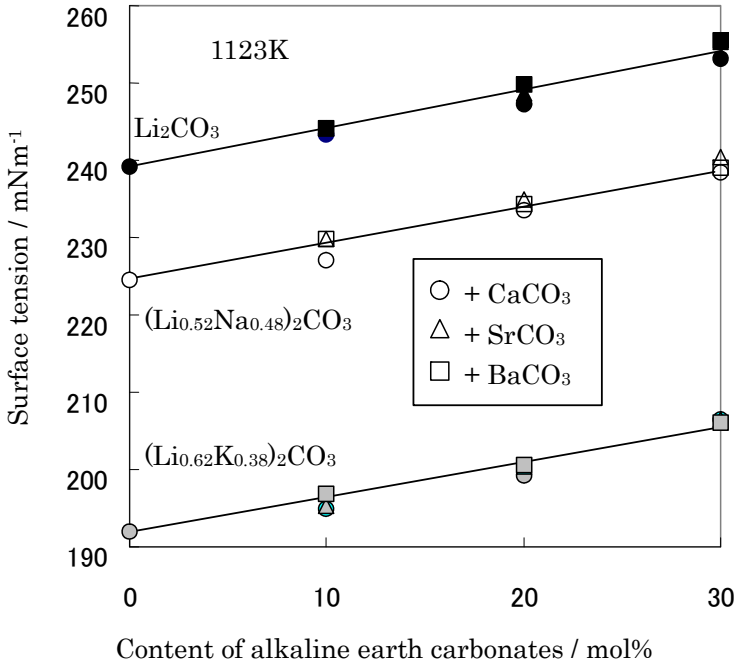

Fig. 3-19. Surface tension of molten carbonate mixtures Li_2CO_3, $(Li_{0.52}Na_{0.48})_2CO_3$, and $(Li_{0.62}K_{0.38})_2CO_3$ with an added alkaline earth carbonate ($CaCO_3$, $SrCO_3$, and $BaCO_3$) at 1123K.

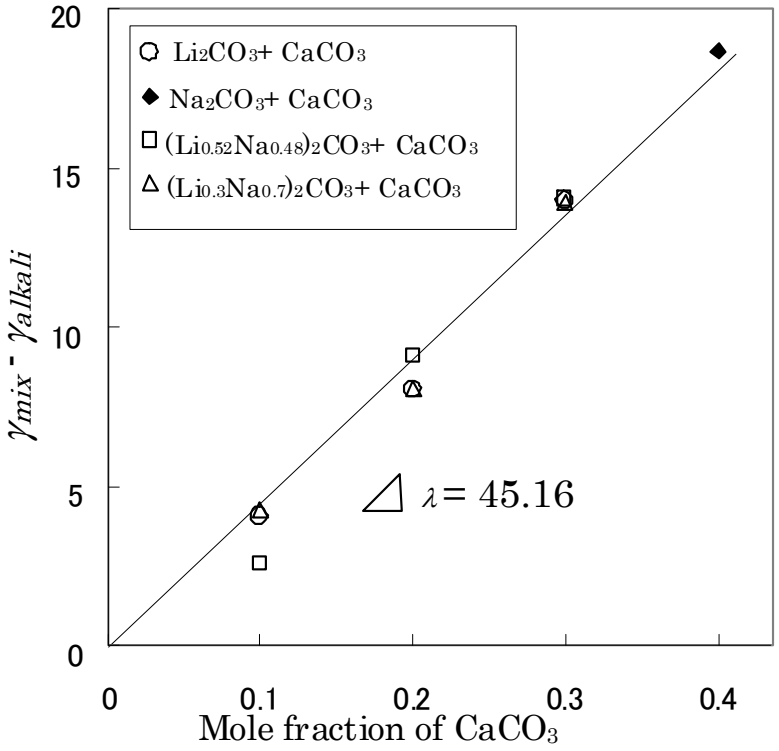

Fig. 3-20. $\gamma_{mix} - \gamma_{alkali}$ as a function of the mole fraction of $CaCO_3$ for molten Li_2CO_3-Na_2CO_3-$CaCO_3$ system at 1123K .

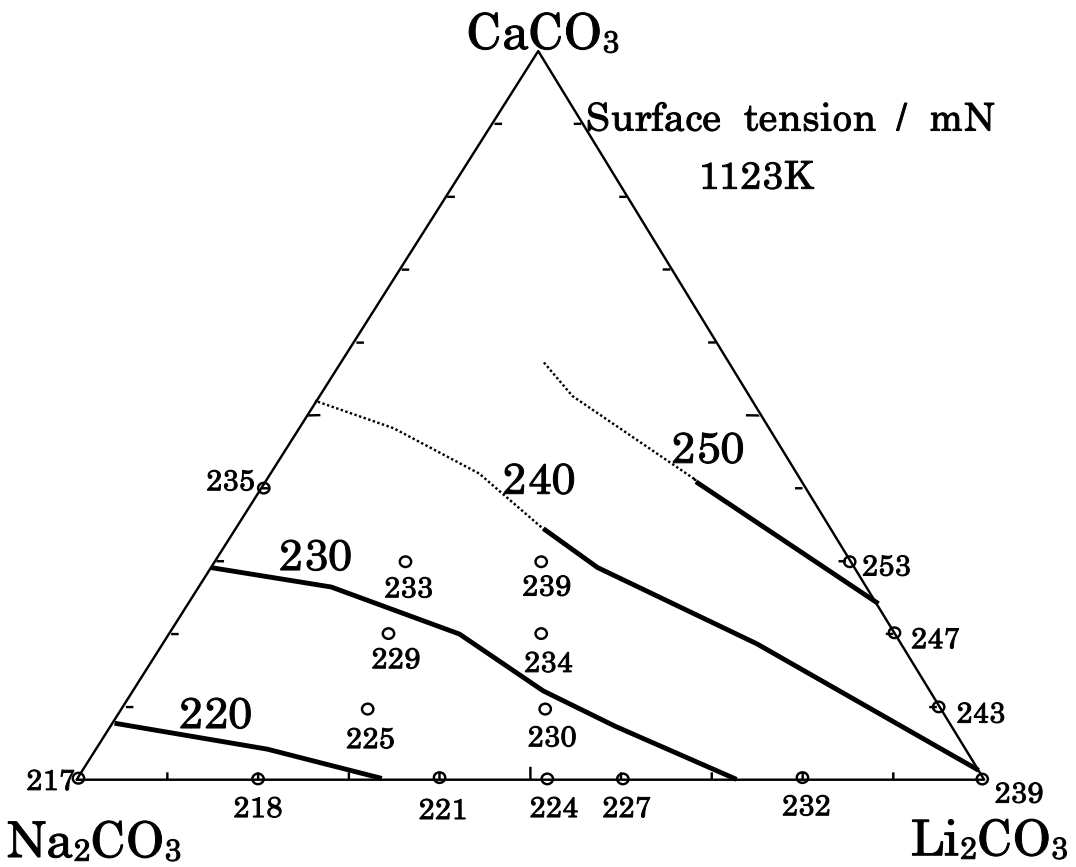

Fig. 3-21. The surface tension of molten Li_2CO_3-Na_2CO_3-$CaCO_3$ at 1123K and a calculated contour diagram using the relationship $\gamma_{mix} = \gamma_{alkali} + \lambda X_{AE}$.

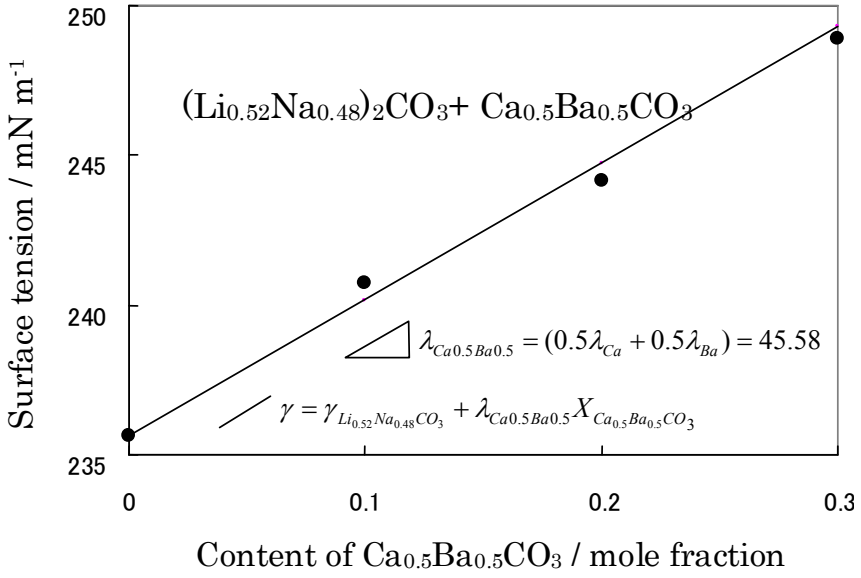

Fig.3-22. Surface tension of $(Li_{0.52}Na_{0.48})_2CO_3$ with added $Ca_{0.5}Ba_{0.5}CO_3$ at 923K and estimated values shown as a line.

3.4.5. *Estimation of surface tension of quaternary system*

Recently it has been reported that quaternary carbonate mixtures such as $(Li_{0.52}Na_{0.48})CO_3+Ca_{0.5}Ba_{0.5}CO_3$ (in the amounts of 10, 20 and 30 mol%) are promising as MCFC electrolytes[18].

The surface tension of $(Li_{0.52}Na_{0.48})CO_3$-$Ca_{0.5}Ba_{0.5}CO_3$ at 923K was estimated by equation [3-20] using $\lambda_{Ca0.5Ba0.5}$, which is an average of the λs for $CaCO_3$ and $BaCO_3$, obtained through the plots like Fig. 3-22 at 923K. The estimated values showed good agreement with measured data within an error of 0.3% as shown in Fig. 3-22.

3.5. Conclusion

The surface tension of molten carbonate mixtures were measured using maximum bubble pressure technique. The accuracies of the measurements were estimated to be $\pm 1.0\%$ for surface tension measurements.

It was found that there is a linear relationship between the surface tension of molten alkali carbonates and the cubic root of molar volume or cation radius.

The addition of Rb_2CO_3 or Cs_2CO_3 to Li_2CO_3 or Na_2CO_3 resulted in decrease of the surface tension of mixtures. Cs_2CO_3 and Rb_2CO_3 can be surfactant, which effectively decreases the surface tension of molten carbonate thus would increase gas solubility.

At constant temperature, the relationship between composition and measured surface tension in all binary carbonate systems is correlated by Guggenheim's equation for regular solution using interaction parameter W.

The addition of Rb_2CO_3 or Cs_2CO_3 increase the distance between carbonate ions in the surface layer. This would not only make surface tension lower but also by mixing with Li_2CO_3 bring the structural change of melt and result in deviation of molar volume from additive property.

It was shown that a mixture of two components having the same surface tension has almost the same surface tension in the Li_2CO_3-Na_2CO_3-K_2CO_3 system. It has been found that the estimated surface tension of ternary carbonates agreed well with measured data within 1.2%.

The addition of alkaline earth carbonates resulted in an increase in surface tension of molten carbonate mixtures.

The surface tension of alkali-alkaline earth ternary systems increased linearly with an increase in the alkaline earth carbonate content. The gain of surface tension by adding an alkaline earth carbonate is proportional to its mole fraction. The ratios of gain of surface tension to mole fraction of an alkaline earth carbonate depend on the carbonate system and are obtained from the data of mixtures in ternary molten carbonate systems. Using these ratios, the surface tension of an alkali-alkaline earth carbonate mixture can be estimated with good agreement.

These methods for estimating the surface tension of molten alkali - alkaline earth carbonates can be

extended to multi-component systems and lower temperature than the melting point of single molten carbonates with good agreement.

Reference

[1] H. H. Uhlig, *J. Phys. Chem.*, **41**, 1215 (1937).

[2] G. J. Janz and M. R. Lorenz, "Precise Measurement of Density and Surface Tension at Temperatures up to 1000 °C in one Apparatus," *Rev. Sci. Instr.*, **31**, 18-22 (1960).

[3] G. J. Janz and M. R. Lorenz, "Molten carbonate electrolytes: physical properties, structure, and mechanism of electrical conductance," *J. Electrochem. Soc.*, 108, 1052 (1961).

[4] A. T. Ward and G. J. Janz, "Molten carbonate electrolytes: electrical conductance, density and surface tension of binary and ternary mixtures," *Electrochimica Acta*, 10, 849 (1965).

[5] M. V. Smirnov and V. P. Stepanov, *Electrochimca Acta*, **27**, 1551 (1982).

[6] Q. Liu and R. A. Lange, *Contrib. Mineral Petrol.*, **146**, 370 (2003).

[7] R. Schrödinger, *Ann. Physik*., **46**, 413 (1915).

[8] G. J. Janz, *J. Phys. Chem. Ref. Data*, **17**, 1 (1988).

[9] R. D. Shannon, *Acta Crystallogr., Sect. A: Cryst. Phys., Diffr., Theor. Gen. Crystallogr*., **A32**, 751 (1976).

[10] P. L. Spedding, *J. Electrochem. Soc*., **117**, 177 (1970).

[11] M. Blander, W. R. Grimes, N. V. Smith and G. M. Watson, *J. Phys. Chem.*, **63**, 1164 (1959).

[12] E. A. Guggenheim, *Trans.Farad. Soc.*, **41**, 150 (1945).

[13] M. Blander, W. R. Grimes, N. V. Smith and G. M. Watson, *J. Phys. Chem.*, **63**, 1164 (1959).

[14] B. K. Andersen and O. J. Kleppa, *Acta Chem. Scand.* **A 30**, 751 (1976).

[15] T. Fujisawa, T. Utigard, and J. M. Toguri, *Can. J. Chem.*, **63**, 1132 (1985).

[16] G. Liu, T. Utlgard, and J. M. Toguri, *J. Chem. Eng. Data*, **31**, 342 (1986).

[17] K. Yajima, H. Moriyama, Y. Tominaga, T. Hara, and J. Oishi, *J. Chem. Eng. Data* **29**, 122 (1984).

[18] A. C. Schoeler, T. D. Kaun, I. Bloom, M. Lanagan, and M. Krumpelt, *J. Electrochem. Soc*., **147**, 916(2000).

4. Electrical Conductivity of Molten Carbonates

4-1. Introduction

One of physical properties of molten carbonates, electrical conductivity of molten carbonates determines resistance of electrolyte and directly affects the output of Molten Carbonate Fuel Cell. Furthermore, electrical conductivity of molten carbonate is important not only for the good choice of new electrolyte, but also for better understanding of the behavior of ionic species in the melt. There are, however, few known data of electrical conductivity of molten carbonate mixtures.

For the study of the electrical conductivity of molten carbonate, Janz and Lorenz[1], Ward and Janz [2],and Spedding[3] reported single alkali, binary and ternary alkali carbonate systems of Li_2CO_3, Na_2CO_3, K_2CO_3.

No data have been reported for binary and ternary carbonate mixtures containing Rb_2CO_3, Cs_2CO_3, $CaCO_3$, $SrCO_3$, $BaCO_3$ and the mixtures added with MO_4^{2-} (SO_4^{2-}, CrO_4^{2-}, MoO_4^{2-}, and WO_4^{2-}).

In this section, several molten carbonate mixtures mentioned at section 1.5 are investigated for electrical conductivity measurement. The influence of ionic size to physical properties of cations (Li^+, Na^+, K^+, Rb^+, Cs^+, Ca^{2+}, Sr^{2+}, and Ba^{2+}) and additives MO_4^{2-} (SO_4^{2-}, CrO_4^{2-}, MoO_4^{2-}, and WO_4^{2-}) was interesting for predict unknown data and understanding the nature of molten salts. I will present interesting relationship between electrical conductivity and composition in ternary molten carbonate system.

4.2. Experimental

4.2.1. Measurement method for the electrical conductivity of molten carbonates

For the measurement of electrical conductivity of molten salt, AC two probe technique utilizing vertical capillary cell is popular. Janz et al.[1-2], and Spedding[3] used MgO single crystal capillaries and AC bridge. Janz et al. utilized AC of frequency 1, 2, 5, and 20 kHz, and Spedding utilized 2kHz-40kHz.. In this thesis, I also adopted AC two probe technique and utilize high purity alumina conductance cell and impedance measurement using Frequency Response Analyzer (FRA) utilizing 10 Hz to 10^6 Hz.

Recently, Kim[4] also used FRA but they use unique method utilizing movable electrodes in capillaries for the measurement of molten fluorides. Schematic diagrams of measurements are shown in Fig. 4-1. In capillary cell of AC two probe technique, electrodes do not move. On the other hand, movable electrodes show increase resistance with increase of molten salt path length by drawing-up electrode. The difference of resistance by known length of electrode displacement has direct relationship to the resistance of molten salt inside capillary of known length without impedance of electrode-molten salt interface.

In this work, movable electrode method also used to verify result.

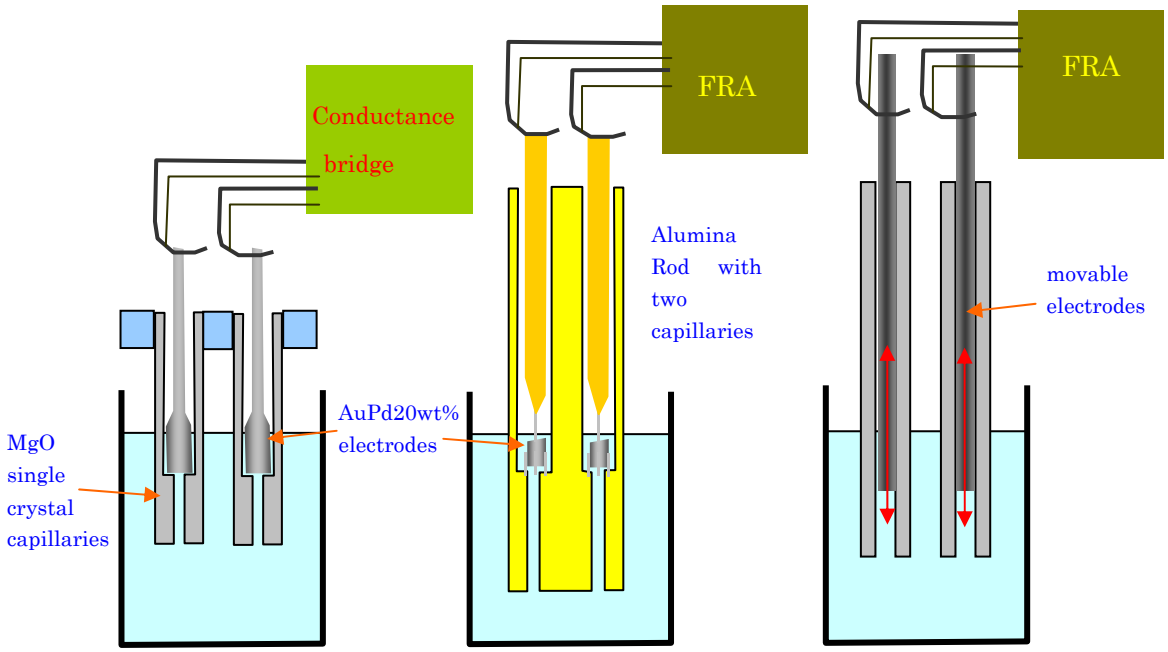

Fig. 4-1. Measurement methods of electrical conductivity of molten salts, a)Janz et al. and Spedding, b) This work, c)Kim and Sadoway et al.

4.2.2. Measurement procedures

The sample preparation method is the same as section 2.2.3 except for crucible size, 20mmOD 40mm h containing about 12 cm^3 molten salt.

The electrical conductivity of molten alkali carbonates were measured in the temperature range from about 1100 K to a temperature higher than their liquidus by 30 K.

Sample temperatures were as measured by a Platinel thermocouple covered with an alumina tube that was inserted into the sample melts.

The measurements were made by an AC two probe technique and AC impedance spectroscopy using a Solatron 1186 electrochemical interface and a Solatron 1170 frequency response analyzer (FRA). The frequency range of the impedance measurements was from 10 Hz to 10 kHz. In the Nyquist plots of impedance a part of one semicircle appeared. The higher frequency intercept of the semicircle with the real axis was taken to be the resistance of the electrolyte[5].

A conductance cell with two capillaries which were machined in a sintered high purity Al_2O_3 rod was used in these measurements, and its cell constant was designed to be about 200 cm^{-1}. Two Au-Pd (80:20wt%) alloy electrode were used as probes in the cell. The cell constant were calibrated using standard materials of molten KNO_3 and molten NaCl[6]. The values of cell constant measured in each standard materials accorded well within ±1%.

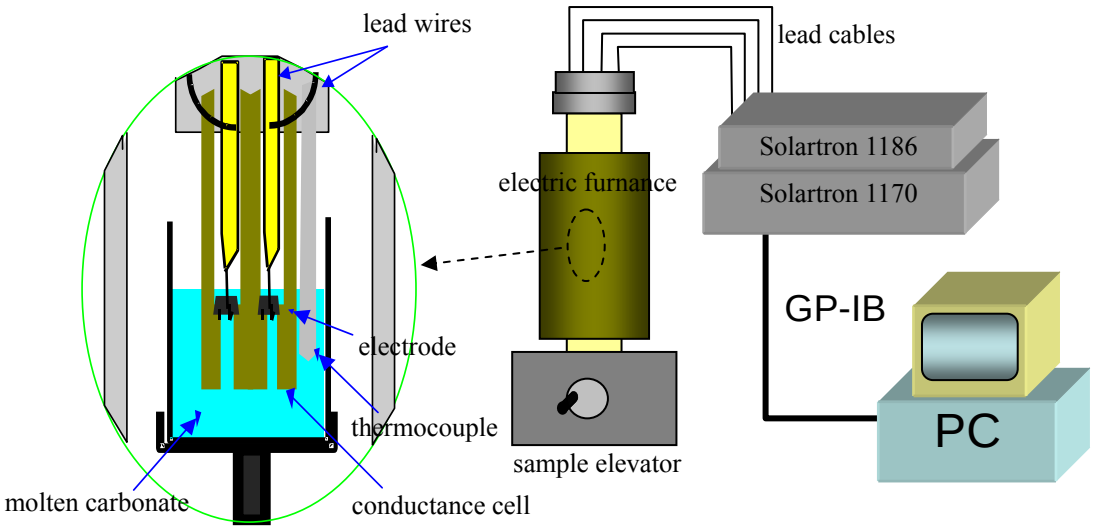

Fig. 4-2. Measurement apparatus for electrical conductivity of molten carbonate mixtures

4.3. Results

4.3.1. Temperature dependence of electrical conductivities of molten carbonates

The temperature dependencies of the conductivity are shown for molten single carbonate in Fig. 4-3. A comparison of our data with that in the literature showed good agreement for Li_2CO_3 and K_2CO_3[1,3]. However the datum for Na_2CO_3 was lower than the reported value by 3%[1,3]. For binary carbonates, the results of Li_2CO_3-Rb_2CO_3, Li_2CO_3-Cs_2CO_3, Na_2CO_3-Rb_2CO_3, and Na_2CO_3-Cs_2CO_3 are shown in Figs. 4-4 to 4-7, respectively.

The conductivities of binary systems of molten Li_2CO_3 - X_2CO_3 (X: Na, K, Rb, and Cs) and Na_2CO_3 - Z_2CO_3 (Z: K, Rb, and Cs) at 1173 K, are shown in Figs. 4-8 and 4-9, respectively. The data for binary carbonates measured in this work also showed good agreement with those reported by Ward and Janz[2], but there were some discrepancies in the Li_2CO_3-K_2CO_3 system, especially for Li-rich compositions reported by Spedding[3]. Spedding measured the resistance of the cell by AC bridge utilizing 2 kHz - 40 kHz signal and used standard material of KCl aqueous solution, while we used a FRA utilizing AC signal of 1 Hz - 10 kHz and standard materials of molten KNO_3 and NaCl. The discrepancy of the data may arise from the difference of experimental arrangement or technique such as standard material, measurement circuit and measurement frequency.

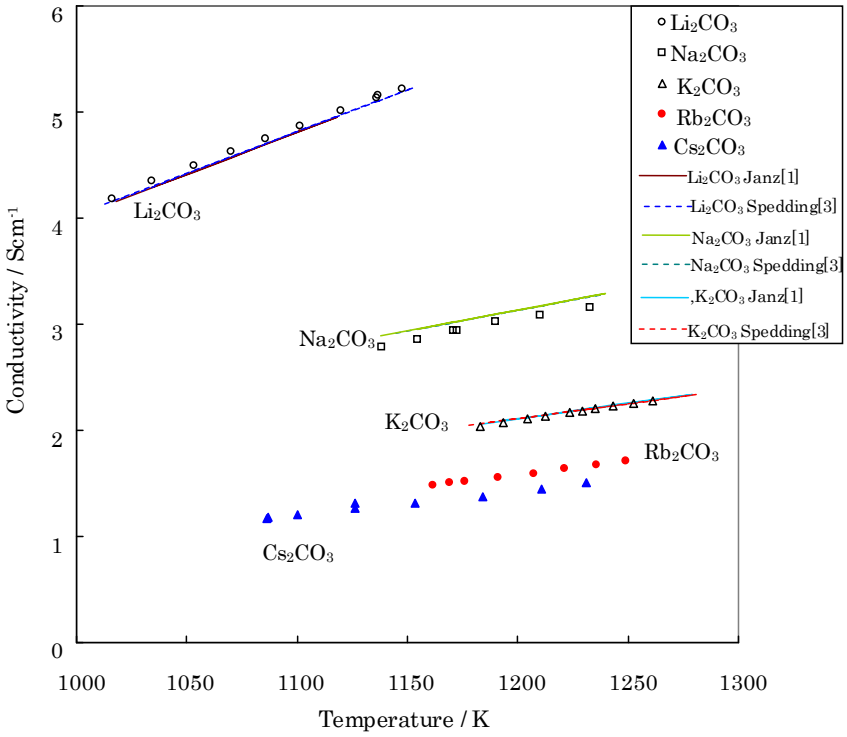

Fig. 4-3. Temperature dependence of electrical conductivity of molten carbonates.

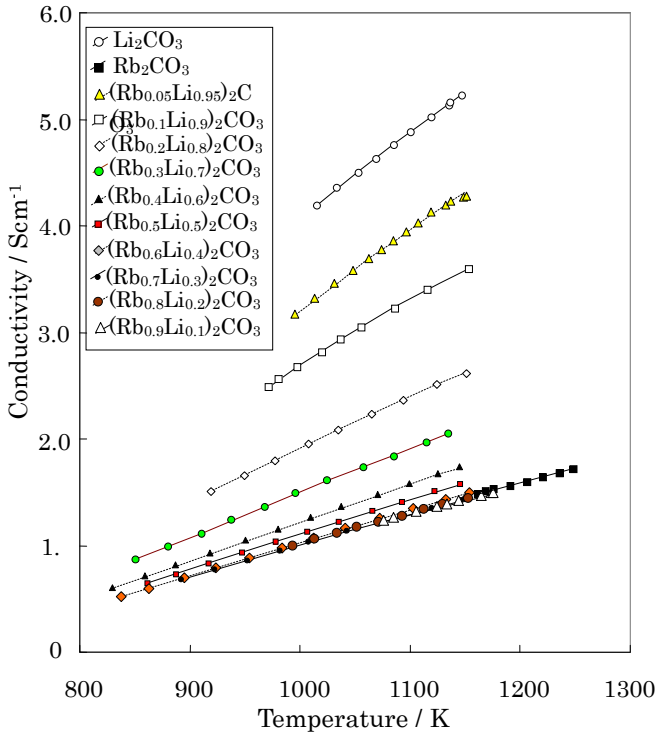

Fig. 4-4. Temperature dependence of the conductivity of molten alkali carbonates: Li_2CO_3-Rb_2CO_3 mixtures.

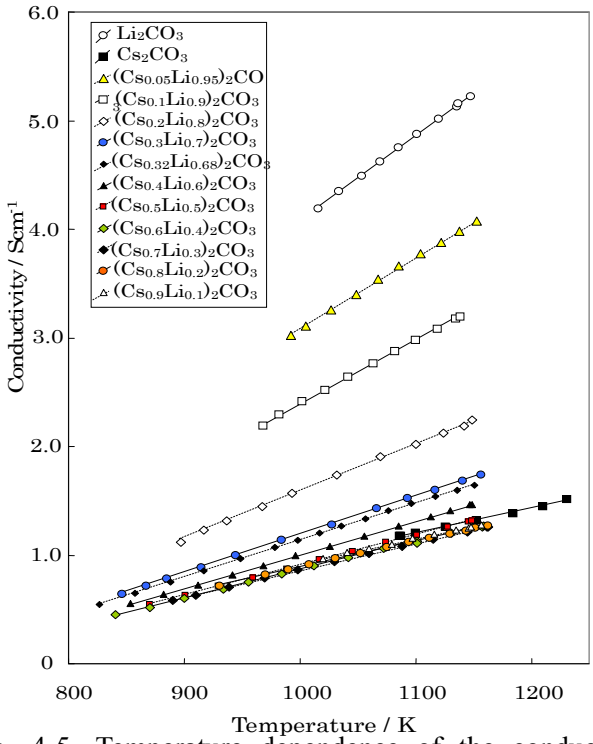

Fig. 4-5. Temperature dependence of the conductivity of molten alkali carbonates: Li_2CO_3-Cs_2CO_3 mixtures.

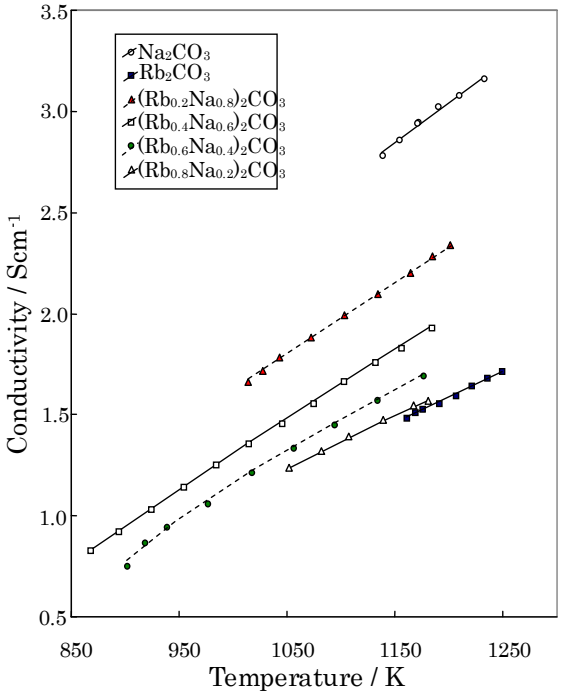

Fig. 4-6 Temperature dependence of the conductivity of molten alkali carbonates: Na_2CO_3-Rb_2CO_3 mixtures.

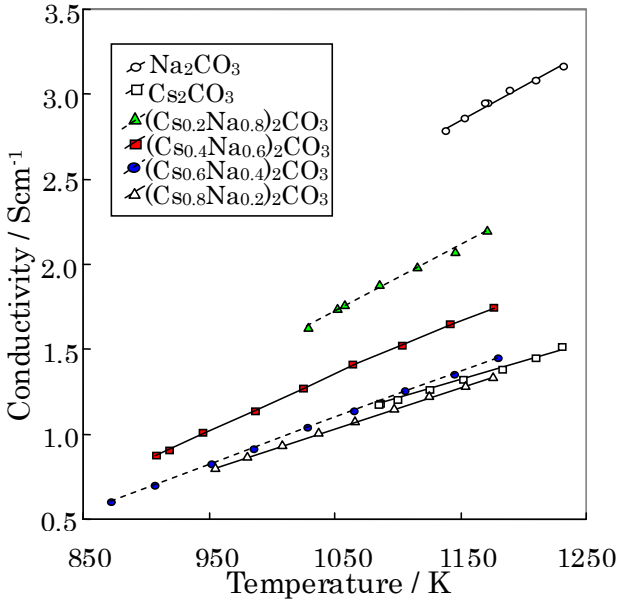

Fig.4-7. Temperature dependence of the conductivity of molten alkali carbonates: Na_2CO_3-Cs_2CO_3 mixtures.

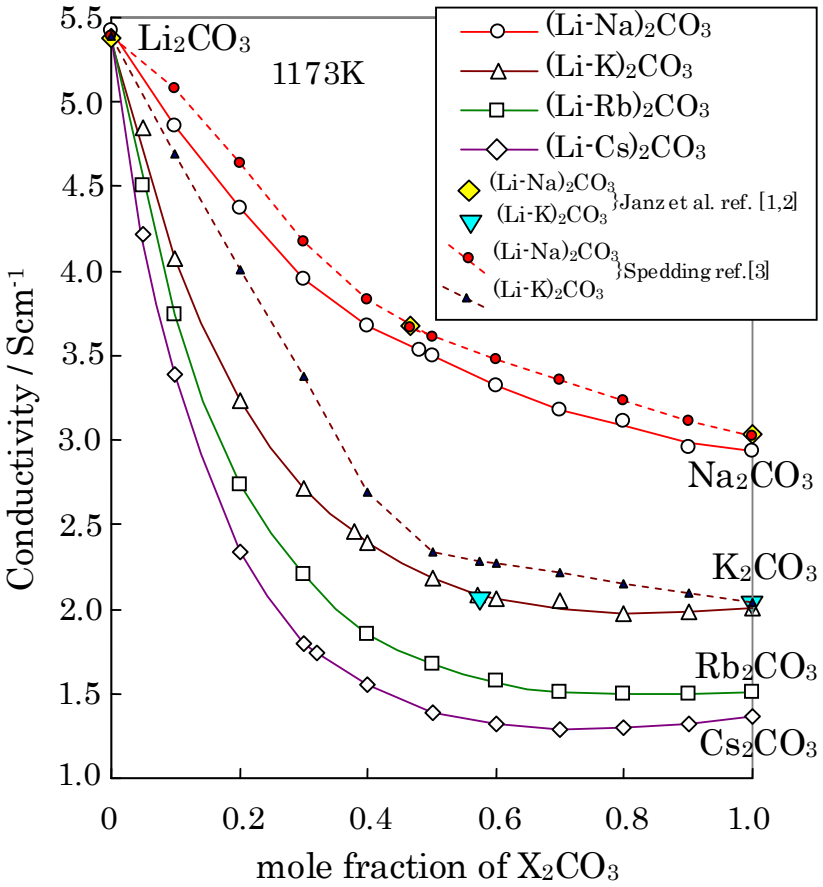

Figure 4-8. The conductivity of the binary molten carbonates Li_2CO_3-X_2CO_3 (X: Na, K, Rb, and Cs) at 1173 K

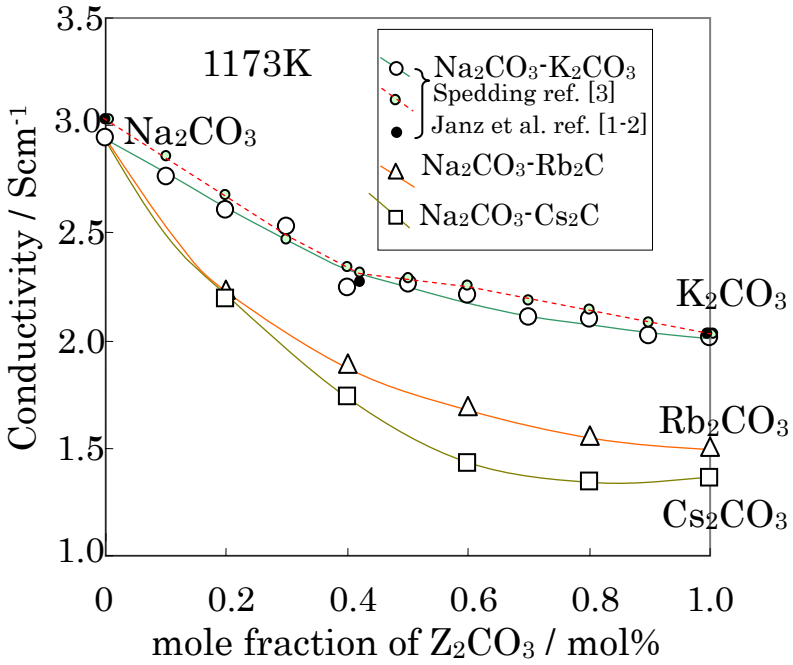

Fig. 4-9. The conductivity of the binary molten carbonates Na_2CO_3-Z_2CO_3 (Z: K, Rb, and Cs) at 1173 K

For high temperature measurement, long lead wires were used, which may bring small capacitance and inductance to the circuit. It was observed that these small circuit elements make small circle at high frequency area in Cole-Cole plot, and resistance decrease steeper than at lower frequency. Spedding obtained resistance by plotting resistance and square root of frequency utilizing 2,000-40,000 Hz. In that frequency region, obtained resistance is apt to become smaller than that obtained below 10 kHz, therefore conductivity seems to be larger.

A re-measurement for $(Li_{0.7}K_{0.3})_2CO_3$ in the frequency range 1 Hz to 100 kHz showed that about 2% increase of conductivity by tracing Spedding method utilizing 2,000-40,000 Hz as shown in Fig 4-10. However discrepancy is more than 20% between our data and that of Spedding.

In order to check our result we use another cell constitution, utilizing twin capillary and movable Au-Pd (80:20 wt%) electrode like reported by Kim[4]. The result of re-measurement using another method showed good agreement with our previous data as shown in Fig. 4-10. The reason for the large discrepancy is not only measurement frequency but also other factors like standard material and measurement circuit.

The temperature dependencies of the conductivity of molten $(Li_{0.62}K_{0.38})_2CO_3$ and $(Li_{0.52}Na_{0.48})_2CO_3$ are shown in Fig. 4-11.

The temperature dependencies of the conductivity of ternary molten alkali carbonate is shown in Fig. 4-12.

The result for alkali-alkaline earth carbonate, Li_2CO_3-Na_2CO_3-$CaCO_3$ for example is shown in Fig. 4-14.

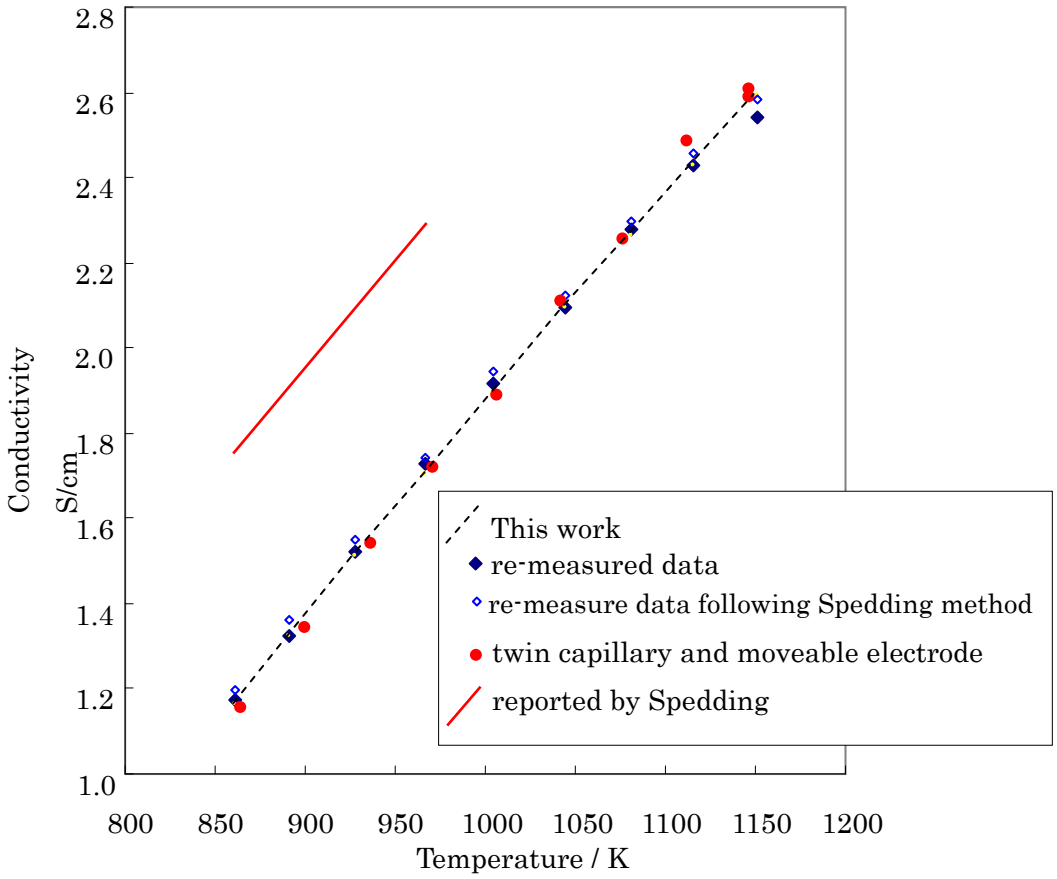

Fig 4-10. Results of conductivity measurement for $(Li_{0.7}K_{0.3})_2CO_3$

Electrical conductivity of molten carbonates are plotted as a function of temperature in Fig. 4-13 for alkali ion (Rb^+ or Cs^+) addition, Fig. 4-14 for $CaCO_3$ addition, Fig. 4-15 for CrO_4^{2-} addition and Fig. 4-16 for SO_4^{2-}, MoO_4^{2-}, WO_4^{2-} and Cl^- addition, respectively.

Precise measurements of conductivity had been done for CrO_4^{2-} addition. The results of small amount addition such as 1, 3 or 5 mol% showed that difference in the measurement even 2 mol% composition difference. Good resolution of data can be seen clearly in Fig 4-15 for CrO_4^{2-} addition.

The electrical conductivity of molten carbonates increased with an increase in temperature. The conductivity values were fit to Arrhenius' equation as given by Janz[6].

$$\sigma = \sigma_0 \exp(-\frac{E_a}{RT}) \qquad [4\text{-}1]$$

where σ (S cm^{-1}) is the conductivity of the molten carbonate, σ_0 (S cm^{-1}) is a pre-exponential factor, E_a (J mol^{-1}) is the apparent activation energy, R (J $K^{-1}mol^{-1}$) is the gas constant, and T (K) is absolute temperature. The parameters of Arrhenius' equation for the data at temperatures higher than about

973 K are summarized in Table 4-1 for single and binary alkali carbonate. The measurement temperature range for some of the molten binary alkali carbonates was extended to below 973K to take account of their lower melting points. It was found that Arrhenius' equation showed significant deviations as shown in Fig. 4-11 from the data at temperatures lower than 973K, an important temperature range from the viewpoint of MCFC operation.

Typical compositions of MCFC electrolytes are $(Li_{0.52}Na_{0.48})_2CO_3$ and $(Li_{0.62}K_{0.38})_2CO_3$. As far as we know, the conductivity values for these compositions given in Fig 4-11 have not yet been previously reported. The conductivities of $(Li_{0.52}Na_{0.48})_2CO_3$ and $(Li_{0.62}K_{0.38})_2CO_3$ at 923 K were 2.06 and 1.31 S cm^{-1}, respectively.

Janz and Lorenz[1], Ward and Janz[2], and Spedding[3] also reported that activation energy of Arrhenius' equation changed with temperature. Therefore the deviation from Arrhenius' equation was observed for the data of large temperature range. Janz well discussed about temperature dependence of activation energy[1].

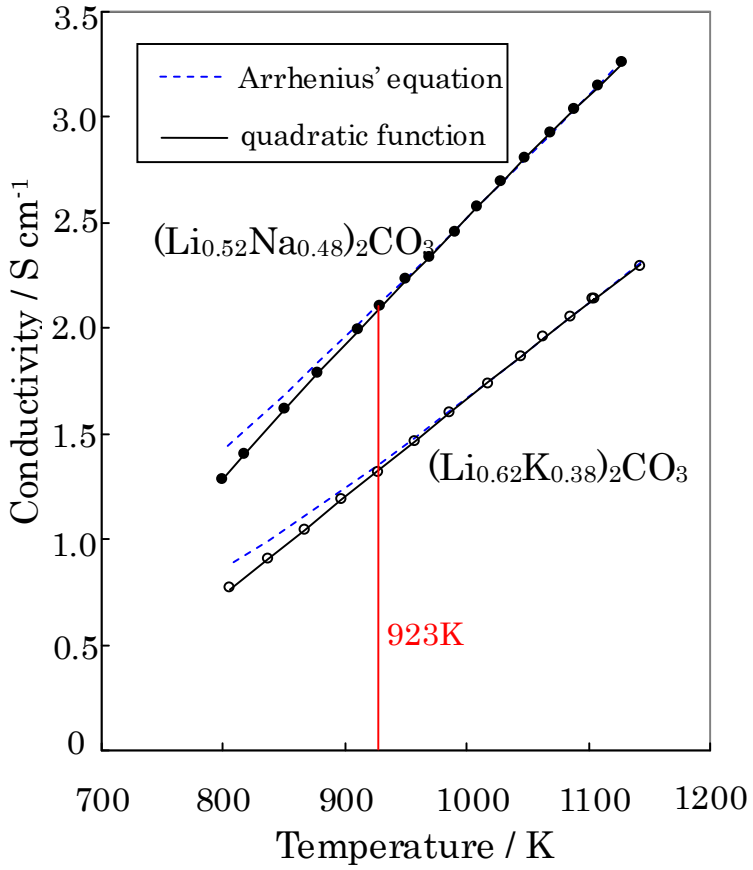

Fig. 4-11. Temperature dependence of the conductivity of the binary molten carbonate mixtures, $(Li_{0.52}Na_{0.48})_2CO_3$ and $(Li_{0.62}K_{0.38})_2CO_3$.

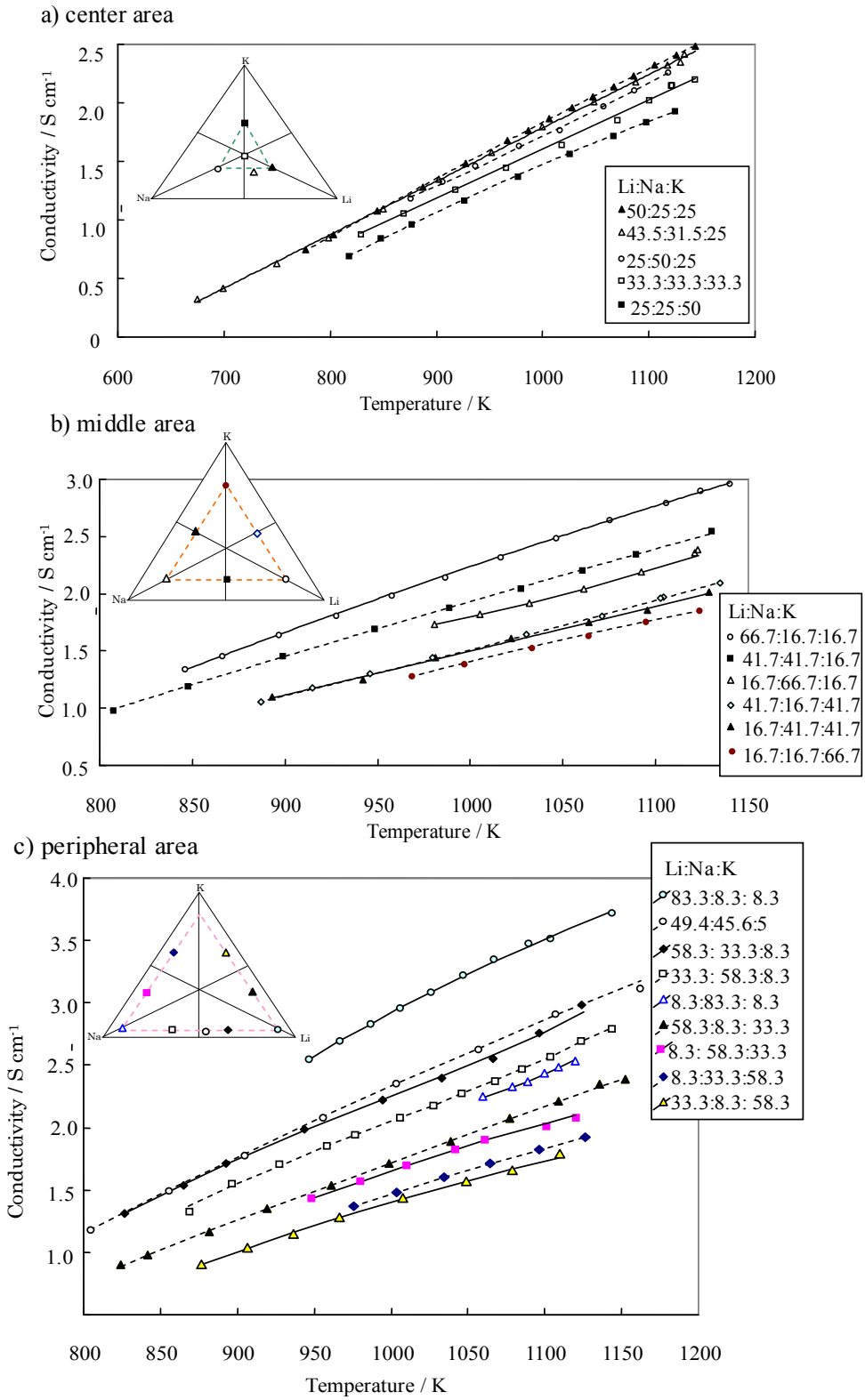

Fig.4-12. Temperature dependence of the conductivity of molten Li_2CO_3 - Na_2CO_3 - K_2CO_3 ternary carbonates of a) center area, b) middle area, and c) peripheral area in the triangular composition diagram.

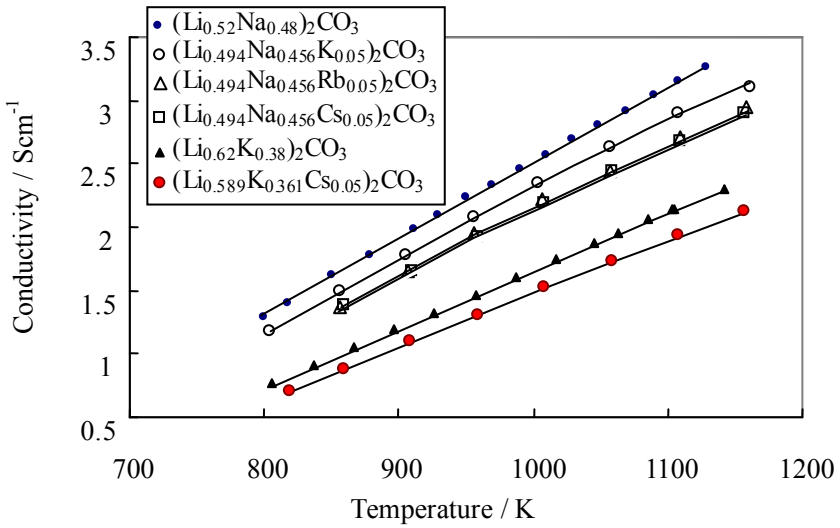

Fig.4-13. Temperature dependence of electrical conductivity of molten $(Li_{0.52}Na_{0.48})_2CO_3$ and $(Li_{0.62}K_{0.38})_2CO_3$ containing alkali ion (K^+, Rb^+, or Cs^+).

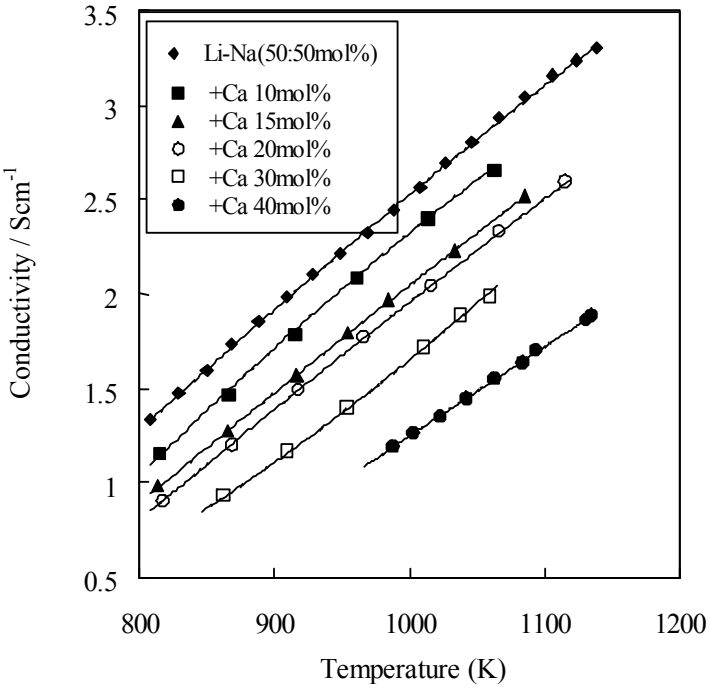

Fig.4-14. The temperature dependence of electrical conductivity of molten Li_2CO_3-Na_2CO_3 (50:50mol%) containing $CaCO_3$.

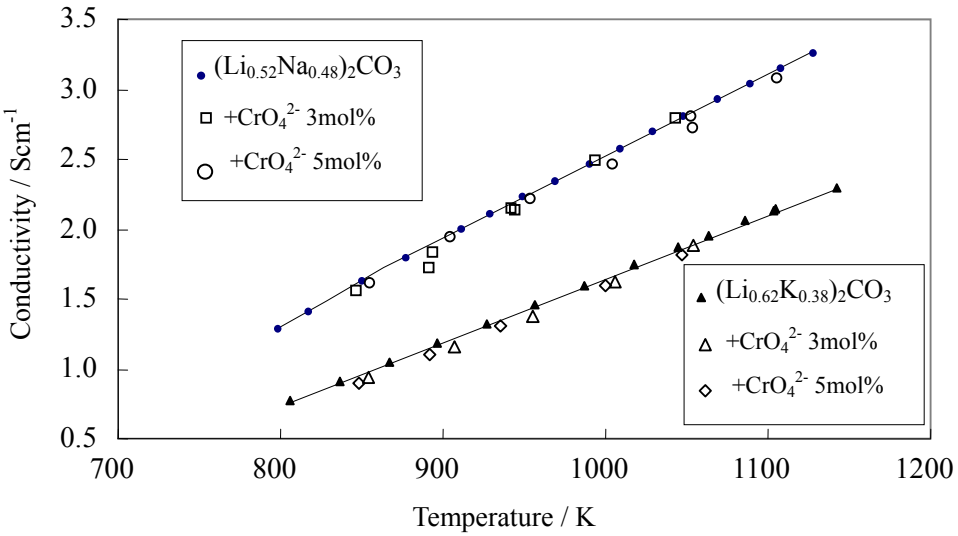

Fig.4-15. Temperature dependence of electrical conductivity of molten $(Li_{0.52}Na_{0.48})_2CO_3$, $(Li_{0.62}K_{0.38})_2CO_3$ and $(K_{0.573}Li_{0.437})_2CO_3$ containing CrO_4^{2-}.

For conductivity data taken over a wide temperature range, including values below 973K, the following quadratic functions of temperature accurately fitted the data.

$$\sigma = a + bT + cT^2 \qquad [4\text{-}2]$$

Here, a (S cm^{-1}), b (S cm^{-1} K^{-1}), and c (S cm^{-1} K^{-2}) are experimentally determined constants; they are summarized in Table 4-2 for single and binary alkali carbonate, Table 4-3 for alkali-alkaline earth carbonate Table 4-4 for ternary alkali carbonate, and Table 4-5 for alkali carbonate containing additives.

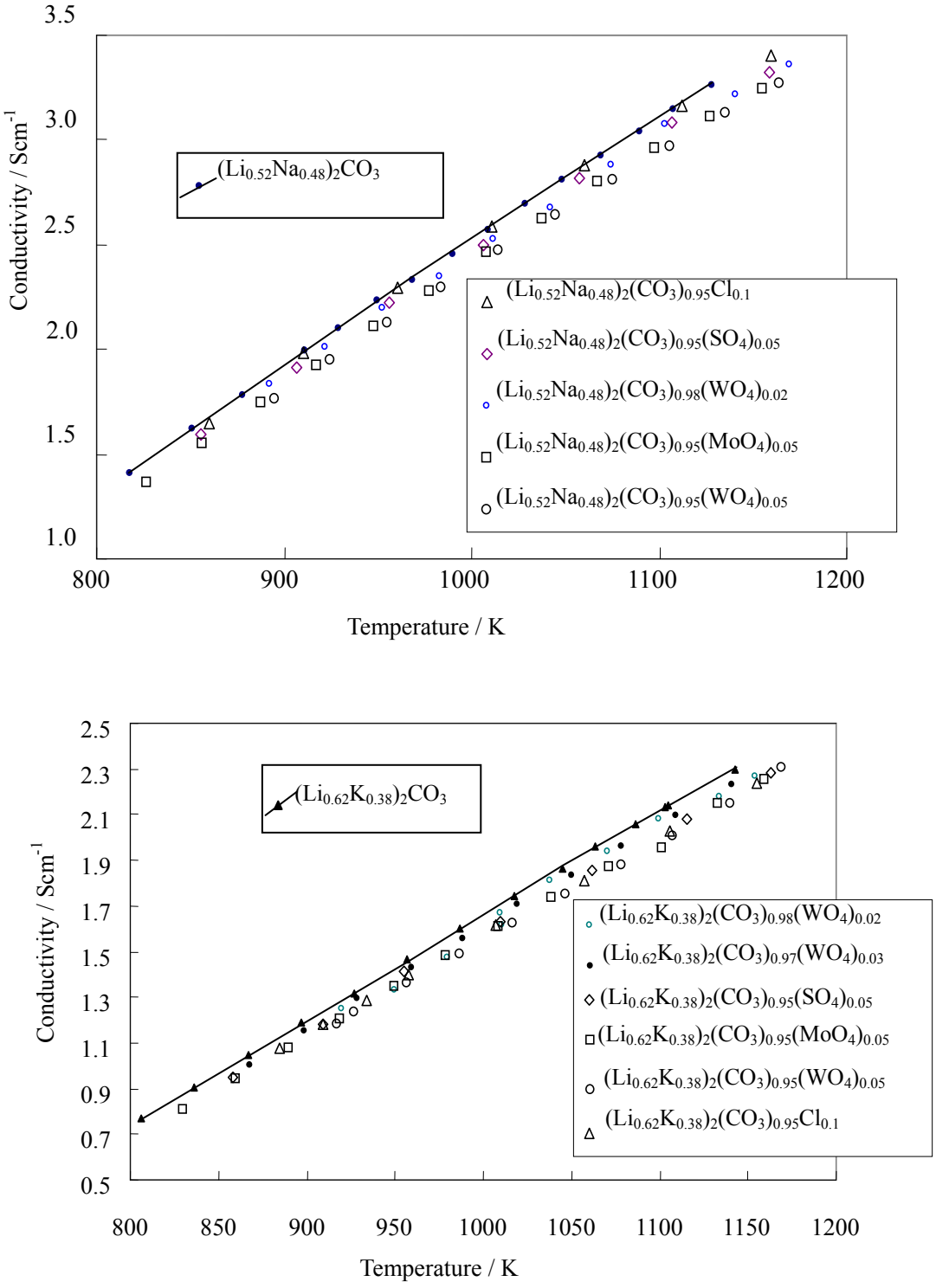

Fig.4-16. Temperature dependence of electrical conductivity of molten $(Li_{0.52}Na_{0.48})_2CO_3$ and $(Li_{0.62}K_{0.38})_2CO_3$ containing SO_4^{2-}, MoO_4^{2-}, WO_4^{2-}, or Cl^-.

Table 4-1. Arrhenius parameters of the electrical conductivity of molten single and binary alkali carbonates.

Composition (mol%)		Pre-exponential factor	Apparent activation energy	Conductivity value at 1173K	Square of correlation coefficient	Estimated standard error	Temperature (K)		
		σ_0 (Scm^{-1})	E_a (kJmol^{-1})	σ_{1173}(Scm^{-1})	r^2		T		
Li/Na	100/0[a]	28.52	16.19	5.42	0.999	0.002	1016	-	1148
	90/10[b]	26.05	16.38	4.86	0.999	0.004	978	-	1147
	80/20	24.29	16.72	4.37	0.999	0.003	988	-	1139
	70/30[b]	23.59	17.44	3.95	0.996	0.010	973	-	1134
	60/40	19.06	16.04	3.68	0.998	0.004	986	-	1145
	52/48	24.68	18.97	3.53	1.000	0.007	979	-	1147
	50/50	21.77	17.82	3.50	0.998	0.012	985	-	1169
	40/60	24.22	19.37	3.32	0.998	0.006	982	-	1141
	30/70	18.84	17.34	3.18	0.999	0.004	994	-	1142
	20/80	21.44	18.84	3.11	0.997	0.004	1058	-	1136
	10/90	16.05	16.49	2.96	1.000	0.002	1105	-	1202
	0/100[a]	13.49	14.85	2.94	0.991	0.004	1139	-	1233
Li/K	95/5	37.66	19.99	4.85	0.970	0.019	1008	-	1118
	90/10	27.98	18.80	4.07	0.998	0.006	976	-	1133
	80/20	22.29	18.83	3.23	0.998	0.006	997	-	1137
	70/30	22.87	20.80	2.71	0.999	0.004	972	-	1150
	62/38	23.22	21.91	2.46	0.999	0.004	987	-	1142
	60/40	23.54	22.32	2.39	1.000	0.002	978	-	1141
	50/50	19.89	21.55	2.18	0.999	0.005	983	-	1139
	43/57	22.75	23.31	2.08	1.000	0.002	980	-	1146
	40/60	20.23	22.29	2.06	0.999	0.006	980	-	1159
	30/70	20.12	22.27	2.05	0.998	0.006	970	-	1097
	20/80	16.05	20.46	1.97	0.999	0.003	1027	-	1162
	10/90	16.00	20.36	1.98	0.996	0.004	1145	-	1219
	0/100[a]	11.70	17.17	2.01	0.998	0.002	1183	-	1261
Li/Rb	95/5	30.62	18.71	4.50	0.998	0.005	995	-	1148
	90/10	25.82	18.84	3.74	0.998	0.006	972	-	1154
	80/20	22.12	20.36	2.74	0.999	0.005	978	-	1151
	70/30	19.50	21.29	2.20	0.999	0.004	996	-	1135
	60/40	19.39	22.92	1.85	0.999	0.004	980	-	1145
	50/50	18.37	23.37	1.67	0.999	0.005	978	-	1146
	40/60	17.44	23.51	1.57	0.999	0.004	983	-	1154
	30/70	15.88	22.93	1.51	0.999	0.005	982	-	1147
	20/80	14.11	21.83	1.50	0.999	0.004	993	-	1153
	10/90	11.63	20.00	1.50	0.999	0.003	1076	-	1174
	0/100[a]	11.31	19.63	1.51	0.996	0.003	1162	-	1249
Li/Cs	95/5	25.69	17.62	4.22	0.999	0.003	992	-	1153
	90/10	25.45	19.65	3.39	1.000	0.001	983	-	1139
	80/20	21.3	21.53	2.34	0.999	0.005	993	-	1149
	70/30	20.35	23.63	1.80	1.000	0.003	984	-	1156
	68/32	19.26	23.47	1.74	0.999	0.004	978		1151
	60/40	18.98	24.43	1.55	1.000	0.002	997	-	1149
	50/50	15.87	23.78	1.39	1.000	0.003	989	-	1149
	40/60	14.40	23.33	1.32	0.999	0.006	985	-	1159
	30/70	12.43	22.13	1.29	1.000	0.003	998	-	1163
	20/80	11.34	21.14	1.30	0.999	0.005	990	-	1163

Table 4-1. (*continued*)

Composition (mol%)		Pre-exponential factor σ_0 (Scm^{-1})	Apparent activation energy E_a ($kJmol^{-1}$)	Conductivity value at 1173K σ_{1173}(Scm^{-1})	Square of correlation coefficient r^2	Estimated standard error	Temperature (K) T_1	-	T_2
Li/Cs	10/90	9.78	19.56	1.32	0.999	0.003	1020	-	1157
	0/100 [a]	9.38	18.80	1.36	0.997	0.006	1086	-	1231
Na/K	90/10 [b]	16.72	17.57	2.76	0.997	0.003	1147	-	1220
	80/20 [b]	23.09	21.25	2.61	0.997	0.006	1108	-	1197
	70/30 [b]	28.56	23.64	2.53	0.986	0.015	1048	-	1176
	60/40	13.95	17.78	2.25	0.997	0.011	1060	-	1223
	50/50 [b]	35.92	26.98	2.26	0.997	0.010	1016	-	1146
	40/60 [b]	25.74	23.93	2.21	0.996	0.007	1060	-	1164
	30/70 [b]	20.23	22.04	2.11	0.999	0.005	1058	-	1190
	20/80 [b]	22.78	23.24	2.10	0.997	0.005	1172	-	1263
	10/90 [b]	16.80	20.65	2.02	0.998	0.003	1158	-	1237
Na/Rb	80/20	14.41	18.16	2.24	1.000	0.003	1014	-	1201
	60/40	16.52	21.13	1.89	0.999	0.004	985	-	1184
	40/60	16.65	22.27	1.70	0.996	0.012	977	-	1177
	20/80	11.11	19.16	1.56	0.998	0.005	1051	-	1180
Na/Cs	80/20	16.14	19.46	2.19	0.997	0.006	1052	-	1172
	60/40	16.18	21.74	1.74	0.998	0.009	987	-	1177
	40/60	15.07	22.97	1.43	0.999	0.006	987	-	1180
	20/80	11.48	20.98	1.34	1.000	0.003	981	-	1177

[a] replotted data from ref .[7] [b] replotted data from ref . [8].

Table 4-2. Empirical equations for the electrical conductivity for molten binary alkali carbonates. $\sigma = a + bT + cT^2$ (σ:S cm^{-1}, T:K).

Composition (mol%)	Electrical conductivity (Scm^{-1}) $\sigma = a + bT + cT^2$			Value at 923K (Scm^{-1})	Square of correlation coefficient	Estimated standard deviation (Scm^{-1})	Temperature (K)
	a	$b\times10^3$	$c\times10^6$	σ_{923}	r^2		T_1 - T_2
Li/Na							
80/20	-5.2564	10.2826	-1.7750	2.72[a]	1.000	0.010	947 - 1139
70/30[b]	-11.8484	22.6452	-7.8914	2.33 [a]	1.000	0.007	924 - 1134
60/40	-8.4447	16.3433	-5.1447	2.26	0.999	0.014	829 - 1145
52/48	-4.6866	8.5330	-1.3250	2.06	1.000	0.004	799 - 1128
50/50	-6.4705	12.0172	-3.0089	2.06	0.999	0.014	852 - 1169
40/60	-5.2162	9.2958	-1.7306	1.89	0.999	0.015	874 - 1141
Li/K							
80/20	-5.6063	10.1898	-2.2765	1.86	0.999	0.013	920 - 1137
70/30 [b]	-4.1526	7.1192	-1.0926	1.49	1.000	0.006	851 - 1150
62/38	-3.2403	5.2415	-0.3389	1.31	1.000	0.005	806 - 1142
60/40	-2.8431	4.4599	-0.0091	1.27	1.000	0.005	829 - 1141
50/50	-3.8240	6.5057	-1.1949	1.16	1.000	0.005	837 - 1139
43/57	-2.5501	3.9141	0.0194	1.08	1.000	0.010	789 - 1146
40/60	-3.1680	5.1689	-0.6170	1.08	1.000	0.006	821 - 1159
30/70	-3.7021	6.3018	-1.2170	1.08 [a]	0.998	0.008	944 - 1097
Li/Rb							
80/20	-4.6678	8.2105	-1.6305	1.52	1.00	0.005	919 - 1151
70/30	-3.5640	5.9748	-0.9138	1.17	1.00	0.003	851 - 1135
60/40	-2.8092	4.4812	-0.4425	0.95	1.00	0.003	829 - 1145
50/50	-2.7886	4.4877	-0.5947	0.85	1.00	0.002	862 - 1146
40/60	-2.3282	3.6238	-0.2656	0.79	1.00	0.002	838 - 1154
30/70	-2.6505	4.3322	-0.6764	0.77	1.00	0.001	893 - 1150
Li/Cs							
90/10	-5.4858	9.7332	-1.8575	1.92 [a]	1.000	0.005	969 - 1139
80/20	-3.8564	6.4646	-1.0156	1.25	0.999	0.010	897 - 1149
70/30	-2.3872	3.6160	-0.0428	0.91	1.000	0.003	846 - 1156
68/32	-2.5532	3.9856	-0.2893	0.88	1.000	0.002	827 1151
60/40	-1.9705	2.8246	0.1469	0.76	1.000	0.002	854 - 1149
50/50	-2.0322	3.1117	-0.1733	0.69	1.000	0.002	871 - 1149
40/60	-2.1182	3.3595	-0.3737	0.66	1.000	0.003	841 - 1159
30/70	-2.1769	3.5730	-0.5330	0.67	1.000	0.001	890 - 1163
20/80	-2.4072	4.1389	-0.8419	0.70 [a]	1.000	0.002	930 - 1163
Na/Rb							
60/40	-2.7814	4.6463	-0.5678	1.02	1.000	0.005	869 - 1184
40/60	-3.6087	6.1633	-1.4098	0.88	1.000	0.005	918 - 1177
Na/Cs							
60/40	-3.4942	5.9766	-1.2974	0.92	1.000	0.005	909 - 1177
40/60	-1.8941	2.9255	-0.0814	0.74	1.000	0.003	873 - 1180
20/80	-2.0088	3.3912	-0.4635	0.73 [a]	1.000	0.002	955 - 1177

[a] extrapolated values; [b] replotted from ref . [8]

Table 4-3. Empirical equations of the electrical conductivity of molten Li_2CO_3-Na_2CO_3-K_2CO_3 ternary carbonates.

Composition Li_2CO_3: Na_2CO_3: K_2CO_3 (mol%)	Electrical conductivity $\sigma = a + bT + cT^2$ (S cm^{-1})			Value at 1073K (S cm^{-1})	Square of correlation coefficient	Estimated standard deviation (S cm^{-1})	Equivalent conductivity at 1073 K (Scm^{2}equiv^{-1})	Equivalent conductivity estimated (diff.%) † (Scm^{2}equiv^{-1})	Temperature range (K)
	a	$b\times10^3$	$c\times10^6$	σ_{1073}	r^2				T_1 - T_2
33.3:33.3:33.3	-1.1240	1.1224	1.5744	1.89	0.998	0.026	104.5	105.9 (0.5)	829 - 1144
25:25:50	-3.9633	6.9372	-1.5161	1.73	1.000	0.006	102.8	102.8 (0.0)	818 - 1125
25:50:25	-1.2854	1.6260	1.3725	2.04	0.999	0.012	111.6	111.5 (-0.1)	876 - 1118
50:25:25	-3.5829	6.1187	-0.7085	2.17	1.000	0.005	111.9	109.8 (-1.9)	777 - 1144
16.7:16.7:66.7	-3.7377	6.4521	-1.3207	1.66	1.000	0.004	105.4	105.9 (0.5)	969 - 1124
16.7:66.7:16.7	9.8336	-19.3437	11.3088	2.10	0.999	0.007	113.7	118.4 (4.0)	980 - 1123
66.7:16.7:16.7	-4.8019	8.4895	-1.4686	2.62	1.000	0.006	125.8	123.0 (-2.3)	846 - 1140
16.7:41.7:41.7	-2.2311	3.5883	0.1462	1.79	0.997	0.022	105.0	106.2 (1.2)	893 - 1129
41.7:16.7:41.7	-1.8568	2.5850	0.7919	1.83	0.999	0.011	101.9	102.1 (0.2)	887 - 1135
41.7:41.7:16.7	-3.4927	6.0761	-0.6600	2.27	1.000	0.010	115.9	114.8 (-0.9)	807 - 1130
8.3:33.3:58.3	-5.7423	10.3767	-3.1834	1.73	1.000	0.003	108.5	107.3 (-1.1)	976 - 1126
8.3:58.3:33.3	-8.4941	16.1697	-6.0196	1.93	0.999	0.010	112.2	110.8 (-1.3)	949 - 1121
33.3:8.3:58.3	-4.5031	8.0861	-2.1970	1.64	0.999	0.013	98.3	101.3 (3.0)	877 - 1109
33.3:58.3:8.3	-0.9437	1.0965	1.8882	2.41	1.000	0.010	121.9	121.7 (-0.2)	869 - 1144
58.3:8.3:33.3	-3.4779	5.8199	-0.6230	2.05	1.000	0.008	106.9	106.8 (-0.1)	824 - 1152
58.3:33.3:8.3	-2.0955	3.2969	1.0454	2.65	0.996	0.041	126.0	127.2 (1.0)	827 - 1124
83.3:8.3:8.3	-11.8432	22.8176	-8.0555	3.37	0.999	0.001	150.0	148.6 (-1.0)	947 - 1090
8.3:83.3:8.3	21.8017	-40.4848	20.7943	2.30	0.998	0.005	123.7	126.5 (2.3)	1060 - 1120
43.5:31.5:25.0	-2.7970	4.6114	-0.0291	2.12	1.000	0.017	111.1	109.3 (-1.6)	675 - 1134
49.4:45.6:5.0	-5.7651	10.7711	-2.6814	2.71	0.9995	0.041	130.1	127.7 (-1.8)	805 - 1162

†: difference % between measured data and those estimated using equations [4-14]- [4-18]

Table 4-4. Empirical equations of electrical conductivity of molten Li_2CO_3-Na_2CO_3 and Li_2CO_3-K_2CO_3 containing alkaline earth (Ca, Sr and Ba) carbonate. $\sigma = a + bT + cT^2$ (σ :Scm^{-1}, T:K).

Composition (mol%)	Electrical conductivity $\sigma = a + bT + cT^2$ (Scm^{-1})			Value at 1073K (Scm^{-1})	Square of Correlation Coefficient	Standard deviation of estimated σ (Scm^{-1})	Temperature (K)
	a	$b\times10^3$	$c\times10^6$	σ_{1073}	r^2		T
Li/Ca							
95/5	-11.7337	22.2563	-6.7891	4.33	1.000	0.009	998 - 1142
90/10	-8.85194	16.5179	-4.1884	4.05	1.000	0.008	991 - 1146
85/15	-7.6267	14.1316	-3.2877	3.75	0.998	0.018	978 - 1135
80/20	-9.2631	16.5438	-4.3768	3.45	1.000	0.006	989 - 1142
75/25	-9.9350	17.6391	-5.0642	3.16	1.000	0.004	986 - 1142
70/30	-8.0066	13.5938	-3.2062	2.89	1.000	0.008	972 - 1149
65/35	-7.2407	12.0686	-2.6774	2.63	1.000	0.006	989 - 1147
60/40	-7.1185	11.6521	-2.6137	2.38	1.000	0.004	998 - 1144
55/45	-11.7906	19.9511	-6.5056	2.13	0.999	0.005	1080 - 1150
Li/Sr							
95/5	-10.4910	19.8019	-5.5929	4.32	0.998	0.019	1008 - 1139
90/10	-8.0331	15.1112	-3.6398	3.99	1.000	0.003	1006 - 1134
85/15	6.9673	-13.5826	9.7292	3.60	0.997	0.026	987 - 1135
80/20	-7.0360	12.6025	-2.7885	3.28	0.996	0.027	970 - 1125
75/25	-1.5092	1.8360	2.1763	2.97	1.000	0.005	980 - 1136
70/30	0.9322	-3.6502	4.9462	2.71	0.998	0.016	1017 - 1138
65/35	-48.3795	85.6460	-35.6605	2.46	1.000	0.002	1075 - 1126
Li/Ba							
95/5	-4.5677	8.5772	-0.3368	4.25	1.000	0.005	1008 - 1136
90/10	-9.5404	17.6827	-4.8529	3.85	1.000	0.008	989 - 1140
85/15	-9.9630	17.9521	-5.0302	3.51	1.000	0.007	982 - 1138
80/20	-5.1857	8.9009	-1.0613	3.14	1.000	0.010	995 - 1140
75/25	-5.8732	9.6278	-1.3447	2.91	0.999	0.012	975 - 1139
70/30	-4.6293	7.4541	-0.7608	2.49	1.000	0.004	976 - 1135
65/35	-1.5975	1.3188	2.1219	2.26	1.000	0.010	992 - 1137
60/40	-0.4089	-1.3038	3.3286	2.03	1.000	0.005	991 - 1140
55/45	3.2139	-8.1222	6.2898	1.74	1.000	0.005	1004 - 1131
Li/Na/Ca							
27/63/10	-6.99258	12.5596	-3.4843	2.47	1.000	0.003	964 - 1111
24/56/20	-9.3277	16.6133	-5.5178	2.15	0.998	0.020	923 - 1114
21/49/30	-3.9549	5.9850	-0.5489	1.84	1.000	0.004	931 - 1113
18/42/40	-4.0191	5.7028	-0.5008	1.52	1.000	0.004	971 - 1120
15/35/50	-22.1381	38.4870	-15.5305	1.28	0.995	0.008	1078 - 1122
0/60/40	-8.3086	13.6814	-4.3676	1.34	0.998	0.007	1073 - 1148
45/45/10	-3.0650	4.6149	0.6325	2.62	0.999	0.014	848 - 1052
42.5/42.5/15	-4.3076	7.0939	-0.7400	2.45	1.000	0.005	814 - 1085
40/40/20	-4.6089	7.5324	-0.9583	2.37	1.000	0.008	817 - 1114
35/35/30	-1.4299	0.5488	2.5431	2.09	1.000	0.011	862 - 1059

Table 4-4. (*continued*)

Composition (mol%)	Electrical conductivity $\sigma = a + bT + cT^2$ (Scm^{-1})			Value at 1073K (Scm^{-1})	Square of Correlation Coefficient	Standard deviation of estimated σ (Scm^{-1})	Temperature (K)
	a	$b\times10^3$	$c\times10^6$	σ_{1073}	r^2		T
Li/Na/Ca							
30/30/40	1.6198	-5.2261	4.8943	1.65	0.998	0.014	979 - 1100
63/27/10	-6.1110	10.9784	-2.3296	2.99	1.000	0.010	865 - 1145
56/24/20	-7.6855	12.9200	-3.1789	2.52	0.998	0.020	936 - 1098
49/21/30	-2.0180	1.8155	1.9398	2.16	1.000	0.004	896 - 1041
42/18/40	-2.9682	3.6298	0.7841	1.83	1.000	0.005	1011 - 1144
Li/Na/Sr							
27/63/10	-4.3039	7.1612	-0.9104	2.33	1.000	0.008	946 - 1092
24/56/20	-2.4252	3.2852	0.7395	1.95	1.000	0.006	910 - 1100
21/49/30	-2.4258	2.9765	0.8792	1.78	0.999	0.007	961 - 1087
18/42/40	2.5393	-6.3364	4.9033	1.39	1.000	0.003	1057 - 1139
0/60/40	-1.6748	1.6504	1.0369	1.29	1.000	0.001	1056 - 1150
45/45/10	-2.2048	3.2512	1.0396	2.48	0.998	0.025	836 - 1076
40/40/20	-4.4852	7.2770	-0.9886	2.19	1.000	0.005	907 - 1091
35/35/30	-3.6639	5.3225	-0.1604	1.86	1.000	0.007	931 - 1093
30/30/40	2.4492	-6.5843	5.3145	1.50	0.996	0.007	1065 - 1110
63/27/10	-11.4591	22.1692	-8.2627	2.82	0.997	0.035	874 - 1069
56/24/20	-4.0810	6.6916	-0.5515	2.46	0.999	0.020	860 - 1100
49/21/30	-10.5780	18.4066	-6.1493	2.09	0.999	0.012	968 - 1098
42/18/40	-2.3723	2.5511	1.1368	1.67	0.997	0.005	1078 - 1123
Li/Na/Ba							
27/63/10	-6.7635	12.7764	-3.9976	2.34	1.000	0.003	926 - 1073
24/56/20	-2.0958	2.7920	0.9387	1.98	1.000	0.004	934 - 1107
21/49/30	-12.7214	24.2116	-9.9951	1.75	0.996	0.020	925 - 1102
18/42/40	-7.7577	13.1155	-4.2763	1.39	0.999	0.007	1000 - 1101
15/35/50	-2.4670	3.3316	0.0109	1.12	1.000	0.000	1081 - 1142
0/60/40	-0.0251	-1.3369	2.4158	1.32	1.000	0.002	1056 - 1150
45/45/10	-2.9137	4.4324	0.5585	2.49	0.999	0.022	1031 - 1125
40/40/20	-5.2919	9.0848	-1.9300	2.23	0.999	0.015	854 - 1130
35/35/30	-1.8414	1.7700	1.5560	1.85	0.999	0.014	856 - 1085
30/30/40	-2.1343	2.1189	1.1906	1.51	1.000	0.003	1011 - 1129
63/27/10	-6.6763	12.3865	-3.1457	2.99	1.000	0.003	896 - 1130
56/24/20	-5.6660	9.7531	-2.0536	2.44	1.000	0.003	887 - 1137
49/21/30	-2.7702	3.6329	0.8121	2.06	1.000	0.003	867 - 1139
42/18/40	-6.4556	10.9528	-3.1706	1.65	0.998	0.010	1002 - 1104
Li/K/Ca							
27/63/10	-4.0019	6.4579	-1.2517	1.49	0.999	0.011	919 - 1121
24/56/20	-4.7211	7.6087	-1.8612	1.30	0.990	0.029	938 - 1116
21/49/30	-3.1558	3.8344	0.2166	1.21	0.999	0.010	972 - 1119
18/42/40	2.7199	-7.0099	4.9986	0.95	1.000	0.002	999 - 1082
0/65/35	4.6260	-9.6365	5.8077	0.97	0.999	0.005	1046 - 1144
45/45/10	-3.2502	5.1884	-0.6501	1.57	1.000	0.010	832 - 1053
40/40/20	-2.1928	2.7807	0.5297	1.40	0.999	0.017	843 - 1139

Table 4-4. (*continued*)

Composition (mol%)	Electrical conductivity $\sigma = a + bT + cT^2$ (Scm^{-1})			Value at 1073K (Scm^{-1})	Square of Correlation Coefficient	Standard deviation of estimated σ (Scm^{-1})	Temperature (K)
	a	$b\times10^3$	$c\times10^6$	σ_{1073}	r^2		T
Li/K/Ca							
35/35/30	-1.2857	0.6804	1.5699	1.25	0.999	0.012	846 - 1120
30/30/40	-0.7678	-0.4402	2.0032	1.07	0.998	0.015	923 - 1122
25/25/50	-1.6589	1.1152	1.1987	0.92	0.995	0.123	1022 - 1122
72/18/10	0.6027	-3.5860	5.0213	2.54	0.998	0.025	921 - 1120
64/16/20	-5.3674	8.6012	-1.4744	2.16	0.998	0.028	913 - 1130
56/14/30	1.4546	-5.3033	5.2353	1.79	1.000	0.009	920 - 1122
48/12/40	3.3548	-7.5196	5.4210	1.53	0.986	0.023	1014 - 1117
Li/K/Sr							
27/63/10	1.8734	-4.8489	4.1014	1.39	0.997	0.016	920 - 1113
24/56/20	-3.45835	5.1560	-0.7264	1.24	0.998	0.000	967 - 1092
21/49/30	8.0935	-17.3060	10.0322	1.08	0.999	0.037	1012 - 1105
47.5/47.5/5	-1.8350	2.0755	1.1590	1.73	0.999	0.018	837 - 1130
45/45/10	-2.3406	3.2173	0.4141	1.59	0.999	0.015	819 - 1129
40/40/20	-0.3040	-0.8659	2.2767	1.39	0.996	0.016	968 - 1146
35/35/30	-2.9899	4.2778	-0.3472	1.20	0.996	0.011	1043 - 1148
32.5/32.5/35	-5.0561	8.2290	-2.3038	1.12	0.986	0.015	1077 - 1176
63/27/10	-2.8369	4.2213	0.2269	1.95	1.000	0.011	822 - 1142
56/24/20	-4.9529	7.9778	-1.5846	1.78	1.000	0.012	878 - 1135
49/21/30	3.9484	-8.7567	6.0313	1.50	0.999	0.006	1033 - 1124
Li/K/Ba							
27/63/10	-2.5367	3.7723	-0.0746	1.43	0.999	0.009	915 - 1136
24/56/20	-2.7119	3.9727	-0.2441	1.27	1.000	0.002	901 - 1149
21/49/30	-2.5599	3.4476	-0.0129	1.13	1.000	0.006	910 - 1138
18/42/40	-8.9805	15.4093	-5.7074	0.98	1.000	0.003	1029 - 1141
0/65/35	-10.2069	16.8845	-6.0126	0.99	0.997	0.008	1131 - 1144
45/45/10	-1.2114	0.4209	2.1462	1.71	0.999	0.021	823 - 1131
42.5/42.5/15	-0.9999	0.0590	2.2024	1.60	0.998	0.025	822 - 1126
40/40/20	-1.5910	1.4437	1.3254	1.48	0.999	0.015	810 - 1132
37.5/37.5/25	-1.9877	2.3675	0.6799	1.34	0.997	0.022	875 - 1129
35/35/30	-0.6506	-0.1523	1.7563	1.21	0.999	0.010	960 - 1128
30/30/40	1.7341	-4.2910	3.3923	1.04	0.998	0.007	1069 - 1160
63/27/10	-3.1451	4.9006	-0.1237	1.97	1.000	0.003	825 - 1135
56/24/20	-2.6065	3.6249	0.4107	1.76	0.997	0.027	832 - 1140
49/21/30	-1.3418	1.0023	1.5466	1.52	1.000	0.006	887 - 1142
42/18/40	5.4734	-11.7567	7.2664	1.23	0.997	0.009	1028 - 1130

Table 4-5. Experimental equations for conductivity of molten $(Li_{0.52}Na_{0.48})_2CO_3$ and $(Li_{0.62}K_{0.38})_2CO_3$ containing additives.

Composition	Conductivity $\sigma = a + bT + cT^2$			Value at 923K	Square of Correlation Coefficient	Standard deviation of estimated σ	Equivalent conductivity	Temperature		
(mol%)	(Scm^{-1})			(Scm^{-1})		(Scm^{-1})	(eqScm^2)	(K)		
	a	$b\times10^3$	$c\times10^6$	σ_{923}	r^2			T_1	-	T_2
$(Li_{0.52}Na_{0.48})_2CO_3$				2.06[a]			93.4			
$(Li_{0.52}Na_{0.48})_2(CO_3)_{0.97}(CrO_4)_{0.03}$	-1.671	1.747	2.433	2.01	0.999	0.012	92.1	894	-	1043
$(Li_{0.52}Na_{0.48})_2(CO_3)_{0.95}(CrO_4)_{0.05}$	-3.862	6.937	-0.6125	2.02	0.997	0.029	92.9	855	-	1053
$(Li_{0.52}Na_{0.48})_2(CO_3)_{0.98}(MoO_4)_{0.02}$	-4.925	9.13	-1.742	2.02	0.999	0.02	*92.5*[c]	892	-	1170
$(Li_{0.52}Na_{0.48})_2(CO_3)_{0.95}(MoO_4)_{0.05}$	-5.444	9.985	-2.134	1.95	1.000	0.007	90.5	827	-	1155
$(Li_{0.52}Na_{0.48})_2(CO_3)_{0.95}(WO_4)_{0.05}$	-5.416	9.906	-2.101	1.94	1.000	0.003	89.7	895	-	1164
$(Li_{0.52}Na_{0.48})_2(CO_3)_{0.95}(SO_4)_{0.05}$	-6.231	11.62	-2.912	2.01	1.000	0.013	91.5	856	-	1159
$(Li_{0.52}Na_{0.48})_2(CO_3)_{0.95}Cl_{0.1}$	-5.995	11.13	-2.607	2.06	1.000	0.004	94.3	860	-	1159
$(Li_{0.52}Na_{0.48})_2(CO_3)_{0.95}F_{0.1}$	-6.649	12.87	-3.645	2.13	0.999	0.018	96.2	803	-	1076
$(Li_{0.52}Na_{0.48})_2(CO_3)_{0.95}I_{0.1}$	-1.835	2.111	2.11	1.91	1.000	0.004	92.6	899	-	988
$(Li_{0.494}Na_{0.456}K_{0.05})_2CO_3$				1.89[b]			87.7			
$(Li_{0.494}Na_{0.456}Rb_{0.05})_2CO_3$	-5.07	9.248	-2.008	1.76	0.999	0.013	82.0	856	-	1158
$(Li_{0.494}Na_{0.456}Cs_{0.05})_2CO_3$	-5.176	9.468	-2.145	1.74	1.000	0.022	82.9	859	-	1157
$(Li_{0.62}K_{0.38})_2CO_3$				1.31[a]			66.6			
$(Li_{0.62}K_{0.38})_2(CO_3)_{0.97}(CrO_4)_{0.03}$	-3.681	6.092	-0.7975	1.26	1.000	0.002	64.4	867	-	1141
$(Li_{0.62}K_{0.38})_2(CO_3)_{0.95}(CrO_4)_{0.05}$	-2.834	4.264	0.1662	1.24	1.000	0.002	63.6	852	-	1054
$(Li_{0.62}K_{0.38})_2(CO_3)_{0.97}(MoO_4)_{0.03}$	-4.706	8.220	-1.880	1.28	0.999	0.016	*65.8*[c]	830	-	1160
$(Li_{0.62}K_{0.38})_2(CO_3)_{0.95}(MoO_4)_{0.05}$	-3.184	5.136	-0.3904	1.22	0.999	0.014	63.2	830	-	1160
$(Li_{0.62}K_{0.38})_2(CO_3)_{0.97}(MoO_4)_{0.03}$	-5.287	9.074	-2.184	1.23	0.993	0.029	63.2	920	-	1154
$(Li_{0.62}K_{0.38})_2(CO_3)_{0.95}(WO_4)_{0.05}$	-4.100	6.984	-1.323	1.22	1.000	0.009	63.5	834	-	1165
$(Li_{0.62}K_{0.38})_2(CO_3)_{0.95}(SO_4)_{0.05}$	-4.016	6.839	-1.229	1.25	0.999	0.014	63.8	858	-	1160
$(Li_{0.589}K_{0.361}Cs_{0.05})_2CO_3$	-3.324	5.416	-0.6048	1.16	1.000	0.004	*61.7*[d]	819	-	1157
$(Li_{0.62}K_{0.38})_2(CO_3)_{0.95}Cl_{0.1}$	-3.164	5.152	-0.4104	1.24	1.000	0.006	65.0	885	-	1155
$(Li_{0.62}K_{0.38})_2(CO_3)_{0.95}F_{0.1}$	-3.352	5.436	-0.3949	1.33	1.000	0.003	67.1	788	-	1071

[a] data from Table. 4-2, [b] data from Table 4-3, [c] molar volume were estimated from 5 mol% MoO_4^{2-} addition. [d] molar volume were estimated using additivity

4.4. Discussion

4.4.1. Equivalent conductivity of molten single carbonates

The equivalent conductivities of molten carbonates, Λ (S cm^2 equiv^{-1}) were computed from the conductivity data and the molar volumes, V_m (cm^3 equiv^{-1}), from the equation

$$\Lambda = \sigma V_m \qquad [4\text{-}3]$$

The Arrhenius plots of equivalent conductivity vs. reciprocal temperature of molten single carbonates are shown in Fig. 4-17. For small radii, up to Rb the equivalent conductivity decreases with increasing cationic radius. The equivalent conductivity of molten Cs_2CO_3 was higher than that

of molten Rb_2CO_3. The same behavior can be seen for RbX and CsX (X= Cl, Br, I, and NO_3)[6]. It looks strange because of larger radius of Cs^+ than that of Rb^+.

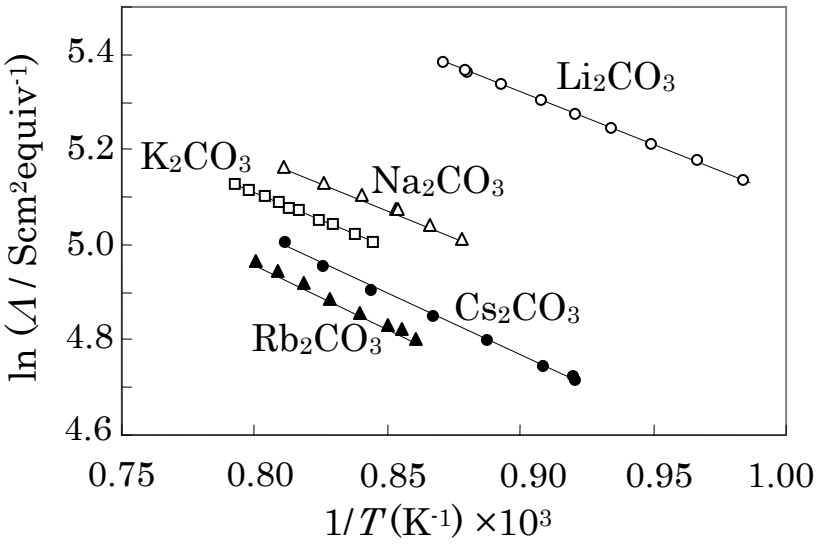

Fig 4-17. Arrhenius plots of the equivalent conductivity vs. reciprocal temperature of molten single carbonates.

Nakamura et al. [9] reported that empirical plots of the electrical conductivity of the molten alkali halides AX (A=Li, Na, K, Rb, and Cs) for a common X (X=F, Cl, Br, and I) obey

$$\sigma = k(r_A^{-2.5} + r_X^{-2.5}) \quad [4\text{-}4]$$

where, r_A, r_X, and k are the ionic radius of the alkali cations, the ionic radius of the halide ions and a constant, respectively. This equation is applied to the molten carbonates studied here using Shannon's ionic radii for 6 coordination[10] and is found to be good agreement with the data. This relationship can be used to estimate the electrical conductivity of the hypothetical molten carbonates, Ag_2CO_3, Tl_2CO_3, and Fr_2CO_3 as shown in Fig. 4-18. The physical properties of these carbonate are unknown. From the viewpoint of molten salt physical chemistry, it is interesting to predict unknown physical properties of the carbonates.

It was reported that in section *2.4.2* a linear relationship between the molar volume of molten carbonates and the ionic volume of cations estimated using their ionic radii[10,11]; they are shown in Fig. 4-19 with the estimated molar volumes of the hypothetical molten carbonates, Ag_2CO_3, Tl_2CO_3, and Fr_2CO_3.

The relationship between equivalent conductivity at 1173 K and ionic radius is plotted in Fig. 4-20. The curved line shows the relationship between the ionic radii and the calculated equivalent conductivity, that being the product of electrical conductivities estimated using equation [4-4] and the molar volumes, both being estimated from ionic radii. The equivalent conductivity of Fr_2CO_3 is predicted to be higher than those of Rb_2CO_3 and Cs_2CO_3 in spite of the cation radius of Fr^+ being

larger than those of Rb^+ and Cs^+. Fig. 4-17 shows that the electrical conductivity decreases with an increase in ionic radius. On the other hand, Fig 4-18 shows that the molar volume becomes larger with increasing ionic radius. This means that the molar volume has a stronger influence on the equivalent conductivity for the cations larger than Rb^+ than does the conductivity. A similar relationship is expected for molten salts with other anions such as chloride, bromide, iodide, and nitrate.

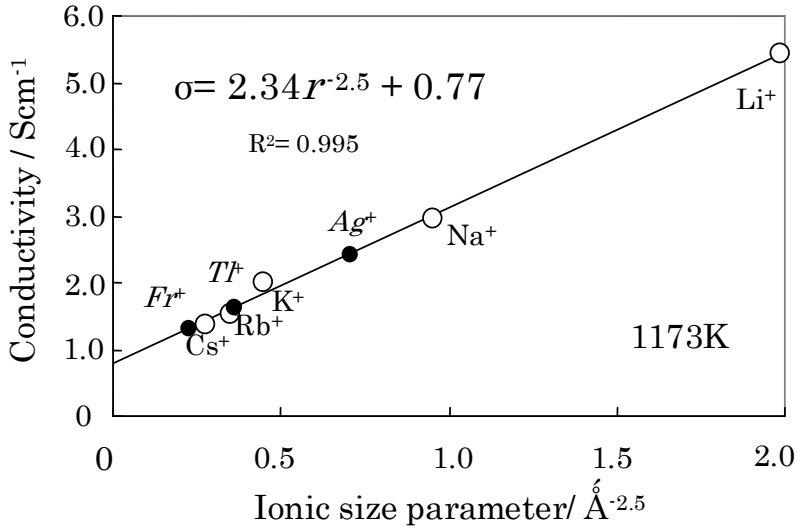

Fig 4-18. Empirical relationship between the electrical conductivity of single molten carbonates and the ionic radii of their cations; the conductivities of Ag_2CO_3, Tl_2CO_3, and Fr_2CO_3 were estimated from their ionic radii and the equation [4-4].

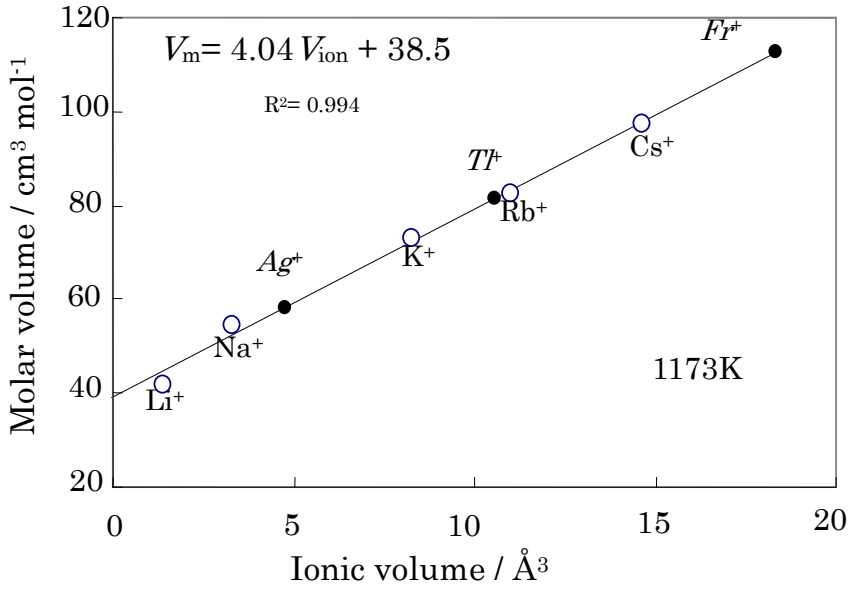

Fig 4-19. Relationship between the molar volume of single molten carbonates and the ionic volume of cations; the molar volumes of Ag_2CO_3, Tl_2CO_3, and Fr_2CO_3 were estimated from their ionic radii.

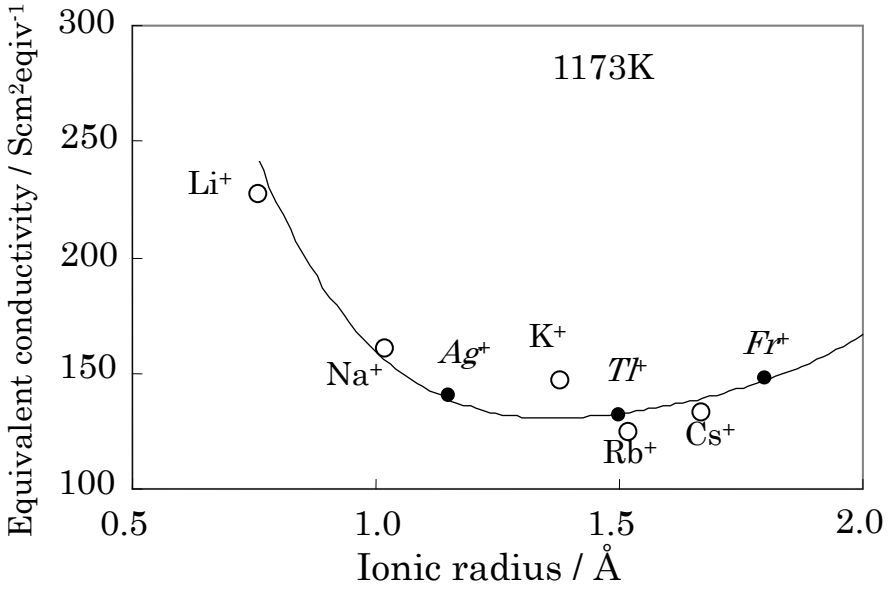

Fig 4-20. Relationship between the equivalent conductivities of single molten carbonates and their cationic radii; the equivalent conductivities of Ag_2CO_3, Tl_2CO_3, and Fr_2CO_3 were estimated from their ionic radii.

4.4.2. Equivalent conductivity of molten binary carbonate systems

In the molten binary carbonate systems containing Li_2CO_3 or Na_2CO_3, the addition of Rb_2CO_3 or Cs_2CO_3 decreases the conductivity, as shown in Figs. 4-8 and 4-9. The conductivity of molten Li_2CO_3-X_2CO_3 (X: Na, K, Rb, and Cs) and Na_2CO_3-Z_2CO_3 (Z: K, Rb, and Cs) decrease with an increase of ionic radius of X and Z.

To provide a more theoretical discussion, we examined the equivalent conductivities of molten Li_2CO_3-X_2CO_3 (X: Na, K, Rb, and Cs) (Fig. 4-21) and Na_2CO_3- Z_2CO_3 (Z: K, Rb, and Cs), (Fig. 4-22) as a function of the mole fraction. The binary systems with Rb or Cs carbonates have relatively deep minimum in the equivalent conductivity.

Spedding[3], as well as Ward and Janz[2] tried to correlate the equivalent conductivity of molten binary carbonates (Li_2CO_3-Na_2CO_3 , Li_2CO_3-K_2CO_3 and Na_2CO_3-K_2CO_3), and composition using the following Markov equation.

$$\Lambda = x_A^2\Lambda_A + x_B^2\Lambda_B + 2x_Ax_B\Lambda_B \qquad [4\text{-}5]$$

where, Λ is equivalent conductivity of the mixture, Λ_A and Λ_B are the equivalent conductivities of the pure components A and B (assuming that $\Lambda_A > \Lambda_B$), and x_A and x_B are the mole fractions of component A and B. We applied equation [4-5] to the equivalent conductivity data for of molten binary carbonates, but as Spedding reported, there were large differences between the estimated and experimental values, ranging up to 45% as shown in Fig. 4-21.

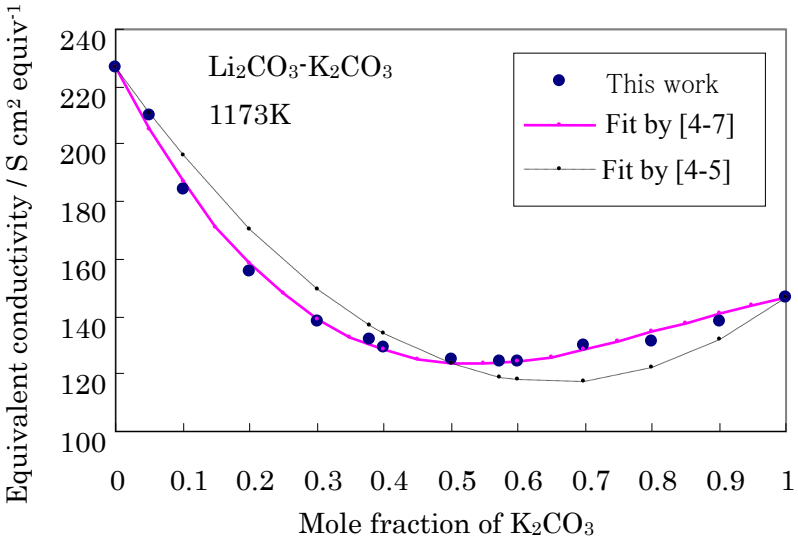

Fig 4-21. The comparison of equations [4-5] and [4-7] fitting Li_2CO_3-K_2CO_3 system

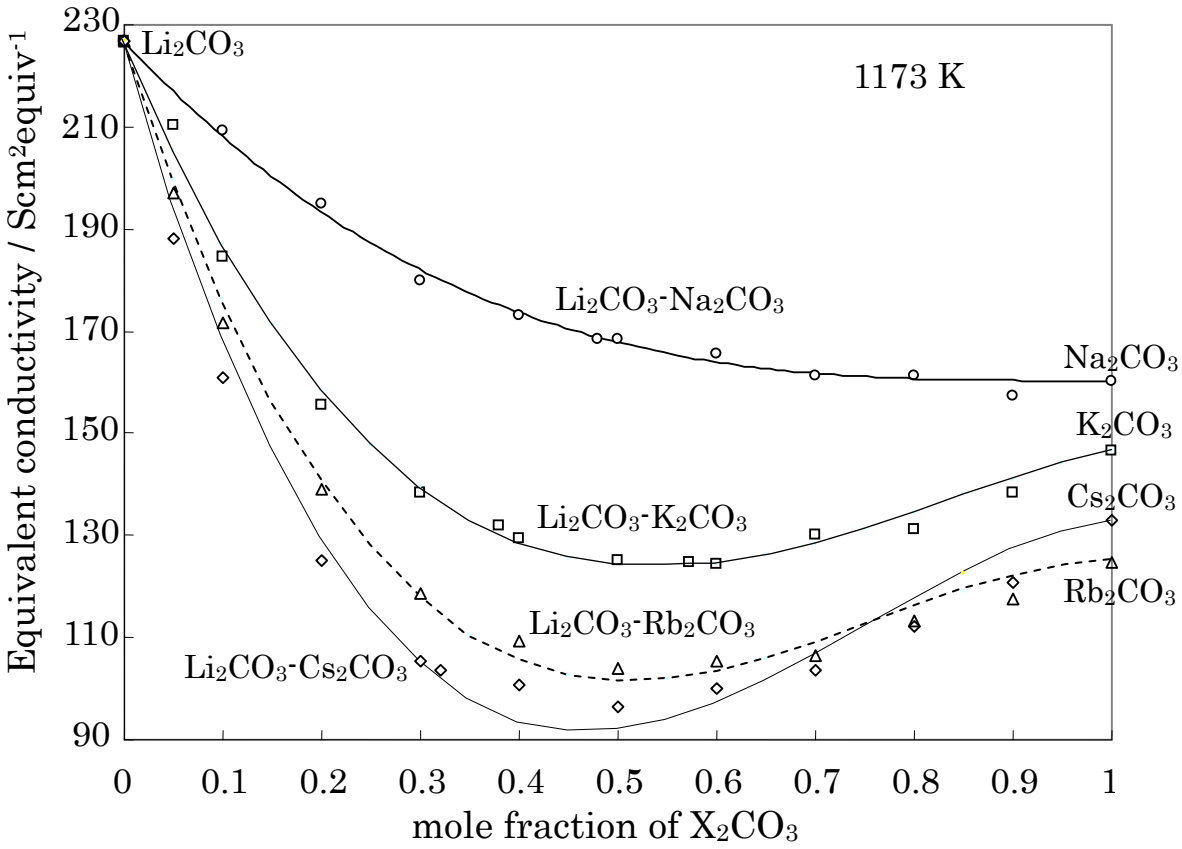

Fig 4-22. The equivalent conductivity of the binary molten carbonates Li_2CO_3-X_2CO_3 (X: Na, K, Rb, and Cs) at 1173 K; the curves were calculated using equation [4-7].

As $x_A + x_B = 1$, $x_A = 1 - x_B$. In equation [4-5], substituting x_A with $1-x_B$, and adding $x_B\Lambda_B - x_B\Lambda_B$, the equation is transformed to equation [4-5'].

$$\Lambda = (1-x_B)\Lambda_A + x_B\Lambda_B - x_B(1-x_B)\Lambda_A - x_B(1-x_B)\Lambda_B + 2(1-x_B)x_B\Lambda_B \quad [4\text{-}5']$$

Then substituting $1-x_B$ with x_A, following equation is obtained:

$$\Lambda = x_A\Lambda_A + x_B\Lambda_B + x_Ax_B(\Lambda_B - \Lambda_A) \quad [4\text{-}6]$$

This equation has three terms; the first and the second obey an additive rule, and the third is a mixing term. The mixing term has the shape of parabola with an increasing depth with an increasing difference between the two equivalent conductivities of the components. Furthermore Spedding used a mixing term $2x_Ax_B\Lambda_{AB}$ adjusting Λ_{AB} instead of $2x_Ax_B\Lambda_B$ in equation [4-5]. But it was find that such an equation differs from the data by up to 20% and cannot correlate well for the whole range of binary systems. We decided that the mixing term should not have a constant coefficient, but one depending on composition. Therefore, equation [4-5] is modified by adding an $\lambda_Ax_A + \lambda_Bx_B$ term instead of Λ_B as follows:

$$\Lambda = x_A^2\Lambda_A + x_B^2\Lambda_B + x_Ax_B(\lambda_Ax_A + \lambda_Bx_B) \quad [4\text{-}7]$$

Here, λ_A and λ_B are interaction parameters of mixing corresponding to the manner in which each component A and B affected the other component. The comparison of equations [4-5] and [4-7] fitting Li_2CO_3-K_2CO_3 system is shown in Fig. 4-21. It is evident that the equation [4-7] can fit the data better than [4-5].

Figs. 4-22 and 4-23 illustrate that equation [4-7] fitted the equivalent conductivity data of mixtures well. The maximum difference was no more than 6% for 7 systems at 1173 K. The fitting parameters are summarized in Table 4-6.

Table 4-6. Interaction parameters λ_A and λ_B of the equation $\Lambda = x_A^2\Lambda_A + x_B^2\Lambda_B + x_Ax_B(\lambda_Ax_A + \lambda_Bx_B)$ for 7 binary carbonate systems at 1173 K.

Systems	λ_A and λ_B / Scm^2eq^{-1}	
	λ_A	λ_B
Li_2CO_3 - Na_2CO_3	246.5	321.6
Li_2CO_3 - K_2CO_3	-4.3	249.0
Li_2CO_3 - Rb_2CO_3	-133.8	242.6
Li_2CO_3 - Cs_2CO_3	-220.6	236.0
Na_2CO_3 - K_2CO_3	277.5	267.7
Na_2CO_3 - Rb_2CO_3	156.7	234.0
Na_2CO_3 - Cs_2CO_3	210.0	146.0

Furthermore, equation [4-7] also fitted well to data from the other molten salt systems of chlorides, iodides, nitrates, and sulfates[6]. Further analysis of these systems will be reported elsewhere.

In equation [4-7], substituting x_A with $1-x_B$, and adding $x_B\Lambda_B - x_B\Lambda_B$, the equation is transformed to equation [4-7'].

$$\Lambda = (1-x_B)\Lambda_A + x_B\Lambda_B - x_B(1-x_B)\Lambda_A - x_B(1-x_B)\Lambda_B + (1-x_B)x_B[\lambda_A(1-x_B) + \lambda_Bx_B] \quad [4\text{-}7']$$

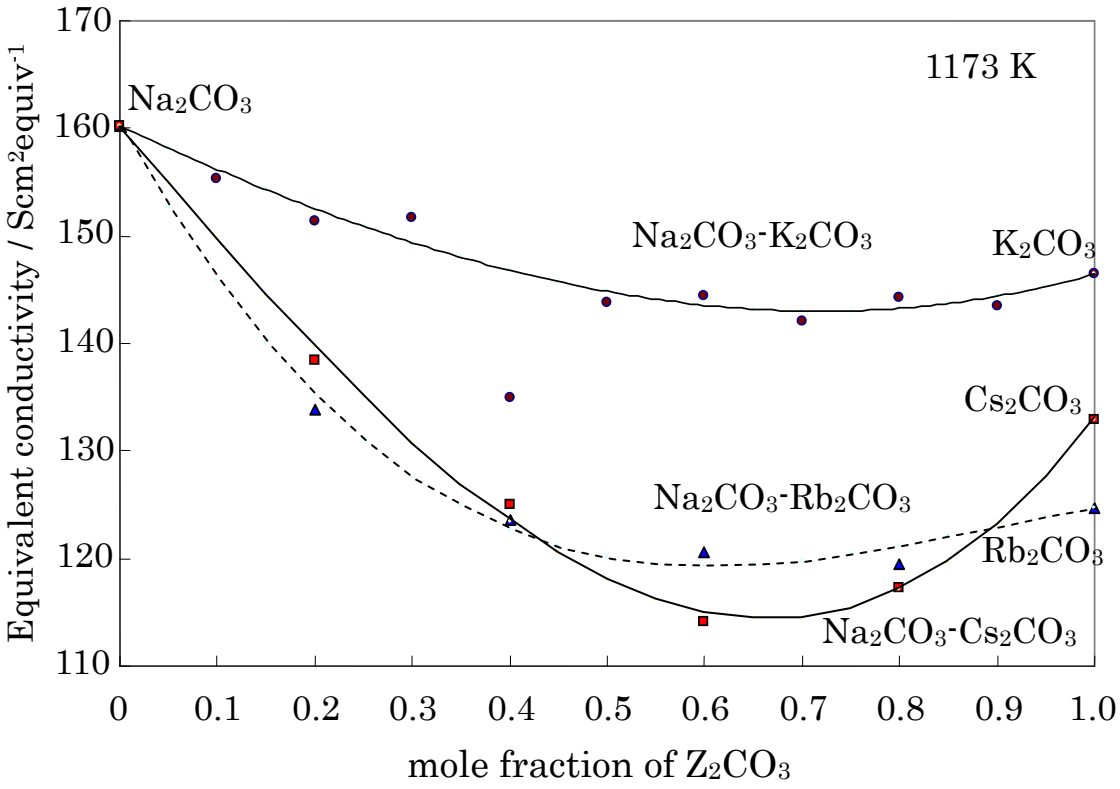

Fig 4-23. The equivalent conductivity of binary molten carbonates Na_2CO_3-Z_2CO_3 (Z: K, Rb, and Cs) at 1173 K; the curves were calculated using equation [4-7].

Then substituting 1-x_B with x_A, following equation is obtained:

$$\Lambda = x_A\Lambda_A + x_B\Lambda_B + x_Ax_B(\lambda_Ax_A + \lambda_Bx_B - \Lambda_A - \Lambda_B) \qquad [4\text{-}8]$$

Therefore, when $\lambda_A = \lambda_B = \Lambda_A + \Lambda_B$, the mixing term $W(x_B) = x_Ax_B(\lambda_Ax_A + \lambda_Bx_B - \Lambda_A - \Lambda_B)$ becomes zero (because $x_A + x_B = 1$), and equation [4-8] then obeys an additivity rule. In most cases, the values of Λ were lower than those from the additivity rule, meaning that λ_A and $\lambda_B < \Lambda_A + \Lambda_B$. Furthermore, by differentiating the mixing term, $d\,W(x_B)/dx_B = W'(x_B)$, one can obtain the increment of the curve at the composition close to that corresponding to a single A salt ($x_B = 0$) as $W'(0) = \lambda_A - (\Lambda_A + \Lambda_B)$, and to a single B salt ($x_B = 1$) as $W'(1) = -\lambda_B + (\Lambda_A + \Lambda_B)$. We obtained the rate of decrease of the equivalent conductivity for compositions near single carbonates as a difference from the additive terms. Their absolute values are $(\Lambda_A + \Lambda_B - \lambda_A)$ for adding B to pure A and $(\Lambda_A + \Lambda_B - \lambda_B)$ for adding A to pure B. It should be noted that the parameters λ_A and λ_B, which describe the equivalent conductivity of the whole binary system in equation [4-7], have a special significance. They are related to the rate of decrease in the mixing term of equivalent conductivity produced by the addition of a second component to a pure component. The additivity correction ($\Delta\Lambda$) to the rate of decrease of the equivalent conductivity at compositions near those of the single carbonates can be expressed in

the following manner, normalized to the equivalent conductivity in the pure carbonate, Λ_i:

$$\Delta\Lambda \equiv (\Lambda_A + \Lambda_B - \lambda_i) / \Lambda_i \qquad [4\text{-}9]$$

where 'i' denotes a pure component of either A or B.

It can be seen that $\Delta\Lambda$ increases with an increasing difference between the sizes of the cation of the pure carbonate and that of the added carbonate. We found that $\Delta\Lambda$ has a relatively good correlation with the relative ionic size difference ΔR, which is defined as the ratio of the change in the cation ionic radius produced by exchanging component A with B, normalized to the cation radius in the pure carbonate, r_i:

$$\Delta R \equiv \left| r_B - r_A \right| / r_i \qquad [4\text{-}10]$$

The plot of $\Delta\Lambda$ against ΔR is shown in Fig. 4-24. Each point in Fig. 4-24 showed the value of the pair of pure carbonate and additive carbonate depicted as 'Pure carbonate←additive carbonate'. It can be seen that $\Delta\Lambda$ is in proportion to ΔR. In the plot, relatively large scatter can be seen for Na←Z or Z←Na (Z: K, Rb, and Cs) data points. It is because of fewer data points of binary carbonate of Na_2CO_3 - Rb_2CO_3 and Na_2CO_3 - Cs_2CO_3 than that of Li_2CO_3 - X_2CO_3 (X: Na, K, Rb, and Cs), in which small error of conductivity affect largely λ values and hence $\Delta\Lambda$, and because of relatively scattered conductivity data of Na_2CO_3- K_2CO_3. This correlation confirmed that ionic size difference plays an important role in the decrease in equivalent conductivity with addition of the second component. The addition of ions of different sizes changes the potential distribution around the additive ion, and this inconsistency may disturb the ionic conduction of the pure component. In order to elucidate the manner in which additives decrease the equivalent conductivity, further data and analysis is needed.

Using the relationship used to construct Fig. 4-24, one can estimate the values of λ_A and λ_B for each binary carbonate system from equations [4-9] and [4-10] using the ionic radii and equivalent conductivities of the pure molten carbonates. The slope of the $\Delta\Lambda/\Delta R$ plot was determined to be 1.88 at 1173 K from seven binary carbonate data as shown in Fig. 4-24 and we defined this value as $k_{carbonate}$. The value $k_{carbonate}$ correlates relative excess decrease of equivalent conductivity from additivity by additive with the relative difference of ionic radii between pure carbonate and additive in binary carbonate systems.

$$\Delta\Lambda \approx k_{carbonate}\Delta R \qquad [4\text{-}11]$$

In addition, from equations [4-9] and [4-10], λ_i is obtained as the following equation:

$$\lambda_i = \Lambda_A + \Lambda_B - \Lambda_i k_{carbonate} \left| r_B - r_A \right| / r_i \qquad [4\text{-}12]$$

Substituting this expression for λ_i into equation [4-8], one can obtain an equation for the conductivity of a mixture based solely on the ionic radii and equivalent conductivity of the pure components:

$$\Lambda = x_A\Lambda_A + x_B\Lambda_B - x_A x_B\, k_{carbonate} \left| r_B - r_A \right| (\Lambda_A x_A / r_A + \Lambda_B x_B / r_B) \qquad [4\text{-}13]$$

We used equation [4-13] to estimate the equivalent conductivities of 7 binary carbonate systems with a standard deviation of 6.6 S cm^2 $equiv^{-1}$ and a maximum deviation of 13%.

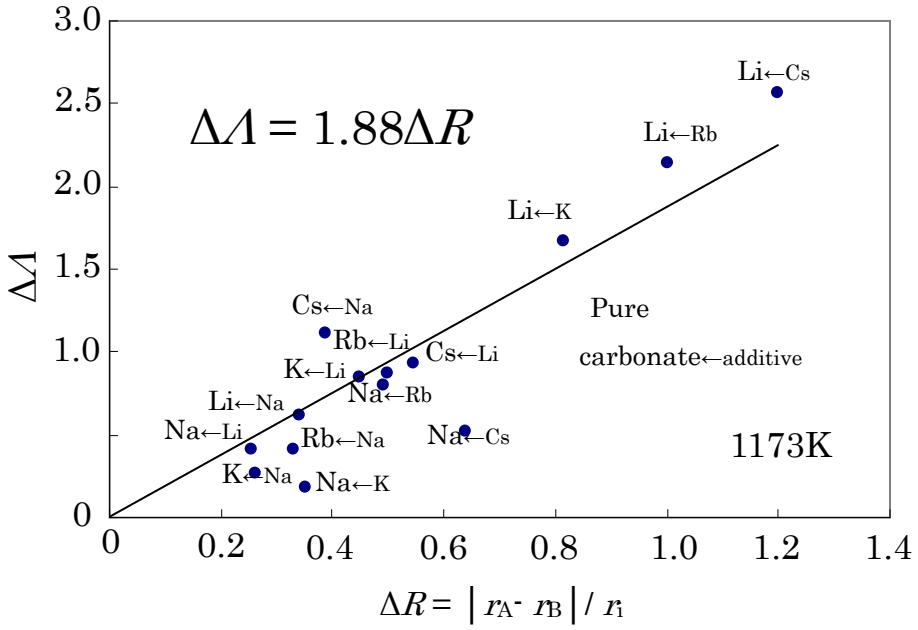

Fig. 4-24. The relationship between the relative rate of decrease of the equivalent conductivity for single carbonates using the additivity correction $\Delta\Lambda$ and the relative ionic size difference ΔR of the binary molten carbonates at 1173 K.

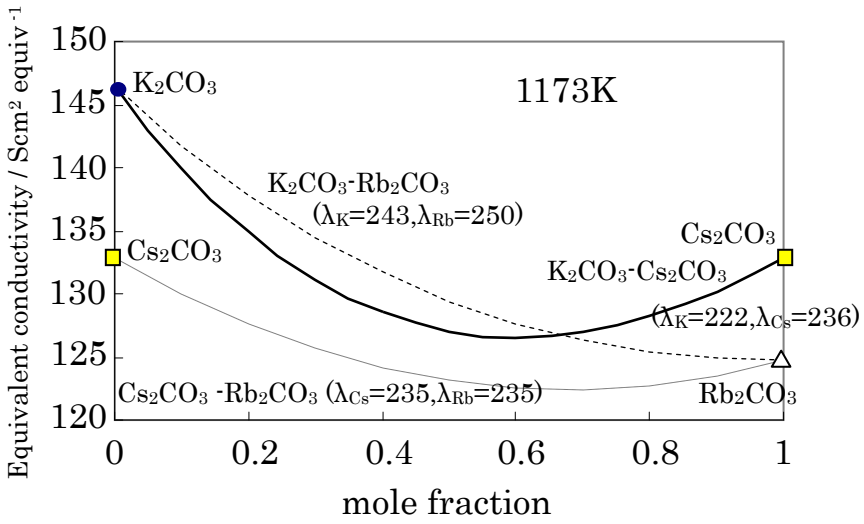

Fig 4-25. Predicted equivalent conductivity of the binary molten carbonates K_2CO_3-Rb_2CO_3, K_2CO_3-Cs_2CO_3, and Rb_2CO_3-Cs_2CO_3 at 1173 K.

It should be pointed out that one can estimate the equivalent conductivities of binary carbonate systems using just the ionic radii and equivalent conductivities of pure components without introducing large errors, even for binary systems where no measured data for the electrical conductivity exists. The conductivity, molar volume, and equivalent conductivity of any binary

carbonate systems consisting of Li_2CO_3, Na_2CO_3, K_2CO_3, Rb_2CO_3, Cs_2CO_3, Ag_2CO_3, Tl_2CO_3 or Fr_2CO_3 can be predicted with reasonable accuracy using equation [4-13], together with known cationic radii[10] and estimated values of the equivalent conductivity. For example, Fig. 4-24 shows the predicted results for K_2CO_3-Rb_2CO_3, K_2CO_3-Cs_2CO_3, and Rb_2CO_3-Cs_2CO_3.

4.4.3. Equivalent conductivity of ternary molten carbonates

The electrical conductivity of the Li_2CO_3 - Na_2CO_3 - K_2CO_3 ternary system at 1073 K is shown in Fig. 4-26 together with contour lines obtained through the interpolation using neighboring measured data.

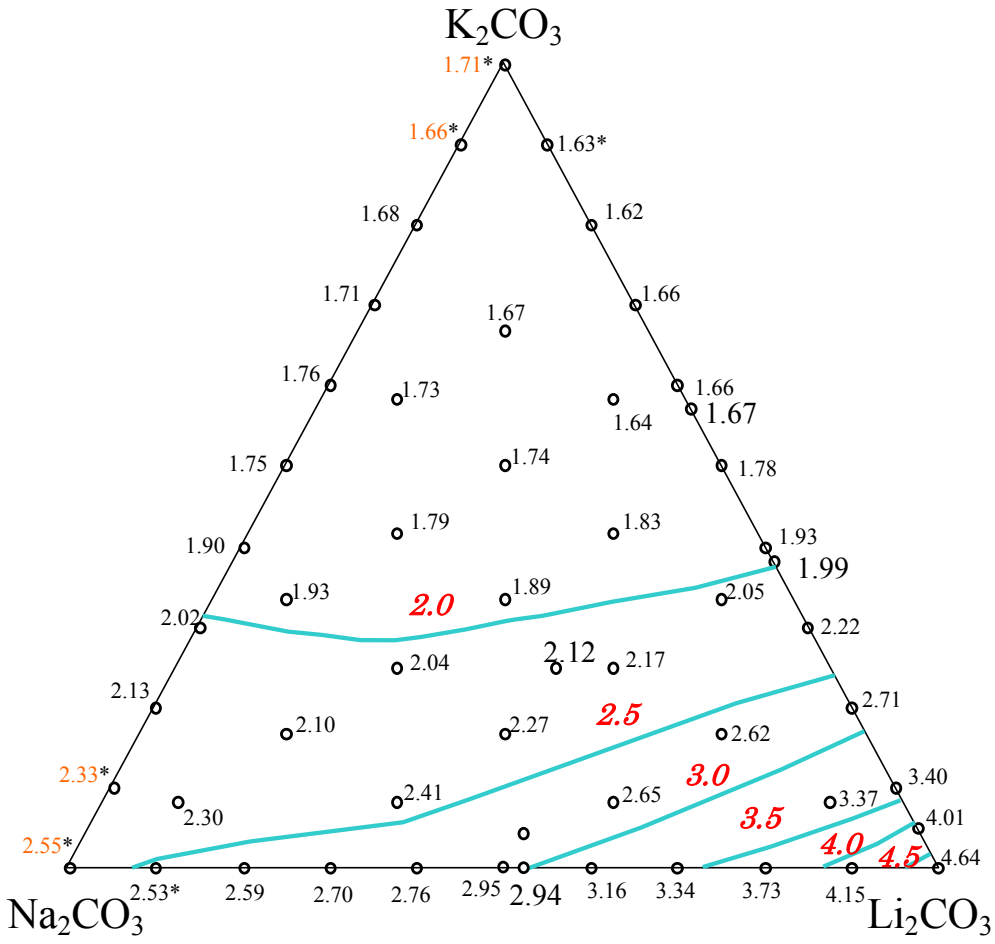

Fig. 4-26. Contour diagram of the conductivity in the molten Li_2CO_3-Na_2CO_3-K_2CO_3 system at 1073 K (S cm^{-1}). (*extrapolated value)

To provide a more theoretical framework, the equivalent conductivities of molten Li_2CO_3-Na_2CO_3-K_2CO_3 are examined as a function of the mole fraction. The equivalent conductivities of the molten carbonates, Λ (S cm^2 $equiv^{-1}$), were computed using the following equation

$$\Lambda = \sigma V_m \qquad [4\text{-}3]$$

The molar volumes of mixtures were estimated with the additivity rule in order to calculate the equivalent conductivity.

For binary molten carbonate systems, we have demonstrated that the following equation correlates the equivalent conductivity with composition in previous section:

$$\Lambda_{A\text{-}B} = x_A\Lambda_A + x_B\Lambda_B - x_Ax_Bk_{carbonate} \mid r_B - r_A \mid (x_A\Lambda_A/r_A + x_B\Lambda_B/r_B) \qquad [4\text{-}14]$$

where x_A and x_B are the mole fraction of components A and B, Λ_A, Λ_B and $\Lambda_{A\text{-}B}$ are the equivalent conductivities of pure components A, B and the binary mixture of A and B, r_A and r_B are Shannon's ionic radii for 6 coordination[10] (Å) in A and B, respectively, and $k_{carbonate}$ was a constant at a particular temperature. The value of $k_{carbonate}$ at other temperatures (T: K) has been obtained by fitting equation [4-14] to seven binary systems and has the following equation:

$$k_{carbonate} = 4.381 - 2.099\times10^{-3}T \qquad [4\text{-}15]$$

The equation [4-14] for molten binary carbonate systems is tried to extend to ternary molten carbonate. In order to predict the equivalent conductivity of ternary molten carbonates consisting of three pure carbonates, A, B, and C, the pure component B in [4-14] is substituted by the mixture of B and C (denoted as BC), and treated the ternary system of A and BC as a pseudo binary system using the following equation:

$$\Lambda_{A\text{-}BC} = x_A\Lambda_A + x_{BC}\Lambda_{B\text{-}C} - x_A\,x_{BC}k_{carbonate} \mid r_{BC} - r_A \mid (x_A\Lambda_A/r_A + x_{BC}\Lambda_{B\text{-}C}/r_{BC}) \qquad [4\text{-}16]$$

where x_{BC} is the sum of mole fractions of B and C, $\Lambda_{B\text{-}C}$ is the equivalent conductivities of the binary mixture of B and C. For the cationic radius of BC we used the average cation radius of B and C from the following equation:

$$r_{BC} = (1-c)r_B + cr_C \qquad [4\text{-}17]$$

where c is the mole fraction of C in the BC binary system.

For example, the equivalent conductivity of the pseudo binary systems of A-BC (B:C=1:1), B-CA (C:A=1:1), and C-AB (A:B=1:1) as Li_2CO_3-$(Na_{0.5}K_{0.5})_2CO_3$, Na_2CO_3-$(Li_{0.5}K_{0.5})_2CO_3$, and K_2CO_3-$(Li_{0.5}Na_{0.5})_2CO_3$ and the fit to equation [4-16] are shown in Fig. 4-27. In this calculation using equation [4-16], measured data for single and binary compositions were used. It can be seen that the equation correlated the data of ternary carbonate with good accuracy using the data of single and binary carbonate mixture. It was found that ternary carbonate mixtures can be treated as pseudo binary mixtures for calculation of equivalent conductivity and the equation [4-16] extended from equation [4-14] of binary carbonate can be used for estimating the equivalent conductivity of ternary carbonate.

Next the equivalent conductivity of a ternary molten carbonate at a composition of (x_A, x_B, x_C), Λ_{ABC}, is tried to estimate only from equivalent conductivities of three single carbonates, Λ_A, Λ_B, and Λ_C without measured data of binary carbonates. At first equivalent conductivities of binary carbonates, $\Lambda_{A\text{-}B}$, $\Lambda_{B\text{-}C}$, and $\Lambda_{C\text{-}A}$ were estimated using Λ_A, Λ_B, Λ_C, and equation [4-14]. Then, $\Lambda_{A\text{-}BC}$,

$\Lambda_{B\text{-}CA}$, and $\Lambda_{C\text{-}AB}$, were estimated using equation [4-16]. The obtained equivalent conductivities $\Lambda_{A\text{-}BC}$, $\Lambda_{B\text{-}CA}$, and $\Lambda_{C\text{-}AB}$ at the same composition of Λ_{ABC}, however, shows small differences from each other. These differences may come from calculating $\Lambda_{A\text{-}B}$, $\Lambda_{B\text{-}C}$, and $\Lambda_{C\text{-}A}$ using equation [4-14]. The nearer composition to BC, CA, or AB, $\Lambda_{A\text{-}BC}$, $\Lambda_{B\text{-}CA}$, or $\Lambda_{C\text{-}AB}$ would contain the larger calculation difference of $\Lambda_{A\text{-}B}$, $\Lambda_{B\text{-}C}$, or $\Lambda_{C\text{-}A}$. In order to minimize the difference by averaging the contributions from Λ_A, Λ_B, Λ_C, $\Lambda_{A\text{-}B}$, $\Lambda_{B\text{-}C}$, and $\Lambda_{C\text{-}A}$, we use following equation;

$$\Lambda_{ABC} = \frac{1}{3}(\Lambda_{A\text{-}BC} + \Lambda_{B\text{-}CA} + \Lambda_{C\text{-}AB}) \qquad [4\text{-}18]$$

Equivalent conductivity of Li_2CO_3 - Na_2CO_3 - K_2CO_3 mixtures were calculated using the conductivity and density data of molten Li_2CO_3, Na_2CO_3, K_2CO_3 and equations [4-14]-[4-18]. The calculated values were in good agreement with the measured values listed in Table 4-3 within 4%. A contour diagram of the equivalent conductivity in Li_2CO_3-Na_2CO_3-K_2CO_3 system is shown in Fig. 4-28 with the contour curves through calculated values. The composition of minimum equivalent conductivity occurs near $(Li_{0.427}K_{0.573})_2CO_3$ at 1073 K.

In section 4.4.1, it is estimated that the molar volume and electrical conductivity using cationic radii for Ag_2CO_3, Tl_2CO_3 and Fr_2CO_3. Using the relationships developed above one can predict the equivalent conductivity, molar volume, and electrical conductivity for any composition of whole ternary systems using the cationic radii, molar volume and electrical conductivity of any trio of pure components, such as Li_2CO_3, Na_2CO_3, K_2CO_3, Rb_2CO_3, Cs_2CO_3, Ag_2CO_3, Tl_2CO_3, and Fr_2CO_3.

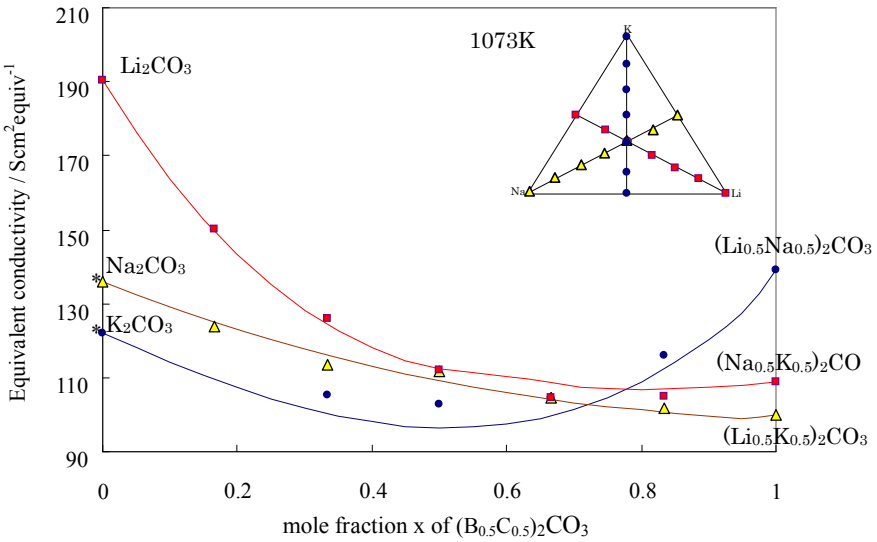

Fig. 4-27. Equivalent conductivity of pseudo binary molten carbonates, Li_2CO_3-$(Na_{0.5}K_{0.5})_2CO_3$, Na_2CO_3-$(Li_{0.5}K_{0.5})_2CO_3$, and K_2CO_3-$(Li_{0.5}K_{0.5})_2CO_3$ fitted by equation [4-16] at 1073 K.(*extrapolated value)

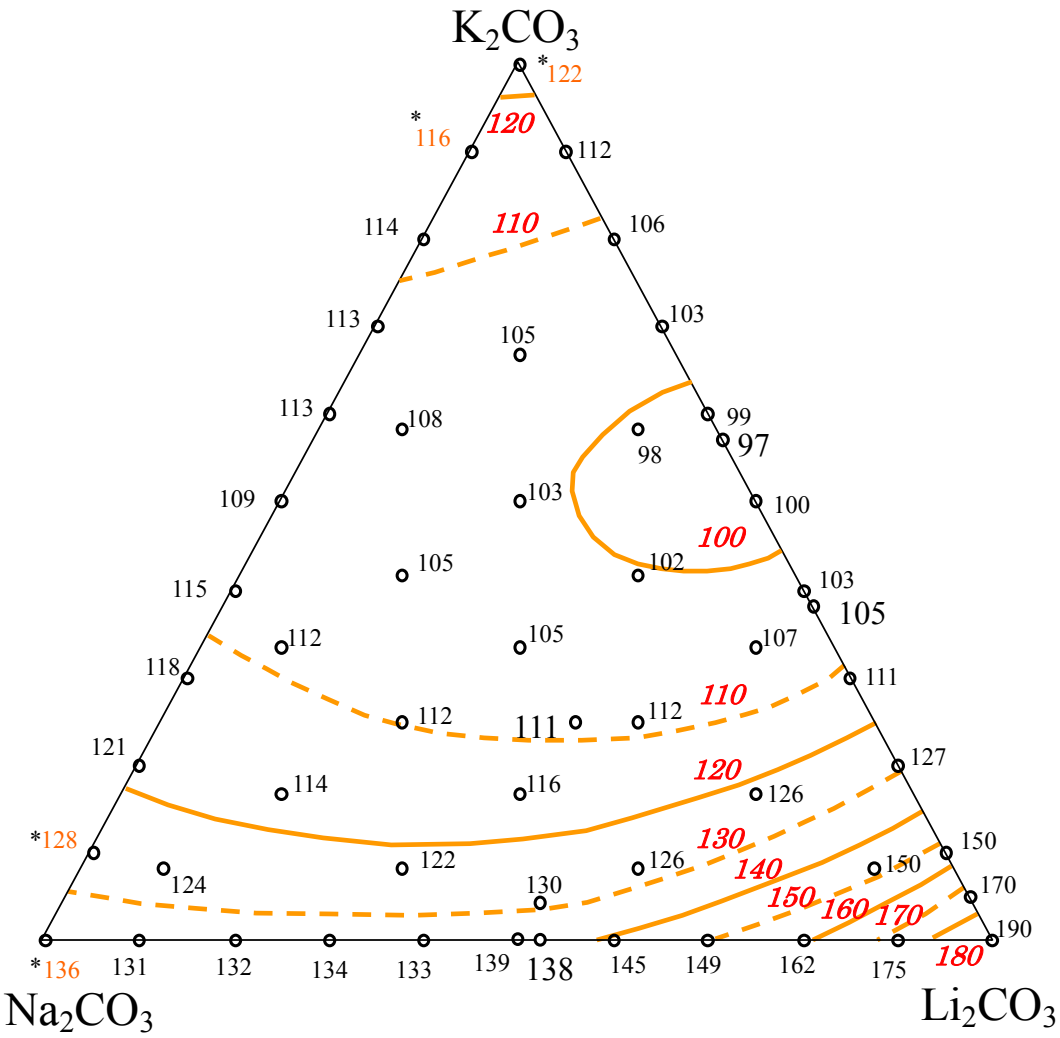

Fig. 4-28. Equivalent conductivity in the molten Li_2CO_3-Na_2CO_3-K_2CO_3 system at 1073 K (Scm^2equiv^{-1}) and predicted contour lines using equations from [4-14] to [4-18]. (*extrapolated value)

4.4.4. Estimation method for the conductivity of molten alkali-alkaline earth carbonates

The results of the electrical conductivity at 1073K of molten Li_2CO_3-Na_2CO_3, Li_2CO_3-K_2CO_3 and Li_2CO_3-alkaline earth (Ca, Sr and Ba) carbonates are shown in Fig.4-29. Additon of alkaline earth carbonate to molten Li_2CO_3 resulted in linear decrease of the electrical conductivity. The additives' effects of decreasing electrical conductivity in these systems follows $K_2CO_3 > BaCO_3 \geq SrCO_3 \geq CaCO_3 > Na_2CO_3$. Although the difference of ionic radii[10] between Ca^{2+}(100pm) and Ba^{2+}(140pm) is as much as that between Na^+ (100pm) and K^+(150pm), there is greater difference in the effect of decreasing electrical conductivity between Na_2CO_3 and K_2CO_3 than that among alkaline earth carbonates. This means that the sizes of alkali cations have stronger influence on the conductivity than those of alkaline earth cations.

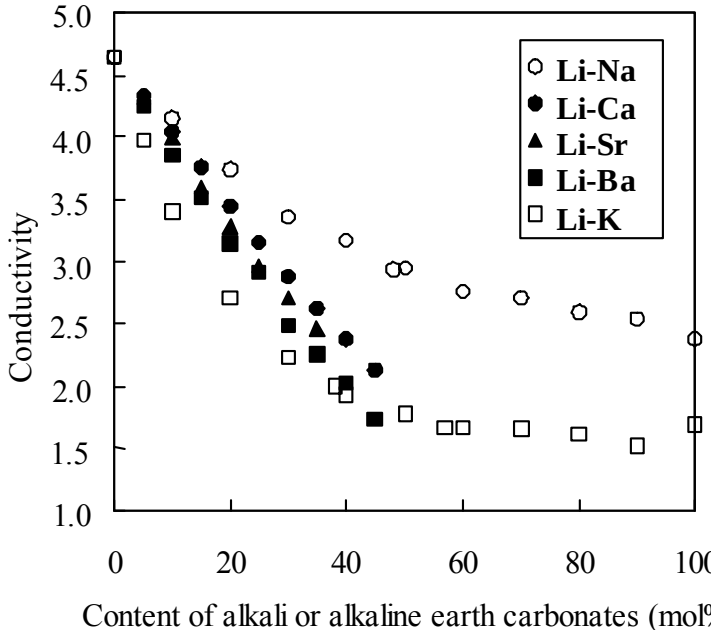

Fig.4-29. The composition dependence of electrical conductivity in molten Li_2CO_3-$CaCO_3$, Li_2CO_3-$SrCO_3$, Li_2CO_3-$BaCO_3$, Li_2CO_3-Na_2CO_3 and Li_2CO_3-K_2CO_3 systems at 1073K.

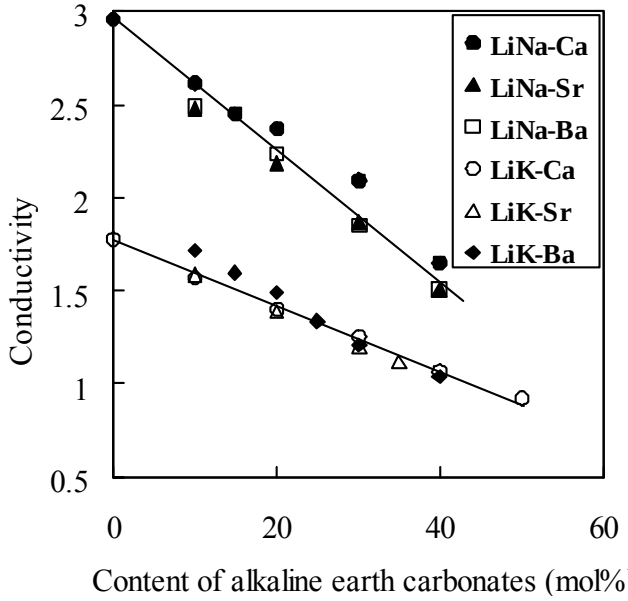

Fig.4-30. The electrical conductibity of molten Li_2CO_3-Na_2CO_3 (50:50mol%) and Li_2CO_3-K_2CO_3 (50:50mol%) containing alkaline earth carbonates at 1073K.

The conductivity of Li_2CO_3-Na_2CO_3 (50:50mol%) and Li_2CO_3-K_2CO_3 (50:50mol%) added with alkaline earth carbonate at 1073K are shown in Fig. 4-30. The addition of each alkaline earth carbonate to Li_2CO_3-Na_2CO_3 (50:50mol%) and Li_2CO_3-K_2CO_3 (50:50mol%) results in linear decrease of the electrical conductivity with increase of the mole fraction of the additives. There is also not so much difference among the alkaline earth carbonates in the effect of decreasing the electrical conductivity. The electrical conductivity of molten Li_2CO_3-Na_2CO_3 (70:30mol%), (30:70mol%), and Li_2CO_3-K_2CO_3 (80:20mol%), (30:70mol%) containing alkaline earth carbonates are also measured. The results shows that the addition of alkaline earth carbonate makes the electrical conductivity of these melt decrease linearly with increase of the mole fraction of the additives. And there is also little difference in the effect of decreasing the electrical conductivity among the additives.

Since the electrical conductivity of these carbonate melts linearly decrease with increase of the content of alkaline earth carbonate, one can correlate the electrical conductivity of these melt with content of alkaline earth carbonate by using following equation:

$$\sigma_{mix} = \sigma_{alkali}(1 - kX_{A.E.}/100) \qquad [4\text{-}19]$$

where σ_{alkali} and σ_{mix} are the conductivity of molten alkali carbonate and one added with alkaline earth carbonate by the content of $X_{A.E.}$ (mol%), respectively. k is the constant which is determined from the slope of the plot of $\sigma_{mix}/\sigma_{alkali}$ vs. $X_{A.E.}$. For example, k was determined to be 1.14 from the data of whole composition in molten Li_2CO_3-Na_2CO_3-$CaCO_3$ system at 1073K shown in Fig.4-31. The values of k at 1073K of other systems are summarized in Table 4-7. The k values for any measured carbonate systems containing alkaline earth carbonates are not so much different. They show quite similar values around 1.2.

The electrical conductivity of any composition in the systems of Li_2CO_3-Na_2CO_3-alkaline earth or Li_2CO_3-K_2CO_3-alkaline earth can be approximately estimated using k values and the electrical conductivity data of molten Li_2CO_3-Na_2CO_3 and Li_2CO_3-K_2CO_3 binary systems. The measured values and calculated contour diagrams of Li_2CO_3-Na_2CO_3-$CaCO_3$ and Li_2CO_3-K_2CO_3-$CaCO_3$ at 1073K are shown in Fig. 4-32 and Fig. 4-33, respectively. It can be seen that calculated contour diagrams agree well with the measured values.

The k is greater than 1 means added alkaline earth cation prevent the conduction of alkali cations, while k is less than 1 means alkaline earth cation contribute the total conduction. The vale of k, about 1.2 indicate that there is little contribution and prevention to the total conduction in molten carbonate.

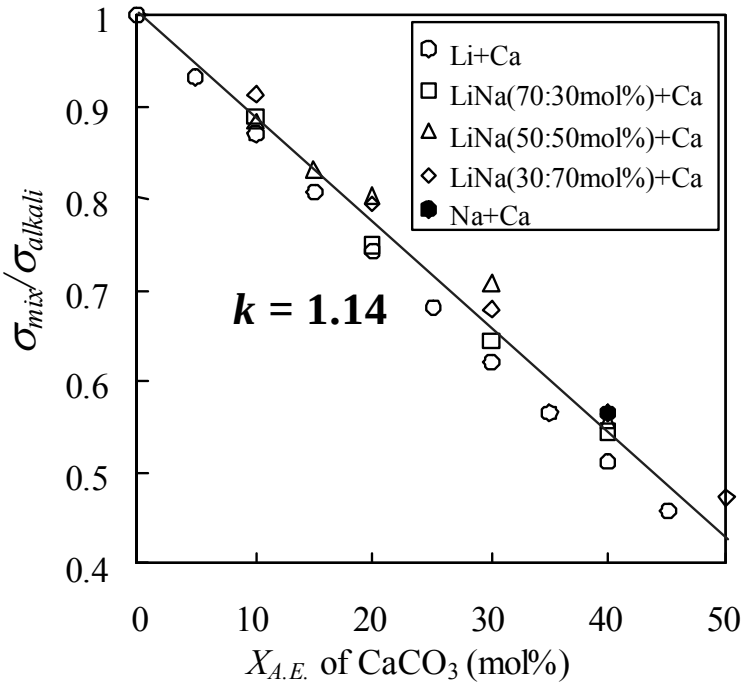

Fig.4-31. Plot of $\sigma_{mix}/\sigma_{alkali}$ vs. content of $CaCO_3$, $X_{A.E.}$ for molten Li_2CO_3-Na_2CO_3-$CaCO_3$ carbonate system at 1073K .

Table 4-7. The *k* values for molten Li_2CO_3-Na_2CO_3 and Li_2CO_3-K_2CO_3 containing alkaline earth (Ca, Sr and Ba) carbonates at 1073K.

Ternary system of molten carbonate	*k*	Square of Correlation Coefficient r^2	Standard deviation for estimation of $\sigma_{mix}/\sigma_{alkali}$
Li-Na-Ca	**1.14**	**0.97**	**0.027**
Li-Na-Sr	**1.17**	**0.98**	**0.028**
Li-Na-Ba	**1.31**	**0.95**	**0.042**
Li-K-Ca	**1.10**	**0.95**	**0.036**
Li-K-Sr	**1.23**	**0.93**	**0.038**
Li-K-Ba	**1.22**	**0.86**	**0.064**

In alkali (Li, Na and K) carbonate melt, alkali cation which is relatively smaller than carbonate ion is thought to contribute to most of the electrical conduction of the molten carbonate. Since each alkali earth cation has double charge of an alkali cation, it should strongly attract the carbonate ions and this restricts its movement greater than alkali cations. From the facts that *k* are about 1.2, and there is little difference in the effect of decreasing conductivity among the alkaline earth carbonate in spite of the difference of cation radii, it can be concluded that alkaline earth cations should have no contribution to conduction. Therefore the decrease of electrical conductivity of molten Li_2CO_3-K_2CO_3 and Li_2CO_3-Na_2CO_3 added with alkaline earth (Ca, Sr and Ba) carbonates are simply brought by the exchanging conductive alkali cations for relatively no conductive alkaline earth cation.

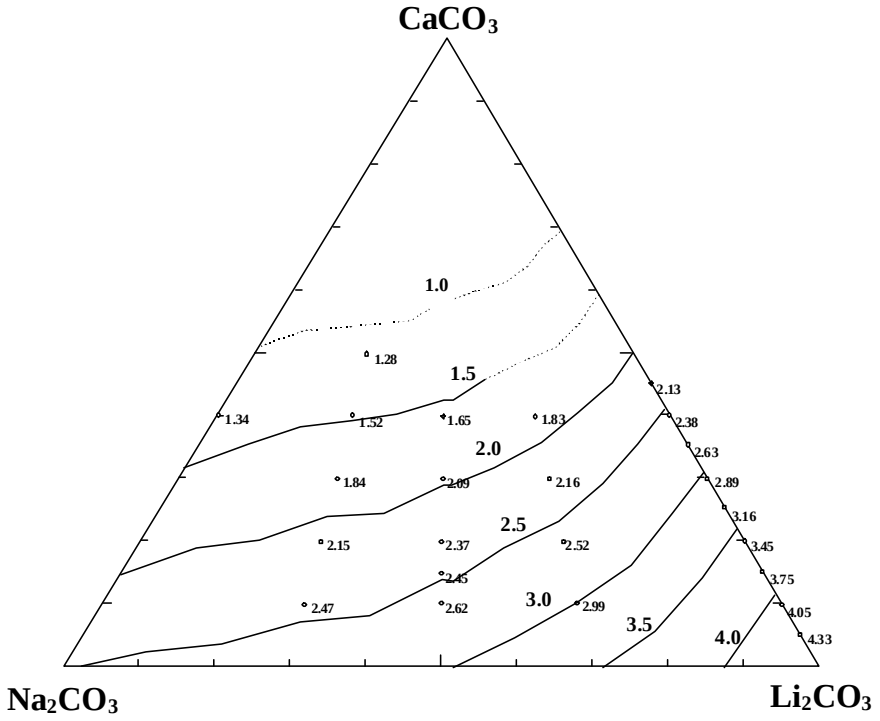

Fig.4-32. The electrical conductivity (Scm^{-1}) of molten Li_2CO_3-Na_2CO_3-$CaCO_3$ at 1073K and calculated contour curves from *k* value.

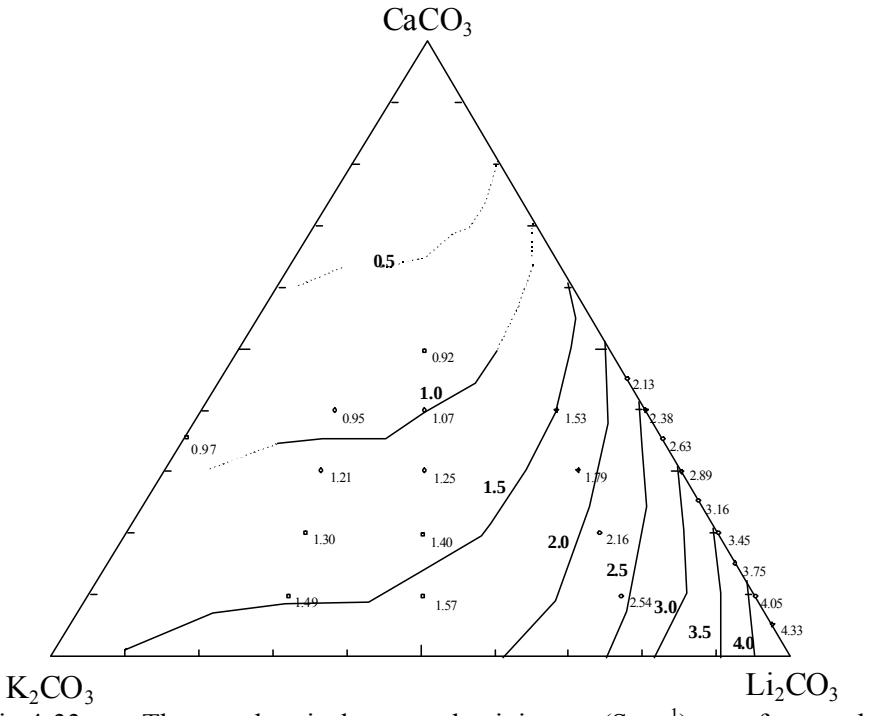

Fig.4-33. The electrical conductivity (Scm^{-1}) of molten Li_2CO_3-K_2CO_3-$CaCO_3$ at 1073K and calculated contour curves from *k* value.

4.5. Conclusion

The electrical conductivities of the molten binary salts Li_2CO_3-X_2CO_3 (X: Na, K, Rb, and Cs) and Na_2CO_3-Z_2CO_3 (Z: K, Rb, and Cs) were measured by an AC two probe technique and electrochemical impedance spectroscopy.

The electrical conductivities of the important eutectic compositions for the MCFC electrolytes $(Li_{0.52}Na_{0.48})_2CO_3$ and $(Li_{0.62}K_{0.38})_2CO_3$ were 2.06 and 1.31 S cm^{-1} at 923 K.

The conductivity of molten Li_2CO_3-X_2CO_3 (X: Na, K, Rb, and Cs) or Na_2CO_3-Z_2CO_3 (Z: K, Rb, and Cs) at the same composition of additives (X_2CO_3 or Z_2CO_3) decreased with an increase in the ionic radius of X or Z.

The equivalent conductivity of Cs_2CO_3 was larger than that of Rb_2CO_3. For cations larger than Rb^+, the molar volume plays a more important role in determining the equivalent conductivity than does the electrical conductivity.

The equivalent conductivities of binary carbonate mixtures Λ, were well correlated with the composition (x_A and x_B), the equivalent conductivities (Λ_A and Λ_B) of the pure components A and B, and two interaction parameters (λ_A and λ_B) as $\Lambda = x_A^2\Lambda_A + x_B^2\Lambda_B + x_Ax_B(\lambda_Ax_A+\lambda_Bx_B)$.

The interaction parameters (λ_A and λ_B) can be estimated from the equivalent conductivity of the pure components and their cationic radii.

The conductivity, molar volume, and equivalent conductivity of any binary carbonate systems consisting of Li_2CO_3, Na_2CO_3, K_2CO_3, Rb_2CO_3, Cs_2CO_3, Ag_2CO_3, Tl_2CO_3 or Fr_2CO_3 can be predicted using simply the ionic radii and equivalent conductivities of the pure components with a reasonable degree of accuracy.

The method for estimating the equivalent conductivity and composition of molten binary carbonate systems was extended to ternary molten carbonate systems. We have succeeded in estimating the equivalent conductivities of the ternary molten carbonates listed in Table III within 4% by dealing them as pseudo binary systems, and using the cationic radii and equivalent conductivity of the three constituent single molten carbonates.

The addition of alkaline earth carbonates to molten Li_2CO_3-K_2CO_3 and Li_2CO_3-Na_2CO_3 results in linear decrease of electrical conductivity with increase of the mole fraction of the additives. There is not so much difference among the alkaline earth carbonates in the effect of decreasing electrical conductivity at the same content of addition.

Reference

[1] G. J. Janz and M. R. Lorenz, "Molten Carbonate Electrolyte: Physical Properties, Structure, and Mechanism of Electrical Conductance," *J. Electrochem. Soc*., **108**, 1052-1058 (1961).

[2] A. T. Ward and G. J. Janz, "Molten Carbonate Electrolytes: Electrical Conductance, Density and Surface Tension of Binary and Ternary Mixtures," *Electrochimica Acta*, **10**, 849-857 (1965).

[3] P. L. Spedding, “Electrical Conductance of Molten Alkali Carbonate Binary Mixtures,” *J. Electrochem. Soc*., **120**, 1049-1052 (1973).

[4] K. B. Kim and D. R. Sadoway, “Electrical Conductivity Measurements of Molten Alkaline-Earth Fluorides,” *J. Electrochem. Soc*., **139**, 1027 (1992).

[5] Y. Miyazaki, M. Yanagida, K. Tanimoto, T. Kodama, and S. Tanase, “An Apparatus for Electrical Conductance Measurements with Molten Carbonates,” *J. Electrochem. Soc*., **133**, 1402-1404 (1986).

[6] G. J. Janz, *J. Phys. Chem. Ref. Data*, **17**, 1 (1988).

[7] T. Kojima, Y. Miyazaki, M. Yanagida, K. Tanimoto, H. Okuyama, T. Kodama, and S. Tanase, “Conductance measurements in molten carbonates I. alkali carbonates,” *Denki Kagaku*, **59**, 247-249 (1991).

[8] S. Tanase, Y. Miyazaki, M. Yanagida, K. Tanimoto, and T. Kodama, *Prog. Batteries Sol. Cells*, **7**, 389 (1988).

[9] T. Nakamura and M. Itoh, “Specific conductance and free-ion behavior of component ions in molten alkali halides,” *J. Electrochem. Soc*., 137, 1166 (1990).

[10] R. D. Shannon, *Acta Crystallogr., Sect. A: Cryst. Phys., Diffr., Theor. Gen. Crystallogr.*, **A32**, 751 (1976).

[11] T. Kojima, Y. Miyazaki, K. Nomura, and K. Tanimoto, “Density, molar volume, and surface tension of molten Li_2CO_3-Na_2CO_3 and Li_2CO_3-K_2CO_3 containing alkaline earth (Ca, Sr, and Ba) carbonates”, *J. Electrochem. Soc.*, **150**, E535-E542 (2003).

5. Reaction of materials with lanthanum in molten carbonates

5.1. Introduction

Lanthanum-containing perovskites have been used as materials for electronic devices, sensors, catalysts, and fuel cell components. In general, these compounds have been synthesized through a process involving the sintering of mixed oxides. In particular, the usage of the less reactive La_2O_3 as one of the reagents requires a multi-step time-consuming procedure of mixing and heating at temperatures higher than 1200 K.

Lower temperature syntheses of lanthanum-containing perovskites are favorable because of the advantages of reducing the production cost and of controlling particle size and composition of product. The compound $LaMnO_{3\pm d}$ was synthesized at 623 K using reactive amorphous precursors obtained from a stoichiometric citrate solution[1]. $LaAlO_3$ was prepared through a gelation-precipitation technique at 873 K.[2]

Molten salts have been used for new synthesis method of precise compositions and (or) structure control at relatively low temperatures. $LaCrO_3$ was produced in molten KOH at 513 K[3]. $LaMn_{0.8}Na_{0.2}O_3$ was produced in molten NaOH at 723 K[4]. Alkali-doped $LaNiO_3$ was synthesized in molten KOH at 673 K[5].

Molten carbonates have been used as a flux of perovskite synthesis. For example, $LaNiO_3$ was produced with the aid of a Na_2CO_3 flux at 1073 K[6]. K_2CO_3 was used for the structure controlling synthesis of $Ba_{11}Rh_{10}O_{30}$ and $Ba_{32}Rh_{29}O_{87}$ at 1323K, aiming at the synthesis of 2H-$BaRhO_3$[7]. As far as we know, however, there are quite a few reports for the synthesis of $LaMO_3$ perovskites using molten carbonates.

In this section, it have been investigated novel methods for the synthesis of $LaMO_3$ using mainly molten $(Li_{0.52}Na_{0.48})_2CO_3$, which has been studied as the electrolyte of molten carbonate fuel cells[8],and applied the method to synthesize several lanthanum perovskites at (or lower than) 923 K. Then a $LaMO_3$ coating method is presented on metal or ceramic substrates. Lastly the reaction mechanism of $LaAlO_3$ formation in molten carbonate is discussed on the basis of in-situ X-ray diffraction data.

5.2. Experimental

5.2.1 Powder $LaMO_3$ synthesis

Schematic view of a reactor vessel is shown in Fig. 5-1.

Li_2CO_3 (Nakarai Tesque, 99%), Na_2CO_3 (Nakarai Tesque, 99.5%), and K_2CO_3 (Nakarai Tesque, 99.5%) were used for preparing molten carbonate mixtures. These carbonates were mixed to the eutectic compositions of $(Li_{0.52}Na_{0.48})_2CO_3$, $(Li_{0.62}K_{0.38})_2CO_3$, $(K_{0.573}Li_{0.427})_2CO_3$, or $(Li_{0.435}Na_{0.315}K_{0.25})_2CO_3$**;** after having been melted at 923 K, they were stored in an electric oven at

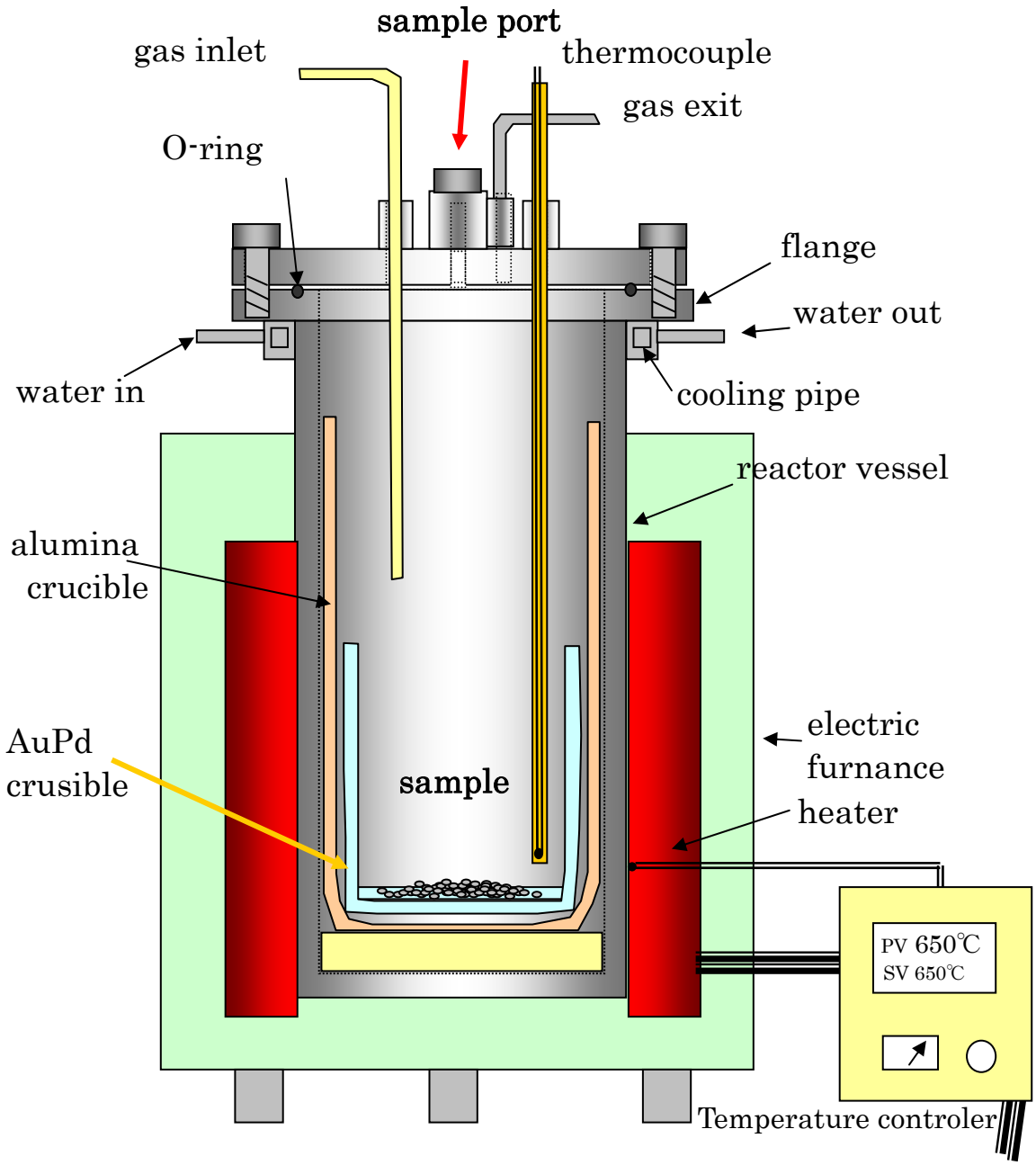

Fig.5-1. Schematic view of a reactor vessel for $LaMO_3$ synthesis.

373K before use. $(Li_{0.52}Na_{0.48})_2CO_3$ was mainly used as a flux of perovskite synthesis. For the lower temperature synthesis at 773K, molten $(Li_{0.435}Na_{0.315}K_{0.25})_2CO_3$ was used for several lanthanum perovskites synthesis. Other carbonates were used for the synthesis of $LaAlO_3$.

The following oxides and a acetate were used as the metal (M) source of $LaMO_3$: α-Al_2O_3 (Aldrich,

99.998%), Sc_2O_3 (Aldrich, 99.999%), Fe_2O_3 (Kishida Chemical, 99.97%), Co_3O_4 (Kanto Kagaku, 99.95%), Ga_2O_3 (Cerac, 99.995%), and $Mn(CH_3COO)_3{\cdot}2H_2O$ (Merck, 98%). The oxide or acetate needed to synthesize 10mmol of $LaMO_3$ were mixed with 5 mmol of $La_2(CO_3)_3{\cdot}8H_2O$ and about 2 g of the alkali carbonate mixture.

To prepare the precursor through co-precipitation, the following metal nitrates or acetate was used as starting materials: $Cr(NO_3)_3{\cdot}9H_2O$ (Kishida Chemical, 98%), $Ni(NO_3)_2{\cdot}6H_2O$ (Kanto Kagaku, 98%), $In(NO_3)_3{\cdot}3H_2O$ (Mitsuwa Chemical, 99%), and $Mn(CH_3COO)_3{\cdot}2H_2O$ (Merck, 98%). An appropriate amount of $La_2(CO_3)_3{\cdot}8H_2O$ and the metal nitrate or acetate needed for 10mmol of $LaMO_3$ synthesis were dissolved in dilute nitric acid. A saturated hot aqueous solution of Na_2CO_3 was poured into the La-M nitrate or acetate mixture solutions in order to form the precipitates. The precipitates were vacuum-filtered**,** washed with distilled water, and then dried. The cake obtained was crushed and mixed with about 2 g of the alkali carbonate mixture.

The precursor mixtures were placed in a Au-Pd (80:20wt.%) alloy crucible (40mmϕ inner diameter, 60mm high) and kept at elevated temperatures.

The mixtures obtained were ground, washed with distilled water, and filtered in order to remove alkali carbonates. Then, the $LaMO_3$ products (M=Al, Sc, Cr, Fe, Co, Ni, Ga, and In) were washed with 12M HCl for further purification.

The materials used and the experimental conditions (reaction temperature, reaction time, and atmosphere) for powder $LaMO_3$ synthesis are summarized in Table 5-1.

5.2.2 $LaMO_3$ production on the metal and ceramic surfaces

The following substrates were placed in a Au-Pd (80:20wt.%) crucible containing the mixture of $(Li_{0.52}Na_{0.48})_2CO_3$ and $La_2(CO_3)_3{\cdot}8H_2O$ (1:1 by weight): the metals aluminum (Nilaco, 99.999%, 20×20×0.1mm), chromium (Nilaco, 99.9%,20×5×5mm), iron (Nilaco, 99.98%, 20×20×0.5mm), cobalt (Nilaco, 99.98%, 20×20×0.5mm), and nickel (Nilaco, 99.7%, 20×20×0.5mm), and α -Al_2O_3 ceramics (Nikkato, SSA-S, 20×20×3mm). A single crystal α -Al_2O_3 (Dalian Danning Opt-electronics Technology, 99.99%, C-plane (0001) , 10×10×0.5mm) was suspended by a gold wire (0.3mmϕ) in the mixture of $(Li_{0.52}Na_{0.48})_2CO_3$ and $La_2(CO_3)_3{\cdot}8H_2O$ (10:1 by weight). The single crystal plane was set face below in order to prevent the floating particles from accumulating on the plane. These samples were kept at 923 K.

The samples, after the immersion in molten carbonates containing lanthanum carbonate, were washed with distilled water in order to remove the carbonate from their surfaces. The materials used and the experimental conditions are summarized in Table 5-1.

Table 5.1. Reaction conditions and results of the synthesis of $LaMO_3$ (M= Al, Sc, Cr, Mn, Fe, Co, Ni, Ga, and In) powder in alkali carbonate.

Materials	Alkali carbonates	Precursors	Temperature (K)	Atmospheres	Reaction time (h)	Product
Al	$(Li_{0.52}Na_{0.48})_2CO_3$	Immersion[c)]	923	CO_2	12h	$LaAlO_3$
α-Al_2O_3	$(Li_{0.52}Na_{0.48})_2CO_3$	Mixture [a)]	923	CO_2	12h	$LaAlO_3$
α-Al_2O_3	$(Li_{0.62}K_{0.38})_2CO_3$	Mixture [a)]	923	CO_2	12h	$LaAlO_3$
α-Al_2O_3	$(K_{0.573}Li_{0.427})_2CO_3$	Mixture [a)]	923	CO_2	12h	$LaAlO_3$
α-Al_2O_3	$(Li_{0.435}Na_{0.315}K_{0.25})_2CO_3$	Mixture [a)]	923	CO_2	12h	$LaAlO_3$
α-Al_2O_3	$(Li_{0.435}Na_{0.315}K_{0.25})_2CO_3$	Mixture [a)]	773	N_2	72h	$LaAlO_3$
α-Al_2O_3 (alumina)	$(Li_{0.52}Na_{0.48})_2CO_3$	Immersion[c)]	923	CO_2	12h	$LaAlO_3$ on the surface
α-Al_2O_3 (sapphire)	$(Li_{0.52}Na_{0.48})_2CO_3$	Immersion[c)]	923	CO_2	72h	$LaAlO_3$ on the surface
α-$LiAlO_2$	$(Li_{0.52}Na_{0.48})_2CO_3$	Mixture [a)]	923	CO_2	18h	$LaAlO_3$
α-$LiAlO_2$	$(Li_{0.52}Na_{0.48})_2CO_3$	Mixture [a)]	923	N_2	3h	$LaAlO_3$
Sc_2O_3	$(Li_{0.52}Na_{0.48})_2CO_3$	Mixture [a)]	923	CO_2	72h	$LaScO_3$
Sc_2O_3	$(Li_{0.435}Na_{0.315}K_{0.25})_2CO_3$	Mixture [a)]	773	N_2	72h	Sc_2O_3 + $La_2O_2CO_3$
$Cr(NO_3)_3{\cdot}9H_2O$	$(Li_{0.52}Na_{0.48})_2CO_3$	Co-precipitated mixture [b)]	923	CO_2	72h	$LaCrO_3$
$Cr(NO_3)_3{\cdot}9H_2O$	$(Li_{0.435}Na_{0.315}K_{0.25})_2CO_3$	Co-precipitated mixture [b)]	773	CO_2	12h	$LaCrO_3$
Cr	$(Li_{0.52}Na_{0.48})_2CO_3$	Immersion[c)]	923	CO_2/ O_2=2/1	12h	$LaCrO_3$ on the surface
$Mn(CH_3COO)_3{\cdot}2H_2O$	$(Li_{0.52}Na_{0.48})_2CO_3$	Co-precipitated mixture [b)]	923	CO_2	72h	$LaMnO_3$
$Mn(CH_3COO)_3{\cdot}2H_2O$	$(Li_{0.435}Na_{0.315}K_{0.25})_2CO_3$	Mixture [a)]	773	Air	12h	$LaMnO_3$
Fe_2O_3	$(Li_{0.52}Na_{0.48})_2CO_3$	Mixture [a)]	923	CO_2	16h	$LaFeO_3$
Fe_2O_3	$(Li_{0.435}Na_{0.315}K_{0.25})_2CO_3$	Mixture [a)]	773	CO_2	12h	$LaFeO_3$
Fe	$(Li_{0.52}Na_{0.48})_2CO_3$	Immersion[c)]	923	CO_2/ O_2=2/1	12h	$LaFeO_3$ on the surface
Co_3O_4	$(Li_{0.52}Na_{0.48})_2CO_3$	Mixture [a)]	923	O_2/CO_2=1/2	12h	$LaCoO_3$
Co_3O_4	$(Li_{0.435}Na_{0.315}K_{0.25})_2CO_3$	Mixture [a)]	773	O_2	72h	unidentified + $La_2O_2CO_3$
Co	$(Li_{0.52}Na_{0.48})_2CO_3$	Immersion[c)]	923	CO_2/ O_2=2/1	12h	CoO on the surface
$Ni(NO_3)_2{\cdot}6H_2O$	$(Li_{0.52}Na_{0.48})_2CO_3$	Co-precipitated mixture [b)]	923	O_2	72h	$LaNiO_3$
Ni_2O_3	$(Li_{0.435}Na_{0.315}K_{0.25})_2CO_3$	Co-precipitated mixture [b)]	773	O_2	12h	$LaNiO_3$ + NiO + $La_2O_2CO_3$
Ni	$(Li_{0.52}Na_{0.48})_2CO_3$	Immersion[c)]	923	CO_2/ O_2=2/1	12h	NiO on the surface
Ga_2O_3	$(Li_{0.52}Na_{0.48})_2CO_3$	Mixture [a)]	923	CO_2,	72h	$LaGaO_3$
Ga_2O_3	$(Li_{0.435}Na_{0.315}K_{0.25})_2CO_3$	Mixture [a)]	773	N_2	72h	$LaGaO_3$
$In(NO_3)_3{\cdot}3H_2O$	$(Li_{0.52}Na_{0.48})_2CO_3$	Co-precipitated mixture [b)]	1173	CO_2,	72h	$LaInO_3$

a) mixed with $La_2(CO_3)_3{\cdot}8H_2O$ and alkali carbonate. b) co-precipitated with equimolar lanthanum, then mixed with alkali carbonate.

c) solid immersed in a mixture of $La_2(CO_3)_3{\cdot}8H_2O$ and alkali carbonate.

5.2.3 XRD analysis and in-situ XRD observations

X-ray diffraction (XRD) patterns of the powder products and the surfaces of the metals and ceramics immersed in the above mentioned molten carbonate mixtures were taken using CuKα radiation at operating conditions of 45kV and 40mA (X'Pert Pro system, Spectris). The XRD patterns of the synthesized powders were taken using Bragg-Brentano focusing optics, while those of the pure or purified products using parallel beam optics (from 20 to 90 deg, scan step: 0.02deg, time per step: 2 sec). The data were analyzed using a Rietveld analysis computer program RIETAN-2000 for the evaluation of phase purity[9]. A split pseudo-Voigt profile function was used for pattern fitting.

In-situ X-ray diffractometry was carried out to investigate the reaction mechanism between α-$LiAlO_2$ (Nippon Chemical Industrial) and $La_2(CO_3)_3 \cdot 8H_2O$. In molten carbonate α-$LiAlO_2$ is more stable than α-Al_2O_3, which reacts with lithium to produce α-$LiAlO_2$[10].Thus we did not use α-Al_2O_3 but α-$LiAlO_2$ for the in-situ reaction observation. The mixture of α-$LiAlO_2$ and $La_2(CO_3)_3 \cdot 8H_2O$ (molar ratio Al: La =1:1) was mixed with $(Li_{0.52}Na_{0.48})_2CO_3$, 1:1 by weight. Then the mixture was set in a gold pan (30mmϕ, 2mmt, 0.5mm depth) in the high temperature reactor chamber (XRK 900, Anton Paar) under CO_2 or N_2 atmosphere. The XRD patterns were recorded at several temperatures up to 923 K.

5.3. Result and Discussion

5.3.1. The $LaMO_3$ powders synthesis

The results of the perovskites synthesis in molten carbonates are summarized in Table 5-1. The desired $LaMO_3$ compounds (M= Al, Sc, Cr, Mn, Fe, Co, Ni, Ga, and In) were successfully obtained. In order to remove $(Li_{0.52}Na_{0.48})_2CO_3$, the products were washed with distilled water. As a typical result, the XRD profile of crude $LaGaO_3$ is shown in Fig. 5-2. The product, after a wash with distilled water, contained the $LaGaO_3$ and $La_2O_2CO_3$**.** We obtained $LaAlO_3$, $LaFeO_3$, $LaMnO_3$, and $LaNiO_3$ perovskites as powders containing small amount of impurities only after washing with water. The XRD pattern of $LaMnO_3$, shown in Fig. 5-3, could be assigned as $LaMnO_3$ (JCPDS: 35-1353). The In-containing perovskite, $LaInO_3$, could be produced at temperatures higher than 1073K; almost pure phase was obtained by keeping the mixture at 1173 K for 72h and then washing the powder with distilled water. $(Li_{0.435}Na_{0.315}K_{0.25})_2CO_3$ has the lowest melting point (671 K) of the four molten carbonate mixtures. This carbonate mixture was used for the $LaMO_3$ (M=Al, Sc, Cr, Mn, Fe, Co, Ni, and Ga) synthesis at 773 K; Table 5-1 summarizes the reaction conditions and results of this work. The XRD observations revealed some $LaMO_3$ in the crude products. In molten $(Li_{0.435}Na_{0.315}K_{0.25})_2CO_3$, the compounds $LaAlO_3$, $LaCrO_3$, $LaMnO_3$, $LaFeO_3$, $LaNiO_3$, and $LaGaO_3$ could be produced at a low temperature of 773 K.

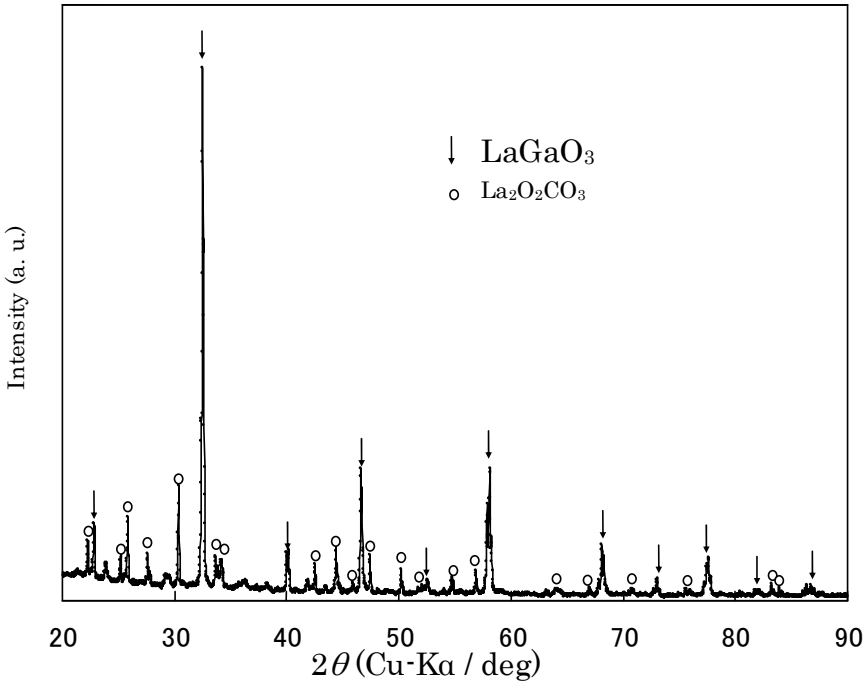

Fig. 5-2. XRD profile of $LaGaO_3$ synthesized in molten $(Li_{0.52}Na_{0.48})_2CO_3$ at 923 K for 72 hours under CO_2, and then washed with distilled water.

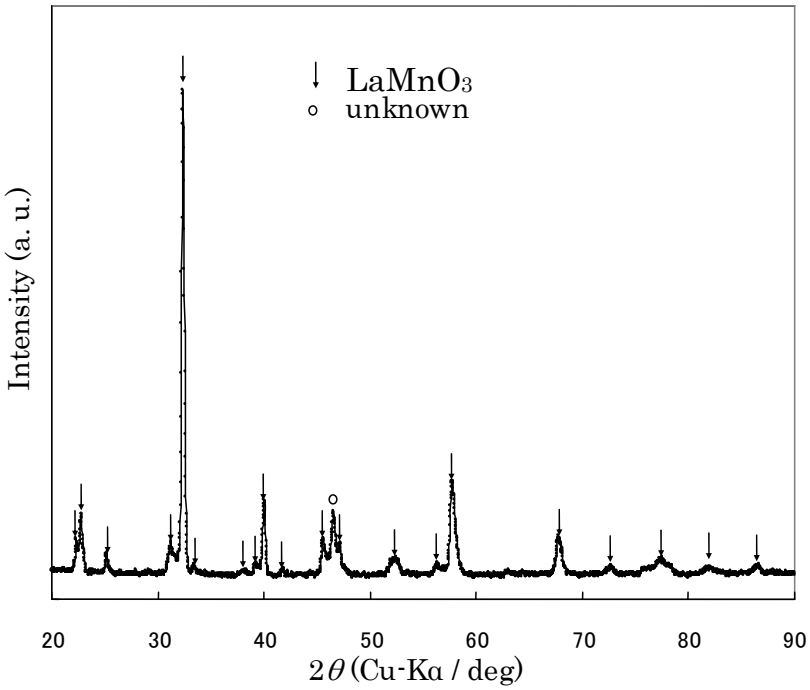

Fig. 5-3. XRD pattern**,** assigned as $LaMnO_3$, of $LaMnO_3$ synthesized in molten $(Li_{0.52}Na_{0.48})_2CO_3$ at 923 K for 72 hours under CO_2**,** then washed with distilled water.

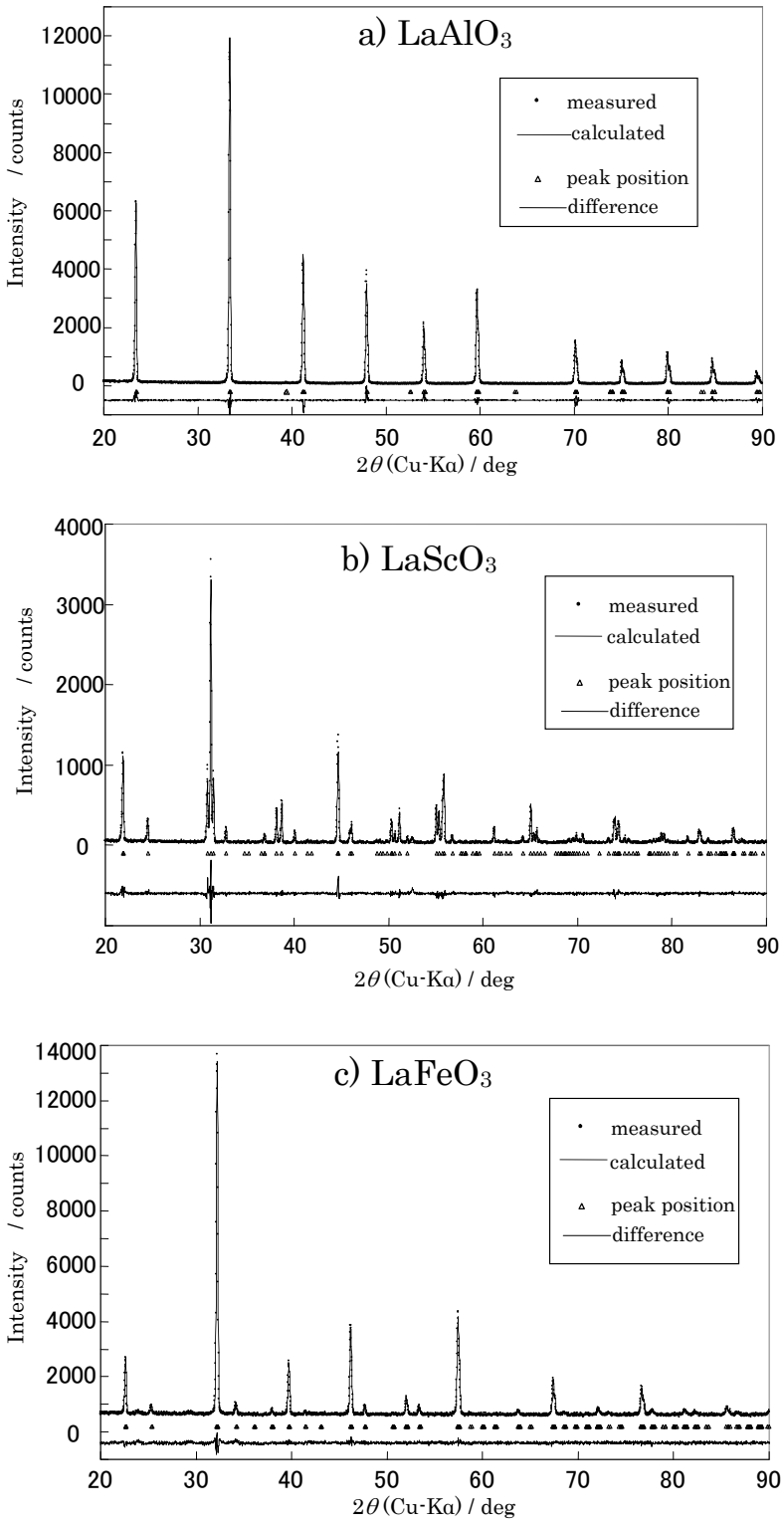

Fig. 5-4. Rietveld refinement results for XRD data of a) $LaAlO_3$, b) $LaScO_3$ and c) $LaFeO_3$.

From the viewpoint of low temperature synthesis, $LaAlO_3$ (773K) [2], $LaScO_3$ (773K) [11],$LaGaO_3$ (773K) [12],and $LaInO_3$ (1073K) [13]were synthesized at lower temperature than that of the papers so far reported. As for $LaGaO_3$, Huang et al. reported that Sr- and Mg- doped $LaGaO_3$ perovskite was produced at 873K[14].

The four eutectic carbonates $(Li_{0.52}Na_{0.48})_2CO_3$, $(Li_{0.62}K_{0.38})_2CO_3$, $(K_{0.573}Li_{0.427})_2CO_3$, or $(Li_{0.435}Na_{0.315}K_{0.25})_2CO_3$ were used as solvents for the reaction with α-Al_2O_3 and $La_2(CO_3)_3{\cdot}8H_2O$ at 923 K under CO_2 for 12h in order to compare the reactivity among these carbonates. For all carbonate mixtures, reaction proceeded completely to produce $LaAlO_3$. Every carbonate showed vigorous reactivity to α-Al_2O_3 for the production of $LaAlO_3$. Any of these carbonates could be used as solvents for $LaMO_3$ synthesis.

Although the desired products had been successfully obtained, after just a water wash the crude products contained unreacted metal oxides and lanthanum oxide carbonate, $La_2O_2CO_3$. Some of the crude powders could be purified from these impurities by washing with 12M HCl. Pure phase powders of $LaMO_3$ (M = Al, Sc, and Fe), and the powders of $LaMO_3$ (M = Ni, Co, Cr, Ga, and In) with small amount of impurity were obtained by HCl wash. Although $LaNiO_3$ and $LaCoO_3$ partly dissolved in 12M HCl with gas evolution, these lanthanum perovskites could be purified by such an acid wash. On the other hand, $LaMnO_3$ dissolved quickly in 12M HCl and was not obtained purified powder through this method.

In order to verify the phase purity, we analyzed the XRD data by the Rietveld method using the computer program RIETAN-2000[9].As examples, the results of $LaAlO_3$, $LaFeO_3$, and $LaScO_3$ are shown in Fig 5-4. The "goodness of fit" indicator, S ($=R_{wp}/R_e$ values ideally 1) were under 1.3 and indicated good fit[15].These results confirmed that the lanthanum perovskite compounds obtained by our method were single phases. Although trace amount of impurity phase can be seen in XRD patterns, the goodness of refinement S for $LaCrO_3$ (S =1.69), $LaCoO_3$ (S = 1.35), $LaNiO_3$ (S = 1.35), $LaGaO_3$ (S = 1.35), and $LaInO_3$ (S = 1.35), indicate successful refinement. These results of Rietveld analysis for $LaMO_3$ (M = Al, Sc, Fe, Co, Cr, Ga, and In) are summarized in Table 5-2. The obtained lattice parameters accord well with reported ones[13, 16, 17].

For further analysis of composition, $LaAlO_3$, $LaScO_3$, and $LaFeO_3$, in which little impurity phases can be seen in XRD (Fig. 5-4), were dissolved in nitric acid and elemental analysis was done using ICP (SPS-1700HVR: Seiko Instruments). The results were shown in Table 5-3. It was found that the sample of $LaScO_3$ was almost pure (atomic ratio: Li/La = 0.008, Na/La = 0.004). On the other hand, the sample of $LaAlO_3$ contained relatively large amount of lithium (atomic ratio: Li/La=0.15). Both lithium and sodium can be found in the sample of $LaFeO_3$ (atomic ratio: Li/La = 0.021, Na/La = 0.015). These lithium and sodium would be inside perovskite lattice or constitutes of amorphous phases such as $LiAlO_2$ or $LiFeO_2$. Several alkali doped lanthanum perovskites such as $La_{0.97}K_{0.03}NiO_3$[5], $LaMn_{0.8}Na_{0.2}O_{3+\delta}$[4] and $La_{2/3-x}Li_{3x}TiO_3$[18, 19]have been synthesized. The condition

of incorporated lithium and sodium needs more precise investigation. For the synthesis of product with less impurity, further optimizations of reaction condition and purification method are needed.

Table 5.2. Results of Rietveld analysis of XRDs for synthesized $LaMO_3$ (M= Al, Sc, Cr, Fe, Co, Ni, Ga, and In)

$LaMO_3$	Space Group	Reliability factors, and goodness-of-fit indicator of Rietveld analysis[9]	Lattice parameters / Å	Fractional coordinates (x, y, z)
$LaAlO_3$	*R-3c*	*R*wp= 9.27, *R*p = 6.97, *R*e = 7.62, *S*=1.24,	*a*=*b*=5.3637(1), *c*=13.1302(9) (*a*=*b*=5.3648, *c*=13.1113)[16]	La (0,0,1/4) Al (0,0,0) O (0.524(1),0,1/4)
$LaScO_3$	*Pnma*	*R*wp = 14.57, *R*p = 11.02, *R*e = 11.92, *S* = 1.22	*a*=5.7652(1), *b*=8.0556(2), *c*=5.6507(1) (*a*=5.787, *b*=8.098, *c*=5.678) [17]	La (0.0431(1),1/4,-0.089(4)) Sc (0,0,1/2) O1 (0.473(2),1/4,0.086(2)) O2 (-0.791(1),-0.447(1), -0.794(2))
$LaCrO_3$	*Pnma*	*R*wp = 9.66, *R*p = 7.65, *R*e = 6.19, *S* = 1.56	*a*=5.5107(3), *b*=7.7538(4), *c*=5.4733(3) (*a*=5.514, *b*=7.755, *c*=5.477) [17]	La (0.0136(3),1/4,-0.004(1)) Cr (0,0,1/2) O1 (0.487(3),1/4,-0.036(9)) O2 (-0.728(4),-0.538(3),-0.732(5))
$LaFeO_3$	*Pnma*	*R*wp = 4.17, *R*p = 3.29, *R*e = 3.73, *S* = 1.12	*a*=5.5648(2), *b*=7.8527(3), *c*=5.5562(2) (*a*=5.565, *b*=7.862, *c*=5.556) [17]	La (0.0296(2),1/4,-0.003(2)) Fe (0,0,1/2) O1 (0.513(3),1/4,0.072(7)) O2 (-0.755(3),-0.452(2),-0.767(3))
$LaCoO_3$	*R-3m*	*R*wp = 2.96, *R*p = 2.26, *R*e = 2.25, *S* = 1.32	*a*=*b*=*c*=3.8229(1), α =90.682(1) (*a*=*b*=*c*=3.824, α =90.70) [17]	La (0,0,0) Co (1/2,1/2,1/2) O (1/2,1/2,0)
$LaNiO_3$	*R-3c*	*R*wp = 14.87, *R*p = 11.00 *R*e = 9.28, *S* = 1.60	*a*=*b*=5.4596(2), *c*=13.1421(4) (*a*=*b*=5.4573, *c*=13.1462) [JCPDS Card No.79-2451]	La (0,0,1/4) Ni (0,0,0) O (0.548(1),0,1/4)
$LaGaO_3$	*Pnma*	*R*wp = 19.00, *R*p = 13.23 *R*e = 11.58, *S* = 1.64	*a*=5.5267(2), *b*=7.7792(2), *c*=5.4947(1) (*a*=5.524, *b*=7.787, *c*=5. 496) [17]	La (0.074(5),1/4,0.0043(8)) Ga (0,0,1/2) O1 (0.429(4),1/4,0.000(14)) O2 (-0.719(4),-0.462(2),-0.705(4))
$LaInO_3$	*Pnma*	*R*wp = 14.64, *R*p =10.76, *R*e = 9.20, *S* = 1.59	*a*=5.9366(1), *b*=8.2099(2),*c*=5.7185(1) (*a*=5.935, *b*=8.221, *c*=5.726) [13]	La (0.0550(2),1/4,0.0138(4)) In (0,0,1/2) O1 (0.457(3),1/4,-0.095(3)) O2 (-0.682(2),-0.548(2),-0.688(2))

Table 5.3. Elemental analysis of synthesized lanthanum perovskites, $LaAlO_3$, $LaScO_3$, and $LaFeO_3$ after purified with 12M HCl

Perovskites	Weight percent (%)				Elemental ratio			
	La	M	Li	Na	La	M	Li	Na
$LaAlO_3$	62.6	12.9	0.49	0.16	1	1.036	0.151	0.004
$LaScO_3$	57.9	20.1	0.02	0.04	1	1.073	0.008	0.004
$LaFeO_3$	56.0	23.8	0.06	0.14	1	1.057	0.021	0.015

5.3.2.Surface coverage of $LaMO_3$ on metal and ceramics substrates

The metals aluminum, chromium, iron, α-Al_2O_3 ceramic plate, and single crystal α-Al_2O_3 reacted with lanthanum carbonate in molten $(Li_{0.52}Na_{0.48})_2CO_3$ at 923 K and produced perovskite compounds on their surfaces. The results are summarized in Table 5-1. Under a CO_2 atmosphere, the aluminum was covered with a $LaAlO_3$ scale.

The compound $LaCrO_3$ was produced on the surface of the metal chromium under a CO_2/O_2=2/1 atmosphere. An adhesive scale of $LaCrO_3$ formed, but a further oxidation reaction proceeded, which introduced yellow colored CrO_4^{2-} ion into the molten carbonate. The coating of $LaCrO_3$ on the surface of Cr metal would be important because it might provide a means of coating metal interconnect in SOFC to resist oxidation and to decrease contact resistance[20, 21].Microscope (Lasertec, VL2000D) observation of surface morphology is shown in Fig 5-5. It was shown that cubic crystals less than 5 μm of $LaCrO_3$ were covered metal chromium surface without holes or clacks.

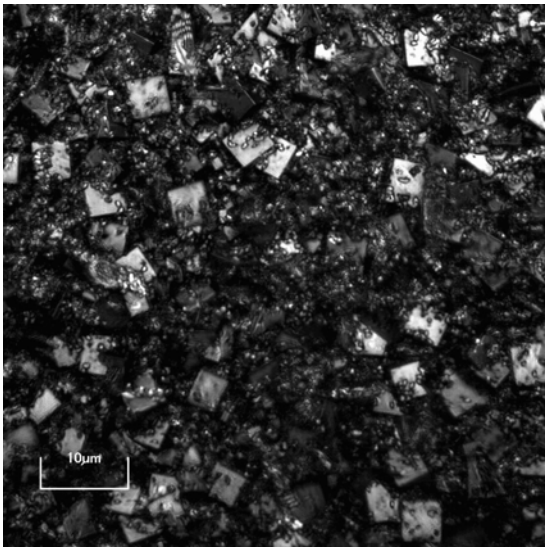

Figure 5-5. Microscope photograph of the surface of chromium immersed in molten $(Li_{0.52}Na_{0.48})_2CO_3$ added with lanthanum carbonate at 923 K for 12 hours under O_2/CO_2=1/2.

Under the same atmosphere, iron was covered with $LaFeO_3$ scale. The scale was fragile and easily removable.

On the other hand, Cobalt and nickel plates immersed in molten $(Li_{0.52}Na_{0.48})_2CO_3$ containing lanthanum carbonate under a CO_2/O_2 atmosphere were covered with CoO and NiO, respectively, not with perovskite compounds. These divalent oxides existed in a stable form on each metal plate, and did not produce trivalent oxides, which can react with lanthanum to generate perovskites. It was confirmed that for the formation of $LaMO_3$ in molten carbonate, M(III) should be stable.

Molten carbonate fuel cells utilized many materials which we mentioned above[8].Fine powder of α-$LiAlO_2$ is utilized as the electrolyte matrix. The eutectic carbonates $(Li_{0.52}Na_{0.48})_2CO_3$ and $(Li_{0.62}K_{0.38})_2CO_3$ have been used as the electrolyte. Porous ceramics of NiO, $LiCoO_2$, and $LiFeO_2$ are used as the cathode materials. Stainless steel is used as the separator and current corrector material and made of iron, chromium and nickel. Matsuzawa et al. reported that La_2O_3 addition reduce the solubility of NiO cathode into molten carbonate electrolyte[22].Böhme et al. reported La_2O_3 addition enhanced the NiO cathode conductivity[23].Tagawa et al. try to use La_2O_3 as anode catalyst for MCFC internal reforming of methane[24].It should be noted that the addition of lanthanum compound to MCFC would influence not only electrode but also electrolyte matrix and stainless steel housing because of $LaMO_3$ formation. Our preliminary study showed that in molten carbonates with lanthanum carbonate added stainless steel was covered with fragile $LaFeO_3$ scale, and the electrode materials $LiFeO_2$ and $LiCoO_2$ were changed to $LaFeO_3$ and $LaCoO_3$, respectively. The addition of lanthanum compound to MCFC needs more study for establishing whole system stability.

Following their immersion in the molten eutectic solvent/lanthanum mixture, and under a CO_2 atmosphere, the surfaces of the single crystal α-Al_2O_3 (sapphire (0001) plane) and α-Al_2O_3 ceramic plates were found to be coated with $LaAlO_3$**.** The XRD pattern of $LaAlO_3$ on α-Al_2O_3 ceramic was similar to that of powder $LaAlO_3$. On the other hand, the XRD pattern of $LaAlO_3$ produced on single crystal α-Al_2O_3 was different. Two peaks of the $LaAlO_3$ film were much larger than the corresponding peaks of powder $LaAlO_3$, as illustrated in Fig. 5-6. These two peaks originated from (012) plane of $LaAlO_3$. This suggests that the (012) plane of $LaAlO_3$ covered the crystal surface. Microscope (VL2000D, Lasertec, Japan) observation is shown in Fig. 5-7 of the surface of single crystal α-Al_2O_3 (sapphire) immersed in molten $(Li_{0.52}Na_{0.48})_2CO_3$ with lanthanum carbonate added. On the surface there were produced square crystal planes of about 5 μm size. These crystal planes were parallel to substrate and should be the cause of strong reflection of the (012) plane of $LaAlO_3$. It seemed that $LaAlO_3$ grew epitaxially on single crystal Al_2O_3. The plane on which crystal grew was set faced below, therefore floating $La_2O_2CO_3$ particle in molten carbonate did not pile up on the surface and did not contact. Lanthanum species dissolved in molten carbonate should react with the surface of sapphire to grow $LaAlO_3$ crystal. It should be noted that lanthanum species dissolved in molten carbonates play an important role for producing $LaMO_3$.

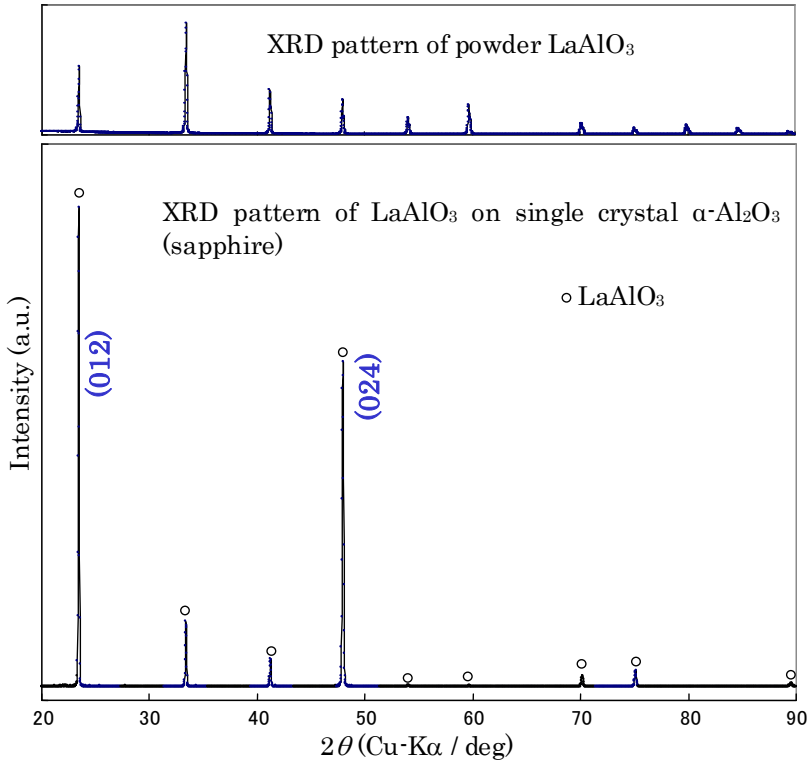

Fig. 5-6. X-ray diffraction (XRD) pattern of $LaAlO_3$ produced on the surface of single-crystal α-Al_2O_3 (sapphire) immersed in molten $(Li_{0.52}Na_{0.48})_2CO_3$ added with lanthanum carbonate at 923 K for 72 hours under CO_2.

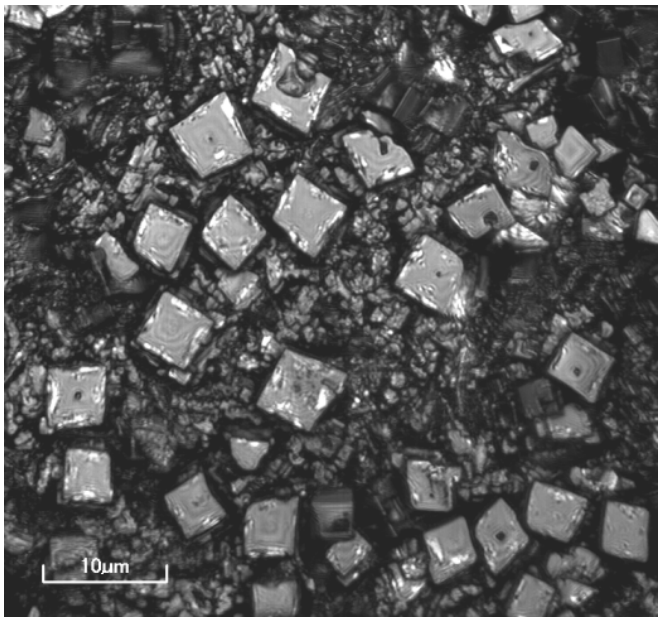

Figure 5-7. Microscope photograph of the surface of single crystal α-Al_2O_3 (sapphire) immersed in molten $(Li_{0.52}Na_{0.48})_2CO_3$ added with lanthanum carbonate at 923 K for 72 hours under CO_2.

5.3.3. In-situ XRD observation of the $LaAlO_3$ formation reaction

Figure 5-8 shows the XRD patterns of the mixture of α-$LiAlO_2$, $La_2(CO_3)_3 \cdot 8H_2O$ and $(Li_{0.52}Na_{0.48})_2CO_3$ heated up to 923 K under a CO_2 atmosphere. Under the melting point of $(Li_{0.52}Na_{0.48})_2CO_3$, up to 773 K (Fig.5-8, a and b), the XRD patterns showed carbonates peaks. Above the melting point of carbonate mixture, the patterns simplified, with the disappearance of the carbonates peaks, then, the $La_2O_2CO_3$ peaks appeared which suggests that the following reaction proceeded up to 823 K (Fig. 5-8, c):

$$La_2(CO_3)_3 \cdot 8H_2O \rightarrow La_2O_2CO_3 + 2CO_2 + 8H_2O \qquad [5\text{-}1]$$

After holding the temperature at 923 K for 2 hours (Fig. 5-8(d)), we could see only the $La_2O_2CO_3$ peaks. After 18 hours, small $LaAlO_3$ peaks appeared (Fig. 5-8(e)). After the sample cooling to room temperature, it was found that a large part of sample had changed to $LaAlO_3$ (Fig. 5-8(f)). From these results, we suppose that the following reaction occurs:

$$2LiAlO_2 + La_2O_2CO_3 \rightarrow 2LaAlO_3 + Li_2CO_3 \qquad [5\text{-}2]$$

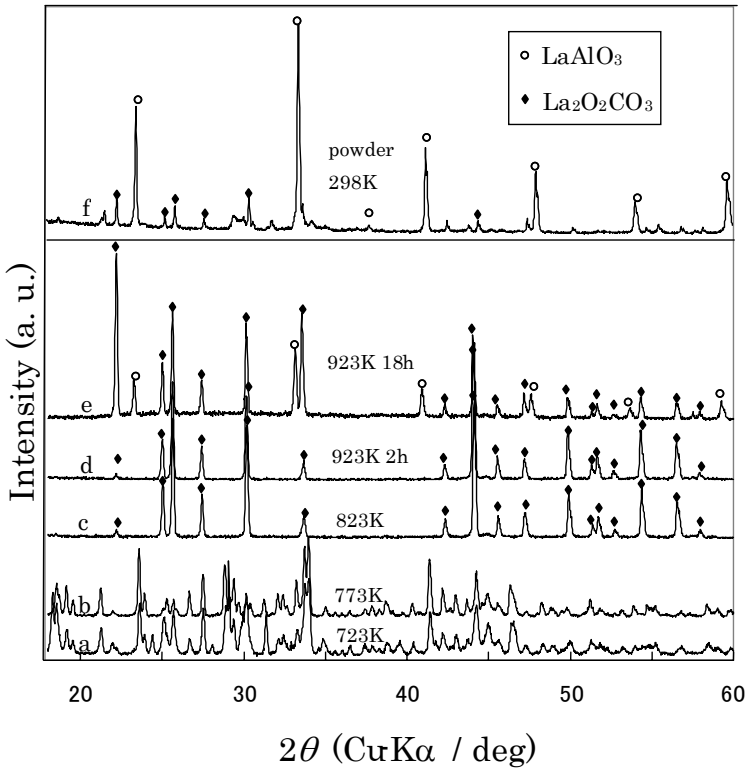

Fig. 5-8. XRD patterns of a mixture of α-$LiAlO_2$, $La_2(CO_3)_3 \cdot 8H_2O$, and $(Li_{0.52}Na_{0.48})_2CO_3$ under CO_2 atmosphere at several temperatures up to 923 K. (a) 723 K, (b) 773 K, (c) 823 K, (d) 923 K after 2h, (e) 923 K after 18h, (f) ex-situ, powder pattern at 298 K after 18 h at 923 K.

Under a N_2 atmosphere, the XRD patterns higher than 873 K exhibited a different profile assigned as La_4LiAlO_8 (JCPDS: 01-084-1470) (Fig. 5-9, c-g). $LaAlO_3$ peaks could be seen in the pattern at

923 K (Fig. 5-9, d), and after 3h, a large part of the sample changed to $LaAlO_3$ (Fig. 5-9, f). XRD pattern of the sample kept at 923 K under a N_2 atmosphere for 3 hours, and after that cooled to room temperature, showed that much of the sample had transformed into $LaAlO_3$ (Fig. 5-9, g) via the following reactions:

$$LiAlO_2 + 2La_2O_2CO_3 \rightarrow La_4LiAlO_8 + 2CO_2 \quad [5\text{-}3]$$

$$La_4LiAlO_8 + 3LiAlO_2 \rightarrow 4LaAlO_3 + 2Li_2O \quad [5\text{-}4]$$

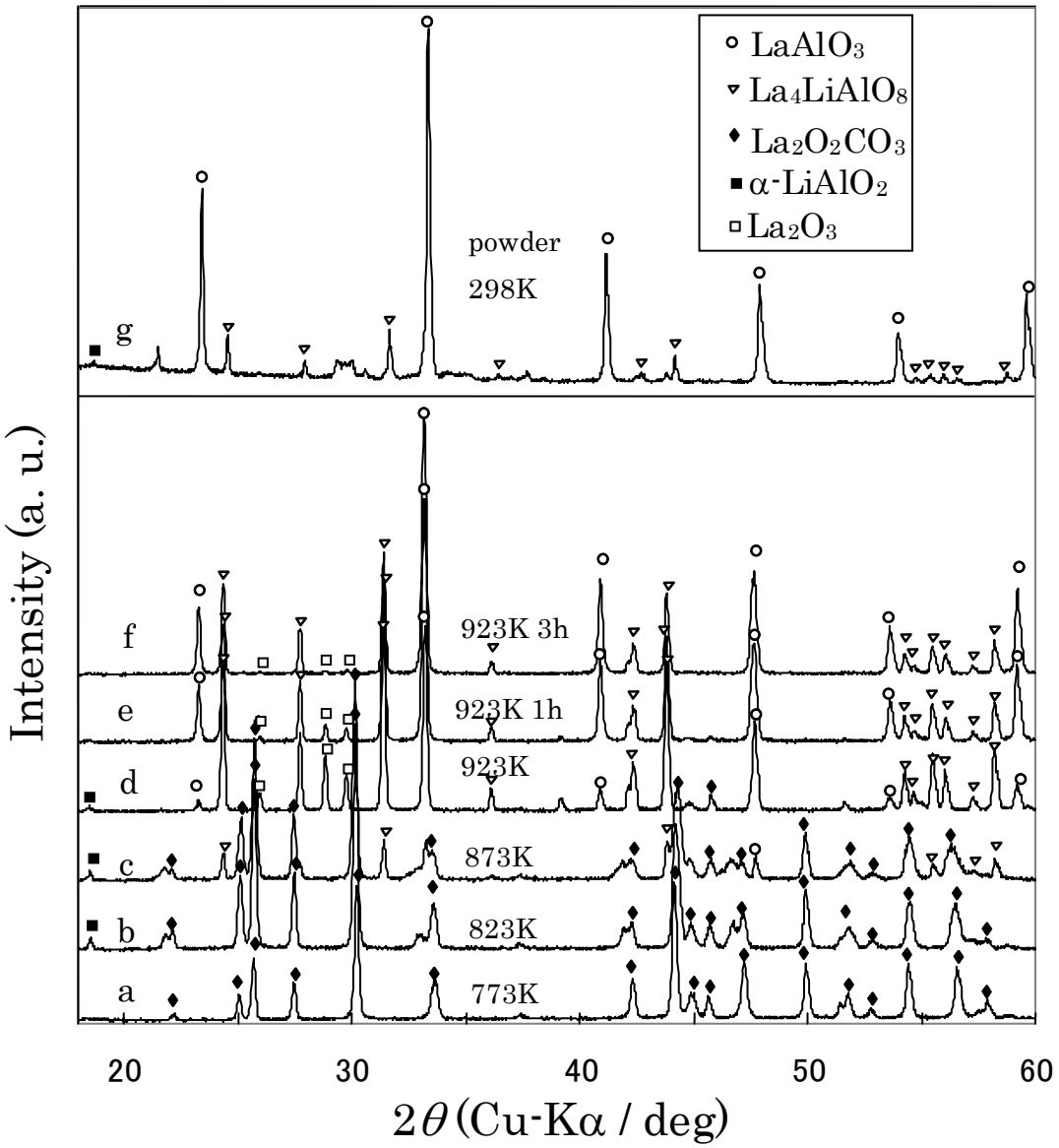

Fig. 5.9. X-ray diffraction patterns of a mixture of α-$LiAlO_2$, $La_2(CO_3)_3 \cdot 8H_2O$, and $(Li_{0.52}Na_{0.48})_2CO_3$ under N_2 atmosphere at several temperatures up to 923 K. (a) 773 K, (b) 823 K, (c) 873 K, (d) 923 K after 0.5h, (e) 923 K after 1h, (f)923 K after 3h, (g) *ex situ*, powder pattern at 298 K after 3 h at 923 K.

After holding at 923 K for only 3 hours under CO_2, then cooling down, a very weak $LaAlO_3$ peak can be seen in the powder sample. On the other hand, after 3 hours under N_2, a large part of sample changed to $LaAlO_3$. Therefore, it was confirmed that the $LaAlO_3$ production reaction will proceed faster in N_2 than in CO_2. This means the reaction proceed faster with decomposition of carbonate ion.

In general, the reaction between an M containing oxide and $La_2O_2CO_3$ is expected to proceed as follows:

$$M_2O_3 + La_2O_2CO_3 \rightarrow 2LaMO_3 + CO_2 \qquad [5\text{-}5]$$

It should be noted that carbonate ion is consumed as the oxide ion source to produce perovskite at the reaction site. It is also expected that reaction [5-5] will proceed faster in the atmosphere free from CO_2, such as N_2 or O_2. Actually it was found that $LaGaO_3$ can be produced at 773K under N_2, and at 923 K under CO_2, but no production can be seen at 773K under CO_2. This means that the condition of high temperature and atmosphere without CO_2 is favorable for $LaMO_3$ production.

It was also confirmed that the reaction producing $LaAlO_3$ did not proceed without the presence of the $(Li_{0.52}Na_{0.48})_2CO_3$ solvent after 12 h at 923 K. The rate of the $LaMO_3$ production reaction in molten carbonates at 923 K seems faster than that of a solid state reaction. Matsuzawa et al. reported that La_2O_3 was changed to $La_2O_2CO_3$ at 923K and solubility of lanthanum species was 1.0×10^{-2} mole fraction in molten $(Li_{0.52}Na_{0.48})_2CO_3$[18].

It was also observed that a planar-shaped $La_2O_2CO_3$ crystal of a few mm size grew in the molten $(Li_{0.52}Na_{0.48})_2CO_3$ added with $La_2(CO_3)_3 \cdot 8H_2O$ after 12h at 923 K under air. The crystal growth suggests that vigorous dissolution and precipitation of lanthanum species would occur in molten carbonate containing $La_2O_2CO_3$. The schematic view of reaction mechanism is shown in Fig. 5-10. The molten carbonates do not only act as a source of oxide ion but also as a flux conveying lanthanum to the reaction site. Consequently, the dissolved lanthanum species can attack the metal oxide surface to produce lanthanum perovskites more effectively and at lower temperatures than that by solid state reactions.

5.4. Conclusion

A successful new method for the synthesis of lanthanum perovskites $LaMO_3$ (M= Al, Sc, Cr, Mn, Fe, Co, Ni, Ga, and In) in molten carbonates has been found.

The metals aluminum, chromium, and iron, immersed in the mixture of molten $(Li_{0.52}Na_{0.48})_2CO_3$ and lanthanum carbonate were covered with $LaAlO_3$, $LaCrO_3$, and $LaFeO_3$, respectively. An α-Al_2O_3 ceramic and single crystal α-Al_2O_3 immersed in the same mixture were also covered with $LaAlO_3$. On the surface of single crystal α-Al_2O_3, the (012) plane of $LaAlO_3$ predominated.

Our in-situ XRD investigation of the reaction mechanism between $LiAlO_2$ and $La_2(CO_3)_3 \cdot 8H_2O$ in molten $(Li_{0.52}Na_{0.48})_2CO_3$ under a CO_2 or N_2 atmosphere revealed that $La_2O_2CO_3$ was produced first.

Then, however, a reaction ensued that produced $LaAlO_3$. Under a N_2 atmosphere, this latter reaction took place via La_4LiAlO_8, and at a faster rate than the reaction under CO_2.

The molten carbonates play an important role to facilitate $LaMO_3$ production reaction through dissolving and conveying lanthanum to the reaction site and acting as a source of oxide ion for perovskite formation.

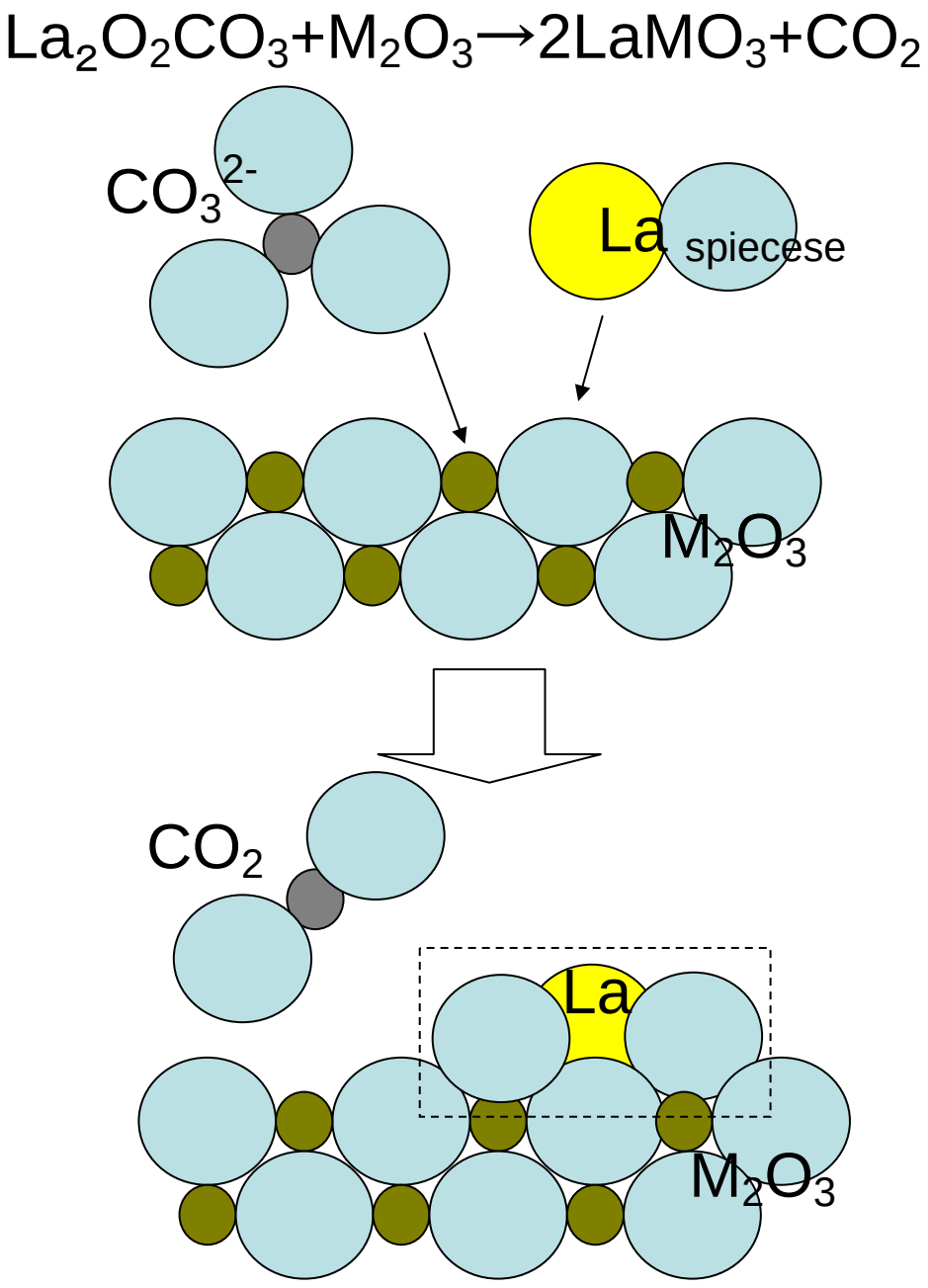

Fig.5-10. Schematic view of reaction mechanism of lanthanum perovskite formation in molten carbonate.

Reference

[1] F. Licci, G. Turilli, P. Ferro, and A. Ciccarone, "Low-Temperature Synthesis and Properties of $LaMnO_{3\pm d}$ and $La_{0.67}R_{0.33}Mn_{3\pm d}$ (R = Ca, Sr, Ba) from Citrate Precursors," *J. Am. Ceram. Soc.*, **86**, 413-19 (2003).

[2] P. K. Sahu, S. K. Behera, S. K. Partihar, and S. Bhattacharyya, "Low temperature synthesis of microwave dielectric $LaAlO_3$ nanoparticles: effect of chloride on phase evolution and morphology," *Ceram. Int.*, **30**, 1231-35 (2004).

[3] W. Zheng, W. Pang, G. Meng, and D. Peng, "Hydrothermal synthesis and characterization of $LaCrO_3$," *J. Mater. Chem*., **9**, 2833-36 (1999).

[4] N. R. Washburn, A. M. Stacy, and A. M. Portis, "Low-temperature, flux-grown, Na-doped $LaMnO_3$: Magnetic properties," *Appl. Phys. Lett*. **70**, 1622-1624 (1997).

[5] C. Shivakumara, M. S. Hegde, A. S. Prakash, A. M. A. Khadar, G. N. Subbanna, and N. P. Lalla, "Low temperature synthesis, structure and properties of alkali-doped La_2NiO_4, $LaNiO_3$ and $LaNi_{0.85}Cu_{0.15}O_3$ from alkali hydroxide fluxes," *Solid State Sci.*, **5**, 351-57 (2003).

[6] A. Wold, B. Post, and E. Banks, "Rare Earth Nickel Oxides," *J. Am. Chem. Soc*., **79**, 4911-13 (1957).

[7] K. E. Stitzer, A. El Abed, J. Darriet, and H-C. zur Loye, "Crystal Growth and Structure Determination of Barium Rhodates: Stepping Stones toward 2H-$BaRhO_3$," *J. Am. Chem. Soc*., **126**, 856-64 (2004).

[8] S. Mitsushima, K. Matsuzawa, N. Kamiya, and K. Ota, "Improvement of MCFC cathode stability by additives," *Electrochimica Acta*, **47**, 3823-30 (2002).

[9] F. Izumi and T. Ikeda, "A Rietveld-Analysis Program RIETAN-98 and its Applications to Zeolites," *Mater. Sci. Forum*, **321-24**, 198-204 (2000).

[10] M. Murai, K. Takizawa, K. Soejima, and H. Sotouchi, "Lithiation of Alumina in Molten Li/K Carbonates," *J. Electrochem. Soc.*, **143**, 3456-62 (1996).

[11] H. Inaba, H. Hayashi, and M. Suzuki, "Structural phase transition of perovskite oxides $LaMO_3$ and $La_{0.9}Sr_{0.1}MO_3$ with different size of B-site ions," *Solid State Ionics*, **144**, 99-108 (2001).

[12] K. Huang, M. Feng, and J. B. Goodenough, "Sol-Gel Synthesis of a New Oxide-Ion Conductor Sr- and Mg-Doped $LaGaO_3$ Perovskite," *J. Am. Ceram. Soc.*, **79**, 1100-04 (1996).

[13] H. He, X. Huang, and L. Chen, "The effects of dopant valence on the structure and electrical conductivity of $LaInO_3$," *Electrochim. Acta*, **46**, 2871-77 (2001).

[14] K. Huang, R. S. Tichy, and J. B. Goodenough, "Superior Perovskite Oxide-Ion Conductor; Strontium- and Magnesium-Doped $LaGaO_3$: II, ac Impedance Spectroscopy," *J. Am. Ceram. Soc.*, **81**, 2576-80 (1998).

[15] R. A. Young, "The Rietveld Method," ed. by R. A. Young, Oxford Univ. Press, Oxford (1993), Chap. 1.

[16] T-Y. Chen and K-Z. Fung, "A and B-site substitution of the solid electrolyte $LaGaO_3$ and $LaAlO_3$ with the alkaline-earth oxides MgO and SrO," *J. Alloys. Compd.,* **368**, 106-15 (2004).

[17] R. W. G. Wyckoff, "Crystal Structures Vol. 2, Second Edition," Interscience Publishers, 1964.

[18] Y. Inaguma, T. Katsumata, M. Itoh, and Y. Morii, "Crystal Structure of a Lithium Ion-Conducting Perovskite $La_{2/3-x}Li_{3x}TiO_3$ (x=0.05)," *J. Solid State Chem.,* **166**, 67-72 (2002).

[19] M. Yashima, M. Itoh, Y. Inaguma, and Y. Morii, "Crystal Structure and Diffusion Path in the Fast Lithium-Ion Conductor $La_{0.62}Li_{0.16}TiO_3$," *J. Am. Chem. Soc.,* **127**, 3491-95 (2005).

[20] N. Q. Minh, "Ceramic Fuel Cells," *J. Am. Ceram. Soc.,* **76**, 563-88 (1993).

[21] E. A Lee, S. Lee, H.J. Hwang and J.-W. Moon, "Sol–gel derived $(La_{0.8}M_{0.2})CrO_3$ (M=Ca, Sr) coating layer on stainless-steel substrate for use as a separator in intermediate-temperature solid oxide fuel cell," *J. Power Sources,* **157**, 709-13 (2006).

[22] K. Matsuzawa, T. Mizusaki, S. Mitsushima, N. Kamiya, K. Ota, "The effect of La oxide additive on the solubility of NiO in molten carbonates," *J. Power Sources*, **140**, 258-63 (2005).

[23] O. Böhme, F. U. Leidich, H. J. Salge, and H. Wendt, "Development of Materials and Production Technologies for molten carbonate fuel cells," *Int. J. Hydrogen Energy*, **19**, 349-55 (1994).

[24] T. Tagawa, A. Yanase, S. Goto, M. Yamaguchi, and M. Kondo, "Ceramic anode catalyst for dry methane type molten carbonate fuel cell," *J. Power Sources*, **126**, 1-7 (2004).

6. Conclusions

6.1. Summery of this work

This work has been devoted to studies for physical properties and chemical properties of molten carbonate mixtures. There are many new and interesting findings for fundamental and industrial aspects.

Density, surface tension and electrical conductivity have been measured with accurate and elaborated measurement methods, studying error factor or refining methods.

The molar volume of molten carbonate obtained through the measurements of density showed additivity and can be estimated using ionic size.

The surface tension of molten carbonate is related to ionic radii and some rules with composition. The surface tension of single, binary and ternary system can be predicted through the method of this work. The method also can be extended to other molten salt systems.

New correlation equation for the equivalent conductivity of molten carbonate systems has been found. The equation has been extended to new universal relationship with composition and ionic radii. The equivalent conductivity of single, binary and ternary system can be predicted using the ionic radii of components through the method of this work. The method also can be extended to other molten salt systems. Using the relationships developed in this thesis one can predict the equivalent conductivity, molar volume, and electrical conductivity for any composition of whole ternary systems using the cationic radii, molar volume and electrical conductivity of any trio of pure components, such as Li_2CO_3, Na_2CO_3, K_2CO_3, Rb_2CO_3, Cs_2CO_3, Ag_2CO_3, Tl_2CO_3, and Fr_2CO_3.

These studies of physical properties of molten carbonate will pave new avenue for the study of molten salts.

Successful new method for the synthesis of lanthanum perovskites $LaMO_3$ (M= Al, Sc, Cr, Mn, Fe, Co, Ni, Ga, and In) in molten carbonates also has been found. These reactions proceed faster and lower temperature than that of ordinal solid state reactions by the help of molten carbonate. It was found that addition of lanthanum species into molten carbonate electrolyte changes the nature of MCFC materials by making lanthanum perovskites.

6.2. New electrolyte for molten carbonate fuel cell

New electrolyte for molten carbonate fuel cell is favorable to have high conductivity and less corrosive to MCFC materials such as NiO cathode and stainless steel separator. Tanimoto showed that the electrolyte of $(Li_{0.52}Na_{0.48})_2CO_3$ containing alkaline earth carbonates such as $CaCO_3$ and/or $BaCO_3$ decrease the solubility of nickel in electrolyte.

Through the study of molten carbonate physical properties, these electrolytes are favorable for MCFC, because they show relatively high conductivity and surface tension. Higher conductivity

reduces cell resistance and enhances cell output. The electrolyte of the higher surface tension prevents cross leakage of gas through electrolyte matrix.

6.3. Future of molten salt and molten carbonate technologies

There are developing many new technologies concerning molten carbonate, not only MCFC but also nuclear fuel processing, solid oxide fuel cell, fuel processing and so on. These technologies would be key stones for industry and our life.

The work of this thesis has stimulated me for many fields concerning molten salt. I have found new materials and phenomenon for future technology, which can not be included here. I will report new materials and technology which come out partly from this study from now on.

I believe that molten carbonate and molten salt technologies would be more important for science and technology in near future.

List of Publications

1) T. Kojima, M. Yanagida, S. Tanase, K. Tanimoto, Y. Tamiya, T. Asai and Y. Miyazaki, "The Electrical Conductivity of Molten Li_2CO_3-Na_2CO_3 and Li_2CO_3-K_2CO_3 Containing Alkaline Earth (Ca, Sr and Ba) Carbonates", *Denki Kagaku* (presently *Electrochemistry*), **64**, 471-477 (1996).

2) T. Kojima, M. Yanagida, K. Tanimoto, Y. Tamiya, H. Matsumoto and Y. Miyazaki, "The surface tension and the density of molten binary alkali carbonate systems," *Electrochemistry*, **67**, 593-602 (1999).

3) T. Kojima, Y. Miyazaki, K. Nomura, and K. Tanimoto, "Density, molar volume, and surface tension of molten Li_2CO_3-Na_2CO_3 and Li_2CO_3-K_2CO_3 containing alkaline earth (Ca, Sr, and Ba) carbonates", *J. Electrochem. Soc.*, **150**, E535-542 (2003).

4) T. Kojima, K. Nomura, Y. Miyazaki, and K. Tanimoto, "Synthesis of Various $LaMO_3$ Perovskites in Molten Carbonates", *J. Am. Ceram. Soc.,* **89**, 3610-16 (2006).

5) T. Kojima, Y. Miyazaki, K. Nomura, and K. Tanimoto, "Electrical Conductivity of Molten Li_2CO_3-X_2CO_3 (X: Na, K, Rb, and Cs) and Na_2CO_3-Z_2CO_3 (Z: K, Rb, and Cs)", *J. Electrochem. Soc.*, **154**, F222-230 (2007).

6) T. Kojima, Y. Miyazaki, K. Nomura, and K. Tanimoto, "Density, Surface Tension, and Electrical Conductivity of Ternary Molten Carbonate System Li_2CO_3 - Na_2CO_3 - K_2CO_3 and Methods for Their Estimation", *J. Electrochem. Soc.*, **155**, F150-156 (2008).

7) T. Kojima, Y. Miyazaki, K. Nomura, and K. Tanimoto, "Effect of additives to the density, surface tension, and electrical conductivity of molten Li_2CO_3-Na_2CO_3 and Li_2CO_3-K_2CO_3", preparing for submission.

Acknowledgment

Author would like to appreciate Professor Tetsuo Sakai, Professor Tetsuhiko Kobayashi, and Professor Keisuke Oguro, who gave me the opportunity to perform the studies presented by this thesis. Author would like to thank Professor Shigehito Deki, Professor Satoru Nishiyama and Professor Minoru Mizuhata for great help, kind suggestion and fruitful discussions.

Special thanks go to Dr. Katsuhiro Nomura, Dr. Kazumi Tanimoto, and Mr. Miyazaki for long-lasting kind cooperation, suggestions and discussions.

Author would like to express gratitude to Dr. Teruo Kodama, who leaded the technology of MCFC in Japan and brought me to this interesting research.

Author would like to show appreciation for Prof. Norikazu Ohtori and Dr. Shigeo Tanase, who started me up for this study.

Author also would like to thank Mr. Masahiro Yanagida, Ms. Yukiko Tamiya and Dr. Hajima Matsumoto, and Dr. Hironobu Okuyama for helpful partnership.

Author finally would like to thank to my family, my mother, my wife, my daughter and sons for supporting me every time.

Toshikatsu Kojima
January 2009
In Ikeda City, Osaka, Japan